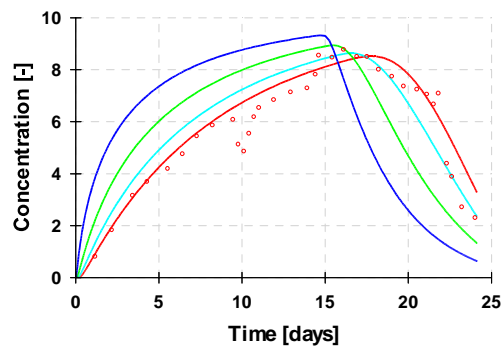*The HYDRUS-1D Software Package for Simulating the*

One-Dimensional Movement of Water, Heat, and

Multiple Solutes in Variably-Saturated Media

Version 4.0

April 2008

DEPARTMENT OF ENVIRONMENTAL SCIENCES
UNIVERSITY OF CALIFORNIA RIVERSIDE
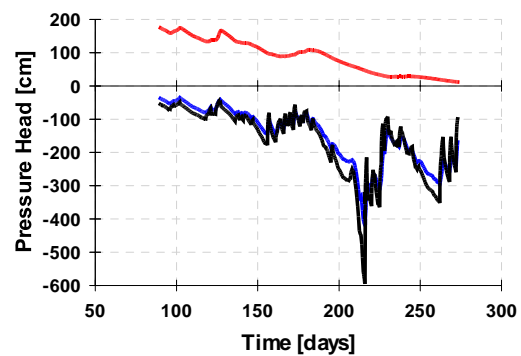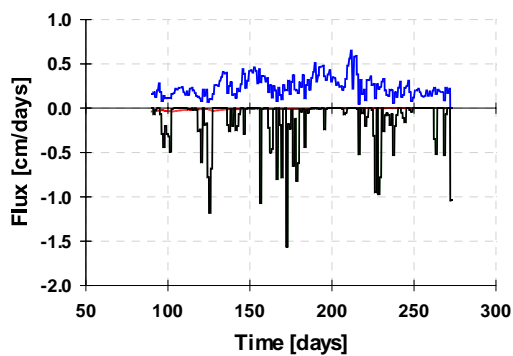RIVERSIDE, CALIFORNIA

The HYDRUS-1D Software Package for Simulating the

One-Dimensional Movement of Water, Heat, and

Multiple Solutes in Variably-Saturated Media

Version 4.0

by

J. Šimůnek, M. Šejna, H. Saito, M. Sakai, and M. Th. van Genuchten

April 2008

DEPARTMENT OF ENVIRONMENTAL SCIENCES
UNIVERSITY OF CALIFORNIA RIVERSIDE
RIVERSIDE, CALIFORNIA

DISCLAIMER

This report documents version 4.0 of HYDRUS-1D, a software package for simulating water, heat and solute movement in one-dimensional variably-saturated media. The software has been verified against a large number of test cases. However, no warranty is given that the program is completely error-free. If you do encounter problems with the code, find errors, or have suggestions for improvement, please contact

Jirka Šimůnek
Department of Environmental Sciences
University of California Riverside
Riverside, CA 92521
USA
Phone/Fax: (951) 827-7854
Email: Jiri.Simunek@ucr.edu

iv

ABSTRACT

Šimůnek, J., M. Šejna, H. Saito, M. Sakai, and M. Th. van Genuchten, The HYDRUS-1D Software Package for Simulating the Movement of Water, Heat, and Multiple Solutes in Variably Saturated Media, Version 4.0, *HYDRUS Software Series 3*, Department of Environmental Sciences, University of California Riverside, Riverside, California, USA, pp. 315, 2008.

This report documents version 4.0 of HYDRUS-1D, a software package for simulating water, heat and solute movement in one-dimensional variably saturated media. The software consists of the HYDRUS computer program, and the HYDRUS1D interactive graphics-based user interface. The HYDRUS program numerically solves the Richards equation for variably-saturated water flow and advection-dispersion type equations for heat and solute transport. The flow equation incorporates a sink term to account for water uptake by plant roots. The flow equation may also consider dual-porosity type flow in which one fraction of the water content is mobile and another fraction immobile, or dual-permeability type flow involving two mobile regions, one representing the matrix and one the macropores. The heat transport equation considers transport due to conduction and convection with flowing water. Coupled water, vapor, and energy transport can be considered as well. The solute transport equations consider advective-dispersive transport in the liquid phase, as well as diffusion in the gaseous phase. The transport equations also include provisions for nonlinear nonequilibrium reactions between the solid and liquid phases, linear equilibrium reactions between the liquid and gaseous phases, zero-order production, and two first-order degradation reactions: one which is independent of other solutes, and one which provides the coupling between solutes involved in sequential first-order decay reactions. In addition, physical nonequilibrium solute transport can be accounted for by assuming a two-region, dual-porosity type formulation which partition the liquid phase into mobile and immobile regions. Alternatively, the transport equations include provisions for kinetic attachment/detachment of solute to the solid phase and it can be thus used to simulate transport of viruses, colloids, or bacteria.

The HYDRUS software package also includes modules for simulating carbon dioxide and major ion solute movement. Diffusion in both liquid and gas phases and convection in the liquid phase are considered as CO_2 transport mechanisms. The CO_2 production model is described. The major variables of the chemical system are Ca, Mg, Na, K, SO_4, Cl, NO_3, H_4SiO_4,

alkalinity, and CO_2. The model accounts for equilibrium chemical reactions between these components such as complexation, cation exchange and precipitation-dissolution. For the precipitation-dissolution of calcite and dissolution of dolomite, either equilibrium or multicomponent kinetic expressions are used which include both forward and back reactions. Other dissolution-precipitation reactions considered include gypsum, hydromagnesite, nesquehonite, and sepiolite. Since the ionic strength of soil solutions can vary considerably with time and space and often reach high values, both modified Debye-Hückel and Pitzer expressions were incorporated into the model as options to calculate single ion activities.

The program may be used to analyze water and solute movement in unsaturated, partially saturated, or fully saturated porous media. The flow region may be composed of nonuniform soils. Flow and transport can occur in the vertical, horizontal, or a generally inclined direction. The water flow part of the model can deal with prescribed head and flux boundaries, boundaries controlled by atmospheric conditions, as well as free drainage boundary conditions. The governing flow and transport equations are solved numerically using Galerkin-type linear finite element schemes. HYDRUS also includes a Marquardt-Levenberg type parameter optimization algorithm for inverse estimation of soil hydraulic and/or solute transport and reaction parameters from measured transient or steady-state flow and/or transport data.

New features in version 4.0 of HYDRUS-1D as compared to version 3.0 include:

a) Vapor flow,
b) Coupled water, vapor, and energy transport,
c) Dual-permeability type water flow and solute transport,
d) Dual-porosity water flow and solute transport, with solute transport subjected to two-site sorption in the mobile zone,
e) Potential evapotranspiration as calculated with the Penman-Monteith combination equation or with Hargreaves equation,
f) Daily variations in the evaporation, transpiration, and precipitation rates,
g) Support for the HP1 code, which was obtained by coupling HYDRUS with the PHREEQC biogechemical code.

This report serves as both a user manual and reference document. Detailed instructions are given for data input preparation. A graphical user interface, HYDRUS1D, for easy data preparation and output display in the MS Windows environment is described in the second part of the manual. The software package can be freely downloaded from www.hydrus2d.com (or www.pc-progress.cz).

TABLE OF CONTENTS

LIST OF FIGURES

xiii

LIST OF TABLES

LIST OF ALL VARIABLES

a	ion activity on the exchange surfaces [-]
a^*	parameter in the exponential depth distribution function [L^{-1}]
a_{dr}	geometry factor for radial flow depending on the flow conditions [-]
a_i	conversion factor from concentration to osmotic head [L^{4}M^{-1}]
a_r	value of coefficient a at reference temperature T_r^A
a_T	value of coefficient a at temperature T^A
a_v	air content [L^{3}L^{-3}]
A	amplitude of temperature sine wave at the soil surface [K]
A_{qh}	empirical parameter in the deep drainage function, Eq. (7.1) [LT^{-1}]
A_s	correction factor [-]
b	normalized root water uptake distribution [L^{-1}]
b'	arbitrary root water uptake distribution [L^{-1}]
b_i	coefficients in the global matrix equations for water flow [T^{-1}] and solute transport [LT^{-1}]
b_1, b_2, b_3	empirical parameters to calculate the soil thermal conductivity, λ_0 [MLT^{-3}K^{-1}] (e.g. Wm^{-1}K^{-1})
B	convective term in the solute transport equation [LT^{-1}]
B_{qh}	empirical parameter in the deep drainage function, Eq. (7.1) [L^{-1}]
c	solution concentration [ML^{-3}]
c'	finite element approximation of c [ML^{-3}]
c_i	initial solution concentration [ML^{-3}]
$c_{im,m}$	solute concentration of the immobile zone of the matrix region [ML^{-3}]
$c_{m,m}$	solute concentration of the mobile zone of the matrix region [ML^{-3}]
c_n	value of the concentration at node n [ML^{-3}]
c_p	specific heat of moist air [L^{2}T^{-2}K^{-1}] (i.e., 1013 J kg^{-1} °C^{-1})
c_r	concentration of the sink term [ML^{-3}]
c_0	prescribed concentration boundary condition [ML^{-3}]
C	soil water capacity [L^{-1}]
C_a	volumetric heat capacity of the gas phase [ML^{-1}T^{-2}K^{-1}] (e.g. Jm^{-3}K^{-1})

C_n volumetric heat capacity of the solid phase [$ML^{-1}T^{-2}K^{-1}$] (e.g. $Jm^{-3}K^{-1}$)

C_o volumetric heat capacity of the organic matter [$ML^{-1}T^{-2}K^{-1}$] (e.g. $Jm^{-3}K^{-1}$)

C_p volumetric heat capacity of the porous medium [$ML^{-1}T^{-2}K^{-1}$] (e.g. $Jm^{-3}K^{-1}$)

C_T total solution concentration [ML^{-3}] ($mmol_c l^{-1}$)

C_w volumetric heat capacity of the liquid phase [$ML^{-1}T^{-2}K^{-1}$] (e.g. $Jm^{-3}K^{-1}$)

Cr_i^e local Courant number for element e [-]

d thickness of stagnant boundary layer above soil surface [L]

d effective 'diffusion' pathlength (i.e. half the aggregate width or half the fracture spacing) [L]

d_c diameter of the sand grains [L]

d_i coefficients in the global matrix equations for water flow [T^{-1}] and solute transport [LT^{-1}]

d_r relative distance between Earth and Sun [-]

D effective dispersion coefficient of the soil matrix [L^2T^{-1}]

D^-, D^+ effective dispersion coefficients corrected for higher-order approximation [L^2T^{-1}]

D_a diffusivity of water vapor in air [L^2T^{-1}] at temperature T

D_{eq} equivalent depth [L]

D^g diffusion coefficient for the gas phase [L^2T^{-1}]

D^w solute dispersion coefficient for the liquid phase [L^2T^{-1}]

D_g molecular diffusion coefficient of the gas phase [L^2T^{-1}]

D_L longitudinal dispersivity [L]

D_L^* additional longitudinal dispersivity [L] to fulfill the performance index ω_s

D_r thickness of layers over which radial drainage flow is considered [L]

D_v thickness of layers over which vertical drainage flow is considered [L]

D_v vapor diffusivity in soil [L^2T^{-1}]

D_w molecular diffusion coefficient in free water [L^2T^{-1}]

e element number [-]

e_a saturation vapor pressure at temperature T [$ML^{-1}T^{-2}$] (e.g., kPa)

(e_a-e_d) vapor pressure deficit [$ML^{-1}T^{-2}$] (e.g., kPa)

e_d vapor pressure at dew point [$ML^{-1}T^{-2}$] (e.g., kPa)

e_i coefficients in the global matrix equations for water flow [T^{-1}] and solute transport [LT^{-1}]

e_R elements located in the root zone [-]

E maximum (potential) rate of infiltration or evaporation under the prevailing atmospheric conditions [LT^{-1}]

E dispersive term in the solute transport equation [L^{2}T^{-1}]

E_a activation energy of a chemical reaction or process [ML^{2}T^{-2}M^{-1}] (e.g., kgm^{2}s^{-2}mol^{-1})

ET_0 reference crop evapotranspiration [LT^{-1}] (e.g., mm d^{-1})

f fraction of exchange sites assumed to be at equilibrium with the solution concentration [-]

f_{em} fraction of sorption sites in equilibrium with the mobile liquid phase (remaining sites are in contact with the mobile liquid phase) (dual-porosity model with two-site sorption in the mobile phase) [-]

f_f fraction of the exchange sites assumed to be in equilibrium with the solution phase [-] of the fracture domain (dual-permeability model) [-]

f_i coefficients in the global matrix equations for water flow [LT^{-1}] and solute transport [ML^{-2}T^{-1}]

f_m fraction of sorption sites in contact with the mobile region of the matrix (dual-permeability model with immobile zone in the matrix) [-]

f_m fraction of the exchange sites assumed to be in equilibrium with the solution phase [-] of the matrix domain (dual-permeability model) [-]

f_{mo} fraction of sorption sites in contact with mobile water (the remainder is in contact with immobile water) (dual-porosity model) [-]

f_r root growth coefficient [-]

$\{f\}$ vector in the global matrix equation for solute transport [MT^{-1}L^{-2}]

F first-order decay term in the solute transport equation [T^{-1}]

$\{F_w\}$ coefficient vector in the global matrix equation for water flow [LT^{-1}]

g gas phase concentration [ML^{-3}]

g gravitational acceleration (= 9.81 m s^{-2}) [LT^{-2}]

g_{atm} gas phase concentration above the stagnant boundary layer [ML^{-3}]

G zero-order decay term in the solute transport equation [ML^{-3}T^{-1}]

G soil heat flux [MT^{-3}] (e.g., MJ m^{-2} d^{-1})

G_{sc} solar constant [MT^{-3}] (e.g., J m^{-2}s^{-1}, 1360 W m^{-2})

G_{wT} gain factor [-] (equal 7 for sand)

h pressure head [L]

h^* scaled pressure head [L]

h' finite element approximation of h [L]

h_A minimum pressure head allowed at the soil surface [L]

h_{dr} watertable height above drain level at midpoint between drains, i.e. hydraulic head needed for calculating subsurface flow into drains [L]

h_f pressure head in the macropore region of the dual-permeability model [L]

h_i initial condition for the pressure head [L]

h_m pressure head in the matrix region of the dual-permeability model [L]

h_n nodal value of the pressure head [L]

h_{ref} pressure head at reference temperature T_{ref} [L]

h_s air-entry value in the Brooks and Corey soil water retention function [L]

h_S maximum pressure head allowed at the soil surface [L]

h_T pressure head at soil temperature T [L]

h_0 surface boundary condition for the pressure head [L]

h_{50} pressure head at which root water uptake is reduced by 50 % [L]

h_ϕ osmotic head [L]

$h_{\phi 50}$ osmotic head at which root water uptake is reduced by 50 % [L]

h_Δ pressure head at the reversal point in a hysteretic retention function [L]

H Hamaker constant (= 1e-20 J) [ML^2T^{-2}]

H_r relative humidity [-]

J number of the day in the year [-]

k kth chain number [-]

k Boltzman constant (= 1.38048e-23 J/K) [$M\ L^2T^{-2}K^{-1}$]

k_a first-order deposition (attachment) coefficient [T^{-1}]

k_d first-order entrainment (detachment) coefficient [T^{-1}]

k_g empirical constant relating the solution and gas phase concentrations [-]

k_s empirical constant relating the solution and adsorbed concentrations [L^3M^{-1}]

K unsaturated soil hydraulic conductivity [LT^{-1}]

K^*	scaled unsaturated soil hydraulic conductivity [LT^{-1}]
K^d	unsaturated hydraulic conductivity of the main drying branch [LT^{-1}]
K^w	unsaturated hydraulic conductivity of the main wetting branch [LT^{-1}]
K_a	effective hydraulic conductivity of the fracture-matrix interface [LT^{-1}]
K_{ex}	dimensionless thermodynamic equilibrium constant [-]
K_f	unsaturated soil hydraulic conductivity of the macropore (fracture) region in the dual-permeability model [LT^{-1}]
K_H	Henry's law constant [MT^{2}M^{-1}L^{-2}]
K_{hBot}	horizontal saturated hydraulic conductivity below the drain system [LT^{-1}]
K_{hTop}	horizontal saturated hydraulic conductivity above the drain system [LT^{-1}]
K_k	measured value of the unsaturated soil hydraulic conductivity at θ_k [LT^{-1}]
K_{LT}	thermal hydraulic conductivity of the liquid phase [L^{2}K^{-1}T^{-1}]
K_m	unsaturated soil hydraulic conductivity of the matrix region in the dual-permeability model [LT^{-1}]
K_r	relative soil hydraulic conductivity [-]
$K_{r'}$	saturated hydraulic conductivity in the layer with radial drainage flow [LT^{-1}]
K_{ref}	hydraulic conductivity at reference temperature T_{ref} [LT^{-1}]
K_s	saturated hydraulic conductivity [LT^{-1}]
$K_s^{\ d}$	saturated hydraulic conductivity associated with the main drying branch [LT^{-1}]
$K_s^{\ w}$	saturated hydraulic conductivity associated with the main wetting branch [LT^{-1}]
K_T	hydraulic conductivity at soil temperature T [LT^{-1}]
K_v	Vanselow selectivity coefficient [-]
$K_{v'}$	saturated hydraulic conductivity in the layer with vertical drainage flow [LT^{-1}]
K_{vh}	isothermal vapor hydraulic conductivity [LT^{-1}]
K_{vT}	thermal vapor hydraulic conductivity [L^{2}K^{-1}T^{-1}]
K_{12}	selectivity coefficient [-]
K_Δ	unsaturated hydraulic conductivity at the reversal point in a hysteretic conductivity function [LT^{-1}]
l	pore-connectivity parameter [-]
L	x-coordinate (depth of the soil profile) of the soil surface above a certain reference plane [L]

L_{dr} drain spacing [L]

L_m maximum rooting depth [L]

L_R root depth [L]

L_0 initial value of the rooting depth at the beginning of the growth period [L]

L_0 volumetric latent heat of vaporization of liquid water [$ML^{-1}T^{-2}$] (e.g., Jm^{-3})

m parameter in the soil water retention function [-]

M total amount of mass in the entire flow domain [ML^{-2}]

M molecular weight of water [$M\ mol^{-1}$] (=0.018015 kg mol^{-1})

M^0 cumulative amount of solute removed from the flow region by zero-order reactions [ML^{-2}]

M^1 cumulative amount of solute removed from the flow region by first-order reactions [ML^{-2}]

M_r cumulative amount of solute removed from the flow region by root water uptake [ML^{-2}]

M_t total amount of solute in the flow region at time t [ML^{-2}]

M_t^e amount of solute in element e at time t [ML^{-2}]

M_0 amount of solute in the flow region at the beginning of the simulation [ML^{-2}]

M_0^e amount of solute in element e at the beginning of the simulation [ML^{-2}]

n exponent in the soil water retention function [-]

n^d exponent in the soil water retention function; drying branch [-]

n^w exponent in the soil water retention function; wetting branch [-]

n_s number of solutes involved in the consecutive solute chain [-]

n/N relative sunshine fraction [-]

N total number of nodes [-]

N_{Pe} Peclet number [-]

N_R interception number [-]

N_G gravitation number [-]

N_{Lo} contribution of particle London-van der Walls attractive forces to particle removal [-]

O actual rate of inflow/outflow to/from a subregion [LT^{-1}]

p exponent in the water and osmotic stress response function [-]

p_t period of time necessary to complete one temperature cycle (1 day) [T]

p_1 exponent in the water stress response function [-]

p_2 exponent in the osmotic stress response function [-]

P atmospheric pressure [$ML^{-1}T^{-2}$] (e.g., kPa)

Pe_i^e local Peclet number for element e [-]

$[P_s]$ coefficient matrix in the global matrix equation for solute transport [LT^{-1}]

$[P_w]$ coefficient matrix in the global matrix equation for water flow [T^{-1}]

q Darcian fluid flux density [LT^{-1}]

q_{drain} drain discharge rate per unit surface area [LT^{-1}]

q_N water flux boundary condition at the soil surface [LT^{-1}]

q_s solute flux [$ML^{-2}T^{-1}$]

q_{s0} solute flux boundary condition at the bottom of the soil profile [LT^{-1}]

q_{sN} solute flux boundary condition at the soil surface [LT^{-1}]

q_v vapor flux density [LT^{-1}]

q_0 water flux boundary condition at the bottom of the soil profile [LT^{-1}]

$[Q]$ coefficient matrix in the global matrix equation for solute transport [L]

r growth rate [T^{-1}]

r_i coefficients in the global matrix equation for solute transport [$ML^{-2}T^{-1}$]

R solute retardation factor [-]

R_a extraterrestrial radiation [MT^{-3}] (e.g., MJ m^{-2}d^{-1})

R_n net radiation at crop surface [MT^{-3}] (e.g., MJ m^{-2}d^{-1})

R_{nl} net longwave radiation [MT^{-3}] (e.g., MJ m^{-2}d^{-1})

R_{ns} net shortwave radiation [MT^{-3}] (e.g., MJ m^{-2}d^{-1})

R_u universal gas constant [$ML^2T^{-2}K^{-1}M^{-1}$] (= 8.314 kg m^{2}s^{-2}K^{-1}mol^{-1}, J mol^{-1}K^{-1})

$\{R\}$ vector in the global matrix equation for solute transport [$ML^{-2}T^{-1}$]

s adsorbed solute concentration [-]

s^e adsorbed solute concentration on type-1 sites [-]

s_f^k sorbed concentration of type-2 (kinetic) sites in the fracture domain (dual-permeability model) [-]

s_i initial value of adsorbed solute concentration [-]

s_{max} maximum solid phase concentration [MM^{-1}]

s^k	adsorbed solute concentration on type-2 sites [-]
s_m^k	sorbed concentration of type-2 (kinetic) sites in the matrix domain (dual-permeability model) [-]
s_{mo}^e	sorbed concentration in equilibrium with the liquid phase concentration of the mobile region of the dual-porosity model [MM^{-1}]
$s_{mo,e}^k$	sorbed concentration of kinetic sites in contact with the mobile region of the dual-porosity model when at equilibrium [MM^{-1}]
S	sink term in the flow equation [T^{-1}]
S_e	effective saturation [-]
S_e^{im}	effective fluid saturation of the immobile (matrix) region
S_e^m	effective fluid saturations of the mobile (fracture) region
S_{ek}	effective saturation at θ_k [-]
S_f	sink term in the flow equation for the macropore (fracture) reqion of the dual-permeability model [T^{-1}]
S_{im}	sink term in the flow equation for the immobile flow region [T^{-1}]
S_m	sink term in the flow equation for the matrix reqion of the dual-permeability model [T^{-1}]
S_{mo}	sink term in the flow equation for the mobile flow region [T^{-1}]
S_p	spatial distribution of the potential transpiration rate over the soil profile [T^{-1}]
S_T	cation exchange capacity [MM^{-1}] (mmol$_c$kg^{-1})
$[S]$	coefficient matrix in the global matrix equation for solute transport [LT^{-1}]
t	time [T]
t_0	time when simulation begins [T]
t_p	period of time covering one complete cycle of the temperature sine wave [T]
T	temperature [K, ^{o}C]
T	average temperature at the soil surface during period t_p [K]
T^A	absolute temperature [K]
T_a	actual transpiration rate per unit soil surface [LT^{-1}]
T_i	initial temperature [K]
T_m	daily mean air temperature [K]
$T_{\max}$	maximum daily air temperature [K]

T_{min}	minimum daily air temperature [K]
T_p	potential transpiration rate [LT^{-1}]
T_r^A	reference absolute temperature [K] (293.15K = 20°C)
T_{ref}	reference temperature [K]
T_0	prescribed temperature boundary condition [K]
TR	temperature range between mean daily maximum and minimum air temperatures [^{o}C]
$[T]$	coefficient matrix in the global matrix equation for solute transport [LT^{-1}]
u	wet perimeter of the drain [L]
U_2	windspeed measured at 2 m height [LT^{-1}] (e.g., m s^{-1})
v	average pore-water velocity [LT^{-1}]
V	volume of water in each subregion [L]
V_{new}	volume of water in each subregion at the new time level [L]
V_{old}	volume of water in each subregion at the previous time level [L]
V_t	volume of water in the flow domain at time t [L]
V_t^e	volume of water in element e at time t [L]
V_0	volume of water in the flow domain at initial time t_0 [L]
V_0^e	volume of water in element e at initial time t_0 [L]
w	ratio of the volumes of the macropore or fracture domain and the total soil system in the dual-permeability model [-]
W	total amount of energy in the flow region [MT^{-2}]
w_i	weighting factors for the two overlapping regions of the dual-porosity model [-]
x	spatial coordinate [L] (positive upward)
x_0	coordinate of the location where the straining process starts [L]
α	dimensionless water stress response function [-]
α	parameter in the soil water retention function [L^{-1}]
α	sticking efficiency (ratio of the rate of particles that stick to a collector to the rate they strike the collector) [-]
α^d	value of α for a drying branch of the soil water retention function [L^{-1}]
α^w	value of α for a wetting branch of the soil water retention function [L^{-1}]
α^w	weighing factor [-]

α_{ch}	first-order rate constant [T^{-1}] accounting for chemical rate processes
$\alpha_{ch,m}$	first-order rate constant for the matrix domain [T^{-1}]
α_h	scaling factor for the pressure head [-]
$\alpha_h{}^*$	temperature scaling factor for the pressure head [-]
α_K	scaling factor for the hydraulic conductivity [-]
$\alpha_K{}^*$	temperature scaling factor for the hydraulic conductivity [-]
α_θ	scaling factor for the water content [-]
α_w	first-order mass transfer coefficient [L^{-1}T^{-1}]
β	empirical constant in the adsorption isotherm [-]
β	empirical factor in the straining function [-]
β	shape factor that depends on the geometry [-]
β_t	thermal dispersivity [L]
γ	surface tension of soil water [MT^{-2}] (e.g., Jm^{-2})
γ	psychrometric constant [ML^{-1}T^{-2}K^{-1}] (e.g., kPa ^{o}C^{-1})
γ_0	surface tension at 25°C [MT^{-2}] (= 71.89 g s^{-2})
γ_{entr}	entrance resistance into the drains [T]
γ_g	zero-order rate constant for solutes in the gas phase [ML^{-3}T^{-1}]
γ_i	activity coefficient in the soil solution [L^{3}M^{-1}] (l mol^{-1})
γ_s	zero-order rate constant for solutes adsorbed onto the solid phase [T^{-1}]
γ_w	zero-order rate constants for solutes in the liquid phase [ML^{-3}T^{-1}]
γ_w	scaling factor in the mass transfer function (=0.4) [-]
Γ_w	transfer rate for water from the inter- to the intra-aggregate pores [T^{-1}]
Γ_{s1}	mass transfer term for solute exchange between the mobile and immobile regions (dual-porosity model) [ML^{-3}T^{-1}]
Γ_{s2}	mass transfer to kinetic sorption sites in the mobile region (two-site sorption model) [ML^{-3}T^{-1}]
$\Gamma_s{}^*$	mass transfer term for solutes between the mobile and immobile regions of the matrix domain (dual-permeability model with immobile region in the matrix) [ML^{-3}T^{-1}]
δ	solar declination [rad]
δ_{ij}	Kronecker delta [-]
Δ	slope of the vapor pressure curve [ML^{-1}T^{-2}K^{-1}] (e.g., kPa ^{o}C^{-1})

Δt	time increment [T]
Δt_{max}	maximum permitted time increment [T]
Δt_{min}	minimum permitted time increment [T]
Δx	size of the elements [L]
ε	temporal weighing factor [-]
ε	ratio of the molecular weights of water vapor and dry air [-], i.e., 0.622
ε_a^c	absolute error in the solute mass balance [ML^{-2}]
ε_a^w	absolute error in the water mass balance [L]
ε_r^c	relative error in the solute mass balance [%]
ε_r^w	relative error in the water mass balance [%]
η	empirical constant in the adsorption isotherm [L^{3}M^{-1}]
η	single-collector efficiency [-]
η_e	enhancement factor [-]
θ	volumetric water content [L^{3}L^{-3}]
θ^*	scaled volumetric water content [L^{3}L^{-3}]
θ_a	parameter in the soil water retention function [L^{3}L^{-3}]
θ_f	volumetric water content of the macropore (fracture) region in the dual-permeability model [L^{3}L^{-3}]
θ_F	volumetric water content (absolute) of the fracture region in the dual-permeability model ($=(1-w)\theta_f$) [L^{3}L^{-3}]
θ_{im}	water content in the immobile (stagnant, intra-aggregate) region [L^{3}L^{-3}]
$\theta_{m,m}$	water content of the immobile (stagnant, intra -aggregate) region in the matrix (dual-permeability model) [L^{3}L^{-3}]
θ_k	volumetric water content corresponding to K_k [L^{3}L^{-3}]
θ_m	parameter in the soil water retention function [L^{3}L^{-3}]
θ_m	volumetric water content of the matrix region in the dual-permeability model [L^{3}L^{-3}]
θ_{mo}	water content in the mobile (flowing, inter-aggregate) region [L^{3}L^{-3}]
θ_m^d	parameter in soil water retention function; drying branch [L^{3}L^{-3}]
θ_m^w	parameter in soil water retention function; wetting branch [L^{3}L^{-3}]
$\theta_{m,m}$	water content of the mobile (flowing, inter-aggregate) region of the matrix (dual-permeability model) [L^{3}L^{-3}]

θ_M	volumetric water content (absolute) of the matrix region in the dual-permeability model ($=w\theta_m$) [L^{3}L^{-3}]
θ_n	volumetric solid phase fraction [L^{3}L^{-3}]
θ_o	volumetric organic matter fraction [L^{3}L^{-3}]
θ_r	residual soil water content [L^{3}L^{-3}]
θ_r^*	scaled residual soil water content [L^{3}L^{-3}]
θ_r^d	residual soil water content of the main drying branch [L^{3}L^{-3}]
θ_r^w	residual soil water content of the main wetting branch [L^{3}L^{-3}]
θ_s	saturated soil water content [L^{3}L^{-3}]
θ_s^d	saturated soil water content of the main drying branch [L^{3}L^{-3}]
θ_s^w	saturated soil water content of the main wetting branch [L^{3}L^{-3}]
θ_T	total volumetric water vapor content (being the sum of θ and θ_v) [L^{3}L^{-3}]
θ_v	volumetric water vapor content (expressed as an equivalent water content) [L^{3}L^{-3}]
θ_Δ	water content at the reversal point of a hysteretic retention function [L^{3}L^{-3}]
λ	apparent thermal conductivity of the soil [MLT^{-3}K^{-1}] (e.g. Wm^{-1}K^{-1})
λ	latent heat of vaporization of water [L^{2}T^{-2}] (e.g., Jkg^{-1})
λ_0	thermal conductivity of porous medium in the absence of water flow [MLT^{-3}K^{-1}] (e.g. Wm^{-1}K^{-1})
λET_0	latent heat flux of evaporation [MT^{-3}] (e.g., J m^{-2}s^{-1})
μ	fluid viscosity [ML^{-1}T^{-1}] (= 0.00093 Pa s)
μ_g	first-order rate constant for solutes in the gas phase [T^{-1}]
μ_{ref}	dynamic viscosity at reference temperature T_{ref} [MT^{-1}L^{-1}]
μ_s	first-order rate constant for solutes adsorbed onto the solid phase [T^{-1}]
μ_T	dynamic viscosity at temperature T [MT^{-1}L^{-1}]
μ_w	first-order rate constant for solutes in the liquid phase [T^{-1}]
μ_g'	first-order rate constant for decay chain solutes in the gas phase [T^{-1}]
μ_s'	first-order rate constant for decay chain solutes adsorbed onto the solid phase [T^{-1}]
μ_w'	first-order rate constant for decay chain solutes in the liquid phase [T^{-1}]
ζ_i	activity coefficient for the exchange surfaces [MM^{-1}] (kg mol^{-1})
ρ	bulk density of porous medium [ML^{-3}]

ρ_f fluid density (= 998 kg m^{-3}) [ML^{-3}]

ρ_{ref} density of soil water at reference temperature T_{ref} [ML^{-3}]

ρ_p bacterial density (= 1080 kg m^{-3}) [ML^{-3}]

ρ_T density of soil water at temperature T [ML^{-3}]

ρ_{vs} saturated vapor density [ML^{-3}]

ρ_w density of liquid water [ML^{-3}]

ψ dimensionless colloid retention function [-]

σ surface tension [MT^{-2}]

σ_{ref} surface tension at reference temperature T_{ref} [MT^{-2}]

σ_T surface tension at temperature T [MT^{-2}]

τ_g tortuosity factor in the gas phase [-]

τ_w tortuosity factor in the liquid phase [-]

$\phi_{mo}, \phi_{mi}, \phi_{mo,k}$ sink/source terms for the equilibrium phases of the mobile zone, the immobile zone, and for the kinetic sorption sites [ML^{-3}T^{-1}], respectively

$\phi_{m,m}, \phi_{im,m}$ various reactions in the mobile and immobile parts of the matrix [ML^{-3}T^{-1}]

φ site latitude [rad]

φ_n linear basis functions [-]

$\varphi_n{}^u$ upstream weighted basis functions [-]

ω first-order adsorption rate constant [T^{-1}]

ω first-order rate coefficient [T^{-1}] in the water mass transfer equation

ω_{dpm} mass transfer coefficient between the mobile and immobile zones of the matrix region [T^{-1}]

ω_{ph} first-order rate constant [T^{-1}] accounting for physical rate processes

ω_s performance index for minimizing or eliminating numerical oscillations [-]

ω_s sunset hour angle [rad]

ξ local coordinate [-]

List of additional variables in the carbon dioxide and major ion chemistry modules

a	parameter in the exponential depth reduction function [L^{-1}]
a_i	activity of the ith ion [-]
A	Debye-Hückel constant ($kg^{0.5}mol^{-0.5}$)
Alk	alkalinity ($mol_c kg^{-1}$)
B	Debye-Hückel constant ($kg^{0.5}cm^{-1}mol^{-0.5}$)
B_{ij}	Pitzer specific virial coefficient for double ion interaction
$\bar{c}$	surface species concentration [MM^{-1}]
$\hat{c}$	solid phase concentration [MM^{-1}]
c_a, c_w	CO_2 concentrations in the gas and liquid phase, respectively [L^3L^{-3}]
c_{ai}	initial CO_2 concentration in the gas phase [L^3L^{-3}]
c_{as}	CO_2 concentration in the soil gas at the soil surface [L^3L^{-3}]
c_{atm}	CO_2 concentration at the top of the stagnant boundary layer [L^3L^{-3}]
c_{a0}	boundary condition for CO_2 concentration in the gas phase [L^3L^{-3}]
c_T	total volumetric CO_2 concentration [L^3L^{-3}]
C_T	cation exchange capacity ($mol_c kg^{-1}$)
C_0	total salt concentration ($mol\ l^{-1}$)
C_{ijk}	Pitzer specific virial coefficient for triple ion interaction
CEC	cation exchange capacity ($mol\ kg^{-1}$)
D_a, D_w	effective soil matrix diffusion coefficients of CO_2 in the gas and liquid phase, respectively [L^2T^{-1}]
D_{as}, D_{ws}	diffusion coefficients of CO_2 in the gas and liquid phase, respectively [L^2T^{-1}]
D_E	effective dispersion coefficient in the soil matrix [L^2T^{-1}]
EC	electric conductivity of the solution ($dS\ m^{-1}$)
ESP	exchangeable sodium percentage
ESP*	adjusted exchangeable sodium percentage
f_{mont}	weight fraction of montmorillonite in soil [-]
f_p, f_s	reduction functions for CO_2 production by plant roots and by soil microorganisms, respectively [-]

h_1, h_3 pressure head when CO_2 production ceases [L]

h_2 pressure head when CO_2 production is optimal [L]

I ionic strength (mol kg^{-1})

IAP^C ion activity product for calcite [-]

IAP^G ion activity product for gypsum [-]

J_{ca}, J_{cw} CO_2 fluxes caused by convection in the gas and liquid phase, respectively [LT^{-1}]

J_{da}, J_{dw} CO_2 fluxes caused by diffusion in the gas and liquid phase, respectively [LT^{-1}]

k_{a1} first dissociation constant of carbonic acid [-]

k_{a2} second dissociation constant of carbonic acid [-]

k_x multiplication factor

K_{CO2} Henry's Law constant [MT^{2}M^{-1}L^{-2}]

K_M, K_M^* Michaelis' constants for O_2 and CO_2 concentrations, respectively [L^{3}L^{-3}]

K_{SP}^C solubility product for calcite [-]

K_{SP}^G solubility product for gypsum [-]

K_{SP}^H solubility product for hydromagnesite [-]

K_{SP}^N solubility product for nesquehonite [-]

K_{SP}^S solubility product for freshly precipitated sepiolite [-]

K_W dissociation constant for water [-]

$K_1,..K_{12}$ equilibrium constants for complexation reactions [-]

$K_{13},..K_{15}$ selectivity constants for cation exchange reactions [-]

m_i molality (mol kg^{-1})

m^0 unit molality (1 mol kg^{-1})

M number of species in the solution mixture [-]

M_{CO} total amount of CO_2 in the entire flow domain [L]

M_l amount of solute in the liquid phase in the flow region at time t [ML^{-2}]

M_p amount of solute in the precipitated phase in the flow region at time t [ML^{-2}]

M_s amount of solute in the sorbed phase in the flow region at time t [ML^{-2}]

M_S molar weight (mol^{-1})

P production/sink term for CO_2 [L^{3}L^{-3}T^{-1}]

P_{CO2} partial pressure of CO_2 [ML^{-1}T^{-2}] (atm)

P_T actual CO_2 production rate $[L^3L^{-2}T^{-1}]$

P_φ osmotic pressure of electrolyte solution $[ML^{-1}T^{-2}]$ (Pa)

pH   negative logarithm of hydrogen activity [-]

pIAP   negative logarithm of the ion activity product [-]

q oxygen uptake rate $[L^3L^{-3}T^{-1}]$

q_a, q_w soil air and soil water fluxes, respectively $[LT^{-1}]$

q_E CO_2 effective velocity $[LT^{-1}]$

q_{E0} prescribed CO_2 effective boundary flux $[LT^{-1}]$

q_{max} maximum oxygen uptake rate $[L^3L^{-3}T^{-1}]$

r scaling factor which represents the effect of solution composition (SAR, C_0, pH) on the hydraulic conductivity [-]

r_1 scaling factor which represents the effect of solution composition (SAR, C_0) on the hydraulic conductivity [-]

r_2 scaling factor which represents the effect of solution pH on the hydraulic conductivity [-]

R universal gas constant $[ML^2T^{-2}K^{-1}M^{-1}]$

R^C calcite dissolution-precipitation rate (mmol cm^{-2}s^{-1})

R^D dolomite dissolution rate (mmol cm^{-2}s^{-1})

s surface species concentration [-]

S^* CO_2 uptake rate associated with root water uptake $[T^{-1}]$

SAR   sodium adsorption ratio (mmol$^{0.5}$l$^{-0.5}$)

W molecular weight of water

x swelling factor [-]

γ_i activity coefficient of the ith solute ion [-]

γ_i^{DH} modified Debye-Hückel activity coefficient of the ith solute ion [-]

γ_p, γ_s actual CO_2 production rate of plant roots and soil microorganisms, respectively $[L^3L^{-3}T^{-1}]$

γ_{p0}, γ_{s0} optimal CO_2 production rate of plant roots and soil microorganisms (20°C), respectively $[L^3L^{-2}T^{-1}]$

GENERAL INTRODUCTION AND OVERVIEW OF HYDRUS-1D

The importance of the unsaturated zone as an integral part of the hydrological cycle has long been recognized. The vadose zone plays an inextricable role in many aspects of hydrology, including infiltration, soil moisture storage, evaporation, plant water uptake, groundwater recharge, runoff and erosion. Initial studies of the unsaturated (vadose) zone focused primarily on water supply studies, inspired in part by attempts to optimally manage the root zone of agricultural soils for maximum crop production. Interest in the unsaturated zone has dramatically increased in recent years because of growing concern that the quality of the subsurface environment is being adversely affected by agricultural, industrial and municipal activities. Federal, state and local action and planning agencies, as well as the public at large, are now scrutinizing the intentional or accidental release of surface-applied and soil-incorporated chemicals into the environment. Fertilizers and pesticides applied to agricultural lands inevitably move below the soil root zone and may contaminate underlying groundwater reservoirs. Chemicals migrating from municipal and industrial disposal sites also represent environmental hazards. The same is true for radionuclides emanating from energy waste disposal facilities.

The past several decades has seen considerable progress in the conceptual understanding and mathematical description of water flow and solute transport processes in the unsaturated zone. A variety of analytical and numerical models are now available to predict water and/or solute transfer processes between the soil surface and the groundwater table. The most popular models remain the Richards equation for variably saturated flow, and the Fickian-based convection-dispersion equation for solute transport. Deterministic solutions of these classical equations have been used, and likely will continue to be used in the near future, for predicting water and solute movement in the vadose zone, and for analyzing specific laboratory or field experiments involving unsaturated water flow and/or solute transport. Models of this type are also helpful tools for extrapolating information from a limited number of field experiments to different soil, crop and climatic conditions, as well as to different tillage and water management schemes.

Once released into the subsurface environment, industrial and agricultural chemicals are generally subjected to a large number of simultaneous physical, chemical, and biological processes, including sorption-desorption, volatilization, photolysis, and biodegradation, as well as their kinetics. The extent of degradation, sorption and volatilization largely determines the persistence of a pollutant in the subsurface [*Chiou*, 1989]. For example, the fate of organic

chemicals in soils is known to be strongly affected by the kinetics of biological degradation. *Alexander and Scow* [1989] gave a review of some of the equations used to represent the kinetics of biodegradation. These equations include zero-order, half-order, first-order, three-half-order, mixed-order, logistic, logarithmic, Michaelis-Menton, and Monod type (with or without growth) expressions. While most of these expressions have a theoretical basis, they are commonly used only in an empirical fashion by fitting the equations to observed data. Zero- and first-order kinetic equations remain the most popular for describing biodegradation of organic compounds, mostly because of their simplicity and the ease at which they can be incorporated in solute transport models. Conditions for the application of these two equations are described by *Alexander and Scow* [1989].

One special group of degradation reactions involves decay chains in which solutes are subject to sequential (or consecutive) decay reactions. Problems of solute transport involving sequential first-order decay reactions frequently occur in soil and groundwater systems. Examples are the migration of various radionuclides [*Lester et al.*, 1975; *Rogers,* 1978; *Gureghian*, 1981; *Gureghian and Jansen*, 1983], the simultaneous movement of interacting nitrogen species [*Cho*, 1971; *Misra et al.*, 1974; *Wagenet et al.*, 1976; *Tillotson et al.*, 1980], organic phosphate transport [*Castro and Rolston*, 1977], the transport of certain pesticides and their metabolites [*Bromilow and Leistra,* 1980; *Wagenet and Hutson*, 1987], the transport of sequential biodegradation of chlorinated hydrocarbons [e.g., *Schaerlaekens et al.*, 1999; *Casey and Šimůnek*, 2001], and the transport of various hormones such as estrogen and testosterone [e.g., *Casey et al.*, 2003, 2004].

While in the past most pesticides were regarded as involatile, volatilization is now increasingly recognized as being an important process affecting the fate of pesticides in field soils [*Glotfelty and Schomburg*, 1989; *Spencer*, 1991]. Another process affecting pesticide fate and transport is the relative reactivity of solutes in the sorbed and solution phases. Several processes such as gaseous and liquid phase molecular diffusion, and convective-dispersive transport, act only on solutes that are not adsorbed. Degradation of organic compounds likely occurs mainly, or even exclusively, in the liquid phase [*Pignatello*, 1989]. On the other side, radioactive decay takes place equally in the solution and adsorbed phases, while other reactions or transformations may occur only or primarily in the sorbed phase.

Several analytical solutions have been published for simplified transport systems involving consecutive decay reactions [*Cho*, 1971; *Wagenet et al.*, 1976; *Harada et al.*, 1980; *Higashi and Pigford,* 1980; *van Genuchten*, 1985]. Unfortunately, analytical solutions for more

complex situations, such as for transient water flow or the nonequilibrium solute transport with nonlinear reactions, are not available and/or cannot be derived, in which case numerical models must be employed. To be useful, such numerical models must allow for different reaction rates to take place in the solid, liquid, and gaseous phases, as well as for a correct distribution of the solutes among the different phases.

The processes of evaporation and plant transpiration also exert a major influence on water and solute distributions in near-surface environments. These processes concentrate salts by decreasing the amount of water in the soil, and when combined with irrigation in arid regions can lead to highly saline conditions. Ion activities for such chemical conditions should be calculated with expressions suitable for use in brines, rather than with the more standard formulations for dilute solutions. The interaction of evapotranspiration, changing soil gas composition, ion exchange and soil-water reactions may cause precipitation and dissolution of a variety of minerals. Major ions (mainly of Ca^{2+}, Mg^{2+}, Na^+, K^+, Cl^-, SO_4^{2-}, HCO_3^-, CO_3^{2-}, and NO_3^-) may accumulate in certain parts of the soil profile in such amounts that crop yield can be seriously reduced. Hence, models used to predict the solution chemistry of major ions in the unsaturated zone should include all of these processes and variables [*Šimůnek et al.*, 1987].

The purpose of this report is to document the HYDRUS-1D software package for simulating one-dimensional variably saturated water flow, heat movement, and the transport of solutes involved in sequential first-order decay reactions. To be able to simulate the salinization processes described in the previous paragraph, we also implemented into the HYDRUS software the carbon dioxide transport and production, and major ion chemistry modules originally developed for the UNSATCHEM program [*Šimůnek et al.*, 1996]. HYDRUS-1D consists of the HYDRUS computer program, and the HYDRUS1D interactive graphics-based user interface. The HYDRUS program numerically solves the Richards equation for saturated-unsaturated water flow and advection-dispersion type equations for heat and solute transport. The water flow equation incorporates a sink term to account for water uptake by plant roots. The flow equation may also consider dual-porosity type flow in which one fraction of water content is mobile and another fraction immobile, or dual-permeability type flow involving two mobile regions, one representing the matrix and one the macropores. The heat transport equation considers movement by conduction as well as convection with flowing water. Coupled water, vapor, and energy transport can be considered as well. The governing advection-dispersion solute transport equations are written in a very general form by including provisions for nonlinear nonequilibrium reactions between the solid and liquid phases, and linear equilibrium reaction

between the liquid and gaseous phases. Hence, both adsorbed and volatile solutes such as pesticides can be considered. The solute transport equations also incorporate the effects of zero-order production, first-order degradation independent of other solutes, and first-order production/decay reactions that provide the required coupling between the solutes involved in the sequential first-order decay chain. The transport models also account for advection and dispersion in the liquid phase, as well as for diffusion in the gas phase, thus permitting one to simulate solute transport simultaneously in both the liquid and gaseous phases. HYDRUS-1D at present considers up to five solutes, which can be either coupled in a unidirectional chain or may move independently of each other. Physical nonequilibrium solute transport can be accounted for by assuming a two-region, dual-porosity type formulation which partition the liquid phase into separate mobile and immobile regions. Additionally, the transport equations may include provisions for kinetic attachment/detachment of solutes to the solid phase, thus permitting simulations of the transport of viruses, colloids, or bacteria.

The HYDRUS software package also includes modules for simulating carbon dioxide and major ion solute movement. Diffusion in both liquid and gas phases and convection in the liquid phase are considered as CO_2 transport mechanisms. The CO_2 production model is described. The major variables of the chemical system are Ca, Mg, Na, K, SO_4, Cl, NO_3, H_4SiO_4, alkalinity, and CO_2. The model accounts for equilibrium chemical reactions between these components such as complexation, cation exchange and precipitation-dissolution. For the precipitation-dissolution of calcite and dissolution of dolomite, either equilibrium or multicomponent kinetic expressions are used which include both forward and back reactions. Other dissolution-precipitation reactions considered include gypsum, hydromagnesite, nesquehonite, and sepiolite. Since the ionic strength of soil solutions can vary considerably with time and space and often reach high values, both modified Debye-Hückel and Pitzer expressions were incorporated into the model as options to calculate single ion activities.

The HYDRUS-1D code may be used to analyze water and solute movement in unsaturated, partially saturated, or fully saturated porous media. The flow region itself may be composed of nonuniform soils. Flow and transport can occur in the vertical, horizontal, or in a generally inclined direction. The water flow part of the model considers prescribed head and flux boundaries, as well as boundaries controlled by atmospheric conditions, free drainage, or flow to horizontal drains. First and third-type boundary conditions can be implemented in both the solute and heat transport parts of the model. In addition, HYDRUS-1D implements a Marquardt-Levenberg type parameter estimation technique for inverse estimation of soil hydraulic and/or

solute transport and reaction parameters from measured transient or steady-state flow and/or transport data.

The governing flow and transport equations are solved numerically using standard Galerkin-type linear finite element schemes, or modification thereof. The program is a one-dimensional version of the HYDRUS-2D and HYDRUS (2D/3D) codes simulating water, heat and solute movement in two- or three-dimensional variably saturated media [*Šimůnek et al.*, 1999; 2006a,b], while incorporating various features of earlier related codes such as SUMATRA [*van Genuchten*, 1978], WORM [*van Genuchten*, 1987], HYDRUS 3.0 [*Kool and van Genuchten*, 1991], SWMI [*Vogel*, 1990], SWMI_ST [*Šimůnek*, 1993], HYDRUS 5.0 [*Vogel et al.*, 1996], and HYDRUS-1D, version 3.0 [*Šimůnek et al.*, 2005]. The method of incorporating hysteresis in the soil hydraulic properties, as well as several other features, was adopted from HYDRUS 5.0 [*Vogel et al.*, 1996]. Carbon dioxide transport and major ion chemistry modules were adopted from the UNSATCHEM program [*Šimůnek et al.*, 1996]. The text in this manual draws heavily upon texts in the early versions of these various programs. The source code was developed and tested on a Pentium 4 PC using the Microsoft's Fortran PowerStation compiler. Several extensions of the MS Fortran beyond the ANSI standard were used to enable communication with graphic based user-friendly interface. New main features of the version 3.0, compared to version 2.0, were a) new analytical models for the soil hydraulic properties, b) compensated root water uptake, c) the dual-porosity features for water flow, d) the attachment/detachment models for solute transport to allow simulations of the virus, colloid, and bacteria transport, and e) the carbon dioxide and f) major ion chemistry modules. Major new features of the current version 4.0, compared to version 3.0, are consideration of a) vapor flow, b) coupled water, vapor, and energy transport, c) dual-permeability type water flow and solute transport, d) dual-porosity water flow with solute transport considering two-site sorption in the mobile zone, e) potential evapotranspiration as calculated with the Penman-Monteith combination and Hargreaves equations, f) daily variations in evaporation, transpiration, and precipitation, and g) support for the HP1 code [*Jacques and Šimůnek*, 2005; *Šimůnek et al.*, 2006c; *Jacques et al.*, 2007], obtained by coupling HYDRUS with the PHREEQC biogechemical code [*Parkhurst and Appelo*, 1999].

One major problem which often prevents the widespread use of otherwise well-documented numerical computer codes is the extensive work generally required for input data preparation, finite element grid design, and graphical presentation of the output results. Hence, techniques are needed which make it easier to create, manipulate and display large data files, and

which facilitate interactive data management. Such techniques will free users from cumbersome manual data processing, and should enhance the efficiency in which programs are being implemented for a particular problem. To avoid or simplify the preparation and management of relatively complex input data files for flow problems, and to graphically display the final simulation results, we developed the HYDRUS1D interactive graphics-based user-friendly interface for the MS Windows environment. The HYDRUS1D interface is directly connected to the HYDRUS computational programs. The software package is distributed on a CD-ROM containing all necessary files needed to run the interface, the input and output files of various examples discussed in this report and several other examples. The software package can also be freely downloaded from www.hydrus2d.com (orm www.pc-progress.cz).

A general overview of the HYDRUS1D graphics-based interface is described in Part B of this manual. We note that in addition to the detailed descriptions in this section, extensive on-line help files are also available in each module of the user interface.

PART A

The HYDRUS Code for Simulating the One-Dimensional

Movement of Water, Heat, and Multiple Solutes

in Variably-Saturated Porous Media

by

J. Šimůnek and M. Th. van Genuchten

1. INTRODUCTION

This part of the manual gives a detailed description of the HYDRUS computer code, which numerically solves the Richards equation for variably-saturated water flow and advection-dispersion type equations for heat and solute transport. The flow equation incorporates a sink term to account for water uptake by plant roots. The flow equation may also consider dual-porosity type flow in which one fraction of the water content is mobile and another fraction immobile, or dual-permeability type flow involving two mobile regions, one representing the matrix and one the macropores. The heat transport equation considers transport due to conduction and convection with flowing water. Coupled water, vapor, and energy transport can be considered as well. The solute transport equations consider advective-dispersive transport in the liquid phase, as well as diffusion in the gaseous phase. The transport equations also include provisions for nonlinear nonequilibrium reactions between the solid and liquid phases, linear equilibrium reactions between the liquid and gaseous phases, zero-order production, and two first-order degradation reactions: one which is independent of other solutes, and one which provides the coupling between solutes involved in sequential first-order decay reactions. Physical nonequilibrium solute transport can be accounted for by assuming a two-region, dual-porosity type formulation which partitions the liquid phase into separate mobile and immobile regions. Additionally, the transport equations may include provisions for kinetic attachment/detachment of solutes to the solid phase, thus permitting simulations of the transport of viruses, colloids, or bacteria.

The program may be used to analyze water and solute movement in unsaturated, partially saturated, or fully saturated porous media. The flow region may be composed of nonuniform soils. Flow and transport can occur in the vertical, horizontal, or a generally inclined direction. The water flow part of the model can deal with prescribed head and flux boundaries, boundaries controlled by atmospheric conditions, as well as free drainage boundary conditions. The governing flow and transport equations are solved numerically using Galerkin-type linear finite element schemes. HYDRUS-1D also includes a Marquardt-Levenberg type parameter optimization algorithm for inverse estimation of soil hydraulic and/or solute transport and reaction parameters from measured transient or steady-state flow and/or transport data.

HYDRUS-1D further incorporates modules simulating carbon dioxide production and major ion solute movement. The CO_2 transport processes include diffusion in both the liquid and gas phases and advection in the liquid phase. The CO_2 production model is described in detail. The major variables of the chemical system are Ca, Mg, Na, K, SO_4, Cl, NO_3, H_4SiO_4, alkalinity,

and CO_2. The model accounts for equilibrium chemical reactions between these components such as complexation, cation exchange and precipitation-dissolution. For the precipitation-dissolution of calcite and dissolution of dolomite, either equilibrium or multicomponent kinetic expressions are used which include both forward and back reactions. Other dissolution-precipitation reactions considered include gypsum, hydromagnesite, nesquehonite, and sepiolite. Since the ionic strength of soil solutions can vary considerably with time and space and often reach high values, both modified Debye-Hückel and Pitzer expressions were incorporated into the model as options to calculate single ion activities.

2. VARIABLY SATURATED WATER FLOW

2.1. *Governing Water Flow Equations*

2.1.1. *Uniform Water Flow*

One-dimensional uniform (equilibrium) water movement in a partially saturated rigid porous medium (Fig. 2.1a) is described by a modified form of the Richards equation using the assumptions that the air phase plays an insignificant role in the liquid flow process and that water flow due to thermal gradients can be neglected:

$$\frac{\partial \theta}{\partial t} = \frac{\partial}{\partial x}\left[K\left(\frac{\partial h}{\partial x} + \cos \alpha\right)\right] - S \tag{2.1}$$

where h is the water pressure head [L], θ is the volumetric water content [L^3L^{-3}], t is time [T], x is the spatial coordinate [L] (positive upward), S is the sink term [$L^3L^{-3}T^{-1}$], α is the angle between the flow direction and the vertical axis (i.e., $\alpha = 0^0$ for vertical flow, 90^0 for horizontal flow, and $0^0 < \alpha < 90^0$ for inclined flow), and K is the unsaturated hydraulic conductivity function [LT^{-1}] given by

$$K(h,x) = K_s(x)K_r(h,x) \tag{2.2}$$

where K_r is the relative hydraulic conductivity [-] and K_s the saturated hydraulic conductivity [LT^{-1}].

2.1.2. *Uniform Water Flow and Vapor Transport*

The Richards equation (2.1) considers only water flow in the liquid phase and ignores the effects of the vapor phase on the overall water mass balance. While this assumption is justified for the majority of applications, a number of problems exist in which the effect of vapor flow can not be neglected. Vapor movement is often an important part of the total water flux when the soil is relatively dry. *Scanlon et al.* [2003] showed that water fluxes in deep vadose zone profiles of

11

the arid and semiarid regions of the western U.S. are often dominated by thermal vapor fluxes. Nonisothermal liquid and vapor flow in HYDRUS is described as follows (e.g., *Saito et al.* [2006]):

$$\frac{\partial \theta_T(h)}{\partial t} = \frac{\partial}{\partial x}\left[\left(K + K_{vh}\right)\left(\frac{\partial h}{\partial x} + \cos\alpha\right) + \left(K_{LT} + K_{vT}\right)\frac{\partial T}{\partial x}\right] - S(h) \qquad (2.3)$$

where θ_T is the total volumetric water content [L^3L^{-3}], being the sum ($\theta_T = \theta + \theta_v$) of the volumetric liquid water content, θ, and the volumetric water vapor content, θ_v (both expressed in terms of equivalent water contents) [L^3L^{-3}]; T is temperature [K]; K is the isothermal hydraulic conductivity of the liquid phase [LT^{-1}]; K_{LT} is the thermal hydraulic conductivity of the liquid phase [$L^2K^{-1}T^{-1}$]; K_{vh} is the isothermal vapor hydraulic conductivity [LT^{-1}]; and K_{vT} is the thermal vapor hydraulic conductivity [$L^2K^{-1}T^{-1}$]. Overall water flow in (2.3) is given as the sum of isothermal liquid flow, isothermal vapor flow, gravitational liquid flow, thermal liquid flow, and thermal vapor flow. Since several terms of (2.3) are a function of temperature, this equation should be solved simultaneously with the heat transport equation (4.5) to properly account for temporal and spatial changes in soil temperature.

2.1.3. *Flow in a Dual-Porosity System*

Dual-porosity models assume that water flow is restricted to the fractures (or inter-aggregate pores and macropores), and that water in the matrix (the intra-aggregate pores or the rock matrix) does not move at all (Fig. 2.1bc). These models assume that the matrix, consisting of immobile water pockets, can exchange, retain, and store water, but does not permit convective flow. This conceptualization leads to two-region, dual-porosity type flow and transport models [*Philip*, 1968; *van Genuchten and Wierenga*, 1976] that partition the liquid phase into mobile (flowing, inter-aggregate), θ_{mo}, and immobile (stagnant, intra-aggregate), θ_{im}, regions:

$$\theta = \theta_{mo} + \theta_{im} \qquad (2.4)$$

with some exchange of water and/or solutes possible between the two regions, usually calculated by means of a first-order rate equation. We will use here the subscript m to represent fractures, inter-aggregate pores, or macropores, and the subscript im to represent the soil matrix, intra-

aggregate pores, or the rock matrix.

The dual-porosity formulation for water flow as used in HYDRUS-1D is based on a mixed formulation, which uses Richards equation (2.1) to describe water flow in the fractures (macropores), and a simple mass balance equation to describe moisture dynamics in the matrix as follows [*Šimůnek et al.*, 2003]:

$$\frac{\partial \theta_{mo}}{\partial t} = \frac{\partial}{\partial x}\left[K(h)\left(\frac{\partial h}{\partial x} + \cos\alpha\right)\right] - S_{mo} - \Gamma_w$$

$$\frac{\partial \theta_{im}}{\partial t} = \qquad\qquad\qquad - S_{im} + \Gamma_w$$

(2.5)

where S_m and S_{im} are sink terms for both regions, and Γ_w is the transfer rate for water from the inter- to the intra-aggregate pores.

An alternative dual-porosity approach, not implemented in HYDRUS-1D, was suggested by *Germann* [1985] and *Germann and Beven* [1985], who used a kinematic wave equation to describe gravitational movement of water in macropores. Although dual-porosity models have been popularly used for solute transport studies (e.g. *van Genuchten* [1981]), they have thus far not been used extensively for water flow problems.

2.1.4. *Flow in a Dual-Permeability System*

While dual-porosity models assume that water in the matrix is stagnant, dual-permeability models (Fig. 2.1de) allow for water flow in the matrix as well. The approach of *Gerke and van Genuchten* [1993a, 1996], who applied Richards equations to each of two pore regions is implemented in HYDRUS-1D. The flow equations for the macropore or fracture (subscript *f*) and matrix (subscript *m*) pore systems in this approach are given by:

$$\frac{\partial \theta_f(h_f)}{\partial t} = \frac{\partial}{\partial x}\left[K_f(h_f)\left(\frac{\partial h_f}{\partial x} + + \cos\alpha\right)\right] - S_f(h_f) - \frac{\Gamma_w}{w}$$

$$\frac{\partial \theta_m(h_m)}{\partial t} = \frac{\partial}{\partial x}\left[K_m(h_m)\left(\frac{\partial h_m}{\partial x} + + \cos\alpha\right)\right] - S_m(h_m) + \frac{\Gamma_w}{1-w}$$

(2.6)

13

Equilibrium Model -------------------------------------Non-Equilibrium Models --------------------------------------

a. Uniform Flow   b. Mobile-Immobile Water   c. Dual-Porosity   d. Dual-Permeability e. Dual-Permeability with MIM

$$\theta$$
$$S = \theta c$$

$$\theta = \theta_{im} + \theta_{mo}$$
$$S = \theta_{im} c_{im} + \theta_{mo} c_{mo}$$

$$\theta = \theta_{im} + \theta_{mo}$$
$$S = \theta_{im} c_{im} + \theta_{mo} c_{mo}$$

$$\theta = \theta_{M} + \theta_{F}$$
$$S = \theta_{M} c_{m} + \theta_{F} c_{f}$$

$$\theta = \theta_{M,im} + \theta_{M,mo} + \theta_{F}$$
$$S = \theta_{M,im} c_{M,im} + \theta_{M,mo} c_{M,mo} + \theta_{F} c_{f}$$
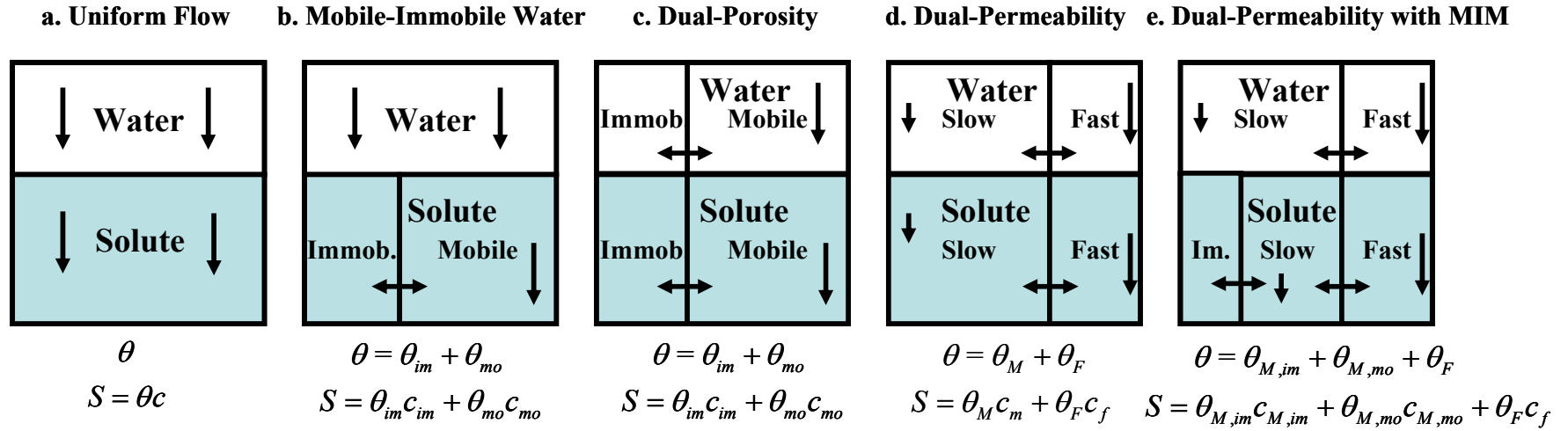
Figure 2.1.   Conceptual physical nonequilibrium models for water flow and solute transport. In the plots, θ is the water content, θ_{mo} and θ_{im} in (b) and (c) are water contents of the mobile and immobile flow regions, respectively; θ_{M} and θ_{F} in (d) are water contents of the matrix and macropore (fracture) regions, respectively, and $\theta_{M,mo}$, $\theta_{M,im}$, and θ_{F} in (e) are water contents of the mobile and immobile flow regions of the matrix domain, and of the macropore (fracture) domain, respectively; c are concentrations of corresponding regions, with subscripts having the same meaning as for water contents, while S is the total solute content of the liquid phase.

respectively, where w is the ratio of the volumes of the macropore or fracture domain and the total soil system [-]. Note that the water contents θ_f and θ_m in (2.6) have different meanings than those in (2.5) where they represented water contents of the total pore space (i.e., $\theta = \theta_{mo} + \theta_{im}$), while in (2.6) they refer to water contents of the two separate (fracture or matrix) pore domains such that $\theta = w\theta_f + (1-w)\theta_m (= \theta_F + \theta_M$, where θ_M and θ_F are absolute water contents in the matrix and macropore (fracture) regions, respectively).

2.2. *Root Water Uptake*

2.2.1. *Root Water Uptake Without Compensation*

The sink term, S, is defined as the volume of water removed from a unit volume of soil per unit time due to plant water uptake. *Feddes et al.* [1978] defined S as

$$S(h) = \alpha(h)S_p \tag{2.7}$$

where the root-water uptake water stress response function $\alpha(h)$ is a prescribed dimensionless function (Fig. 2.1) of the soil water pressure head ($0 \le \alpha \le 1$), and S_p the potential water uptake rate [T^{-1}]. Figure 2.1 gives a schematic of the stress response function as used by *Feddes et al.* [1978]. Notice that water uptake is assumed to be zero close to saturation (i.e., wetter than some arbitrary "anaerobiosis point", h_1). For $h < h_4$ (the wilting point pressure head), water uptake is also assumed to be zero. Water uptake is considered optimal between pressure heads h_2 and h_3, whereas for pressure head between h_3 and h_4 (or h_1 and h_2), water uptake decreases (or increases) linearly with h. The variable S_p in (2.7) is equal to the water uptake rate during periods of no water stress when $\alpha(h)=1$.

Van Genuchten [1987] expanded formulation of *Feddes et al.* [1978] by including osmotic stress as follows

$$S(h,h_\phi) = \alpha(h,h_\phi)S_p \tag{2.8}$$

where h_ϕ is the osmotic head [L], which is assumed here to be given by a linear combination of the concentrations, c_i, of all solutes present, i.e.,

$$h_\phi = a_i c_i \qquad (2.9)$$

in which a_i are experimental coefficients [L^{4}M] converting concentrations into osmotic heads. *van Genuchten* [1987] proposed an alternative S-shaped function to describe the water uptake stress response function (Fig. 2.1), and suggested that the influence of the osmotic head reduction can be either additive or multiplicative as follows

$$\alpha(h, h_\phi) = \frac{1}{1 + \left(\dfrac{h + h_\phi}{h_{50}}\right)^p} \qquad (2.10)$$

or

$$\alpha(h, h_\phi) = \frac{1}{1 + (h/h_{50})^{p_1}} \frac{1}{1 + (h_\phi/h_{\phi 50})^{p_2}} \qquad (2.11)$$

respectively, where p, p_1, and p_2 are experimental constants. The exponent p was found to be approximately 3 when applied to salinity stress data only [*van Genuchten*, 1987]. The parameter h_{50} in (2.10) and (2.11) represents the pressure head at which the water extraction rate is reduced by 50% during conditions of negligible osmotic stress. Similarly, $h_{\phi 50}$ represents the osmotic head at which the water extraction rate is reduced by 50% during conditions of negligible water stress. Note that, in contrast to the expression of *Feddes et al.* [1978], this formulation of the stress response function, $\alpha(h, h_\phi)$, does not consider the transpiration reduction near saturation. This simplification seems justified when saturated or near-saturated conditions occur for only relatively short periods of time.

When the potential water uptake rate is equally distributed over the root zone, S_p becomes

$$S_p = \frac{1}{L_R} T_p \qquad (2.12)$$

where T_p is the potential transpiration rate $[LT^{-1}]$ and L_R the depth $[L]$ of the root zone. Equation (2.12) may be generalized by introducing a non-uniform distribution of the potential water uptake rate over a root zone of arbitrary shape:

$$S_p = b(x)T_p \qquad (2.13)$$
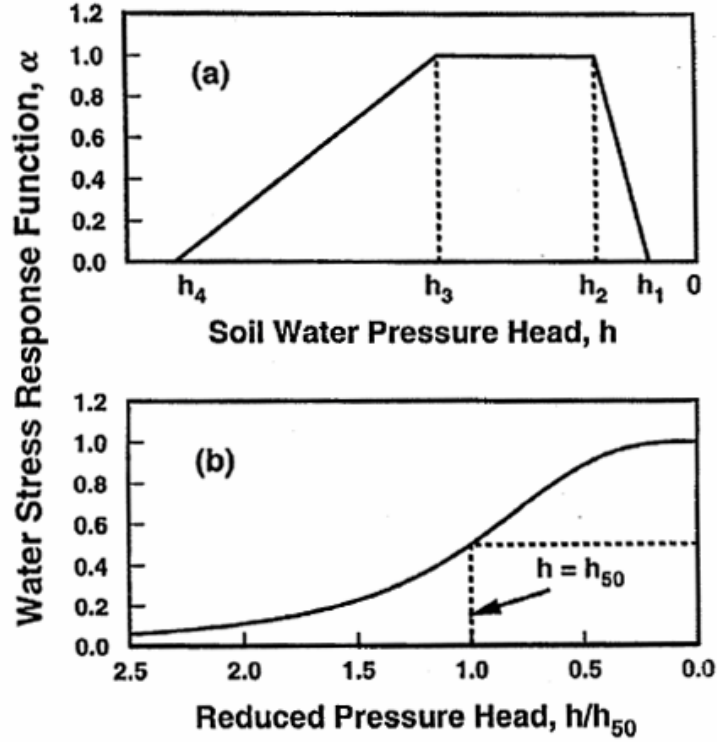
Fig. 2.2. Schematic of the plant water stress response function, $\alpha(h)$, as used by a) *Feddes et al.* [1978] and b) *van Genuchten* [1987].

where $b(x)$ is the normalized water uptake distribution $[L^{-1}]$. This function describes the spatial variation of the potential extraction term, S_p, over the root zone (Fig. 2.2), and is obtained by normalizing any arbitrarily measured or prescribed root distribution function, $bN(x)$, as follows

$$b(x) = \frac{b'(x)}{\int_{L_R} b'(x)\,dx} \qquad (2.14)$$

17

where L_R is the region occupied by the root zone. Normalizing the uptake distribution ensures that $b(x)$ integrates to unity over the flow domain, i.e.,

$$\int_{L_R} b(x)dx = 1 \qquad\qquad (2.15)$$
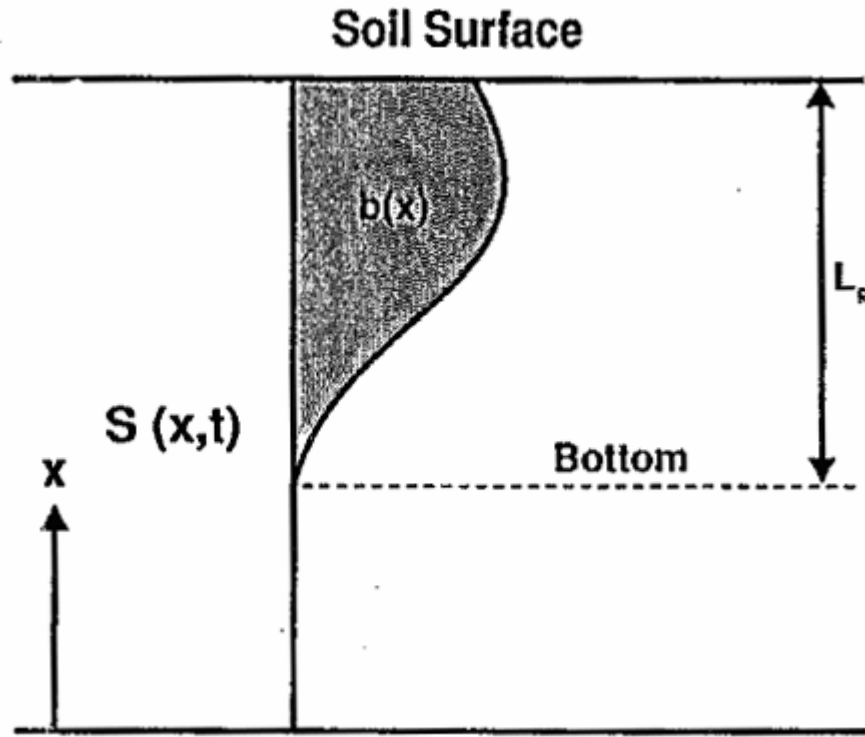
Fig. 2.3. Schematic of the potential water uptake distribution function, $b(x)$, in the soil root zone.

There are many ways to express the function $b(x)$: constant with depth, linear [*Feddes et al.*, 1978], or the following function [*Hoffman and van Genuchten*, 1983]:

$$b(x) = \begin{cases} \dfrac{1.66667}{L_R} & x > L - 0.2L_R \\[2ex] \dfrac{2.0833}{L_R}\left(1 - \dfrac{x_0 - x}{L_R}\right) & x \in \left(L - L_R; L - 0.2L_R\right) \\[2ex] 0 & x < L - L_R \end{cases} \tag{2.16}$$

where L is the x-coordinate of the soil surface [L] and L_R is the root depth [L]. HYDRUS allows a user to prescribe virtually any shape of the water uptake distribution function, provided that this function is constant during the simulation. When the rooting depth varies in time (as described later), only the exponential function is allowed. Note that in the above development, and throughout this manual, the bottom of the soil profile is located at $x = 0$ and the soil surface at $x = L$.

From (2.13) and (2.15) it follows that S_p is related to T_p by the expression

$$\int_{L_R} S_p dx = T_p \tag{2.17}$$

The actual water uptake distribution is obtained by substituting (2.13) into (2.7):

$$S(h, h_\phi, x) = \alpha(h, h_\phi, x)\, b(x) T_p \tag{2.18}$$

whereas the actual transpiration rate, T_a, is obtained by integrating (2.18) as follows

$$T_a = \int_{L_R} S(h, h_\phi, x)\, dx = T_p \int_{L_R} a(h, h_\phi, x)\, b(x)\, dx \tag{2.19}$$

The root depth, L_R, can be either constant or variable during the simulation. For annual vegetation a growth model is required to simulate the change in rooting depth with time. HYDRUS assumes that the actual root depth is the product of the maximum rooting depth, L_m [L], and a root growth coefficient, $f_r(t)$ [-] [*Šimůnek and Suarez*, 1993a]:

$$L_R(t) = L_m \, f_r(t) \qquad\qquad (2.20)$$

For the root growth coefficient, $f_r(t)$, we use the classical Verhulst-Pearl logistic growth function

$$f_r(t) = \frac{L_0}{L_0 + (L_m - L_0)\, e^{-rt}} \qquad\qquad (2.21)$$

where L_0 is the initial value of the rooting depth at the beginning of the growing season [L], and r the growth rate [T^{-1}]. The growth rate is calculated either from the assumption that 50% of the rooting depth will be reached after 50% of the growing season has elapsed, or from given data.

2.2.2. Root Water Uptake With Compensation

The ratio of actual to potential transpiration of the root uptake without compensation is defined as follows:

$$\frac{T_a}{T_p} = \frac{1}{T_p} \int_{L_R} S dx = \int_{L_R} \alpha(h, h_\phi, x) \, b(x) dx = \omega \qquad\qquad (2.22)$$

where ω is a dimensionless water stress index [*Jarvis*, 1989]. Following *Jarvis* [1989], we introduce a critical value of the water stress index ω_c, a so-called the root adaptability factor, which represents a threshold value above which root water uptake reduced in stressed parts of the root zone is fully compensated by increased uptake from other parts. However, some reduction in potential transpiration will occur below this threshold value, although smaller than for water uptake without compensation.

20
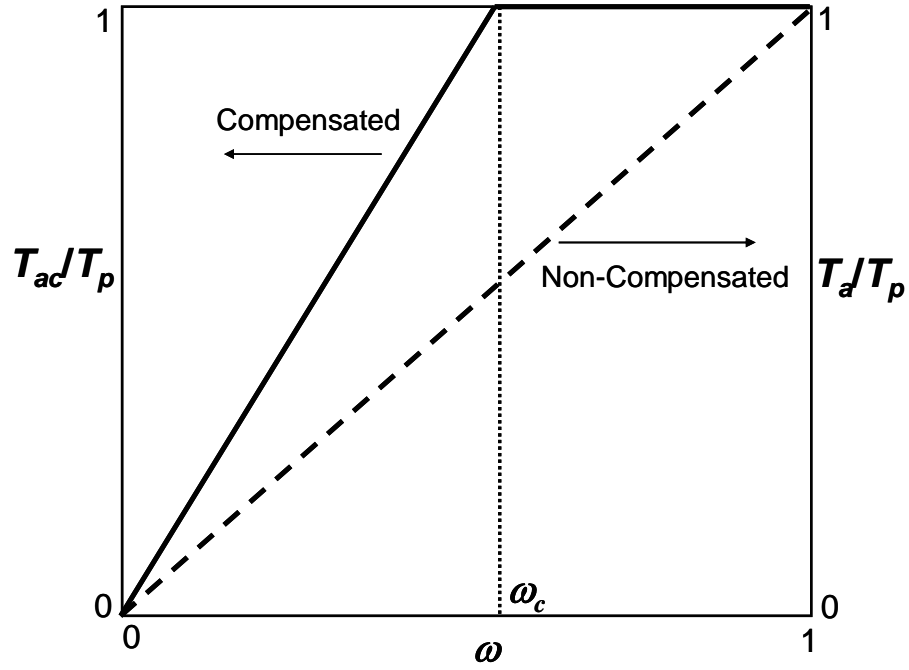
Fig. 2.4. Ratio of actual to potential transpiration as a function of the stress index ω.

Thus, for the interval when ω is larger than the threshold value ω_c (Fig. 2.3), one obtains

$$S(h,h_\phi,x) = \alpha(h,h_\phi,x)b(x)\frac{T_p}{\omega}$$

$$\frac{T_a}{T_p} = \frac{\int_{L_R}\alpha(h,h_\phi,x)b(x)dx}{\omega} = \frac{\omega}{\omega} = 1 \tag{2.23}$$

While for the interval when ω is smaller than the threshold value ω_c, one has

$$S(h,h_\phi,x) = \alpha(h,h_\phi,x)b(x)\frac{T_p}{\omega_c}$$

$$\frac{T_a}{T_p} = \frac{\int_{L_R}\alpha(h,h_\phi,x)b(x)dx}{\omega_c} = \frac{\omega}{\omega_c} < 1 \tag{2.24}$$

When the parameter ω_c is equal to one we hence have noncompensated root water uptake, and

when ω_c is equal to zero we obtain fully compensated uptake.

2.3. *The Unsaturated Soil Hydraulic Properties*

2.3.1. *Uniform Water Flow System*

The unsaturated soil hydraulic properties, $\theta(h)$ and $K(h)$, in (2.1) are in general highly nonlinear functions of the pressure head. HYDRUS permits the use of five different analytical models for the hydraulic properties [*Brooks and Corey*, 1964; *van Genuchten*, 1980; *Vogel and Císlerová*, 1988; *Kosugi*, 1996; and *Durner*, 1994].

The soil water retention, $\theta(h)$, and hydraulic conductivity, $K(h)$, functions according to *Brooks and Corey* [1964] are given by

$$S_e = \begin{cases} |\alpha h|^{-n} & h < -1/\alpha \\ \\ 1 & h \geq -1/\alpha \end{cases} \tag{2.25}$$

$$K = K_s \, S_e^{2/n + l + 2} \tag{2.26}$$

respectively, where S_e is effective saturation:

$$S_e = \frac{\theta - \theta_r}{\theta_s - \theta_r} \tag{2.27}$$

in which θ_r and θ_s denote the residual and saturated water contents, respectively; K_s is the saturated hydraulic conductivity, α is the inverse of the air-entry value (or bubbling pressure), n is a pore-size distribution index, and l is a pore-connectivity parameter assumed to be 2.0 in the original study of *Brooks and Corey* [1964]. The parameters α, n and l in HYDRUS are considered to be empirical coefficients affecting the shape of the hydraulic functions.

HYDRUS also implements the soil-hydraulic functions of *van Genuchten* [1980] who used the statistical pore-size distribution model of *Mualem* [1976] to obtain a predictive equation for the unsaturated hydraulic conductivity function in terms of soil water retention parameters.

The expressions of *van Genuchten* [1980] are given by

$$\theta(h) = \begin{cases} \theta_r + \dfrac{\theta_s - \theta_r}{[1 + |\alpha h|^n]^m} & h < 0 \\[4mm] \theta_s & h \geq 0 \end{cases} \tag{2.28}$$

$$K(h) = K_s S_e^l [1 - (1 - S_e^{1/m})^m]^2 \tag{2.29}$$

where

$$m = 1 - 1/n \ , \quad n > 1 \tag{2.30}$$

The above equations contain five independent parameters: θ_r, θ_s, α, n, and K_s. The pore-connectivity parameter l in the hydraulic conductivity function was estimated [*Mualem*, 1976] to be about 0.5 as an average for many soils.

A third set of hydraulic equations implemented in HYDRUS are those by *Vogel and Císlerová* [1988] who modified the equations of *van Genuchten* [1980] to add flexibility in the description of the hydraulic properties near saturation. The soil water retention, $\theta(h)$, and hydraulic conductivity, $K(h)$, functions of *Vogel and Císlerová* [1988] are given by (Fig. 2.3)

$$\theta(h) = \begin{cases} \theta_a + \dfrac{\theta_m - \theta_a}{(1 + |\alpha h|^n)^m} & h < h_s \\[4mm] \theta_s & h \geq h_s \end{cases} \tag{2.31}$$

and

$$K(h) = \begin{cases} K_s\, K_r(h) & h \le h_k \\[2mm] K_k + \dfrac{(h - h_k)(K_s - K_k)}{h_s - h_k} & h_k < h < h_s \\[2mm] K_s & h \ge h_s \end{cases} \qquad (2.32)$$

respectively, where

$$K_r = \frac{K_k}{K_s}\left(\frac{S_e}{S_{ek}}\right)\left[\frac{F(\theta_r) - F(\theta)}{F(\theta_r) - F(\theta_{kr})}\right]^2 \qquad (2.33)$$

$$F(\theta) = \left[1 - \left(\frac{\theta - \theta_a}{\theta_m - \theta_a}\right)^{1/m}\right]^m \qquad (2.34)$$

$$S_{ek} = \frac{\theta_k - \theta_r}{\theta_s - \theta_r} \qquad (2.35)$$

The above equations allow for a non-zero minimum capillary height, h_s, by replacing the parameter θ_s in van Genuchten's retention function by a fictitious (extrapolated) parameter θ_m slightly larger than θ_s as shown in Fig. 2.4. While this change from θ_s to θ_m has little or no effect on the retention curve, the effect on the shape and value of the hydraulic conductivity function can be considerable, especially for fine-textured soils when n is relatively small (e.g., $1.0 < n < 1.3$). To increase the flexibility of the analytical expressions, the parameter θ_r in the retention function was replaced by the fictitious (extrapolated) parameter $\theta_a \le \theta_r$. The approach maintains the physical meaning of θ_r and θ_s as measurable quantities. Equation (2.33) assumes that the predicted hydraulic conductivity function is matched to a measured value of the hydraulic conductivity, $K_k = K(\theta_k)$, at some water content, θ_k, less that or equal to the saturated water content, i.e., $\theta_k \le \theta_s$ and $K_k \le K_s$ [*Vogel and Císlerová*, 1988; *Luckner et al.*, 1989]. Inspection of (2.31) through (2.34) shows that the hydraulic characteristics contain 9 unknown parameters: θ_r, θ_s, θ_a, θ_m, α, n, K_s, K_k, and θ_k. When $\theta_a = \theta_r$, $\theta_m = \theta_k = \theta_s$ and $K_k = K_s$, the soil hydraulic functions of *Vogel and Císlerová* [1988] reduce to the original expressions of *van Genuchten* [1980].

24
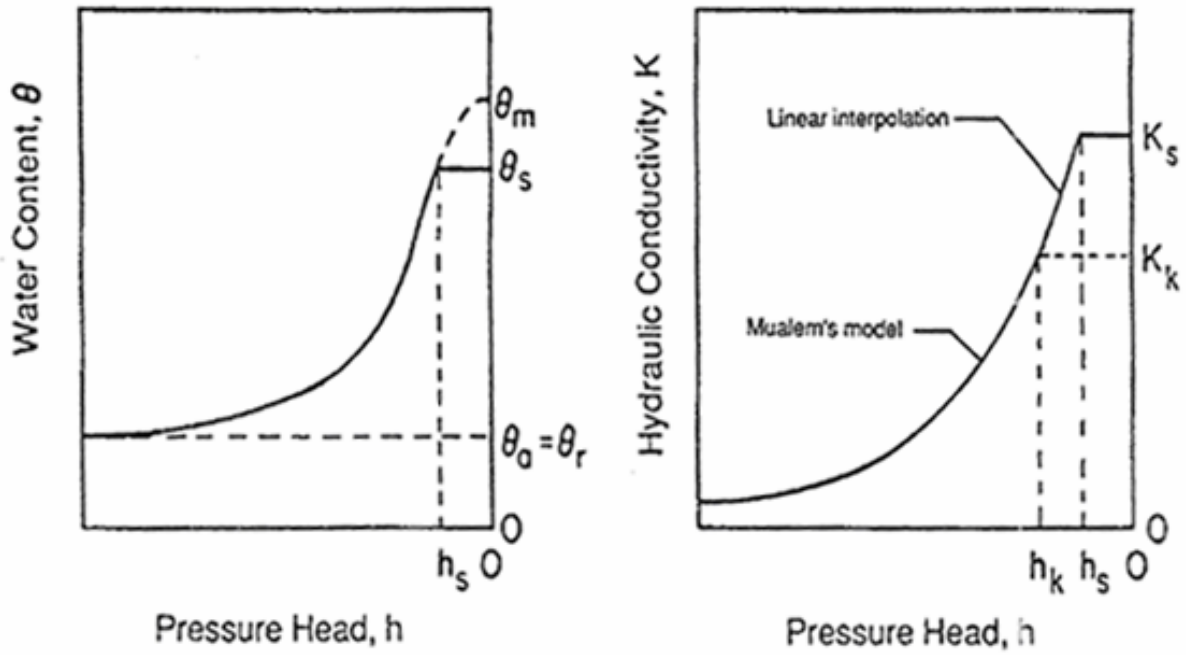
Fig. 2.5. Schematics of the soil water retention (a) and hydraulic conductivity (b) functions as given by equations (2.31) and (2.32), respectively.

Vogel and Císlerová [1988] model (2.31) in which θ_m is calculated so that the air entry value h_s [L] is equal to -2 cm is implemented as "van Genuchten-Mualem with air-entry value of -2 cm". We recommend that this model be used for heavy textured soils (e.g., clays).

Version 4.0 of HYDRUS allows the soil hydraulic properties to be defined also according to *Kosugi* [1996], who suggested the following lognormal distribution model for $S_e(h)$:

$$S_e = \frac{\theta - \theta_r}{\theta_s - \theta_r} = \begin{cases} \dfrac{1}{2}erfc\left\{\dfrac{\ln\left(h/\alpha\right)}{\sqrt{2}n}\right\} & (h < 0) \\ \\ 1 & (h \geq 0) \end{cases} \qquad (2.36)$$

Application of Mualem's pore-size distribution model [*Mualem*, 1976] now leads to the following hydraulic conductivity function:

25

$$K = \begin{cases} K_s S_e^l \left\{ \dfrac{1}{2} erfc \left[\dfrac{\ln(h/\alpha)}{\sqrt{2}n} + \dfrac{n}{\sqrt{2}} \right] \right\}^2 & (h < 0) \\ K_s & (h \geq 0) \end{cases} \qquad (2.37)$$

Note that in this manual we use the symbol α instead of h_0 and n instead of σ as used in *Kosugi* [1996].

Durner [1994] divided the porous medium into two (or more) overlapping regions and suggested to use for each of these regions a van Genuchten-Mualem type function [*van Genuchten*, 1980] of the soil hydraulic properties. Linear superposition of the functions for each particular region gives then the functions for the composite multimodal pore system [*Durner et al.*, 1999]:

$$S_e = w_1 [1 + (\alpha_1 h)^{n_1}]^{-m_1} + w_2 [1 + (\alpha_2 h)^{n_2}]^{-m_2} \qquad (2.38)$$

Combining this retention model with *Mualem*'s [1976] pore-size distribution model leads now to:

$$K(S_e) = K_s \frac{\left(w_1 S_{e_1} + w_2 S_{e_2} \right)^l \left(w_1 \alpha_1 [1 - (1 - S_{e_1}^{1/m_1})^{m_1}] + w_2 \alpha_2 [1 - (1 - S_{e_2}^{1/m_2})^{m_2}] \right)^2}{\left(w_1 \alpha_1 + w_2 \alpha_2 \right)^2} \qquad (2.39)$$

where w_i are the weighting factors for the two overlapping regions, and α_i, n_i, m_i (=1-1/n_i), and l are empirical parameters of the separate hydraulic functions (i=1,2).

An example of composite retention and hydraulic conductivity functions for two overlapping porous media is shown in Figure 2.5. Note that the pressure head axes are on a log scale, which causes the near-saturated values to be significantly enlarged. The fracture domain in this example represents only 2.5% of the entire pore space, but accounts for almost 90% of the hydraulic conductivity close to saturation. Curves similar to those in Figure 2.5 have been used also for fractured rock by *Peters and Klavetter* [1988], *Pruess and Wang* [1987], and *Flint et al.* [2001], among others.

26
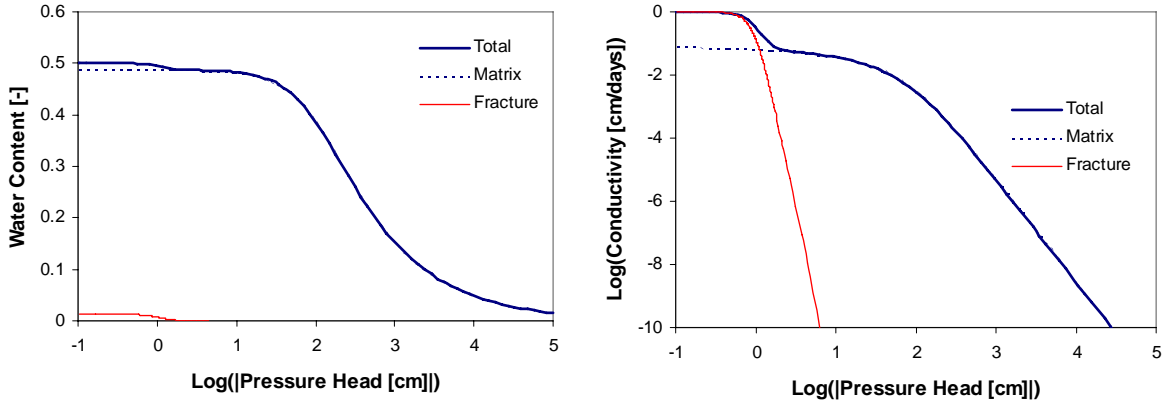
Fig. 2.6. Example of composite retention (left) and hydraulic conductivity (right) functions (θ_r=0.00, θ_s=0.50, α_1=0.01 cm^{-1}, n_1=1.50, l=0.5, K_s=1 cm d^{-1}, w_1=0.975, w_2=0.025, α_2=1.00 cm^{-1}, n_2=5.00).

2.3.2. *Uniform Water Flow and Vapor Transport System*

The thermal hydraulic conductivity function, K_{LT}, in (2.3) may be defined as (e.g., *Noborio et al.* [1996ab], *Saito et al.* [2006]):

$$K_{LT}(T) = K_{Lh}(h)\left(hG_{wT}\frac{1}{\gamma_0}\frac{d\gamma}{dT} \right) \tag{2.40}$$

where G_{wT} is the gain factor (7 for sand), which quantifies the temperature dependence of the soil water retention curve [*Nimmo and Miller*, 1986], γ is the surface tension of soil water [MT^{-2}, Jm^{-2}], and γ_0 is the surface tension at 25°C (= 71.89 g s^{-2}). The temperature dependence of γ is as follows (γ is in [g s^{-2}] and T in [^{o}C]):

$$\gamma = 75.6 - 0.1425T - 2.38 \cdot 10^{-4}T^2 \tag{2.41}$$

The isothermal, K_{vh}, and thermal, K_{vT}, vapor hydraulic conductivities are described as

(e.g., *Nassar and Horton* [1989], *Noborio et al.* [1996b], *Fayer* [2000]):

$$K_{vh} = \frac{D_v}{\rho_w} \rho_{vs} \frac{Mg}{R_u T} H_r \tag{2.42}$$

$$K_{vT} = \frac{D_v}{\rho_w} \eta_e H_r \frac{d\rho_{vs}}{dT} \tag{2.43}$$

where D is the vapor diffusivity in soil [L^2T^{-1}], ρ_{vs} is the saturated vapor density [ML^{-3}], M is the molecular weight of water [M mol^{-1}] (=0.018015 kg mol^{-1}), g is the gravitational acceleration [LT^{-2}] (=9.81 m s^{-2}), R_u is the universal gas constant [J mol^{-1}K^{-1}, ML^2T^{-2}mol^{-1}K^{-1}] (=8.314 J mol^{-1}K^{-1}), η_e is the enhancement factor [-] [*Cass et al.*, 1984], and H_r is the relative humidity [-]. The vapor diffusivity, D_v, in soil is defined as:

$$D_v = \tau_g a_v D_a \tag{2.44}$$

where a_v is the air-filled porosity [-], τ_g is the tortuosity factor as defined by *Millington and Quirk* (1961) and D_a is the diffusivity of water vapor in air [L^2T^{-1}] at temperature T [K]:

$$D_a = 2.12 \cdot 10^{-5} \left(\frac{T}{273.15} \right)^2 \tag{2.45}$$

The saturated vapor density, ρ_{vs} [ML^{-3}] (in kg m^{-3}), as a function of temperature may be expressed as:

$$\rho_{vs} = 10^{-3} \frac{\exp\left(31.3716 - \frac{6014.79}{T} - 7.92495 \cdot 10^{-3} T \right)}{T} \tag{2.46}$$

and the relative humidity, H_r [*Philip and de Vries*, 1957]:

$$H_r = \exp\left[-\frac{hMg}{RT}\right] \tag{2.47}$$

When the liquid and vapor phases of water in soil pores are in equilibrium, the vapor density of the soil can be expressed as the product of the saturated vapor density and the relative humidity:

$$\rho_v = \rho_{vs} H_r \tag{2.48}$$

The volumetric water vapor content, θ_v, is given here in terms of an equivalent water content [$L^3 L^{-3}$] as follows:

$$\theta_v = \rho_v \frac{\theta_s - \theta}{\rho_w} = \rho_{vs} H_r \frac{\theta_s - \theta}{\rho_w} \tag{2.49}$$

The HYDRUS-1D code uses the enhancement factor, η_e, to describe increases in the thermal vapor flux as a result of liquid-island and increased temperature gradients in the air phase [*Philip and de Vries*, 1957]. The enhancement factor as first formulated by *Cass et al.* [1984] may be expressed as [*Campbell*, 1985]:

$$\eta_e = 9.5 + 3\frac{\theta}{\theta_s} - 8.5\exp\left\{-\left[\left(1 + \frac{2.6}{\sqrt{f_c}}\right)\frac{\theta}{\theta_s}\right]^4\right\} \tag{2.50}$$

where f_c is the mass fraction of clay in the soil [-].

2.4. *Scaling in the Soil Hydraulic Functions*

HYDRUS implements a scaling procedure designed to simplify the description of the spatial variability in the unsaturated soil hydraulic properties in the flow domain. The code

29

assumes that variability in the hydraulic properties of a given soil profile can be approximated by means of a set of linear scaling transformations which relate the soil hydraulic characteristics $\theta(h)$ and $K(h)$ of the individual soil layers to reference characteristics $\theta^*(h^*)$ and $K^*(h^*)$. The technique is based on the similar media concept introduced by *Miller and Miller* [1956] for porous media which differ only in the scale of their internal geometry. The concept was extended by *Simmons et al.* [1979] to materials which differ in morphological properties, but which exhibit 'scale-similar' soil hydraulic functions. Three independent scaling factors are embodied in HYDRUS. These three scaling parameters may be used to define a linear model of the actual spatial variability in the soil hydraulic properties as follows [*Vogel et al.*, 1991]:

$$K(h) = \alpha_K \, K^*(h^*)$$
$$\theta(h) = \theta_r + \alpha_\theta \, [\theta^*(h^*) - \theta_r^*] \qquad\qquad (2.51)$$
$$h = \alpha_h \, h^*$$

in which, for the most general case, α_θ, α_h and α_K are mutually independent scaling factors for the water content, the pressure head and the hydraulic conductivity, respectively. Less general scaling methods arise by invoking certain relationships between α_θ, α_h and/or α_K. For example, the original Miller-Miller scaling procedure is obtained by assuming $\alpha_\theta = 1$ (with $\theta_r^* = \theta_r$), and $\alpha_K = \alpha_h^{-2}$. A detailed discussion of the scaling relationships given by (2.51), and their application to the hydraulic description of heterogeneous soil profiles, is given by *Vogel et al.* [1991].

2.5. *Temperature Dependence of the Soil Hydraulic Functions*

A similar scaling technique as described above is used in HYDRUS to express the temperature dependence of the soil hydraulic functions. Based on capillary theory that assumes that the influence of temperature on the soil water pressure head can be quantitatively predicted from the influence of temperature on surface tension, *Philip and de Vries* [1957] derived the following equation

$$\frac{dh}{dT} = \frac{h}{\sigma}\frac{d\sigma}{dT} \qquad\qquad (2.52)$$

where T is temperature [K] and σ is the surface tension at the air-water interface [MT^{-2}]. From (2.52) it follows that

$$h_T = \frac{\sigma_T}{\sigma_{ref}} h_{ref} = \alpha_h^* \, h_{ref} \tag{2.53}$$

where h_T and h_{ref} (σ_T and σ_{ref}) are pressure heads (surface tensions) at temperature T and reference temperature T_{ref}, respectively; and α_h^* is the temperature scaling factor for the pressure head.

Following *Constantz* [1982], the temperature dependence of the hydraulic conductivity can be expressed as

$$K_T(\theta) = \frac{\mu_{ref}}{\mu_T} \frac{\rho_T}{\rho_{ref}} K_{ref}(\theta) = \alpha_K^* \, K_{ref}(\theta) \tag{2.54}$$

where K_{ref} and K_T denote hydraulic conductivities at the reference temperature T_{ref} and soil temperature T, respectively; μ_{ref} and μ_T (ρ_{ref} and ρ_T) represent the dynamic viscosity [ML^{-1}T^{-1}] (density of soil water [ML^{-3}]) at temperatures T_{ref} and T, respectively; and α_K^* is the temperature scaling factor for the hydraulic conductivity.

2.6. *Hysteresis in the Soil Hydraulic Properties*

Applications of unsaturated flow models often assume unique, single-valued (non-hysteretic) functions for $\theta(h)$ and $K(h)$ to characterize the hydraulic properties at a certain point in the soil profile. While such a simplification may be acceptable for many flow simulations, other cases require a more realistic description involving hysteresis in the soil hydraulic properties. The HYDRUS code incorporates hysteresis by using the empirical model introduced by *Scott et al.* [1983]. This model was also employed by *Kool and Parker* [1987], who modified the formulation to account for air entrapment. Following *Vogel et al.* [1996], the present version of HYDRUS further extends the model of *Kool and Parker* by considering also hysteresis in the hydraulic conductivity function.

The adopted procedure for modeling hysteresis in the retention function requires that

both the main drying and main wetting curves are known (Fig. 2.4). These two curves are described with (2.31) using the parameter vectors (θ_r^d, θ_s^d, θ_m^d, α^d, n^d) and (θ_r^w, θ_s^w, θ_m^w, α^w, n^w), respectively, where the subscripts d and w indicate wetting and drying, respectively. The following restrictions are expected to hold in most practical applications:

$$\theta_r^d = \theta_r^w \, , \quad \alpha^d \leq \alpha^w \tag{2.55}$$

We also invoke the often assumed restriction

$$n^d = n^w \tag{2.56}$$

If data are lacking, one may use $\alpha^w = 2\alpha^d$ as a reasonable first approximation [*Kool and Parker*, 1987; *Nielsen and Luckner*, 1992]. We further assume
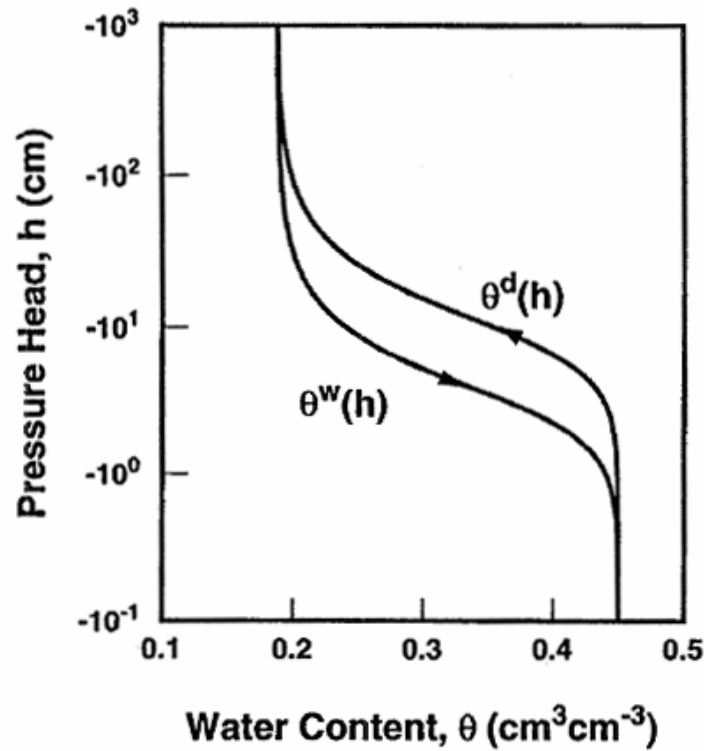
Fig. 2.7. Example of a water retention curve showing hysteresis. Shown are the boundary wetting curve, $\theta^w(h)$, and the boundary drying curve, $\theta^d(h)$.

32

$$\theta_m^w = \theta_r + \frac{\theta_s^w - \theta_r}{\theta_s^d - \theta_r}(\theta_m^d - \theta_r) \qquad (2.57)$$

so that the parameters θ_s and α are the only independent parameters describing hysteresis in the retention function. According to the hysteresis model, drying scanning curves are scaled from the main drying curve, and wetting scanning curves from the main wetting curve. The scaling factors for the drying scanning curves can be obtained by considering the main drying curve as a reference curve in scaling equation (2.51) (keeping $\alpha_h = 1$ to scale only in the water content direction), i.e.:

$$\theta(h) = \theta_r' + \alpha_\theta [\theta^d(h) - \theta_r^d] \qquad (2.58)$$

and forcing each scanning curve, $\theta(h)$, to pass through the point $(\theta_\Delta, h_\Delta)$ characterizing the latest reversal from wetting to drying. Substituting this reversal point into (2.57), and assuming that $\theta_r = \theta_r^d$, leads to

$$\alpha_\theta = \frac{\theta_\Delta - \theta_r}{\theta^d(h_\Delta) - \theta_r} \qquad (2.59)$$

Note that the scaling procedure results in a fictitious value of the parameter θ_s' for the drying scanning curve (this parameter may be located outside of the main hysteresis loop). The scaling relationship is similarly for the wetting scanning curves

$$\theta(h) = \theta_r' + \alpha_\theta [\theta^w(h) - \theta_r] \qquad (2.60)$$

in which the fictitious parameter θ_r' is now used (again possibly scaled outside of the main loop). The scaling factor α_θ for a particular scanning curve can be obtained by substituting the reversal point $(\theta_\Delta, h_\Delta)$ and the full saturation point $(\theta_s, 0)$ into (2.59), and subtracting the two resulting equations to eliminate θ_r' to give

$$\alpha_\theta = \frac{\theta_\Delta - \theta_s}{\theta^w(h_\Delta) - \theta_s^w} \tag{2.61}$$

The parameter θ_r' is subsequently determined from (2.59) as $\theta_r' = \theta_s - \alpha_\theta(\theta_s^w - \theta_r)$. If the main hysteresis loop is not closed at saturation, the water content at saturation for a particular wetting scanning curve is evaluated using the empirical relationship of *Aziz and Settari* [1979]

$$\theta_s = \theta_s^d - \frac{\theta_s^d - \theta_\Delta}{1 + R(\theta_s^d - \theta_\Delta)}, \quad R = \frac{1}{\theta_s^d - \theta_s^w} - \frac{1}{\theta_s^d - \theta_r^d} \tag{2.62}$$

An analogous hysteretic procedure can be applied to the unsaturated hydraulic conductivity function $K(h)$. The main branches $K^d(h)$ and $K^w(h)$ of the hysteresis loop are characterized by the same set of parameters as the corresponding retention curves $\theta^d(h)$ and $\theta^w(h)$, and by the saturated conductivities K_s^d and K_s^w according to Eq. (2.28). For drying scanning curves we obtain from (2.51)

$$K(h) = \alpha_K K^d(h) \tag{2.63}$$

From knowledge of the reversal point (h_Δ, K_Δ) we obtain

$$\alpha_K = \frac{K_\Delta}{K^d(h_\Delta)} \tag{2.64}$$

For a wetting scanning curve we have now

$$K(h) = K_r' + \alpha_K K^w(h) \tag{2.65}$$

where K_r' is a fictitious parameter. Substituting the reversal point (h_Δ, K_Δ) and the saturation point $(0, K_s)$ into (2.64) and solving for α_K yields

$$\alpha_K \;=\; \frac{K_\Delta \; \text{-} \; K_s}{K^w(h_\Delta) \; \text{-} \; K_s^w} \tag{2.66}$$

The fictitious conductivity parameter K_r' may be obtained from (2.64) as $K_r' = K_s - \alpha_K\, K_s^w$. If the main hysteresis loop is not closed at saturation, the hydraulic conductivity at saturation for a wetting scanning curve is evaluated using equations similar to (2.61), i.e.,

$$K_s = K_s^d \;\text{-}\; \frac{K_s^d \;\text{-}\; K_\Delta}{1 + R\,(K_s^d \;\text{-}\; K_\Delta)}, \quad R = \frac{1}{K_s^d \;\text{-}\; K_s^w} \;\text{-}\; \frac{1}{K_s^d} \tag{2.67}$$

While relatively simple to implement, the above model has been found to suffer from a so-called pumping effect, in which the hysteresis loops can move to physically unrealistic parts of the retention function. As an alternative, we also incorporated in HYDRUS the hysteresis model of *Lenhard et al.* [1991] and *Lenhard and Parker* [1992] that eliminates pumping by keeping track of historical reversal points. We greatly acknowledge the help of Robert Lenhard in this effort.

2.7. Initial and Boundary Conditions

The solution of Eq. (2.1) requires knowledge of the initial distribution of the pressure head within the flow domain:

$$h(x,t) = h_i(x) \qquad t = t_0 \tag{2.68}$$

where h_i [L] is a prescribed function of x, and t_o is the time when the simulation begins.

2.7.1. System-Independent Boundary Conditions

One of the following boundary conditions must be specified at the soil surface ($x=L$) or at the bottom of the soil profile ($x=0$):

$$h(x,t) = h_0(t) \qquad \text{at } x = 0 \text{ or } x = L$$

$$-K\left(\frac{\partial h}{\partial x} + \cos\alpha\right) = q_0(t) \quad \text{at } x = 0 \text{ or } x = L \tag{2.69}$$

$$\frac{\partial h}{\partial x} = 0 \qquad \text{at } x = 0$$

where h_0 [L] and q_0 [LT^{-1}] are the prescribed values of the pressure head and the soil water flux at the boundary, respectively.

2.7.2. *System-Dependent Boundary Conditions*

In addition to the system-independent boundary conditions given by (2.68), we consider two system-dependent boundary conditions, which cannot be defined a priori. One of these involves the soil-air interface, which is exposed to atmospheric conditions. The potential fluid flux across this interface is controlled exclusively by external conditions. However, the actual flux depends also on the prevailing (transient) soil moisture conditions near the surface. The soil surface boundary condition may change from a prescribed flux to a prescribed head type condition (and vice-versa). The numerical solution of (2.1) is obtained by limiting the absolute value of the surface flux by the following two conditions [*Neuman et al.*, 1974]:

$$\left| -K\frac{\partial h}{\partial x} - K \right| \leq E \qquad \text{at } x = L \tag{2.70}$$

and

$$h_A \leq h \leq h_S \qquad \text{at } x = L \tag{2.71}$$

where E is the maximum potential rate of infiltration or evaporation under the current atmospheric conditions [LT^{-1}], and h_A and h_S are, respectively, minimum and maximum pressure head at the soil surface allowed under the prevailing soil conditions [L]. The value for h_A is determined from the equilibrium conditions between soil water and atmospheric water vapor, whereas h_S is usually set equal to zero; if positive, h_S represents a small layer of water ponded which can form on top of the soil surface during heavy rains before initiation of runoff. One options in HYDRUS is to assume that any excess water on the soil surface above zero will be

immediately removed. When one of the end points of (2.69) is reached, a prescribed head boundary condition will be used to calculate the actual surface flux. Methods of calculating E and h_A on the basis of atmospheric data have been discussed by *Feddes et al.* [1974]. The minimum pressure head at the soil surface allowed under the prevailing soil conditions, h_A [L], can be calculated from the air humidity, H_r [-], as follows:

$$H_r = \exp\left(-\frac{h_A Mg}{RT}\right)$$
$$h_A = -\frac{RT}{Mg}\ln(H_r)$$

(2.72)

where M is the molecular weight of water [M mol^{-1}] ($=0.018015$ kg mol^{-1}), g is the gravitational acceleration [LT^{-2}], ($=9.81$ m s^{-2}), and R is the gas constant [J mol^{-1} K^{-1}] ($=8.314$ J mol^{-1}K^{-1}) [ML^{2}T^{-2}mol^{-1}K^{-1}].

Variations in potential evaporation and transpiration during the day can be generated with HYDRUS-1D using the assumptions that hourly values between 0-6 a.m. and 18-24 p.m. represent 1% of the total daily value and that a sinusoidal shape is followed during the rest of the day [*Fayer*, 2000], i.e.,

$$T_p(t) = 0.24\overline{T_p} \qquad\qquad t < 0.264\text{d}, t > 0.736\text{d}$$
$$T_p(t) = 2.75\overline{T_p}\sin\left(\frac{2\pi t}{1\,\text{day}} - \frac{\pi}{2}\right) \quad t \in (0.264\text{d}, 0.736\text{d})$$

(2.73)

where $\overline{T_p}$ is the daily value of potential transpiration (or evaporation). Similarly, variation of precipitation can be approximated using a cosine function as follows:

$$P(t) = \overline{P}\left[1 + \cos\left(\frac{2\pi t}{\Delta t} - \pi\right)\right]$$

(2.74)

where $\overline{P}$ is the average precipitation rate of duration Δt.

Potential evaporation and transpiration fluxes can also be calculated from potential

evapotranspiration using Beer's law that partitions the solar radiation component of the energy budget via interception by the canopy [*Ritchie*, 1972] as follows:

$$T_p = ET_p\left(1 - e^{-k \cdot \text{LAI}}\right) = ET_p SCF$$
$$E_p = ET_p e^{-k \cdot \text{LAI}} = ET_p(1 - SCF)$$

(2.75)

where ET_p, T_p, and E_p are potential evapotranspiration, transpiration and evaporation fluxes [LT^{-1}], respectively, LAI is the leaf area index [-], SCF is the soil cover fraction [-], and k is a constant governing the radiation extinction by the canopy [-] as a function of sun angle, the distribution of plants, and the arrangement of leaves (between 0.5-0.75).

Another option in HYDRUS is to permit water to build up on the surface. If surface ponding is expected, a "surface reservoir" boundary condition of the type [*Mls*, 1982]

$$-K\left(\frac{\partial h}{\partial z} + \cos\alpha\right) = q_0(t) - \frac{dh}{dt} \qquad \text{at } x = L$$

(2.76)

may be applied. The flux q_0 in this equation is the net infiltration rate, i.e., the difference between precipitation and evaporation. Equation (2.75) shows that the height $h(L,t)$ of the surface water layer increases due to precipitation, and reduces because of infiltration and evaporation.

A third system-dependent type boundary condition considered in HYDRUS is a seepage face at the bottom of the soil profile through which water can leave the saturated part of the flow domain. This type of boundary condition assumes that a zero-flux boundary condition applies as long as the local pressure head at the bottom of the soil profile ($x = 0$) is negative (or below some specified value *hSeep*). However, a zero pressure head (or the specified value *hSeep*) will be used as soon as the bottom of the profile becomes saturated. This type of boundary condition often applies to finite lysimeters that are allowed to drain under gravity.

Another system-dependent boundary condition, which can be used at the bottom of the soil profile involves flow to a horizontal subsurface tile drains. HYDRUS-1D permits two different analytical solutions to be used to approximate tile drainage. The first solution is known as the Hooghoudt equation [*Houghoudt*, 1940; *van Hoorn*, 1998; *van Dam et al.,* 1997]:

$$q_{drain} = \frac{8K_{hBot}D_{eq}h_{dr} + 4K_{hTop}h_{dr}^2}{L_{dr}^2} + \frac{h_{dr}}{\gamma_{entr}} \qquad (2.77)$$

where q_{drain} is the drain discharge rate per unit surface area [LT^{-1}], K_{hTop} and K_{hBot} are the horizontal saturated hydraulic conductivities above and below the drain system [LT^{-1}], respectively; h_{dr} is the watertable height above the drain at the midpoint between the drains, i.e., the hydraulic head needed for calculating subsurface flow into the drains [L], L_{dr} is the drain spacing [L], γ_{entr} is the entrance resistance into the drains [T], and D_{eq} is the equivalent depth [L]. The equivalent depth as introduced by Hooghoudt is a function of L_{dr}, the depth to an impervious layer, and the drain radius. HYDRUS-1D adopts a numerical scheme as used in the SWAT model [*van Dam et al.,* 1997]. When the drains are located in a homogeneous soil profile just above an impervious layer, (2.76) simplifies as follows:

$$q_{drain} = \frac{4K_h h_{dr}^2}{L_{dr}^2} + \frac{h_{dr}}{\gamma_{entr}} \qquad (2.78)$$

where K_h is the horizontal saturated hydraulic conductivity [LT^{-1}].

The second analytical solution in HYDRUS was derived by Ernst [*Ernst*, 1962; *van Hoorn*, 1997] for a layered soil profile:

$$q_{drain} = \frac{K_{v'} h_{dr}}{D_v} + \frac{8\sum(KD)_h h_{dr}}{L_{dr}^2} + \frac{\pi K_{r'} h_{dr}}{L_{dr}\ln\dfrac{\alpha_{dr} D_r}{u}} + \frac{h_{dr}}{\gamma_{entr}} \qquad (2.79)$$

where $K_{v'}$ and $K_{r'}$ are the saturated hydraulic conductivities in the layers with vertical and radial flow [LT^{-1}], respectively; D_v and D_r are the thicknesses of the layers in which vertical and radial flow is considered [L], respectively; $\sum(KD)_h$ is the transmissivity of the soil layers through which horizontal flow is considered [L^{2}T^{-1}], u is the wet perimeter of the drain [L], and a_{dr} is a geometry factor [-] for radial flow whose value depends on the flow condition (see Table 12.2).

Still another system-dependent lower boundary condition may be imposed in cases where

a functional relationship between the position of the water table and drainage from the soil profile can be established. One possible relationship of this type is discussed in Section 10.3.

HYDRUS additionally allows snow accumulation at the atmospheric boundary when air temperatures are entered. The code in that case assumes that all precipitation is in the form of snow when the air temperature is below -2°C, all precipitation is in the form of liquid when the air temperature is above +2°C, and that a linear transition exists between these two limiting temperatures at -2 and 2 °C [*Jarvis*, 1989]. The code further assumes that when the air temperature is above zero, the existing snow layer (if it exists) melts proportionally to the air temperature.

2.7.3. *Penman-Monteith Combination Equation*

Potential evapotranspiration may be calculated in HYDRUS-1D using either the FAO recommended Penman-Monteith combination equation for evapotranspiration (ET_0) [*Monteith*, 1981; *Monteith and Unsworth*, 1990; *FAO*, 1990] or the Hargreaves equation [*Jensen et al.*, 1997]. With the Penman-Monteith approach, ET_0 is determined using a combination equation that combines the radiation and aerodynamic terms as follows [*FAO*, 1990]:

$$ET_0 = ET_{rad} + ET_{aero} = \frac{1}{\lambda}\left[\frac{\Delta(R_n - G)}{\Delta + \gamma(1 + r_c/r_a)} + \frac{\rho c_p (e_a - e_d)/r_a}{\Delta + \gamma(1 + r_c/r_a)}\right] \tag{2.80}$$

where ET_0 is the evapotranspiration rate [mm d^{-1}], ET_{rad} is the radiation term [mm d^{-1}], ET_{aero} is the aerodynamic term [mm d^{-1}], λ is the latent heat of vaporization [MJ kg^{-1}], R_n is net radiation at surface [MJ m^{-2}d^{-1}], G is the soil heat flux [MJ m^{-2}d^{-1}], ρ is the atmospheric density [kg m^{-3}], c_p is the specific heat of moist air [i.e., 1.013 kJ kg^{-1} °C^{-1}], (e_a-e_d) is the vapor pressure deficit [kPa], e_a is the saturation vapor pressure at temperature T [kPa], e_d is the actual vapor pressure [kPa], r_c is the crop canopy resistance [s m^{-1}], and r_a is the aerodynamic resistance [s m^{-1}]. The slope of the vapor pressure curve, Δ [kPa °C^{-1}] [*Tetens*, 1930; *Murray* 1967], and the psychrometric constant, γ [kPa °C^{-1}] [*Brunt*, 1952], are defined as follows:

$$\Delta = \frac{4098\, e_a}{(T + 237.3)^2} \tag{2.81}$$

$$\gamma = \frac{c_p P}{\varepsilon \lambda} * 10^{-3} = 0.00163 \frac{P}{\lambda} \tag{2.82}$$

respectively, where T is the average air temperature [$^{\circ}$C], P is the atmospheric pressure [kPa], ε is the ratio of the molecular weights of water vapor and dry air (i.e., 0.622), and λ is the latent heat [MJ kg^{-1}].

When no measured radiation data are available, the net radiation can be estimated as:

$$R_n = R_{ns} - R_{nl} \tag{2.83}$$

$$R_{ns} = (1 - \alpha)\left(a_s + b_s \frac{n}{N}\right) R_a \tag{2.84}$$

$$R_{nl} = f \varepsilon' \sigma \frac{\left(T_{max}^4 + T_{min}^4\right)}{2} \tag{2.85}$$

$$G = 0.14(T_{month,n} - T_{month,n-1}) \approx 0 \tag{2.86}$$

where R_n is net radiation [MJ m^{-2}d^{-1}], R_{ns} is net shortwave radiation [MJ m^{-2}d^{-1}], R_{nl} is net longwave radiation [MJ m^{-2}d^{-1}], R_a is extraterrestrial radiation [MJ m^{-2}d^{-1}], α is the albedo or the canopy reflection coefficient (i.e., 0.23), a_s and b_s are parameters for the fraction of radiation (i.e., a_s = 0.25, b_s = 0.5), n/N is the relative sunshine fraction [-], f is the cloudiness factor [-], ε' is the net emissivity, σ is the Stefan-Boltzmann constant (4.90×10^{-9} MJ m^{-2}K^{-4}d^{-1}), T_{max} and T_{min} are the maximum and minimum daily air temperatures [K], e_d is the actual vapor pressure [kPa], and G is the soil heat flux [MJ m^{-2}d^{-1}]. Further details can be found in FAO [1990] and in Appendix A.

2.7.4. Hargreaves Formula

The potential evapotranspiration can also be evaluated using the much simpler Hargreaves formula [e.g., *Jensen et al.*, 1997]:

$$ET_p = 0.0023 R_a \left(T_m + 17.8\right) \sqrt{TR} \tag{2.87}$$

where R_a is extraterrestrial radiation in the same units as ET_p [e.g., mm d^{-1} or J m^{-2}s^{-1}], T_m is the daily mean air temperature, computed as an average of the maximum and minimum air

temperatures [°C], *TR* is the temperature range between the mean daily maximum and minimum air temperatures [°C]. Extraterrestrial radiation, R_a [J m^{-2}s^{-1}], can be calculated as follows

$$R_a = \frac{G_{sc}}{\pi} \, d_r (\omega_s \sin\varphi \sin\delta + \cos\varphi \cos\delta \sin\omega_s) \qquad (2.88)$$

where G_{sc} is the solar constant [J m^{-2}s^{-1}] (1360 W m^{-2}), φ is the site latitude [rad], ω_s is the sunset hour angle [rad], d_r is the relative distance between Earth and Sun [-], and δ is the solar declination [rad]. The last three variables are calculated as follows:

$$\omega_s = \arccos(-\tan\varphi \tan\delta) \qquad (2.89)$$

$$d_r = 1 + 0.033 \cos\left(\frac{2\pi}{365} J\right) \qquad (2.90)$$

$$\delta = 0.409 \sin\left(\frac{2\pi}{365} J - 1.39\right) \qquad (2.91)$$

where *J* is the number of the day in the year [-].

2.8. *Water Mass Transfer*

The mass transfer rate, Γ_w, in (2.5) for water between the fracture and matrix regions in several dual-porosity studies (e.g. *Phillip* [1968]; *Šimůnek et al.* [2003]) has been assumed to be proportional to the difference in effective saturations of the two regions using the first-order rate equation:

$$\Gamma_w = \frac{\partial \theta_{im}}{\partial t} = \omega \left[S_e^m - S_e^{im} \right] \qquad (2.92)$$

where θ_{im} is the matrix water content, ω is a first-order rate coefficient (T^{-1}), and S_e^m and S_e^{im} are effective fluid saturations of the mobile (fracture) and immobile (matrix) regions, respectively. Equation (2.92) assumes that the mass transfer rate is proportional to the difference in effective water contents, rather than pressure heads [*Gerke and van Genuchten*, 1993b], which should

provide a more realistic description of the exchange rate between the fracture and matrix regions. An inherent assumption of (2.92) is that the water retention properties of the matrix and the fracture domains are identical. For this reason, equation (2.92) must be used with some caution and probably only for dual-porosity models. The approach has nevertheless been used successfully in multiple studies (e.g., *Köhne et al.* [2004, 2005]).

An important advantage of (2.92) is the fact that the dual-porosity model based on this mass transfer equation requires significantly fewer parameters since one does not need to know the retention function for the matrix region explicitly, but only its residual and saturated water contents. Coupling (2.92) with a dual-porosity nonequilibrium flow model leads to the usual soil hydraulic parameters needed for the equilibrium model, two additional parameters characterizing the matrix region (i.e. its residual, θ_r^{im}, and saturated, θ_s^{im}, water contents), and the first-order mass transfer coefficient ω. By additionally assuming that the residual water content of the fracture region is equal to zero (and hence that residual water is present only in the immobile region), one could further decrease the number of model parameters.

When the rate of exchange of water between the fracture and matrix regions is assumed to be proportional to the difference in pressure heads between the two pore regions [*Gerke and van Genuchten*, 1993a], the coupling term, Γ_w, becomes:

$$\Gamma_w = \alpha_w \, (h_f - h_m) \tag{2.93}$$

in which α_w is a first-order mass transfer coefficient [$L^{-1}T^{-1}$]. Since pressure heads are now needed for both regions, this approach requires retention curves for both pore regions. For porous media with well-defined geometries, the first-order mass transfer coefficient, α_w, can be defined as follows [*Gerke and van Genuchten*, 1993b]:

$$\alpha_w = \frac{\beta}{d^2} K_a \gamma_w \tag{2.94}$$

where d is an effective 'diffusion' pathlength (i.e. half the aggregate width or half the fracture spacing) [L], β is a shape factor that depends on the geometry [-], and γ_w is a scaling factor (=0.4) obtained by matching the results of the first-order approach at the half-time level of the cumulative infiltration curve to the numerical solution of the horizontal infiltration equation (Gerke and van Genuchten, 1993b). *Gerke and van Genuchten* [1996] evaluated the effective

hydraulic conductivity K_a [LT^{-1}] of the fracture-matrix interface using a simple arithmetic average involving both h_f and h_m as follows

$$K_a(h) = 0.5\left[K_a(h_f) + K_a(h_m)\right]$$ (2.95)

The use of (2.94) implies that the medium contains geometrically well-defined rectangular or other types of macropores or fractures (e.g. *Edwards et al.* [1979], *van Genuchten and Dalton* [1986], and *Gerke and van Genuchten* [1996]). While geometrically based models are conceptually attractive, they may be too difficult to use for field applications, partly because structured soils and rocks usually contain mixtures of aggregates and matrix blocks of various sizes and shapes, but also because the parameters in (2.94) may not be identifiable. Hence, rather than using (2.94) directly, one could also lump β, d, and γ_w into one effective hydraulic conductivity K_a^* of the fracture-matrix interface to give

$$\alpha_w = K_a^*(h)$$ (2.96)

in which case K_a^* can be used as a calibration parameter (this variable is an input parameter to HYDRUS).

3. NONEQUILIBRIUM TRANSPORT OF SOLUTES INVOLVED IN SEQUENTIAL FIRST-ORDER DECAY REACTIONS

3.1. *Governing Solute Transport Equations*

We assume that solutes can exist in all three phases (liquid, solid, and gaseous) and that the decay and production processes can be different in each phase. Interactions between the solid and liquid phases may be described by nonlinear nonequilibrium equations, while interactions between the liquid and gaseous phases are assumed to be linear and instantaneous. We further assume that the solutes are transported by convection and dispersion in the liquid phase, as well as by diffusion in the gas phase. A general structure of the system of first-order decay reactions for three solutes (A, B and C) is as follows [*Šimůnek and van Genuchten*, 1995]:
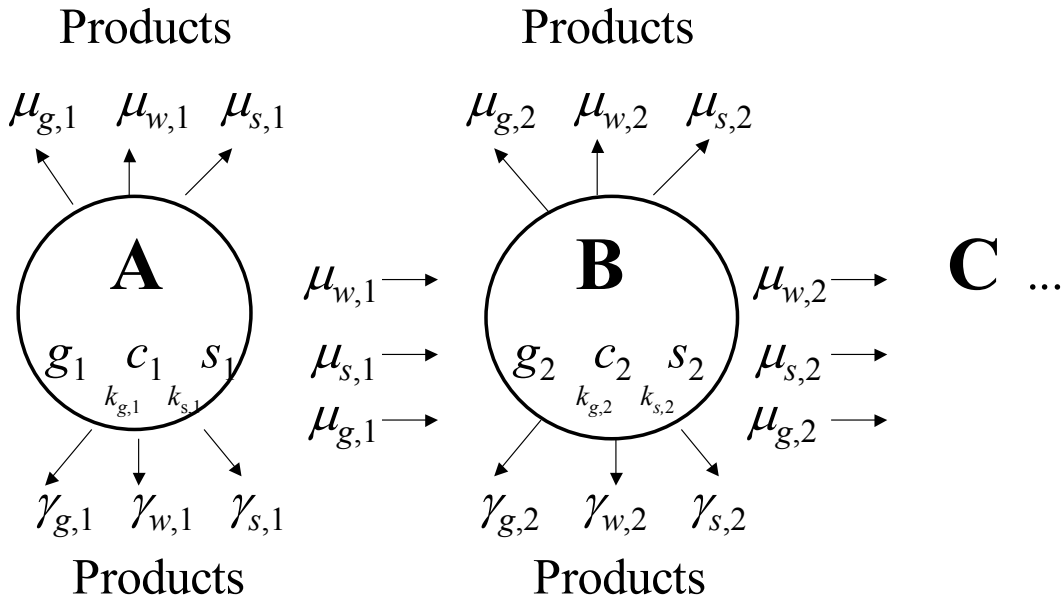
where c, s, and g represent concentrations in the liquid, solid, and gaseous phases, respectively; the subscripts s, w, and g refer to solid, liquid and gaseous phases, respectively; straight arrows represent the different zero-order (γ) and first-order (μ, μ') rate reactions, and circular arrows (k_g, k_s) indicate equilibrium distribution coefficients between phases.

Typical examples of sequential first-order decay chains are:

1. Radionuclides [*van Genuchten*, 1985]

$$^{238}Pu \longrightarrow ^{234}U \longrightarrow ^{230}Th \longrightarrow ^{226}Ra$$

$$c_1 \ s_1 \qquad\qquad c_2 \ s_2 \qquad\qquad c_3 \ s_3 \qquad\qquad c_4 \ s_4$$
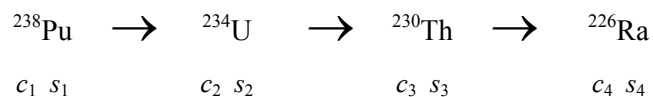
2. Nitrogen [*Tillotson et al.*, 1980]

g_2 ↑

$$(NH_2)_2CO \longrightarrow NH_4^+ \longrightarrow NO_2^- \longrightarrow NO_3^-$$

$$c_1 \ s_1 \qquad\qquad c_2 \ s_2 \qquad\qquad c_3 \qquad\qquad c_4$$

N_2

N_2O
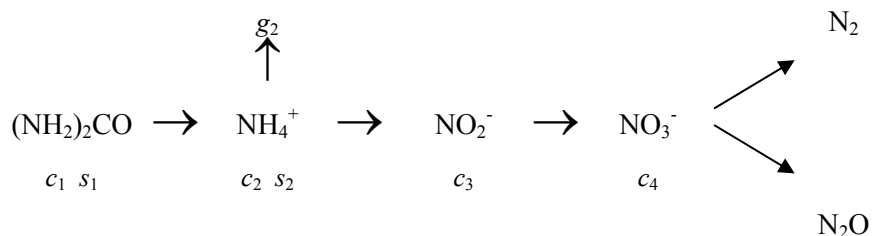
3. Pesticides [*Wagenet and Hutson*, 1987]:

    a) Uninterrupted chain - one reaction path:

Gas

g_1 ↑

Parent pesticide	→	Daughter product 1	→	Daughter product 2	→	Products
$c_1 \ s_1$		$c_2 \ s_2$		$c_3 \ s_3$		
↓		↓		↓		
Product		Product		Product		
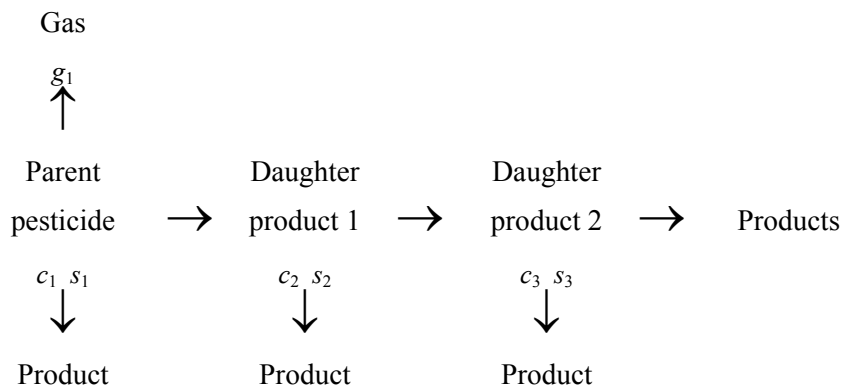
    b) Interrupted chain - two independent reaction paths:

Gas   Gas

g_1 ↑ g_4 ↑

Parent pesticide 1	→	Daughter product 1	→	Product		Parent Pesticide 2	→	Product
$c_1 \ s_1$		$c_2 \ s_2$		$c_3 \ s_3$		$c_4 \ s_4$		
↓		↓				↓		
Product		Product				Product		
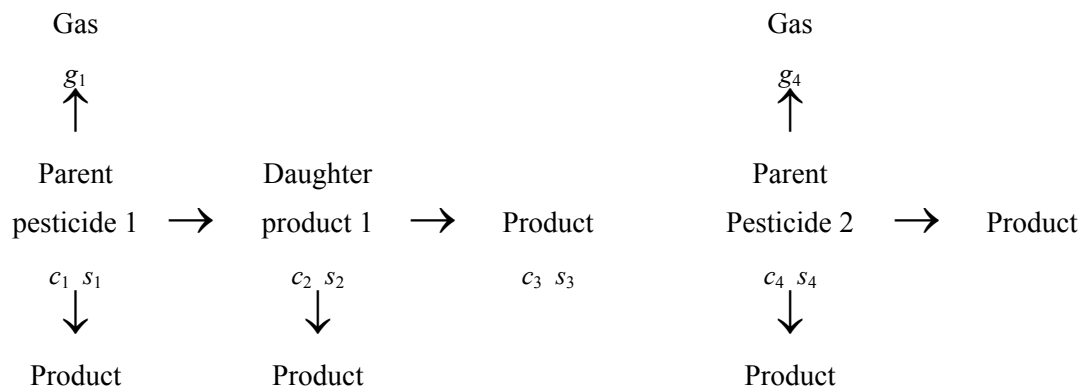
Other examples of chemicals involved in sequential biodegradation chains are hormones [*Casey et al.*, 2003, 2004], chlorinated aliphatic hydrocarbons [*Schaerlaekens et al.*, 1999; *Casey and Šimůnek*, 2001], and explosives [*Dontsova et al.*, 2006]. HYDRUS at present considers up to ten solutes (five for the dual-permeability model), which either can be coupled in a unidirectional chain or are allowed to move independently of each other.

The partial differential equations governing one-dimensional nonequilibrium chemical transport of solutes involved in a sequential first-order decay chain during transient water flow in a variably saturated rigid porous medium are taken as [*Šimůnek and van Genuchten*, 1995]:

$$
\begin{aligned}
&\frac{\partial \theta c_1}{\partial t} + \frac{\partial \rho s_1}{\partial t} + \frac{\partial a_v g_1}{\partial t} = \frac{\partial}{\partial x}\left(\theta D_1^w \frac{\partial c_1}{\partial x}\right) + \frac{\partial}{\partial x}\left(a_v D_1^g \frac{\partial g_1}{\partial x}\right) - \frac{\partial q c_1}{\partial x} - S c_{r,1} - \\
&-(\mu_{w,1} + \mu'_{w,1})\theta c_1 - (\mu_{s,1} + \mu'_{s,1})\rho s_1 - (\mu_{g,1} + \mu'_{g,1})a_v g_1 + \gamma_{w,1}\theta + \gamma_{s,1}\rho + \gamma_{g,1}a_v
\end{aligned}
\tag{3.1}
$$

$$
\begin{aligned}
&\frac{\partial \theta c_k}{\partial t} + \frac{\partial \rho s_k}{\partial t} + \frac{\partial a_v g_k}{\partial t} = \frac{\partial}{\partial x}\left(\theta D_k^w \frac{\partial c_k}{\partial x}\right) + \frac{\partial}{\partial x}\left(a_v D_k^g \frac{\partial g_k}{\partial x}\right) - \frac{\partial q c_k}{\partial x} - \\
&-(\mu_{w,k} + \mu'_{w,k})\theta c_k - (\mu_{s,k} + \mu'_{s,k})\rho s_k - (\mu_{g,k} + \mu'_{g,k})a_v g_k + \mu'_{w,k-1}\theta c_{k-1} + \\
&+ \mu'_{s,k-1}\rho s_{k-1} + \mu'_{g,k-1}a_v g_{k-1} + \gamma_{w,k}\theta + \gamma_{s,k}\rho + \gamma_{g,k}a_v - S c_{r,k} \qquad k \, \varepsilon \, (2, n_s)
\end{aligned}
\tag{3.2}
$$

where c, s, and g are solute concentrations in the liquid [ML^{-3}], solid [MM^{-1}], and gaseous [ML^{-3}], phases, respectively; q is the volumetric flux density [LT^{-1}], μ_w, μ_s, and μ_g are first-order rate constants for solutes in the liquid, solid, and gas phases [T^{-1}], respectively; μ_w', μ_s', and μ_g' are similar first-order rate constants providing connections between individual chain species, γ_w, γ_s, and γ_g are zero-order rate constants for the liquid [ML^{-3}T^{-1}], solid [T^{-1}], and gas [ML^{-3}T^{-1}] phases, respectively; ρ is the soil bulk density [M L^{-3}], a_v is the air content [L^{3}L^{-3}], S is the sink term in the water flow equation (2.1), c_r is the concentration of the sink term [ML^{-3}], D^w is the dispersion coefficient [L^{2}T^{-1}] for the liquid phase, and D^g is the diffusion coefficient [L^{2}T^{-1}] for the gas phase. As before, the subscripts w, s, and g correspond with the liquid, solid and gas phases, respectively; while the subscript k represents the kth chain number, and n_s is the number of solutes involved in the chain reaction. The nine zero- and first-order rate constants in (3.1) and (3.2) may be used to represent a variety of reactions or transformations including biodegradation, volatilization, and precipitation.

HYDRUS assumes nonequilibrium interaction between the solution (c) and adsorbed (s) concentrations, and equilibrium interaction between the solution (c) and gas (g) concentrations of the solute in the soil system. The adsorption isotherm relating s_k and c_k is described by a generalized nonlinear equation of the form

$$s_k = \frac{k_{s,k} c_k^{\beta_k}}{1 + \eta_k c_k^{\beta_k}} \qquad k\,\varepsilon\,(1, n_s)$$

$$\frac{\partial s_k}{\partial t} = \frac{k_{s,k} \beta_k c_k^{\beta_k - 1}}{(1 + \eta_k c_k^{\beta_k})^2} \frac{\partial c_k}{\partial t} + \frac{c_k^{\beta_k}}{1 + \eta_k c_k^{\beta_k}} \frac{\partial k_{s,k}}{\partial t} - \frac{k_{s,k} c_k^{2\beta_k}}{(1 + \eta_k c_k^{\beta_k})^2} \frac{\partial \eta_k}{\partial t} + \frac{k_{s,k} c_k^{\beta_k} \ln c_k}{(1 + \eta_k c_k^{\beta_k})^2} \frac{\partial \beta_k}{\partial t}$$

$$(3.3)$$

where $k_{s,k}$ [L^{3}M^{-1}], β_k [-] and η_k [L^{3}M^{-1}] are empirical coefficients. The Freundlich, Langmuir, and linear adsorption equations are special cases of equation (3.3). When β_k=1, equation (3.3) becomes the Langmuir equation, when η_k=0, equation (3.3) becomes the Freundlich equation, and when both β_k=1 and η_k=0, equation (3.3) leads to a linear adsorption isotherm. Solute transport without adsorption is described with $k_{s,k}$=0. While the coefficients $k_{s,k}$, β_k, and η_k in equation (3.3) are assumed to be independent of concentration, they are permitted to change as a function of time through their dependency on temperature. This feature will be discussed later.

The concentrations g_k and c_k are related by a linear expression of the form

$$g_k = k_{g,k} c_k \qquad k\,\varepsilon\,(1, n_s) \qquad\qquad (3.4)$$

where $k_{g,k}$ is an empirical constant [-] equal to $(K_H R_u T^A)^{-1}$ [*Stumm and Morgan*, 1981], in which K_H is Henry's Law constant [MT^{2}M^{-1}L^{-2}], R_u is the universal gas constant [ML^{2}T^{-2}K^{-1}M^{-1}] and T^A is absolute temperature [K].

3.1.1. *Two-Site Sorption Model (Chemical Nonequilibrium)*

The concept of two-site sorption [*Selim et al.*, 1977; *van Genuchten and Wagenet*, 1989] (Fig. 3.1b) is implemented in HYDRUS to permit consideration of nonequilibrium adsorption-desorption reactions. The two-site sorption concept assumes that the sorption sites can be divided into two fractions:

$$s_k = s_k^e + s_k^k \qquad k \; \varepsilon \; (1, n_s) \qquad (3.5)$$

Sorption, s_k^e [MM^{-1}], on one fraction of the sites (the type-1 sites) is assumed to be instantaneous, while sorption, s_k^k [MM^{-1}], on the remaining (type-2) sites is considered to be time-dependent. At equilibrium we have for the type-1 (equilibrium) and type-2 (kinetic) sites, respectively

$$s_k^e = f s_k \qquad k \; \varepsilon \; (1, n_s) \qquad (3.6)$$

where f is the fraction of exchange sites assumed to be in equilibrium with the solution phase [-]. Because type-1 sorption sites are always at equilibrium, differentiation of (3.6) gives immediately the sorption rate for the type-1 equilibrium sites:

$$s_k^k = (1 - f) s_k \qquad k \; \varepsilon \; (1, n_s) \qquad (3.7)$$

$$\frac{\partial s_k^e}{\partial t} = f \frac{\partial s_k}{\partial t} \qquad k \; \varepsilon \; (1, n_s) \qquad (3.8)$$

Sorption on the type-2 nonequilibrium sites is assumed to be a first-order kinetic rate process. Following *Toride et al.* [1993], the mass balance equation for the type-2 sites in the presence of production and degradation is given by

$$\frac{\partial s_k^k}{\partial t} = \omega_k \left[(1 - f) \frac{k_{s,k} c_k^{\beta_k}}{1 + \eta_k c_k^{\beta_k}} - s_k^k \right] - (\mu_{s,k} + \mu_{s,k}') s_k^k + (1 - f) \gamma_{s,k} \qquad k \; \varepsilon \; (1, n_s) \qquad (3.9)$$

where ω_k is the first-order rate constant for the kth solute [T^{-1}].

Substituting (3.3) through (3.4) into (3.1) and (3.2) leads to the following equation

$$\frac{\partial \theta R_{k1} c_k}{\partial t} + \theta R_{k2} \frac{\partial c_k}{\partial t} = \frac{\partial}{\partial x} \left(E_k \frac{\partial c_k}{\partial x} \right) - \frac{\partial B_k c_k}{\partial x} + F_k c_k + G_k = 0 \qquad k \, \varepsilon \, (1, n_s) \qquad (3.10)$$

in which E_k [L^2T^{-1}] and B_k [LT^{-1}] are an effective dispersion coefficient and effective velocity given by

$$E_k = \theta D_k^w + a_v D_k^g k_{g,k} \qquad\qquad k\,\varepsilon\,(1, n_s) \qquad\qquad (3.11)$$

$$B_k = q - a_v D_k^g \frac{\partial k_{g,k}}{\partial x} \qquad\qquad k\,\varepsilon\,(1, n_s) \qquad\qquad (3.12)$$

respectively. The coefficients F_k and G_k in (3.10) are defined as

$$F_k(c_k) = -(\mu_{w,k} + \mu'_{w,k})\theta - (\mu_{s,k} + \mu'_{s,k})\rho f \frac{k_{s,k} c_k^{\beta_k - 1}}{1 + \eta_k c_k^{\beta_k}} - (\mu_{g,k} + \mu'_{g,k})\, a_v k_{g,k} -$$
$$-\omega_k \rho\,(1-f)\,\frac{k_{s,k} c_k^{\beta_k - 1}}{1 + \eta_k c_k^{\beta_k}} \qquad\qquad (3.13)$$

$$G_1(c_1) = \gamma_{w,1}\theta + \gamma_{s,1}f\rho + \gamma_{g,1}a_v - Sc_{r,1} + \omega_1 \rho s_1^k - \rho f g_1(c_1)$$
$$G_k(c_k) = (\mu'_{w,k-1}\theta + \mu'_{s,k-1}f\rho \frac{k_{s,k-1}c_{k-1}^{\beta_{k-1}-1}}{1 + \eta_{k-1}c_{k-1}^{\beta_{k-1}}} + \mu'_{g,k-1}a_v k_{g,k-1})\,c_{k-1} + \mu'_{s,k-1}\rho s_{k-1}^k + \gamma_{w,k}\theta + \text{(3.14)}$$
$$+ \gamma_{s,k}f\rho + \gamma_{g,k}a_v - Sc_{r,k} + \omega_k \rho s_k^k - \rho f g_k(c_k) \qquad k\,\varepsilon\,(2, n_s)$$

where the variable g_k accounts for possible changes in the adsorption parameters caused by temperature changes in the system as follows (see also section 3.4):

$$g_k(c_k) = \frac{c_k^{\beta_k}}{1 + \eta_k c_k^{\beta_k}}\frac{\partial k_{s,k}}{\partial t} - \frac{k_{s,k}\,c_k^{2\beta_k}}{(1 + \eta_k c_k^{\beta_k})^2}\frac{\partial \eta_k}{\partial t} + \frac{k_{s,k}\,\ln c_k\, c_k^{\beta_k}}{(1 + \eta_k c_k^{\beta_k})^2}\frac{\partial \beta_k}{\partial t} \qquad k\,\varepsilon\,(1, n_s) \qquad (3.15)$$

Because of numerical and programming consideration, we divided the total retardation factor R_k [-] for use in (3.10) into one part, R_{k1}, associated with the liquid and gaseous phases, and another part, R_{k2}, associated with the solid phase:

$$R_{k1}(c_k) = 1 + \frac{a_v \, k_{g,k}}{\theta} \qquad k \;\; \varepsilon \;\; (1, n_s) \tag{3.16}$$

$$R_{k2}(c_k) = \frac{\rho}{\theta} \frac{fk_{s,k} \, \beta_k c_k^{\beta_k - 1}}{(1 + \eta_k \, c_k^{\beta_k})^2} \qquad k \;\; \varepsilon \;\; (1, n_s) \tag{3.17}$$

3.1.2. *Attachment-Detachment Model (Two Kinetic Sites Model)*

Virus, colloid, and bacteria transport and fate models commonly employ a modified form of the convection-dispersion equation (Fig. 3.1c). In this study we define the mass balance equation for these applications as:

$$\frac{\partial \theta c}{\partial t} + \rho \frac{\partial s_e}{\partial t} + \rho \frac{\partial s_1}{\partial t} + \rho \frac{\partial s_2}{\partial t} = \frac{\partial}{\partial x}\left(\theta D \frac{\partial c}{\partial x} \right) - \frac{\partial q c}{\partial x} - \mu_w \theta c - \mu_s \rho (s_e + s_1 + s_2) \tag{3.18}$$

where c is the (colloid, virus, bacteria) concentration in the aqueous phase [$N_c L^{-3}$], s is the solid phase (colloid, virus, bacteria) concentration [$N_c M^{-1}$], subscripts e, 1, and 2 represent equilibrium and two kinetic sorption sites, respectively, N_c is a number of colloids (particles), and μ_w and μ_s represent inactivation and degradation processes in the liquid and solid phases, respectively.

While sorption to equilibrium sites can be described similarly as before using (3.3), mass transfer between the aqueous and both solid kinetic phases can be described as (note that we now dropped subscripts 1 and 2):

$$\rho \frac{\partial s}{\partial t} = \theta k_a \psi c - k_d \rho s \tag{3.19}$$

where k_a is the first-order deposition (attachment) coefficient [T^{-1}], k_d is the first-order entrainment (detachment) coefficient [T^{-1}], and ψ is a dimensionless colloid retention function [-]. The attachment and detachment coefficients in (3.19) have been found to strongly depend upon water content, with attachment significantly increasing as the water content decreases.

To simulate reductions in the attachment coefficient due to filling of favorable sorption sites, ψ is sometimes assumed to decrease with increasing colloid mass retention. A Langmuirian dynamics [*Adamczyk et al.*, 1994] equation has been proposed for ψ to describe this blocking phenomenon:

51

$$\psi = \frac{s_{max} - s}{s_{max}} = 1 - \frac{s}{s_{max}} \tag{3.20}$$

in which s_{max} is the maximum solid phase concentration [$N_c M^{-1}$]. Conversely, enhanced colloid retention during porous medium ripening can theoretically be described using a functional form of ψ that increases with increasing mass of retained colloids:

$$\psi = \max\left(1, s^{s_{max}}\right) \tag{3.21}$$

Johnson and Elimelech [1995] proposed the so-called random sequential adsorption model to describe blocking of the sorption sites:

$$
\begin{aligned}
\psi &= 1 - 4a + 3.308a^2 + 1.4069a^3 && \text{for} && s < 0.8 s_{max} \\
\psi &= \frac{(1 - bs)^3}{2 d_{50}^2 b^3} && \text{for} && s > 0.8 s_{max} \\
b &= \frac{1}{s_{max}} \\
a &= 0.546 \frac{s}{s_{max}}
\end{aligned}
\tag{3.22}
$$

Finally, *Bradford et al.* [2003] hypothesized that the influence of straining and attachment processes on colloid retention can be separated into two distinct components. They suggested the following depth-dependent blocking coefficient for the straining process:

$$\psi = \left(\frac{d_c + x - x_0}{d_c}\right)^{-\beta} \tag{3.23}$$

where d_c is the diameter of the sand grains [L], x_0 is the coordinate of the location where the straining process starts [L] (the surface of the soil profile, or interface between soil layers), and β is an empirical factor (with an optimal value of 0.43 [*Bradford et al.*, 2003]) [-].

The attachment coefficient is often calculated using filtration theory [*Logan et al.*, 1995], a quasi-empirical formulation in terms of the median grain diameter of the porous medium (often

termed the collector), the pore-water velocity, and collector and collision (or sticking) efficiencies accounting for colloid removal due to diffusion, interception and gravitational sedimentation [*Rajagopalan and Tien*, 1976; *Logan et al.*, 1995]:

$$k_a = \frac{3(1-\theta)}{2d_c} \eta \alpha v \qquad (3.24)$$

where d_c is the diameter of the sand grains [L], α is the sticking efficiency (ratio of the rate of particles that stick to a collector to the rate they strike the collector) [-], v is the pore water velocity [LT^{-1}], and η is the single-collector efficiency [-]:

$$\eta = 4A_s^{1/3} N_{Pe}^{-2/3} + A_s N_{Lo}^{1/8} N_R^{15/8} + 0.00338 A_s N_G^{1.2} N_R^{-0.4} \qquad (3.25)$$

where the first, second, and third terms represent removal by diffusion, interception, and gravitational sedimentation, respectively, and where N_{Pe} is the Peclet number [-], N_R is the interception number [-], N_G is the gravitation number [-], N_{Lo} accounts for the contribution of particle London-van der Walls attractive forces to particle removal [-], and A_s is a correction factor [-] as follows:

$$A_s = \frac{2(1-\gamma^5)}{2 - 3\gamma + 3\gamma^5 - 2\gamma^6} \qquad (3.26)$$
$$\gamma = (1-\theta)^{1/3}$$

The dimensionless Peclet number in (3.25) is calculated as follows:

$$N_{Pe} = \frac{3\pi \mu d_p d_c q}{kT} \qquad (3.27)$$

where μ is the fluid viscosity (= 0.00093 Pa s) [ML^{-1}T^{-1}], d_p is the diameter of the particle (e.g., virus, bacteria) (= 0.95 μm = 0.95e-6 m) [L], q is the Darcy's flux [LT^{-1}], k is the Boltzman constant (= 1.38048e-23 J/K) [M L^{2}T^{-2}K^{-1}], and T is the temperature (= 298 K) [K]. Finally, the interception number, N_R, the gravitation number, N_G, and the number representing London-van

der Walls attractive forces, N_{Lo}, in (3.25) are calculated using:

$$N_R = \frac{d_p}{d_c} \tag{3.28}$$

$$N_G = \frac{g(\rho_p - \rho_f)d_p^2}{18\,\mu\,q} \tag{3.29}$$

$$N_{Lo} = \frac{4H}{9\pi\,\mu\,d_p^2\,q} \tag{3.30}$$

where H is the Hamaker constant (= 1e-20 J) [ML^2T^{-2}], g is the gravitational acceleration (= 9.81 m s^{-2}) [LT^{-2}], ρ_p is the bacterial density (= 1080 kg m^{-3}) [ML^{-3}], and ρ_f is the fluid density (= 998 kg m^{-3}) [ML^{-3}].

    The model described above using equation (3.18) can be used in many different ways. For example, one can assume that the soil has two sorption sites, s_1 and s_2, each having their own attachment and detachment constants. This model has been used to describe virus transport in sand dunes by *Schijven and Šimůnek* [2002]. Sorption sites s_1 and s_2 can be used to describe straining and attachment, respectively, as was done by *Bradford et al.* [2002, 2003, 2004]. One may also assume that one sorption site represents sorption to the solid phase, while the other site represents removal of particles by means of attachment to the air-water interface.

3.1.3. *Dual-Porosity Model (Physical Nonequilibrium)*

    The concept of two-region, dual-porosity type solute transport [*van Genuchten and Wierenga*, 1976] is implemented in HYDRUS to permit consideration of physical nonequilibrium transport. The two-region concept assumes that the liquid phase can be partitioned into mobile (flowing), θ_{mo} [L^3L^{-3}], and immobile (stagnant), θ_{im} [L^3L^{-3}], regions such that:

$$\theta = \theta_{mo} + \theta_{im} \tag{3.31}$$

while solute exchange between the two liquid regions is modeled as a first-order process, i.e.,

$$\left[\theta_{im} + \rho(1-f)\frac{k_{s,k}\beta_k c_{k,im}^{\beta_k-1}}{(1+\eta_k c_{k,im}^{\beta_k})^2}\right]\frac{\partial c_{k,im}}{\partial t} = \omega_k(c_k - c_{k,im}) + \gamma_{w,k}\theta_{im} + (1-f)\rho\gamma_{s,k} -$$

$$-\left[\theta_{im}(\mu_{w,k} + \mu_{w,k}') + \rho(\mu_{s,k} + \mu_{s,k}')(1-f)\frac{k_{s,k}c_{k,im}^{\beta_k-1}}{1+\eta_k c_{k,im}^{\beta_k}}\right]c_{k,im} \qquad k\ \varepsilon\ (1,n_s) \tag{3.32}$$

where c_{im} [ML^{-3}] is the concentration of the immobile region and ω_k is mass transfer coefficient for the kth solute [T^{-1}].

Substituting (3.31) and (3.32) into (3.1) and (3.2), with the latter two equations modified for mobile and immobile regions as shown by *van Genuchten and Wagenet* [1989] for simplified one-dimensional conditions, leads to equation (3.10) in which θ is replaced by θ_{mo} and with the coefficients F_k and G_k redefined as follows

$$F_k(c_k) = -(\mu_{w,k} + \mu_{w,k}')\theta_{mo} - (\mu_{s,k} + \mu_{s,k}')\rho f\frac{k_{s,k}c_k^{\beta_k-1}}{1+\eta_k c_k^{\beta_k}} - (\mu_{g,k} + \mu_{g,k}')a_v k_{g,k} - \omega_k \tag{3.33}$$

$$G_1(c_1) = \gamma_{w,1}\theta_{mo} + \gamma_{s,1}f\rho + \gamma_{g,1}a_v - Sc_{r,1} + \omega_1 c_{1,im} - \rho fg_1(c_1)$$

$$G_k(c_k) = \left[\mu_{w,k-1}'\theta_{mo} + \mu_{s,k-1}'f\rho\frac{k_{s,k-1}c_{k-1}^{\beta_{k-1}-1}}{1+\eta_{k-1}c_{k-1}^{\beta_{k-1}}} + \mu_{g,k-1}'a_v k_{g,k-1}\right]c_{k-1} +$$

$$+\left[\mu_{w,k-1}'\theta_{im} + \mu_{s,k-1}'(1-f)\rho\frac{k_{s,k-1}c_{k-1,im}^{\beta_{k-1}-1}}{1+\mu_{k-1}c_{k-1,im}^{\beta_{k-1}}}\right]c_{k-1,im} + \tag{3.34}$$

$$+\gamma_{w,k}\theta_{mo} + \gamma_{s,k}f\rho + \gamma_{g,k}a_v - Sc_{r,k} + \omega_k c_{k,im} - \rho fg_k(c_k) \qquad k\ \varepsilon\ (2,n_s)$$

In order to solve equation (3.10), it is necessary to know the water content θ and the volumetric flux density q. Both variables are obtained from solutions of the Richards equation. The above equations may appear to be relatively complicated. However, by selecting proper values of particular coefficients (i.e., γ_w , γ_s , γ_g, μ_w, μ_s, μ_g, μ_w', μ_s', μ_g', η, k_s, k_g, f, β, ω) the entire system can be simplified significantly. Assuming for example that μ_w', μ_s', μ_g', η, and k_g are zero, and f and β are equal to one, the entire system of equations (3.1) through (3.17) simplifies into a set of equations describing the transport of mutually independent solutes (i.e., single-ion transport as applicable):

$$\frac{\partial\theta Rc}{\partial t} = \frac{\partial}{\partial x}\left(\theta D^w\frac{\partial c}{\partial x}\right) - \frac{\partial qc}{\partial x} + Fc + G \tag{3.35}$$

55
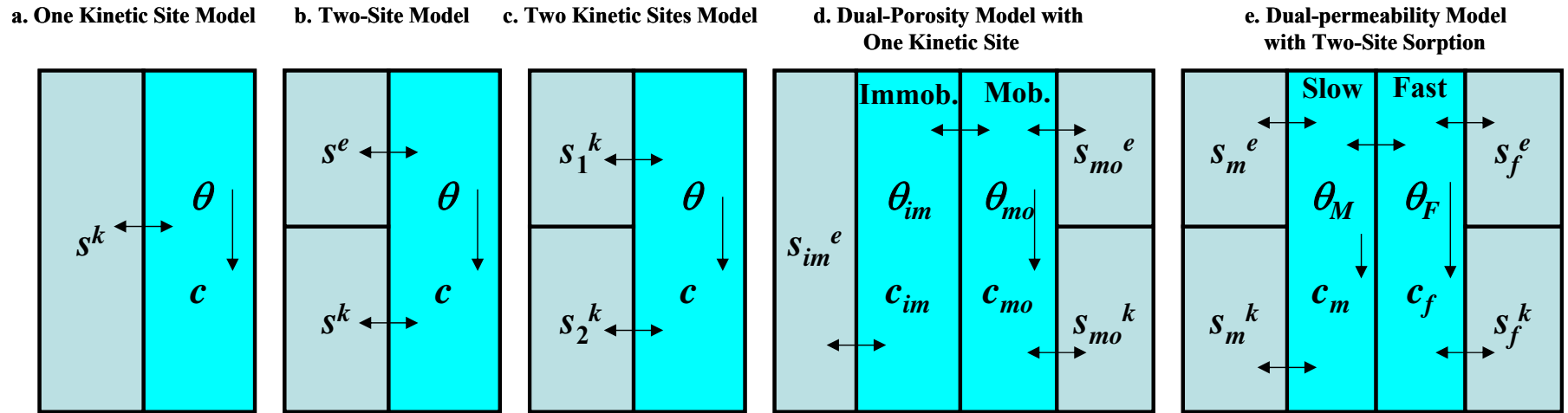
Figure 3.1. Conceptual chemical nonequilibrium models for reactive solute transport. In the plots, θ is the water content, θ_{mo} and θ_{im} in (d) are water contents of the mobile and immobile flow regions, respectively; θ_M and θ_F in (e) are water contents of the matrix and macropore (fracture) regions, respectively; c are concentrations of the corresponding regions, s^e are sorbed concentrations in equilibrium with the liquid concentrations of the corresponding regions, and s^k are kinetically sorbed solute concentrations of the corresponding regions.

3.1.4. *Dual-Porosity Model with One Kinetic Site (Physical and Chemical Nonequilibrium)*

This model (Fig. 3.1d) is similar as the Dual-Porosity Model (section 3.1.3) in that the porous medium is divided into mobile and immobile domains such that $\theta = \theta_{mo} + \theta_{im}$. The current model, however, additionally divides the sorption sites in contact with the mobile zone, similarly as the Two-Site Model (section 3.1.1), into two fractions involving instantaneous and kinetic sorption such that the total sorbed concentration at equilibrium is given by:

$$s = (1 - f_{mo})s_{im} + f_{mo}s_{mo} = (1 - f_{mo})s_{im} + f_{mo}\left(s_{mo}^e + s_{mo,e}^k\right) =$$
$$= (1 - f_{mo})K_d c_{mo} + f_{mo}f_{em}K_d c_{mo} + f_{mo}(1 - f_{em})K_d c_{mo} = K_d c_{mo}$$

(3.36)

where s_{mo}^e is the sorbed concentration in equilibrium with the liquid phase concentration of the mobile region of the Dual-Porosity Model [MM^{-1}], $s_{mo,e}^k$ is the sorbed concentration of the kinetic sites in contact with the mobile region of the Dual-Porosity Model when at equilibrium [MM^{-1}], f_{mo} is the fraction of sorption sites in contact with mobile water (the remainder is in contact with immobile water), and f_{em} is the fraction of sorption sites in equilibrium with the mobile liquid phase (the remaining sites are in contact with the mobile liquid phase). The complete Dual-Porosity Model with One Kinetic Site is described using the following equations [*Šimůnek and van Genuchten*, 2008]:

$$\frac{\partial \theta_{mo} c_{mo}}{\partial t} + f_{mo}\rho \frac{\partial s_{mo}^e}{\partial t} = \frac{\partial}{\partial x}\left(\theta_{mo} D_{mo} \frac{\partial c_{mo}}{\partial x}\right) - \frac{\partial q_{mo} c_{mo}}{\partial z} - \phi_{mo} - \Gamma_{s1} - \Gamma_{s2}$$

$$\frac{\partial \theta_{im} c_{im}}{\partial t} + (1 - f_{mo})\rho \frac{\partial s_{im}}{\partial t} = \Gamma_{s1} - \phi_{im}$$

$$f_{mo}\rho \frac{\partial s_{mo}^k}{\partial t} = \Gamma_{s2} - \phi_{mo,k}$$

$$\Gamma_{s1} = \omega_{ph}(c_{mo} - c_{im})$$

$$\Gamma_{s2} = \alpha_{ch}\left(s_{mo,e}^k - s_{mo}^k\right)$$

$$s_{mo}^e = f_{em}K_d c_{mo}$$

$$s_{mo,e}^k = (1 - f_{em})K_d c_{mo}$$

(3.37)

where ω_{ph} and α_{ch} are first-order rate constants [T^{-1}] accounting for physical and chemical rate processes, respectively; Γ_{s1} is the mass transfer term for solute exchange between the mobile and immobile regions [$ML^{-3}T^{-1}$], Γ_{s2} represents mass transfer to the kinetic sorption sites in the mobile region [$ML^{-3}T^{-1}$], and ϕ_{mo}, ϕ_{mi} and $\phi_{mo,k}$ represent sink/source terms for the equilibrium phases in the mobile zone, for the immobile zone, and for the kinetic sorption sites [$ML^{-3}T^{-1}$], respectively. The first equation of (3.37) describes transport in the mobile phase, the second is a mass balance for the immobile phase, and the third equation a mass balance for the kinetic sorption sites in contact with the mobile zone. The fourth and fifth equations describe mass transfer rates between the mobile and immobile zones, and to the kinetic sorption sites, respectively, while the sixth and seventh equations represent sorption onto the equilibrium and kinetic sorption sites in contact with the mobile zone, respectively. Note that (3.36) and (3.37) (and many of the transport equation later on) are written in terms of the distribution coefficient K_d (instead of $k_{s,k}$ as above), although a full nonlinear Frendlich-Langmuir equation (3.3) can be implemented.

3.1.5. *Dual-Permeability Model (Physical Nonequilibrium)*

Analogous to Eq. (2.6), the dual-permeability formulation for solute transport is based on advection-dispersion type equations for transport in both the fracture and matrix regions as follows [*Gerke and van Genuchten*, 1993a,b] (Figs. 2.1d, 3.1d):

$$\frac{\partial \theta_f c_f}{\partial t} + \rho \frac{\partial s_f}{\partial t} = \frac{\partial}{\partial z}\left(\theta_f D_f \frac{\partial c_f}{\partial z} \right) - \frac{\partial q_f c_f}{\partial z} - \phi_f - \frac{\Gamma_s}{w}$$

$$\frac{\partial \theta_m c_m}{\partial t} + \rho \frac{\partial s_m}{\partial t} = \frac{\partial}{\partial z}\left(\theta_m D_m \frac{\partial c_m}{\partial z} \right) - \frac{\partial q_m c_m}{\partial z} - \phi_m + \frac{\Gamma_s}{1-w} \qquad (3.38)$$

$$\Gamma_s = \omega_{dp}(1-w)\theta_m (c_f - c_m) + \Gamma_w c*$$

The variables in (3.38) have similar meaning as in (3.37), except that they refer now to two overlapping domains, i.e., the matrix (subscript m) and fracture (subscript f) domains. The first equation of (3.38) describes solute transport in the fracture domain, the second equation transport in the matrix domain, and the third equation advective-dispersive mass transfer

58

between the fracture and matrix domains. Equation (3.38) assume complete advective-dispersive transport descriptions for both the fractures and the matrix. *van Genuchten and Dalton* [1986] and *Gerke and van Genuchten* [1996], among others, discussed possible expressions for the first-order solute mass transfer coefficient, ω_{dp}.

3.1.6. *Dual-Permeability Model with Immobile Water (Physical Nonequilibrium)*

The Dual-Permeability Model with Immobile Water (Fig. 2.1e, 3.1e) assumes that the liquid phase of the matrix can be further partitioned into mobile (flowing), $\theta_{m,m}$ [L^{3}L^{-3}], and immobile (stagnant), $\theta_{im,m}$ [L^{3}L^{-3}], regions as follows:

$$\theta_m = \theta_{m,m} + \theta_{im,m} \tag{3.39}$$

where θ_m is the volumetric water content of the matrix pore system [L^{3}L^{-3}]. The governing advection-dispersion equation for transport in the matrix region (second equation of (3.38)) is then replaced [e.g., *Pot et al.*, 2005; *Šimůnek and van Genuchten*, 2008] to yield:

$$\frac{\partial \theta_f c_f}{\partial t} + \rho_f \frac{\partial s_f}{\partial t} = \frac{\partial}{\partial z}\left(\theta_f D_f \frac{\partial c_f}{\partial z}\right) - \frac{\partial q_f c_f}{\partial z} - \phi_f - \frac{\Gamma_s}{w}$$

$$\frac{\partial \theta_{m,m} c_{m,m}}{\partial t} + \rho_m f_m \frac{\partial s_{m,m}}{\partial t} = \frac{\partial}{\partial z}\left(\theta_{m,m} D_m \frac{\partial c_{m,m}}{\partial z}\right) - \frac{\partial q_m c_{m,m}}{\partial z} - \phi_{m,m} + \frac{\Gamma_s}{1-w} - \Gamma_s^*$$

$$\frac{\partial \theta_{im,m} c_{im,m}}{\partial t} + \rho_m (1-f_m)\frac{\partial s_{im,m}}{\partial t} = \Gamma_s^* - \phi_{im,m} \tag{3.40}$$

$$\Gamma_s = \omega_{dp}(1-w)\theta_m(c_f - c_{m,m}) + \Gamma_w c^*$$

$$\Gamma_s^* = \omega_{dpm}(c_{m,m} - c_{im,m})$$

where $c_{im,m}$ and $c_{m,m}$ are solute concentrations in the immobile and mobile zones of the matrix region [ML^{-3}], respectively; $\phi_{m,m}$ and $\phi_{im,m}$ represent various reactions in the mobile and immobile parts of the matrix [ML^{-3}T^{-1}], respectively; f_m is again the fraction of sorption sites in contact with the mobile region of the matrix [-], ω_{dpm} is the mass transfer coefficient between mobile and immobile zones of the matrix region [T^{-1}], and Γ_s^* is the mass transfer term for solutes between the mobile and immobile regions of the matrix domain [ML^{-3}T^{-1}]. The first

equation of (3.40) now describes solute transport in the fracture domain, the second equation transport in the mobile zone of the matrix domain, the third equation is a mass balance for the immobile zone of the matrix domain, the fourth equation describes mass transfer between the fracture and matrix domains, while the fifth equation describes mass transfer between the mobile and immobile zones within the matrix domain.

3.1.7. *Dual-Permeability Model with Two-Site Sorption (Physical and Chemical Nonequilibrium)*

Finally, simultaneous physical and chemical nonequilibrium processes are implemented in HYDRUS-1D by assuming applicability of the Dual-Permeability Model [*Gerke and van Genuchten*, 1993a; *Šimůnek et al.*, 2003; *Šimůnek and van Genuchten*, 2008] and dividing the sorption sites of both the fracture and matrix domains into equilibrium and kinetic sites (Fig. 3.3e). This model leads to the following set of equations [*Pot et al.*, 2005]:

$$
\frac{\partial \theta_f c_f}{\partial t} + \rho_f \frac{\partial s_f^e}{\partial t} = \frac{\partial}{\partial z}\left(\theta_f D_f \frac{\partial c_f}{\partial z}\right) - \frac{\partial q_f c_f}{\partial z} - \phi_f - \frac{\Gamma_s}{w} - \Gamma_f
$$

$$
\frac{\partial \theta_m c_m}{\partial t} + \rho_m \frac{\partial s_m^e}{\partial t} = \frac{\partial}{\partial z}\left(\theta_m D_m \frac{\partial c_m}{\partial z}\right) - \frac{\partial q_m c_m}{\partial z} - \phi_m + \frac{\Gamma_s}{1-w} - \Gamma_m
$$

$$
\rho \frac{\partial s_f^k}{\partial t} = \Gamma_f - \phi_{f,k}
$$

$$
\rho \frac{\partial s_m^k}{\partial t} = \Gamma_m - \phi_{m,k} \tag{3.41}
$$

$$
\Gamma_s = \omega_{dp}(1-w)(c_f - c_m) + \Gamma_w c*
$$

$$
\Gamma_f = \rho_f \alpha_{ch,f}\left[(1-f_f)K_{df}c_f - s_f^k\right]
$$

$$
\Gamma_m = \rho_m \alpha_{ch,m}\left[(1-f_m)K_{dm}c_m - s_m^k\right]
$$

where s_m^k and s_f^k are sorbed concentrations of type-2 (kinetic) sites in the matrix and fracture domains, respectively; f_m and f_f are fractions of the exchange sites assumed to be in equilibrium with the solution phases [-] of the matrix and fracture domains, respectively; ϕ_f, ϕ_m, $\phi_{f,k}$ and $\phi_{m,k}$ represent reactions in the equilibrium phases of the fracture and matrix domains, and at the kinetic

sites of the fracture and matrix domains $[ML^{-3}T^{-1}]$, respectively; and $\alpha_{ch,m}$ and $\alpha_{ch,f}$ are again first-order rate constants for the matrix and fracture domains $[T^{-1}]$, respectively. Note that the distribution coefficients can be different in the different regions (i.e., $K_{df} \neq K_{dm}$).

3.2. *Initial and Boundary Conditions*

The solution of (3.10) requires knowledge of the initial concentration within the flow region, Ω, i.e.,

$$c(x,0) = c_i(x)$$
$$s^k(x,0) = s_i^k(x) \quad\quad\quad (3.42)$$
$$c_{im}(x,0) = c_{im,m}(x)$$

where c_i [ML^{-3}], $c_{im,i}$ [ML^{-3}] and s_i^k [-] are prescribed functions of x. The initial condition for s_i^k must be specified only when nonequilibrium adsorption is considered. The subscript k is dropped in (3.42) and throughout the remainder of this report, thus assuming that the transport-related equations in the theoretical development and the numerical solution apply to each of the solutes in the decay chain.

Two types of boundary conditions (Dirichlet and Cauchy type conditions) can be applied to the upper or lower boundaries. First-type (or Dirichlet type) boundary conditions prescribe the concentration at a boundary:

$$c(x,t) = c_0(x,t) \quad\quad \text{at } x = 0 \text{ or } x = L \quad\quad\quad (3.43)$$

whereas third-type (Cauchy type) boundary conditions may be used to prescribe the concentration flux at the upper or lower boundary as follows:

$$-\theta D\frac{\partial c}{\partial x} + qc = q_0 c_0 \quad\quad \text{at } x = 0 \text{ or } x = L \quad\quad\quad (3.44)$$

in which q_0 represents the upward fluid flux and c_0 is the concentration of the incoming fluid [ML^{-3}]. In some cases, for example when boundary is impermeable ($q_0=0$) or when water flow is directed out of the region, (3.44) reduces to a second-type (Neumann type) boundary condition of the form:

$$\theta D \frac{\partial c}{\partial x} = 0 \qquad\qquad \text{at} \quad x = 0 \text{ or } x = L \qquad\qquad (3.45)$$

A different type of soil surface boundary condition is needed for volatile solutes when they are present in both the liquid and gas phases. This situation requires a third-type boundary condition as before, but with an additional term to account for gaseous diffusion through a stagnant boundary layer of thickness d [L] on the soil surface. The additional solute flux is proportional to the difference in gas concentrations above and below the boundary layer [*Jury et al.*, 1983]. The modified boundary condition has the form

$$-\theta D \frac{\partial c}{\partial x} + qc = q_0 c_0 + \frac{D_g}{d}(k_g c - g_{atm}) \qquad \text{at} \quad x = L \qquad\qquad (3.46)$$

where D_g is the molecular diffusion coefficient in the gas phase [$L^2 T^{-1}$] and g_{atm} is the gas concentration above the stagnant boundary layer [ML^{-3}] (*Jury et al.* [1983] assumed g_{atm} to be zero). Similarly as for (3.44), (3.46) reduces to a second-type (or Neumann type) boundary condition when water flow is zero or directed out of the region:

$$-\theta D \frac{\partial c}{\partial x} = \frac{D_g}{d}(k_g c - g_{atm}) \qquad\qquad \text{at} \quad x = L \qquad\qquad (3.47)$$

Equations (3.46) and (3.47) can only be used when the additional gas diffusion flux is positive. *Jury et al.* [1983] discussed how to estimate the thickness of the boundary layer, d; they recommended a value of 0.5 cm for d as a good average for a bare surface.

3.3. *Effective Dispersion Coefficient*

The dispersion coefficient in the liquid phase, D^w, is given by [*Bear*, 1972]

$$\theta D^w = D_L |q| + \theta D_w \tau_w \tag{3.48}$$

where D_w is the molecular diffusion coefficient in free water [L^2T^{-1}], τ_w is a tortuosity factor in the liquid phase [-], $|q|$ is the absolute value of the Darcian fluid flux density [LT^{-1}], and D_L is the longitudinal dispersivity [L]. After adding the diffusion contribution from the gas phase, the effective dispersion coefficient in the soil matrix for one-dimensional transport is as follows:

$$\theta D = D_L |q| + \theta D_w \tau_w + a_v D_g k_g \tau_g \tag{3.49}$$

where D_g is the molecular diffusion coefficient in the gas phase [L^2T^{-1}] and τ_g is a tortuosity factor in the gas phase [-].

The tortuosity factors for both phases are evaluated in HYDRUS as a function of the water and air contents using the relationship of *Millington and Quirk* [1961]:

$$\begin{aligned} \tau_w &= \frac{\theta^{7/3}}{\theta_s^2} \\ \tau_g &= \frac{a_v^{7/3}}{\theta_s^2} \end{aligned} \tag{3.50}$$

3.4. *Temperature and Water Content Dependence of Transport and Reaction Coefficients*

Several of the diffusion (D_w, D_g), zero-order production (γ_w, γ_s, γ_g), first-order degradation (μ_w', μ_s', μ_g', μ_w, μ_s, and μ_g), and adsorption (k_s, k_g, β, η, ω) coefficients may be strongly dependent upon temperature. HYDRUS assumes that this dependency can be expressed by the Arrhenius equation [*Stumm and Morgan*, 1981]. After some modification, this equation can be expressed in the general form [*Šimůnek and Suarez,* 1993a]

$$a_T = a_r \exp\left[\frac{E_a(T^A - T_r^A)}{R_u T^A T_r^A} \right] \tag{3.51}$$

where a_r and a_T are the values of the coefficient being considered at a reference absolute temperature T_r^A and absolute temperature T^A, respectively; R_u is the universal gas constant, and E_a [$ML^2T^{-2}M^{-1}$] is the activation energy of the particular reaction or process being modeled.

The water content dependence of degradation coefficients is implemented using a modified equation of *Walker* [1974]:

$$a(\theta) = a_r(\theta_{ref}) \min\left[1, \left(\frac{\theta}{\theta_{ref}}\right)^B\right] \tag{3.52}$$

where a_r is the values of the coefficient at a reference water content θ_{ref}, a is the value at the actual water content θ, and B is a solute dependent parameter (usually 0.7). The reference water content, θ_{ref}, which may be different for different soil layers, is calculated from the reference pressure head, h_{ref}, which is considered to be constant for a particular compound.

4. HEAT TRANSPORT

4.1. *Governing Heat Transport Equations*

4.1.1. *Heat Transport Without Vapor Transport*

Neglecting the effect of water vapor diffusion on transport, one-dimensional heat transfer can be described with a convection-dispersion equation of the form

$$\frac{\partial C_p(\theta)T}{\partial t} = \frac{\partial}{\partial x}\left[\lambda(\theta)\frac{\partial T}{\partial x}\right] - C_w\frac{\partial qT}{\partial x} - C_wST \tag{4.1}$$

or equivalently as [*Sophocleous*, 1979]:

$$C_p(\theta)\frac{\partial T}{\partial t} = \frac{\partial}{\partial x}\left[\lambda(\theta)\frac{\partial T}{\partial x}\right] - C_wq\frac{\partial T}{\partial x} \tag{4.2}$$

where $\lambda(\theta)$ is the coefficient of the apparent thermal conductivity of the soil [MLT^{-3}K^{-1}] and $C_p(\theta)$ and C_w are the volumetric heat capacities [ML^{-1}T^{-2}K^{-1}] of the porous medium and the liquid phase, respectively. The volumetric heat capacity is defined as the product of the bulk density and gravimetric heat capacity. The first term on the right-hand side of (4.1) represents heat flow due to conduction, the second term heat transported by flowing water, and the third term energy uptake by plant roots associated with root water uptake. We do not consider the transfer of latent heat by vapor movement. Equation (4.2) is derived from (4.1) by making use of the continuity equation describing isothermal Darcian flow of water in a variably-saturated porous medium

$$\frac{\partial\theta}{\partial t} = -\frac{\partial q}{\partial x} - S \tag{4.3}$$

According to *de Vries* [1963] the volumetric heat capacity is given by

$$C_p(\theta) = C_n\theta_n + C_o\theta_o + C_w\theta + C_a a_v \approx (1.92\theta_n + 2.51\theta_o + 4.18\theta)\,10^6 \quad (\text{J m}^{-3\,\circ}\text{C}^{-1}) \tag{4.4}$$

where θ refers to a volumetric fraction [L^{3}L^{-3}], and subscripts *n, o, a, w* represent solid phase, organic matter, gas phase and liquid phase, respectively.

4.1.2. *Heat Transport With Vapor Transport*

When the effects of water vapor diffusion can not be neglected, the heat transport must be expanded to the form [e.g., *Saito et al.*, 2006]:

$$C_p(\theta)\frac{\partial T}{\partial t} + L_0 \frac{\partial \theta_v}{\partial t} = \frac{\partial}{\partial x}\left(\lambda(\theta)\frac{\partial T}{\partial x}\right) - C_w q \frac{\partial T}{\partial x} - C_v \frac{\partial q_v T}{\partial x} - L_0 \frac{\partial q_v}{\partial x} \qquad (4.5)$$

where L_0 is the volumetric latent heat of vaporization of liquid water [ML^{-1}T^{-2}] (e.g., Jm^{-3}) and q_v is the vapor flux density [LT^{-1}] (see also (2.3)):

$$q_v = -K_{vh}\left(\frac{\partial h}{\partial x} + \cos\alpha\right) - K_{vT}\frac{\partial T}{\partial x} \qquad (4.6)$$

In equation (4.5), the total heat flux density is defined as the sum of the conduction of sensible heat as described by Fourier's law (the first term on the right side), convection of sensible heat by liquid water (the second term) and water vapor (the third term), and convection of latent heat by vapor flow (the fourth term) [*de Vries*, 1958].

4.2. *Apparent Thermal Conductivity*

The apparent thermal conductivity $\lambda(\theta)$ combines the thermal conductivity $\lambda_0(\theta)$ of the porous medium (solid plus water) in the absence of flow and the macrodispersivity, which is a linear function of the velocity [*de Marsily*, 1986]:

$$\lambda(\theta) = \lambda_0(\theta) + \beta_t C_w |q| \qquad (4.7)$$

where β_t is the thermal dispersivity [L]. The volumetric heat capacity of the liquid phase is included in the definition of the thermal conductivity in order to have the dimensions of the thermal dispersivity in length units. *Chung and Horton* [1987] described the thermal

conductivity using the equation

$$\lambda_0(\theta) = b_1 + b_2\theta + b_3\theta^{0.5} \tag{4.8}$$

where b_1, b_2, and b_3 are empirical parameters $[\text{MLT}^{-3}\text{K}^{-1}]$. Alternatively, one can use a function suggested by *Campbell* [1985]:

$$
\begin{aligned}
\lambda_0(\theta) &= A + B\theta - (A - D)\exp[-(C\theta)^E] \\
A &= \frac{0.57 + 1.73\theta_q + 0.93\theta_m}{1 - 0.74\theta_q - 0.49\theta_m} - 2.8\theta_n(1 - \theta_n) \\
B &= 2.8\theta_n \\
C &= 1 + 2.6\theta_c^{-1/2} \\
D &= 0.03 + 0.7\theta_n^2 \\
E &= 4
\end{aligned}
\tag{4.9}
$$

Where the subscripts n, q, c, and m refer to solid, quartz, clay, and other minerals.

4.3. Initial and Boundary Conditions

The solution of (4.1) requires knowledge of the initial temperature within the flow region, i.e.,

$$T(x,0) = T_i(x) \qquad t = 0 \tag{4.10}$$

where T_i is a prescribed function of x.

Two types of boundary conditions (Dirichlet and Cauchy type conditions) can be specified at the top and bottom boundaries of the soil profile. First-type (or Dirichlet type) boundary conditions prescribe the temperature:

$$T(x,t) = T_0(t) \qquad \text{at} \quad x = 0 \text{ or } x = L \tag{4.11}$$

whereas third-type (or Cauchy type) boundary conditions may be used to prescribe the heat flux as follows

$$-\lambda \frac{\partial T}{\partial x} + T C_w q = T_0 C_w q_0 \qquad \text{at} \quad x = 0 \ \text{or} \ x = L \qquad\qquad (4.12)$$

in which T_0 is either the temperature of the incoming fluid or the temperature at the boundary. In some cases, for example for an impermeable boundary ($q=0$) or when water flow is directed out of the region, (4.12) reduces to a second-type (Neumann type) boundary condition of the form:

$$\frac{\partial T}{\partial x} = 0 \qquad\qquad \text{at} \quad x = 0 \qquad\qquad (4.13)$$

Atmospheric boundary conditions for daily fluctuations in soil temperature are often represented by a sine function as follows [*Kirkham and Powers*, 1972]:

$$T_0 = \overline{T} + A \sin\left(\frac{2\pi t}{p_t} - \frac{7\pi}{12} \right) \qquad\qquad (4.14)$$

where p_t is a period of time [T] necessary to complete one cycle of the sine wave (taken to be 1 day), $\overline{T}$ is the average temperature at the soil surface [K] during the period p_t, and A is the amplitude of the sine wave [K]. The second part of the sine term is included to force the maximum in the daily temperature to occur at 1 p.m.

5. CARBON DIOXIDE TRANSPORT AND PRODUCTION

The carbon dioxide transport and production module, as well as the major ion chemistry module described in the next section, were adopted from the UNSATCHEM software package [*Šimůnek et al.*, 1996], and hence their description below closely mirrors those in the UNSATCHEM manual. More detailed analyses of the CO_2 transport and production module, as well as a review of related literature, are presented by *Šimůnek and Suarez* [1993], *Suarez and Šimůnek* [1993], and *Šimůnek et al.* [1996].

5.1. *Governing CO₂ Transport Equations*

We assume that the CO_2 transport in the unsaturated zone can occur in both the liquid and gas phases. We furthermore assume that the CO_2 concentration in the soil is governed by two transport processes [*Patwardhan et al.*, 1988]: convective and diffusive transport in both gas and aqueous phases, and by CO_2 production and/or removal. One-dimensional CO_2 transport hence can be described with the following mass balance equation:

$$\frac{\partial c_T}{\partial t} = -\frac{\partial}{\partial x}(J_{da} + J_{dw} + J_{ca} + J_{cw}) - Sc_w + P \qquad (5.1)$$

where J_{da} describes the CO_2 flux caused by diffusion in the gas phase [LT^{-1}], J_{dw} is the CO_2 flux caused by diffusion and dispersion in the dissolved phase [LT^{-1}], J_{ca} is the CO_2 flux caused by convection in the gas phase [LT^{-1}], and J_{cw} is the CO_2 flux caused by convection in the dissolved phase [LT^{-1}]. The term c_T is the total volumetric concentration of CO_2 [L^3L^{-3}] and P is the CO_2 production/sink term [$L^3L^{-3}T^{-1}$]. The term Sc_w represents dissolved CO_2 removed from the soil by root water uptake. This uptake term assumes that when plants absorb water, dissolved CO_2 is also removed from the soil-water system. The individual flux densities in (5.1) are defined as [*Patwardhan et al.*, 1988]

$$J_{da} = -\theta_a D_a \frac{\partial c_a}{\partial x}$$

$$J_{dw} = -\theta_w D_w \frac{\partial c_w}{\partial x}$$

$$J_{ca} = -q_a c_a$$

$$J_{cw} = -q_w c_w$$

$$(5.2)$$

where c_w and c_a are the volumetric concentrations of CO_2 in the dissolved and gas phases $[L^3 L^{-3}]$, respectively, D_a is the effective soil matrix diffusion coefficient of CO_2 in the gas phase $[L^2 T^{-1}]$, D_w is the effective soil matrix dispersion coefficient of CO_2 in the dissolved phase $[L^2 T^{-1}]$, q_a is the soil air flux $[LT^{-1}]$, q_w is the soil water flux $[LT^{-1}]$, θ_w is the soil water content $[L^3 L^{-3}]$ and θ_a is the volumetric air content $[L^3 L^{-3}]$.

The total CO_2 concentration, c_T $[L^3 L^{-3}]$, is defined as the sum of CO_2 in the gas and dissolved phases as follows

$$c_T = c_a \theta_a + c_w \theta_w \tag{5.3}$$

Substituting (5.2) and (5.3) into (5.1) leads to

$$\frac{\partial(c_a \theta_a + c_w \theta_w)}{\partial t} = \frac{\partial}{\partial x} \theta_a D_a \frac{\partial c_a}{\partial x} + \frac{\partial}{\partial x} \theta_w D_w \frac{\partial c_w}{\partial x} - \frac{\partial}{\partial x} q_a c_a - \frac{\partial}{\partial x} q_w c_w - S c_w + P \tag{5.4}$$

The total aqueous phase CO_2, c_w, defined as the sum of $CO_2(aq)$ and H_2CO_3, is related to the CO_2 concentration in the gas phase by [*Stumm and Morgan*, 1981]

$$c_w = K_{CO_2} RT c_a \tag{5.5}$$

where K_{CO2} is Henry's Law constant [$MT^2M^{-1}L^{-2}$], R is the universal gas constant (8.314 kg m^2 s^{-2}K^{-1}mol^{-1}) [$ML^2T^{-2}K^{-1}M^{-1}$] and T is the absolute temperature [K]. The value of K_{CO2} as a function of temperature was taken from *Harned and Davis* [1943]. Any interaction of dissolved CO_2 with the solid phase is neglected. The quantity of CO_2 added or removed by mineral dissolution/precipitation reactions is relatively small compared to the production and flux values in root-zone environment. The assumption is generally not suitable for saturated conditions or at large depths.

Substituting equation (5.5) into (5.4) gives

$$\frac{\partial R_f c_a}{\partial t} = \frac{\partial}{\partial x} D_E \frac{\partial c_a}{\partial x} - \frac{\partial}{\partial x} q_E c_a - S^* c_a + P \tag{5.6}$$

where R_f is the CO_2 retardation factor [-], D_E is the effective dispersion coefficient for CO_2 in the soil matrix [L^2T^{-1}], q_E is the effective velocity of CO_2 [LT^{-1}], and S^* is the CO_2 uptake rate [T^{-1}] associated with root water uptake. These parameters are defined as

$$R_f = \theta_a + K_{CO_2}RT\theta_w$$
$$D_E = \theta_a D_a + K_{CO_2}RT\theta_w D_w$$
$$q_E = q_a + K_{CO_2}RTq_w \tag{5.7}$$
$$\theta_a = p - \theta_w$$
$$S^* = SK_{CO_2}RT$$

Equation (5.6) is a nonlinear partial differential equation in which all parameters, except for c_a and q_a, are either known or can be obtained from solutions of the variably saturated flow equation. The nonlinearity of (5.6) is caused by the term P, which depends upon the CO_2 concentration, c_a. Since HYDRUS does not consider coupled water and air movement, the flux of air, q_a, is unknown, and thus must be approximated somehow using additional assumptions. One possibility is to assume that advective transport of CO_2 in response to the total pressure gradient is negligible compared to CO_2 diffusion, and therefore to assume a stagnant gas phase in which only diffusive transport occurs (q_a=0). Another possibility is to assume that because of the much lower viscosity of air in comparison to water, a relatively small pressure gradient will lead to significant gas flow. This assumption seems more realistic in that only rarely will the gas

71

phase not be at atmospheric pressure throughout the unsaturated zone. Therefore, under most conditions, the compressibility of the air can be neglected. With the additional assumptions that the air flux is zero at the lower soil boundary and that changes in the total volume of water in the soil profile caused by water flow must be immediately matched by corresponding changes in the gas volume, we obtain then the following equation [*Šimůnek and Suarez*, 1993]:

$$q_a(z) = q_a(0) - q_a(x) + \int_{L-L_R}^{x} S(x)dx \qquad (5.8)$$

This approach seems reasonable since any water leaving the soil system due to evaporation and root water uptake is matched by an equivalent amount of air entering through the soil surface. Similarly, any water entering the soil during precipitation and irrigation events will lead to a similar amount of soil air leaving the soil profile. Only when the soil becomes locally saturated (typically at the soil surface) will air not be able do escape (leading to compressed air below the wetting front).

5.2. *Effective Dispersion Coefficient*

We define the dispersion coefficients, D_w, and the diffusion coefficient, D_a, as

$$D_w = D_{ws}\tau_w + \lambda_w \left| \frac{q_w}{\theta_w} \right| = D_{ws}\frac{\theta_w^{7/3}}{p^2} + \lambda_w \left| \frac{q_w}{\theta_w} \right| \qquad (5.9)$$

$$D_a = D_{as}\tau_a = D_{as}\frac{\theta_a^{7/3}}{p^2} \qquad (5.10)$$

where D_{as} and D_{ws} are the diffusion coefficients [L^2T^{-1}] of CO_2 in the gas and dissolved phases, respectively, τ_a and τ_w are the tortuosity factors [LL^{-1}] in both phases, respectively, p is porosity [L^3L^{-3}] assumed to be equal to the saturated water content, θ_s, and λ_w is the dispersivity in the water phase [L].

72

The tortuosity factors τ_a and τ_w include not only the tortuosity of the flow paths but also the amount of air and liquid space available for diffusion, respectively. The tortuosity factors in both phases are defined in a manner similar to that used by *Millington and Quirk* [1961]. The first term of (5.9) represents the diffusion component and the second term the hydrodynamic dispersion component of the dispersion coefficient. We did not consider mechanical dispersion in the gas phase since diffusion is the dominant process of CO_2 transport in this phase except for very high air velocities. The diffusion coefficients D_{as} and D_{ws}, as functions of temperature, were taken from *Glinski and Stepniewski* [1985].

5.3. *Initial and Boundary Conditions*

The initial condition for the CO_2 concentration in the gas phase is given by

$$c_a(x,t) = c_{ai}(x) \qquad\qquad t = 0 \qquad\qquad (5.11)$$

where $c_{ai}(x)$ is a prescribed function of z [$L^3 L^{-3}$].

First-type or third-type boundary conditions may be specified at the surface (or at the bottom) of the soil profile of the form

$$c_a(x,t) = c_{a0}(t) \qquad\qquad \text{at } x = 0 \text{ or } x = L \qquad\qquad (5.12)$$

or

$$-D_E \frac{\partial c_a}{\partial x} + q_E c_a = q_{E0} c_{a0} \qquad\qquad \text{at } x = 0 \text{ or } x = L \qquad\qquad (5.13)$$

respectively, where q_{E0} is the prescribed effective total CO_2 flux [LT^{-1}] and c_{a0} is concentration [$L^3 L^{-3}$] associated with this flux or prescribed at the boundary. This concentration represents the equilibrium concentration of CO_2 in the atmosphere (0.035%). The first-type boundary condition (5.12) allows the maximum CO_2 flux into the atmosphere. It is difficult to apply the third-type boundary condition (5.13), since the parameter q_E includes both the soil air and soil water fluxes, which are not known a priori and are obtained from solution of the Richards equation. Another option is to neglect the convective fluxes and to assume that a stagnant boundary layer of thickness d [L] exists at the soil surface through which the transport of a gas occurs by vapor diffusion only [*Jury et al.*, 1983,1990; *Sleep and Sykes*, 1989]. This leads to the following

equation

$$-D_E \frac{\partial c_a}{\partial x} + q_E c_a = \frac{D_{as}}{d}(c_{as} - c_{atm}) \quad \text{at } x = L \quad (5.14)$$

where c_{as} is the concentration in the soil gas at the soil surface $[L^3L^{-3}]$ and c_{atm} the concentration at the top of the stagnant boundary layer $[L^3L^{-3}]$. *Jury et al.* [1983] referred to D_{as}/d as the boundary transfer coefficient $[LT^{-1}]$ and discussed various ways of estimating this coefficient.

At the bottom of the soil profile either a continuous concentration profile may be assumed, i.e.,

$$\frac{\partial c_a}{\partial x}(x,t) = 0 \quad \text{at } x = 0 \quad (5.15)$$

or the third-type boundary condition (5.13) may be used, in which case the convective fluxes q_{a0} and q_a are equal to zero as discussed earlier. Boundary condition (5.15) implies that the dispersive flux is equal to zero and that the flux through the lower boundary is only due to convection. A discussion of the applicability of different types of boundary conditions is given by *Baehr* [1987] and *Patwardhan et al.* [1988], among others.

5.4. *Production of Carbon Dioxide*

We assume that the individual CO_2 production processes are additive (5.16) and that it is possible to superpose individual processes which reduce production from the optimal value (5.17) [*Šimůnek and Suarez*, 1993]. The production of CO_2 is then considered as the sum of the production by soil microorganisms, γ_s $[L^3L^{-3}T^{-1}]$, and that by plant roots, γ_p $[L^3L^{-3}T^{-1}]$, as follows:

$$S = \gamma_s + \gamma_p \quad (5.16)$$

$$\gamma_s = \gamma_{s0}\prod_i f_{si} \quad \gamma_p = \gamma_{p0}\prod_i f_{pi} \quad (5.17)$$

74

$$\prod_i f_i = f(x)f(T)f(c_a)f(h)f(h_\phi)f(t) \qquad (5.18)$$

where the subscript s refers to soil microorganisms and the subscript p to plant roots, $f(x)$ is the reduction coefficient as a function of depth [L^{-1}], $f(T)$ is the reduction coefficient as a function of temperature [-], $f(c_a)$ depends similarly on the CO_2 concentration [-], $f(h)$ on the pressure head (or the soil water content) [-], $f(h_\varphi)$ on the osmotic head [-], and $f(t)$ on time [-]. The parameters γ_{s0} and γ_{p0} represent the optimal CO_2 production rates by the soil microorganisms or plant roots, respectively, for the entire soil profile at 20°C under optimal water, solute and CO_2 concentration conditions [L^{3}L^{-2}T^{-1}] [*Šimůnek and Suarez*, 1993]. Definitions of the various reduction coefficients are given by *Šimůnek and Suarez* [1993].

CO$_2$ production generally decreases rapidly with depth because of less root mass and readily decomposable organic matter. *Glinski and Stepniewski* [1985] stated that over 90% of soil respiration activity is concentrated in the humus horizon of the soil. Many expressions are possible to relate the dependence of the production term $f_s(z)$ on soil depth. One example is an expression similar to the normalized distribution function $\beta(z)$ given by *van Genuchten* [1987] for root water uptake. Another possibility is to use again an exponential distribution with depth [*Raats*, 1974]:

$$f_s(x) = ae^{-a(L-x)} \qquad (5.19)$$

where a is an empirical constant [L^{-1}]. We assume that at any time t the dependence of CO$_2$ production by plant roots corresponds to the distribution function $\beta(x)$ used for water uptake by plant roots (see Section 2.2).

The respiration rate of soil microorganisms has been found to decrease at relatively low as well as at high water contents. Poor accessibility of soil water causes a reduction in CO$_2$ production in relatively dry soils (low pressure heads) [*Ekpete and Cornfield*, 1965; *Wilson and Griffin*, 1975]. The observed reduction of the respiration rate near saturation is explained by the unavailability of oxygen because of the high water content and, therefore, its low diffusion rate through the soil. Because of this and consistent with the experimental data of *Williams et al.* [1972] and *Rixon* [1968], the CO$_2$ reduction coefficient $f_s(h)$ as a function of the soil water content for soil microorganisms is expressed as

$$f_s(h) = 1 \qquad\qquad h \ \varepsilon \ (h_2, +\infty)$$

$$f_s(h) = \frac{\log|h| - \log|h_3|}{\log|h_2| - \log|h_3|} \qquad h \ \varepsilon \ (h_3, h_2) \qquad\qquad (5.20)$$

$$f_s(h) = 0 \qquad\qquad h \ \varepsilon \ (-\infty, h_3)$$

where h_2 is the pressure head when CO_2 production is optimal [L] and h_3 is the pressure head when production ceases [L]. Note that no reduction in $f_s(h)$ occurs close to saturation for pressure heads above h_2 [L]. Rather than treating the oxygen stress with a pressure head relation, it seems preferable to consider a separate response function $f(c_a)$. The dependence of the reduction term $f_p(h)$ on the pressure head is represented by expressions similar to the reduction function $\alpha_s(h)$ given by (2.7).

The influence of temperature on chemical processes is described by the Arrhenius equation [*Stumm and Morgan*, 1981]. This equation together with the Van 't Hoff equation has been used successfully by many authors to represent the influence of temperature on soil and root CO_2 production. Assuming that $f(T)=1$ at temperature $T_{20}=293.15$ K (20^oC), the temperature reduction coefficient can be expressed as

$$f(T) = \exp\left[\frac{E(T - T_{20})}{RTT_{20}} \right] \qquad\qquad (5.21)$$

where T is absolute temperature [K] and E the activation energy of the reaction [$ML^2T^{-2}M^{-1}$]. The use of the term "reduction coefficient" for $f(T)$ may seem inappropriate since this coefficient is greater than 1 for temperatures above 20^oC. We use the term to characterize the change in production with temperature, with values greater than 1 above 20 ^oC and less than 1 below 20 ^oC.

The dependence of CO_2 production on its own concentration (actually O_2 deficiency) can be expressed with the Michaelis-Menton equation [*Glinski and Stepniewski*, 1985]

$$q = \frac{q_{max}}{1 + \dfrac{K_M}{c_{O_2}}} \tag{5.22}$$

where K_M is the Michaelis constant [L^3L^{-3}], i.e., the oxygen concentration, c_{O2}, at which oxygen uptake is equal to $1/2 \, q_{max}$, and where q is the oxygen uptake rate and q_{max} is the maximum oxygen uptake rate [$L^3L^{-3}T^{-1}$]. Assuming that the respiratory quotient is equal to unity, then the Michaelis constant for the CO_2 concentration is given by $K_M^* = 0.21 - K_M$, while $c_a = 0.21 - c_{O2}$, in which case the reduction coefficient is given by

$$f(c_a) = \frac{c_{O_2}}{c_{O_2} + K_M} = \frac{0.21 - c_a}{0.42 - c_a - K_m^*} \tag{5.23}$$

Disadvantage of this expression is that if $c_a=0$ the value for $f(c_a)$ is not equal to one. The values for the optimal production rates γ_{p0} and γ_{s0} must therefore be adjusted accordingly.

The coefficient $f(t)$ introduces a time dependence in the production term. This coefficient should describe the diurnal and seasonal dynamics of soil and plant respiration. We assume that the diurnal dynamics for both soil and plant respiration is sufficiently reflected by the temperature dependent coefficient $f(T)$ and that the seasonal dynamics of soil production of CO_2 is sufficiently described by other reduction coefficients. We hence use this coefficient only for changes in CO_2 production caused by the different growth stage of plants. The coefficient $f(t)$ can be described using the growth degree day, *GDD*, concept.

Finally, the actual CO_2 production rate, P_T [$L^3L^{-2}T^{-1}$], is obtained by integrating the CO_2 production rate throughout the entire soil profile as follows

$$P_T = \gamma_{s0}f_s(t)\int_o^L f_s(x)f_s(h)f_s(T)f_s(c_a)f_s(h_\phi)dx + \\ + \gamma_{p0}f_p(t)\int_0^{L_r} f_p(x)f_p(h)f_p(T)f_p(c_a)f_p(h_\phi)dx \tag{5.24}$$

5.5. *Parameter Selection for the CO$_2$ Production Model*

Comprehensive reviews of the selection of the values for optimal CO$_2$ production, as well as coefficients for particular reduction functions, were given by *Suarez and Šimůnek* [1993] and *Šimůnek et al.* [1996]. Values of the different reduction coefficients as suggested in those reviews were used as default values in the graphics-based user interface (see Part B).

6. CARBONATE CHEMISTRY

The carbonate chemistry module, as well as the CO_2 transport and production module as described in the previous section, were adopted from the UNSATCHEM software package [*Šimůnek et al.*, 1996], and thus their description closely mirrors material in the UNSATCHEM manual. Additional details can be found in the original manual [*Šimůnek et al.*, 1996].

When using the ion-association model (and Debye-Hückel activity coefficient calculations) we assume that the chemical system for predicting major ion solute chemistry of the unsaturated zone includes 37 chemical species. These species are divided into six groups as listed in Table 6.1. They include 7 primary dissolved species (calcium, magnesium, sodium, potassium, sulfate, chloride, and nitrate), 10 complex aqueous species, 6 possible solid phases (calcite, gypsum, nesquehonite, hydromagnesite, sepiolite and dolomite), 4 surface species, 7 species which form the CO_2-H_2O system, and 3 silica species. The species from the last two groups could have been included also in other groups (e.g., CO_3^{2-}, $H_2SiO_4^{2-}$, and H^+ could be included in the first group). Their consideration into separate groups is mainly due to their different treatment compared to the other species. For example, complex species of these groups are considered also at high ionic strength when the Pitzer equations are used to calculate activity coefficients, while the species of the second group are in that case dropped from the system, as

Table 6.1. Chemical species considered in the carbonate chemistry module.

1	Aqueous components	7	Ca^{2+}, Mg^{2+}, Na^+, K^+, SO_4^{2-}, Cl^-, NO_3^-
2	Complexed species	10	$CaCO_3^o$, $CaHCO_3^+$, $CaSO_4^o$, $MgCO_3^o$, $MgHCO_3^+$, $MgSO_4^o$, $NaCO_3^-$, $NaHCO_3^o$, $NaSO_4^-$, KSO_4^-
3	Precipitated species	6	$CaCO_3$, $CaSO_4 \cdot 2H_2O$, $MgCO_3 \cdot 3H_2O$, $Mg_5(CO_3)_4(OH)_2 \cdot 4H_2O$, $Mg_2Si_3O_{7.5}(OH) \cdot 3H_2O$, $CaMg(CO_3)_2$
4	Sorbed species	4	Ca,M g,N a,K
5	CO_2-H_2O species	7	P_{CO2}, $H_2CO_3^*$, CO_3^{2-}, HCO_3^-, H^+, OH^-, H_2O
6	Silica species	3	H_4SiO_4, $H_3SiO_4^-$, $H_2SiO_4^{2-}$

discussed later. One of the solid phases (dolomite) is not included in the equilibrium system since its dissolution is always treated kinetically. Also, exclusion of calcite from the equilibrium system is optional since its precipitation-dissolution can be treated as a kinetic process. As a result, either 36 or 35 independent equations are needed to solve this system. In the following sections we present this set of equations, while the method of solution is discussed in *Šimůnek et al.* [1996].

6.1. *Mass and Charge Balance Equations*

Seven mass balance equations for the primary species in the 1st group and one for the silica species in the 6th group of Table 6.1 are defined:

$$Ca_T = [Ca^{2+}] + [CaSO_4^o] + [CaCO_3^o] + [CaHCO_3^+]$$
$$Mg_T = [Mg^{2+}] + [MgSO_4^o] + [MgCO_3^o] + [MgHCO_3^+]$$
$$Na_T = [Na^+] + [NaSO_4^-] + [NaCO_3^-] + [NaHCO_3^o]$$
$$K_T = [K^+] + [KSO_4^-]$$
$$SO_{4T} = [SO_4^{2-}] + [CaSO_4^o] + [MgSO_4^o] + [NaSO_4^-] + [KSO_4^-]$$
$$Cl_T = [Cl^-]$$
$$NO_{3T} = [NO_3^-]$$
$$SiO_{4T} = [H_4SiO_4] + [H_3SiO_4^-] + [H_2SiO_4^{2-}]$$

(6.1)

in which variables with subscript *T* represent the total analytical concentration in solution of that particular species, and where brackets refer to molalities (mol kg^{-1}). Two mass balance equations for the total analytical concentration of carbonate and bicarbonate are defined as follows

$$CO_{3T} = [CO_3^{2-}] + [CaCO_3^o] + [MgCO_3^o] + [NaCO_3^-]$$
$$HCO_{3T} = [HCO_3^-] + [CaHCO_3^+] + [MgHCO_3^+] + [NaHCO_3^o]$$

(6.2)

which are used to calculate inorganic alkalinity, *Alk* (mol$_c$kg^{-1}):

$$Alk = 2\,CO_{3T} + H\,CO_{3T} + [OH^-] - [H^+]$$

(6.3)

Most chemical and multicomponent transport models consider the total inorganic carbon to be a conservative property [e.g., *Westal et al.*, 1986; *Liu and Narasimhan*, 1989; *Yeh and Tripathi*, 1991]. However, this approach can be used only for closed systems. In a soil profile with fluctuating CO_2 concentrations, the approach is inappropriate and use of alkalinity as a conservative property is preferable.

In addition to the mass balance equations, the overall charge balance equation for the solution is given as

$$2[Ca^{2+}]+2[Mg^{2+}]+[Na^+]+[K^+]+[CaHCO_3^+]+[MgHCO_3^+]+[H^+]-2[CO_3^{2-}]-$$
$$-[HCO_3^-]-2[SO_4^{2-}]-[Cl^-]-[NO_3^-]-[OH^-]-[NaCO_3^-]-[NaSO_4^-]-[KSO_4^-]=0 \qquad 6.4)$$

6.2. CO_2 - H_2O System

The activities of the species present in solution at equilibrium are related by the mass-action equations. The dissociation of water is written as follows

$$H_2O \rightleftarrows H^+ + OH^- \qquad K_w = \frac{(H^+)(OH^-)}{(H_2O)} \qquad (6.5)$$
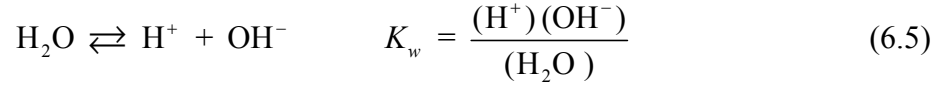
where K_W is the dissociation constant for water [-], while the parentheses denote ion activities. Methods for calculating ion activities will be discussed later.

The solubility of $CO_2(g)$ in water is described with Henry's Law:

$$H_2CO_3^* \rightleftarrows CO_{2(g)}+H_2O \qquad K_{CO_2} = \frac{(H_2CO_3^*)}{P_{CO_2}(H_2O)} \qquad (6.6)$$
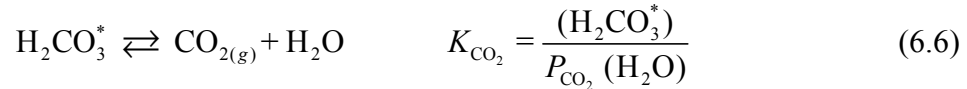
where the activity of $CO_{2(g)}$ is expressed in terms of the partial pressure P_{CO2} (atm), K_{CO2} is Henry's law constant and $H_2CO_3{}^*$ represents both aqueous CO_2 and H_2CO_3.

Protolysis reactions of dissolved CO_2 are written as

$$H_2CO_3^* \rightleftarrows H^+ + HCO_3^- \qquad K_{a1} = \frac{(H^+)(HCO_3^-)}{(H_2CO_3^*)} \qquad (6.7)$$

$$HCO_3^- \rightleftarrows H^+ + CO_3^{2-} \qquad K_{a2} = \frac{(CO_3^{2-})(H^+)}{(HCO_3^-)} \qquad (6.8)$$
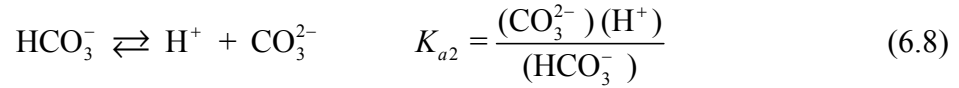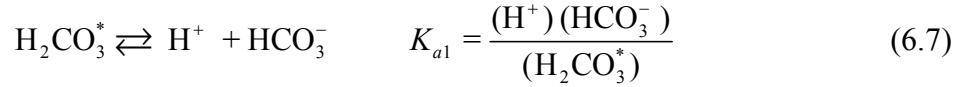
where K_{a1} and K_{a2} are the first and the second dissociation constants of carbonic acid [-], respectively.

6.3. Complexation Reactions

Each complexation reaction for the species in the second group of Table 6.1 and for the silica species can be represented by a mass action law:

$$K_1 = \frac{(Ca^{2+})(SO_4^{2-})}{(CaSO_4^0)} \qquad K_2 = \frac{(Ca^{2+})(CO_3^{2-})}{(CaCO_3^0)} \qquad K_3 = \frac{(Ca^{2+})(HCO_3^-)}{(CaHCO_3^+)} \qquad (6.9)$$

$$K_4 = \frac{(Mg^{2+})(SO_4^{2-})}{(MgSO_4^0)} \qquad K_5 = \frac{(Mg^{2+})(CO_3^{2-})}{(MgCO_3^0)} \qquad K_6 = \frac{(Mg^{2+})(HCO_3^-)}{(MgHCO_3^+)} \qquad (6.10)$$

$$K_7 = \frac{(Na^+)(SO_4^{2-})}{(NaSO_4^-)} \qquad K_8 = \frac{(Na^+)(CO_3^{2-})}{(NaCO_3^-)} \qquad K_9 = \frac{(Na^+)(HCO_3^-)}{(NaHCO_3^0)} \qquad (6.11)$$

$$K_{10} = \frac{(K^+)(SO_4^{2-})}{(KSO_4^-)} \qquad (6.12)$$

$$K_{11} = \frac{(H^+)(H_3SiO_4^-)}{(H_4SiO_4)} \qquad K_{12} = \frac{(H^+)^2(H_2SiO_4^{2-})}{(H_4SiO_4)} \qquad (6.13)$$

where K_i are the equilibrium constants of the ith complexed species [-].

6.4. Cation Exchange and Selectivity

Partitioning between the solid and solution phases is described with the Gapon equation [*White and Zelazny*, 1986]

$$K_{ij} = \frac{\overline{c_i}^{-y+} (c_j^{x+})^{1/x}}{\overline{c_j}^{-x+} (c_i^{y+})^{1/y}} \qquad (6.14)$$

where y and x are the valences of species i and j, respectively, and K_{ij} is the Gapon selectivity coefficient [-]. The adsorbed concentration is expressed in ($mol_c kg^{-1}$ soil). It is assumed that the cation exchange capacity c_T ($mol_c kg^{-1}$ soil) is constant and independent of pH.

$$\overline{c_T} = \Sigma \, \overline{c_i} \qquad (6.15)$$

When four cations ($\overline{Ca}$, $\overline{Mg}$, $\overline{Na}$ and $\overline{K}$) are involved in the exchange reactions, the following system of equations results:

$$\overline{c_T} = \overline{Ca}^{2+} + \overline{Mg}^{2+} + \overline{Na}^{+} + \overline{K}^{+} \qquad (6.16)$$

$$K_{13} = \frac{\overline{Mg}^{2+}}{\overline{Ca}^{2+}} \frac{(Ca^{2+})^{1/2}}{(Mg^{2+})^{1/2}}$$

$$K_{14} = \frac{\overline{Ca}^{2+}}{\overline{Na}^{+}} \frac{(Na^{+})}{(Ca^{2+})^{1/2}} \qquad (6.17)$$

$$K_{15} = \frac{\overline{Ca}^{2+}}{\overline{K}^{+}} \frac{(K^{+})}{(Ca^{2+})^{1/2}}$$

6.5. *Precipitation-Dissolution Reactions*

The carbonate chemistry module considers four solid phases which, if specified or approached from oversaturation, must be in equilibrium with the solution: gypsum, nesquehonite, hydromagnesite and sepiolite. Precipitation-dissolution of calcite can be optionally treated assuming either equilibrium or by means of rate equations. In the latter case the equation corresponding to calcite equilibrium presented in this section is omitted from the equilibrium system and the rate of calcite precipitation-dissolution is calculated from the rate equation as described later. Dissolution of dolomite, which will also be discussed later, is always considered as a kinetic process and never included in an equilibrium system since ordered dolomite almost never precipitates in soils. We refer to *Suarez and Šimůnek* [1997] for a detailed discussion on

how to select and consider these solids. The precipitation or dissolution of gypsum, calcite (if considered in the equilibrium system), nesquehonite, hydromagnesite and sepiolite in the presence of CO_2 are described by

$$CaSO_4 \bullet 2\,H_2O \rightleftarrows Ca^{2+} + SO_4^{2-} + 2\,H_2O \tag{6.18}$$

$$CaCO_3 + CO_2(g) + H_2O \rightleftarrows Ca^{2+} + 2HCO_3^- \tag{6.19}$$

$$MgCO_3 \bullet 3H_2O + CO_2(g) \rightleftarrows Ca^{2+} + 2HCO_3^- + 2H_2O \tag{6.20}$$

$$Mg_5(CO_3)_4(OH)_2 \bullet 4H_2O + 6\,CO_2(g) \rightleftarrows 5\,Mg^{2+} + 10\,HCO_3^- \tag{6.21}$$

$$Mg_2Si_3O_{7.5}(OH) \bullet 3H_2O + 4.5\,H_2O + 4\,CO_2(g) \rightleftarrows 2Mg^{2+} + 3H_4SiO_4 + 4\,HCO_3^- \tag{6.22}$$
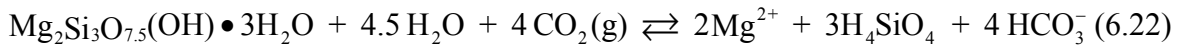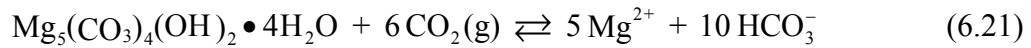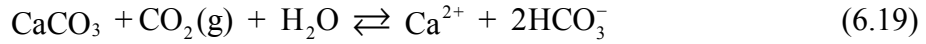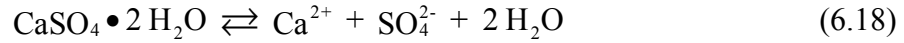
with the corresponding solubility products K_{SP} [-] given by

$$K_{SP}^G = (Ca^{2+})\,(SO_4^{2-})\,(H_2O)^2 \tag{6.23}$$

$$K_{SP}^C = (Ca^{2+})\,(CO_3^{2-}) \tag{6.24}$$

$$K_{SP}^N = (Mg^{2+})\,(CO_3^{2-})(H_2O)^3 \tag{6.25}$$

$$K_{SP}^H = (Mg^{2+})^5\,(CO_3^{2-})^4(OH^-)^2(H_2O)^4 \tag{6.26}$$

$$K_{SP}^S = \frac{(Mg^{2+})^2\,(H_4SiO_4)^3\,(OH^-)^4}{(H_2O)^{4.5}} \tag{6.27}$$

where the indexes *G, C, N, H,* and *S* refer to gypsum, calcite, nesquehonite, hydromagnesite and sepiolite, respectively.

    Substituting (6.5) through (6.8) into (6.24) through (6.27) gives the solubility products for the carbonate solids expressed in terms of bicarbonate, which is almost always the major carbonate ion for conditions (6<pH<10.5) in which the carbonate chemistry module is assumed to be applicable:

$$(\mathrm{Ca}^{2+})(\mathrm{HCO_3^-})^2 = K_{SP}^C \frac{K_{CO2}\,K_{a1}\,P_{CO2}\,(\mathrm{H_2O})}{K_{a2}} \tag{6.28}$$

$$(\mathrm{Mg}^{2+})(\mathrm{HCO_3^-})^2 = K_{SP}^N \frac{K_{CO2}\,K_{a1}}{K_{a2}}\,\frac{P_{CO2}}{(\mathrm{H_2O})^2} \tag{6.29}$$

$$(\mathrm{Mg}^{2+})^5(\mathrm{HCO_3^-})^{10} = K_{SP}^H \frac{K_{CO2}^6\,K_{a1}^6\,P_{CO2}^6}{K_{a2}^4\,K_w^2} \tag{6.30}$$

$$(\mathrm{Mg}^{2+})^2(\mathrm{HCO_3^-})^4 = K_{SP}^S \frac{K_{CO2}^4\,K_{a1}^4\,P_{CO2}^4\,(\mathrm{H_2O})^{4.5}}{K_w^4\,(\mathrm{H_4SiO_4})^3} \tag{6.31}$$

Expressing the solubility products in this way significantly decreases the number of numerical iterations necessary to reach equilibrium as compared to when equations (6.24) through (6.27) are used.

6.6. *Kinetic Model for Calcite Precipitation-Dissolution*

The reaction rates of calcite precipitation-dissolution in the absence of inhibitors such as "foreign ions" and dissolved organic matter, R^C (mmol cm^{-2}s^{-1}), were calculated with the rate equation of *Plummer et al.* [1978]

$$R^C = k_1\,(\mathrm{H^+}) + k_2(\mathrm{H_2CO_3^*}) + k_3(\mathrm{H_2O}) - k_4\,\frac{K_{a2}}{K_{SP}^C}(\mathrm{Ca}^{2+})(\mathrm{HCO_3^-}) \tag{6.32}$$

where

$$k_4 = k_1 + \frac{1}{(\mathrm{H_S^+})}\Big[k_2(\mathrm{H_2CO_3^*}) + k_3\,(\mathrm{H_2O}) \Big] \tag{6.33}$$

and where k_1, k_2, and k_3 are temperature-dependent first-order rate constants representing the forward reactions (mmol cm^{-2}s^{-1}), and k_4 is a function dependent on both temperature and CO_2 concentration representing the back reactions (mmol cm^{-2}s^{-1}). The precipitation-dissolution rate R^C is expressed in mmol of calcite per cm^2 of surface area per second. The term $(\mathrm{H_S^+})$ is the $\mathrm{H^+}$ activity at the calcite surface. Its value is assumed to be $(\mathrm{H^+})$ at calcite saturation where activities of $\mathrm{H_2CO_3^*}$ and H_2O at the calcite surface are equal to their bulk fluid values [*Plummer et al.*,

1978]. The temperature dependency of the constants k_1, k_2, k_3 is expressed as

$$\log k = a_1 + \frac{a_2}{T} \tag{6.34}$$

where values of the empirical constants a_1 and a_2 are given by *Plummer et al.* [1978]. For conditions where $pH>8$ and $pCO_2<1000$ Pa, an alternative expression for the precipitation rate is used, which is considered more accurate for those conditions [*Inskeep and Bloom*, 1985]

$$R^C = -11.82\,[(Ca^{2+})\,(CO_3^{2-}) - K_{SP}^C] \tag{6.35}$$

with an apparent Arrhenius activation energy of 48.1 kJ mol^{-1} for the precipitation rate constant [*Inskeep and Bloom*, 1985].

The precipitation or dissolution rate of calcite is reduced by the presence of various inhibitors. *Suarez and Šimůnek* [1997] developed the following function for the reduction of the precipitation-dissolution rates due to surface poisoning by dissolved organic carbon, based on experimental data from *Inskeep and Bloom* [1986]

$$r = \exp(-b_1 x - b_2 x^2 - b_3 x^{0.5}) \tag{6.36}$$

where r is the reduction constant [-], x is dissolved organic carbon (μmol l^{-1}) and b_1, b_2, and b_3 are regression coefficients (0.005104, 0.000426, 0.069111, respectively).

6.7. *Kinetic Model of Dolomite Dissolution*

The reaction rates of dolomite dissolution, R^D (mmol cm^{-2}s^{-1}), were calculated with the rate equation of *Busenberg and Plummer* [1982]

$$R^D = k_1\,(H^+)^{0.5} + k_2\,(H_2CO_3^*)^{0.5} + k_3\,(H_2O)^{0.5} - k_4\,(HCO_3^-) \tag{6.37}$$

where the temperature dependent first-order rate constants k_1, k_2, k_3 (mmol cm^{-2}s^{-1}), representing

the forward reactions, and k_4 (mmol cm^{-2}s^{-1}), representing the back reaction, are given by (6.34) with empirical constants a_1 and a_2 given by *Busenberg and Plummer* [1982]. The dissolution rate R^D is again expressed in mmol of dolomite per cm^2 of surface area per second. These rate constants are used for ion activity products $IAP^D < 10^{-19}$. For values below 10^{-19} the rate is extremely small and assumed to be zero [*Busenberg and Plummer*, 1982] in the absence of additional data.

6.8. *Silica Concentration in Soil Solution*

Relatively little information exists about Si concentrations in soil water. Use of equilibrium calculations of silica solubility from the stable mineral (quartz) results in the unrealistic prediction that solution concentrations are independent of *p*H up to *p*H 8, above which the solubility will increase due to the dissociation of silicic acid. Si concentrations in soils are usually not fixed by quartz solubility but rather by dissolution (and possibly precipitation) of aluminosilicates including poorly crystallized phases and Si adsorption-desorption onto oxides and aluminosilicates. As a result of these reactions Si concentrations in soil solutions follow a U shaped curve with *p*H, similar to Al oxide solubility, with a Si minimum around *p*H 7.5 [*Suarez*, 1977]. *Suarez* [1977] developed a simple relation between silica content in the soil solution and the soil *p*H:

$$SiO_{4T} = d_1 + d_2\, pH + d_3\, pH^2 \tag{6.38}$$

in which the empirical constants d_1, d_2, and d_3 are equal to 6340, 1430, and 81.9, respectively, and where SiO$_{4T}$ is the sum of all silica species expressed in mol l^{-1}. We utilize this expression and the dissociation expressions for K_{11} and K_{12} (eq. (6.13)) only to obtain estimates of H$_4$SiO$_4$ from total SiO$_4$. As a result sepiolite reactions are not expressed in terms of H$_3$SiO$_4^-$ and H$_2$SiO$_4^{2-}$, which are not included in the charge balance expressions. Only the species H$_4$SiO$_4$ is used in the carbonate chemistry module.

6.9. *Activity Coefficients*

6.9.1. *Extended Debye-Hückel Expression*

Activity coefficient in the dilute to moderately saline solution range are calculated using the extended version of the Debye-Hückel equation [*Truesdell and Jones*, 1974]:

$$\ln \gamma = - \frac{A z^2 \sqrt{I}}{1 + B a \sqrt{I}} + bI \qquad (6.39)$$

where A ($kg^{0.5}mol^{-0.5}$) and B ($kg^{0.5}cm^{-1}mol^{-0.5}$) are constants depending only upon the dielectric constant, density, and temperature, z is the ionic charge in protonic units, a (cm) and b ($kg\ mol^{-1}$) are two adjustable parameters, and I is the ionic strength (mol kg^{-1}):

$$I = 0.5 \sum_{i=1}^{M} z_i^2 c_i \qquad (6.40)$$

where M is the number of species in the solution mixture. The adjustable parameters a and b for individual species are given by *Truesdell and Jones* [1974]. The activities of neutral species are calculated as

$$\ln \gamma = a' I \qquad (6.41)$$

where a' is an empirical parameter.

If the extended Debye-Hückel theory is used to calculate activity coefficients, the activity of water is then calculated in the same way as in the WATEQ program [*Truesdell and Jones*, 1974] using the approximate relation

$$(H_2O) = 1 - 0.017 \sum_{i=1}^{M} m_i \qquad (6.42)$$

6.9.2. *Pitzer Expressions*

At high ionic strength activity coefficients are no longer universal functions of ionic strength, but depend on the relative concentration of the various ions present in solution [*Felmy*

and Weare, 1986]. The activity coefficients can then be expressed in terms of a virial-type expansion of the form [*Pitzer*, 1979]

$$\ln \gamma_i = \ln \gamma_i^{DH} + \sum_j B_{ij}(I)m_j + \sum_j \sum_k C_{ijk}m_j m_k + ... \quad (6.43)$$

where γ_i^{DH} is a modified Debye-Hückel activity coefficient which is a universal function of ionic strength, and B_{ij} and C_{ijk} are specific coefficients for each interaction. The subroutines for calculation of the Pitzer activity coefficients were adopted from the GMIN code [*Felmy*, 1990]. This model is considered accurate also for solutions with very high ionic strength (up to 20 mol kg^{-1}), and can be used down to infinite dilution.

If the Pitzer theory is used, then the activity of water is obtained from the expression [*Felmy and Weare*, 1986]

$$\ln (H_2O) = -\frac{W}{1000}\left(\sum_{i=1}^{M} m_i\right)\phi \quad (6.44)$$

where W is the molecular weight of water and φ the osmotic coefficient (defined in Section 6.11). We refer to *Felmy and Weare* [1986] for a more detailed discussion.

6.10. *Temperature Effects*

Most thermodynamic equilibrium constants depend on both the temperature and pressure of the system. The temperature dependence of the thermodynamic equilibrium constants is often expressed as a power function of the absolute temperature:

$$\log K = a_1 + \frac{a_2}{T} + a_3 T + a_4 \log T + \frac{a_5}{T^2} \quad (6.45)$$

where T is absolute temperature [K], and a_1 through a_5 are empirical constants. The pressure dependence can be neglected for most soils. The empirical constants for the temperature dependent thermodynamic constants used in the calculations are listed in *Šimůnek et al.* [1996].

The temperature dependence of the equilibrium constants for which the constants of equation (6.45) do not exist is expressed with the enthalpy of reaction and the Van 't Hoff expression [*Truesdell and Jones*, 1974].

6.11. *Osmotic Coefficient and Osmotic Pressure Head*

We use the semiempirical equation of *Pitzer* [1973] and co-workers to calculate the osmotic coefficient ϕ. The osmotic pressure of electrolyte solutions, P_ϕ (Pa), is related to the osmotic coefficient ϕ and molality as follows [*Stokes*, 1979]

$$P_\phi = RT \frac{M_s}{V_s} \frac{vm\phi}{m^0} \tag{6.46}$$

where V_s is the partial molar volume of the solvent (cm^3mol^{-1}), m^0 is unit molality (1 mol kg^{-1}), and M_s is molar weight (mol^{-1}). The osmotic pressure head, h_ϕ [L], is related to the osmotic pressure by

$$h_\phi = \frac{P_\phi}{\rho g} \tag{6.47}$$

where ρ is the density of water [ML^{-3}] and g is the gravitational constant [L^2T^{-1}].

6.12. *Effect of Solution Composition on Hydraulic Conductivity*

The accumulation of monovalent cations, such as sodium and potassium, often leads to clay dispersion, swelling, flocculation and overall poor soil physico-mechanical properties. These processes have an adverse effect on the soil hydraulic properties including hydraulic conductivity, infiltration rates and soil water retention as a result of swelling and clay dispersion. These negative effects are usually explained based on the diffuse double layer theory. A consequence of the more diffuse double layer in the presence of monovalent ions as compared to divalent ions is the greater repulsion force or swelling pressure between neighboring clay platelets. These negative effects become more pronounced with decreasing salt concentration

and valence of the adsorbed ions [*Shainberg and Levy*, 1992]. In addition, *Suarez et al*. [1984] determined that elevated levels of pH also had an adverse effect on the saturated hydraulic conductivity.

The effect of solution chemistry on the hydraulic conductivity in the major ion chemistry module is calculated as follows

$$K(h, pH, SAR, C_0) = r(pH, SAR, C_0)\, K(h) \tag{6.48}$$

where *SAR* is the sodium adsorption ratio, C_0 is the total salt concentration of the ambient solution in $mmol_c l^{-1}$, and r is a scaling factor which represents the effect of the solution composition on the final hydraulic conductivity [-], and which is related to pH, *SAR* and salinity. The hydraulic conductivity without the scaling factor r can be assumed to be the optimal value under favorable chemical conditions in terms of optimal pH, *SAR* and salinity. Although soil specific, the effects of solution chemistry are too important to ignore. We include reduction functions calculated for some illitic soils of California based on the experimental work of *McNeal* [1968] and *Suarez et al*. [1981]. The overall scaling factor r in equation (6.48) for this purpose is divided into two parts

$$r(pH,\ SAR,\ C_0) = r_1(SAR,\ C_0)\, r_2(pH) \tag{6.49}$$

where the first part, r_1 [-], reflects the effect of the exchangeable sodium percentage and dilution of the solution on the hydraulic conductivity, while the second part, r_2 [-], represents the effect of the soil solution pH. The first term is based on a simple clay-swelling model, which treats mixed-ions clays as simple mixture of homoionic sodium and calcium clay. Clay swelling is then related to a decrease in soil hydraulic conductivity [*McNeal*, 1974]. The r_1 term was defined by *McNeal* [1968] as

$$r_1 = 1 - \frac{cx^n}{1 + cx^n} \tag{6.50}$$

where c and n are empirical parameters, and x is a swelling factor. The interlayer swelling of soil montmorillonite, x, is defined in the following way

$$x = f_{mont}\, 3.6 \cdot 10^{-4} ESP^* d^* \tag{6.51}$$

where f_{mont} is the weight fraction of montmorillonite in the soil, d^* is the adjusted interlayer spacing [L] and ESP^* is the adjusted exchangeable sodium percentage. For most soils one can use the assumption that f_{mont} = 0.1 [*McNeal*, 1968]. The adjusted exchangeable sodium percentage is calculated as

$$ESP^* = \max[0,\, ESP\text{-}(1.24 + 11.63 \log C_0)] \tag{6.52}$$

where C_0 is total salt concentration of the ambient solution in $mmol_c l^{-1}$, and ESP is defined as

$$ESP = 100 \frac{\overline{Na}}{CEC} \tag{6.53}$$

where CEC is the soil cation exchange capacity ($mmol_c kg^{-1}$) and $\overline{Na}$ the exchangeable sodium concentration ($mmol_c kg^{-1}$). The adjusted interlayer spacing, d^*, is given by

$$\begin{aligned} d^* &= 0 && \text{for } C_0 > 300 \;\; mmol_c \;\; liter^{-1} \\ d^* &= 356.4\, C_0^{-1/2} + 1.2 && \text{for } C_0 < 300 \;\; mmol_c \;\; liter^{-1} \end{aligned} \tag{6.54}$$

McNeal [1968] reported that the values of the empirical factor n in equation (6.50) depends primarily on the soil ESP and that as a first approximation n values may be estimated using

$$\begin{aligned} n &= 1 && \text{for } ESP < 25 \\ n &= 2 && \text{for } 25 \leq ESP \leq 50 \\ n &= 3 && \text{for } ESP > 50 \end{aligned} \tag{6.55}$$

Only the values of the empirical factor c vary from soil to soil. HYDRUS uses values reported by *McNeal* [1968]:

$$
\begin{aligned}
c &= 35 && \text{for } ESP < 25 \\
c &= 932 && \text{for } 25 \leq ESP \leq 50 \\
c &= 25\,000 && \text{for } ESP > 50
\end{aligned}
\tag{6.56}
$$

The reduction factor, r_2, for the effect of pH on hydraulic conductivity was calculated from experimental data of *Suarez et al.* [1984] after first correcting for the adverse effects of low salinity and high exchangeable sodium using the r_1 values. The following equation was used

$$
\begin{aligned}
r_2 &= 1 && \text{for } p\text{H} < 6.83 \\
r_2 &= 3.46 - 0.36\, p\text{H} && \text{for } 6.83 \leq p\text{H} \leq 9.3 \\
r_2 &= 0.1 && \text{for } p\text{H} > 9.3
\end{aligned}
\tag{6.57}
$$

Note, that although the models for reductions in the hydraulic conductivity due to changes in the solution composition were derived from data on the saturated hydraulic conductivity, the same reduction factors were used for the entire range of the pressure heads. The assumption that the r values for saturated conditions can be applied to the entire range of pressure heads has not been closely examined thus far in the literature.

7. NUMERICAL SOLUTION OF THE VARIABLY SATURATED FLOW EQUATION

7.1. *Space and Time Discretization*

The soil profile is first discretized into N-1 adjoining elements, with the ends of the elements located at the nodal points, and N being the number of nodes. The same spatial discretization is used for water flow, solute transport and heat movement. HYDRUS assumes that the vertical coordinate x is directed positive upward.

A mass-lumped linear finite elements scheme was used for discretization of the mixed form of the Richards' equation (2.1) (the numerical solution for equation (2.3) is in principle similar to the solution to equation (2.1)). Since the mass-lumped scheme results in an equivalent and somewhat standard finite difference scheme [e.g., *Vogel et al.*, 1996], we omit the detailed finite element development and give immediately the invoked final finite difference scheme:

$$\frac{\theta_i^{\,j+1,k+1} - \theta_i^{\,j}}{\Delta t} = \frac{1}{\Delta x}\left(K_{i+1/2}^{j+1,k} \frac{h_{i+1}^{j+1,k+1} - h_i^{j+1,k+1}}{\Delta x_i} - K_{i-1/2}^{j+1,k} \frac{h_i^{j+1,k+1} - h_{i-1}^{j+1,k+1}}{\Delta x_{i-1}} \right) + \\ + \frac{K_{i+1/2}^{j+1,k} - K_{i-1/2}^{j+1,k}}{\Delta x}\cos\alpha - S_i^j \tag{7.1}$$

where

$$\Delta t = t^{j+1} - t^j$$

$$\Delta x = \frac{x_{i+1} - x_{i-1}}{2} \qquad \Delta x_i = x_{i+1} - x_i \qquad \Delta x_{i-1} = x_i - x_{i-1} \tag{7.2}$$

$$K_{i+1/2}^{j+1,k} = \frac{K_{i+1}^{j+1,k} + K_i^{j+1,k}}{2} \qquad\qquad K_{i-1/2}^{j+1,k} = \frac{K_i^{j+1,k} + K_{i-1}^{j+1,k}}{2}$$

in which subscripts i-1, i, and i+1 indicate the position in the finite difference mesh; superscripts k and k+1 denote the previous and current iteration levels, respectively; and superscripts j and j+1 represent the previous and current time levels, respectively. Equation (7.1) is based on a fully implicit discretization of the time derivative, and will be solved with a Picard iterative solution scheme. Notice also that the sink term, S, is evaluated at the previous time level. The mass-conservative method proposed by *Celia et al.* [1990], in which $\theta^{j+1,k+1}$ is expanded in a truncated Taylor series with respect to h about the expansion point $h^{j+1,k}$, is used in the time difference scheme of (7.1):

$$\frac{\theta_i^{j+1,k+1} - \theta_i^j}{\Delta t} = C_i^{j+1,k} \frac{h_i^{j+1,k+1} - h_i^{j+1,k}}{\Delta t} + \frac{\theta_i^{j+1,k} - \theta_i^j}{\Delta t} \tag{7.3}$$

where C_i represents the nodal value of the soil water capacity [L^{-1}]:

$$C_i^{j+1,k} = \frac{d\theta}{dh}\Big|^{j+1,k} \tag{7.4}$$

This method has been shown to provide excellent results in terms of minimizing the mass balance error. Notice that the second term on the right hand size of (7.3) is known prior to the current iteration. The first term on the right hand side of (7.3) should vanish at the end of the iteration process if the numerical solution converges. The derivation leads to the following matrix equation with matrix $[P_w]$ and vectors $\{h\}$ and $\{F_w\}$

$$[P_w]^{j+1,k} \{h\}^{j+1,k+1} = \{F_w\} \tag{7.5}$$

The symmetrical tridiagonal matrix $[P_w]$ in (7.5) has the form

$$[P_w] = \begin{vmatrix} d_1 & e_1 & 0 & & & & 0 \\ e_1 & d_2 & e_2 & 0 & & & 0 \\ 0 & e_2 & d_3 & e_3 & 0 & & 0 \\ & & \cdot & \cdot & \cdot & & \\ & & & \cdot & \cdot & \cdot & \\ 0 & & 0 & e_{N-3} & d_{N-2} & e_{N-2} & 0 \\ 0 & & & 0 & e_{N-2} & d_{N-1} & e_{N-1} \\ 0 & & & & 0 & e_{N-1} & d_N \end{vmatrix} \tag{7.6}$$

where the diagonal entries d_i and above-diagonal entries e_i of the matrix $[P_w]$, and the entries f_i of vector $\{F_w\}$, are given by

96

$$d_i = \frac{\Delta x}{\Delta t} C_i^{j+1,k} + \frac{K_{i+1}^{j+1,k} + K_i^{j+1,k}}{2\Delta x_i} + \frac{K_i^{j+1,k} + K_{i-1}^{j+1,k}}{2\Delta x_{i-1}} \qquad (7.7)$$

$$e_i = -\frac{K_i^{j+1,k} + K_{i+1}^{j+1,k}}{2\Delta x_i} \qquad (7.8)$$

$$f_i = \frac{\Delta x}{\Delta t} C_i^{j+1,k} h_i^{j+1,k} - \frac{\Delta x}{\Delta t}(\theta_i^{j+1,k} - \theta_i^j) + \frac{K_{i+1}^{j+1,k} - K_{i-1}^{j+1,k}}{2}\cos\alpha - S_i^j \Delta x \qquad (7.9)$$

The tridiagonal matrix $[P_w]$ is symmetric and therefore the below-diagonal entries are equal to the above-diagonal entries. The entries d_1, e_1, f_1, and e_{N-1}, d_N, f_N are dependent upon the prescribed boundary conditions.

7.2. Treatment of Pressure Head Boundary Conditions

If a first-type (Dirichlet) boundary condition is specified at the top or bottom of the soil profile, then the terms d_1 or d_N are equal to unity, e_1 or e_{N-1} reduce to zero, and f_1 or f_N equal to the prescribed pressure head, h_0. Some additional rearrangement of matrix $[P_w]$ is also necessary to preserve its symmetry. The appropriate entries in the second or $(N-1)$st equations containing the prescribe boundary pressure head h_0 in the left-hand side matrix must then be incorporated into the known vector on the right-hand side of the global matrix equation. When done properly, this rearrangement will restore symmetry in $[P_w]$.

7.3. Treatment of Flux Boundary Conditions

If a third-type (Neumann) boundary condition at the bottom of the profile is specified, then the individual entries are obtained by discretization of Darcy's law, i.e.,

$$q = -K\frac{\partial h}{\partial x} - K \qquad (7.10)$$

such that d_1 and f_1 in $[P_w]$ attain the values

$$d_1 = \frac{K_1^{j+1,k} + K_2^{j+1,k}}{2\Delta x_1} \tag{7.11}$$

$$f_1 = \frac{K_1^{j+1,k} + K_2^{j+1,k}}{2} + q_0^{j+1} \tag{7.12}$$

where q_0 is the prescribed bottom boundary flux [LT^{-1}] and where e_1 is described by (7.8). A similar discretization of Darcy's law is possible to incorporate flux boundary condition at the top of the soil profile. This approach, however, can quickly lead to relatively unstable solutions when the boundary fluxes at the soil surface vary strongly with time (erratic irrigation or rainfall rates). A more stable and mass-conservative solution results when the mass balance equation instead of Darcy's law is discretized.

$$\frac{\partial \theta}{\partial t} = -\frac{\partial q}{\partial x} - S \tag{7.13}$$

Discretization of (7.12) gives

$$\frac{\theta_N^{j+1,k+1} - \theta_N^{j}}{\Delta t} = -\frac{2(q_N^{j+1} - q_{N-1/2}^{j+1,k})}{\Delta x_{N-1}} - S_N^{j} \tag{7.14}$$

Expanding the time derivative on the left hand side of (7.14) as in (7.3), and using the discretized form of Darcy's law for $q_{N-1/2}$ leads to

$$d_N = \frac{\Delta x_{N-1}}{2\Delta t} C_N^{j+1,k} + \frac{K_N^{j+1,k} + K_{N-1}^{j+1,k}}{2\Delta x_{N-1}} \tag{7.15}$$

$$f_N = \frac{\Delta x_{N-1}}{2\Delta t} C_N^{j+1,k} h_N^{j+1,k} - \frac{\Delta x}{2\Delta t}(\theta_N^{j+1,k} - \theta_N^{j}) - \frac{K_N^{j+1,k} + K_{N-1}^{j+1,k}}{2}\cos\alpha - \frac{\Delta x_{N-1}}{2}S_N^{j} - q_N^{j+1} \tag{7.16}$$

where q_N is the prescribed soil surface boundary flux. Implementation of a third-type boundary condition always preserves symmetry of the matrix [P_w].

7.4. *Numerical Solution Strategy*

7.4.1. *Iterative Process*

Because of the nonlinear nature of (7.5), an iterative process must be used to obtain solutions of the global matrix equation at each new time step. For each iteration a system of linearized algebraic equations is first derived from (7.5), which, after incorporation of the boundary conditions, is solved using Gaussian elimination. The Gaussian elimination process takes advantage of the tridiagonal and symmetric features of the coefficient matrix in (7.5). After solving (7.5) the first time, the coefficients in (7.5) are re-evaluated using this first solution, and the new equations are again solved. The iterative process continues until a satisfactory degree of convergence is obtained, i.e., until at all nodes in the saturated (or unsaturated) region the absolute change in pressure head (or water content) between two successive iterations becomes less than some small value determined by the imposed absolute pressure head (or water content) tolerance. The first estimate (at zero iteration) of the unknown pressure heads at each time step is obtained by extrapolation from the pressure head values at the previous two time levels.

7.4.2. *Time Control*

Three different time discretizations are introduced in HYDRUS: (1) time discretizations associated with the numerical solution, (2) time discretizations associated with the implementation of boundary conditions, and (3) time discretizations which provide printed output of the simulation results (e.g., nodal values of dependent variables, water, solute mass balance components, and other information about the flow regime).

Discretizations 2 and 3 are mutually independent; they generally involve variable time steps as described in the input data file. Discretization 1 starts with a prescribed initial time increment, Δt. This time increment is automatically adjusted at each time level according to the following rules [*Mls*, 1982; *Šimůnek et al.*, 1992]:

a. Discretization 1 must coincide with time values resulting from time discretizations 2 and 3.
b. Time increments cannot become less than a preselected minimum time step, Δt_{min}, nor exceed a maximum time step, Δt_{max} (i.e., $\Delta t_{min} \leq \Delta t \leq \Delta t_{max}$).

c. If, during a particular time step, the number of iterations necessary to reach convergence is ≤3, the time increment for the next time step is increased by multiplying Δt by a predetermined constant >1 (usually between 1.1 and 1.5). If the number of iterations is ≥7, Δt for the next time level is multiplied by a constant <1 (usually between 0.3 and 0.9).

d. If, during a particular time step, the number of iterations at any time level becomes greater than a prescribed maximum (usually between 10 and 50), the iterative process for that time level is terminated. The time step is subsequently reset to $\Delta t/3$, and the iterative process restarted.

7.4.3. *Atmospheric Boundary Conditions and Seepage Faces*

Atmospheric boundaries are simulated by applying either prescribed head or prescribed flux boundary conditions depending upon whether equation (2.69) or (2.70) is satisfied [*Neuman*, 1974]. If (2.70) is not satisfied, boundary node *n* becomes a prescribed head boundary. If, at any point in time during the computations, the calculated flux exceeds the specified potential flux in (2.69), the node will be assigned a flux equal to the potential value and treated again as a prescribed flux boundary.

If a seepage face is considered as the lower boundary condition and if during each iteration the lower part of the soil profile is saturated then the last node is treated as a prescribed pressure head boundary with *h*=0. However, if this node is unsaturated then a prescribed flux boundary with *q*=0 is imposed at the lower boundary. Alternatively, a certain non-zero value of *hSeep* can also be specified as the limiting pressure head.

7.4.4. *Water Balance Computations*

The HYDRUS code performs water balance computations at prescribed times for several preselected subregions of the flow domain. The water balance information for each subregion consists of the actual volume of water, *V*, in that subregion, and the rate, *O* [LT^{-1}], of inflow or outflow to or from the subregion. These variables *V* and *O* are evaluated in HYDRUS by means of

$$V = \sum_e \Delta x_i \frac{\theta_i + \theta_{i+1}}{2} \tag{7.17}$$

and

$$O = \frac{V_{new} - V_{old}}{\Delta t} \tag{7.18}$$

respectively, where θ_i and θ_{i+1} are water contents evaluated at the corner nodes of element e, Δx_i is the size of the element, and V_{new} and V_{old} are volumes of water in the subregion computed at the current and previous time levels, respectively. The summation in (7.17) is taken over all elements within the subregion. Similar calculations are carried out for the mobile and immobile regions of the dual-porosity model and for the matrix and fracture regions of the dual-permeability model.

The absolute error in the mass balance of the flow domain is calculated as

$$\varepsilon_a^w = V_t - V_0 + \int_0^t T_a \, dt - \int_0^t (q_0 - q_N) \, dt \tag{7.19}$$

where V_t and V_0 are the volumes of water in the flow domain, Eq. (7.17), evaluated at times t and zero, respectively. The third term on the right-hand side of (7.19) represents the cumulative root water uptake amount, while the fourth term gives the net cumulative flux through both boundaries.

The accuracy of the numerical solution is evaluated by the relative error, ε_r^w [%], in the water mass balance as follows:

$$\varepsilon_r^w = \frac{|\varepsilon_a^w|}{\max\left(\sum_e |V_t^e - V_0^e|, \quad \int_0^t T_a \, dt + \int_0^t (|q_N| + |q_0|) \, dt \right)} 100 \tag{7.20}$$

where V_t^e and V_0^e are the volumes of water in element e at times t and zero, respectively. Note that HYDRUS does not relate the absolute error to the volume of water in the flow domain, but instead to the maximum value of two quantities. The first quantity represents the sum of the

absolute changes in water content over all elements, whereas the second quantity is the sum of the absolute values of all fluxes in and out of the flow domain.

7.4.5. *Computation of Nodal Fluxes*

Components of the Darcian flux are computed at each time level during the simulation only when the water flow and solute (or heat) transport equations are solved simultaneously. When the flow equation is being solved alone, the flux components are calculated only at selected print times. The *x*-components of the nodal fluxes are computed for each node *n* according to

$$q_1^{j+1} = -K_{1+1/2}^{j+1}\left(\frac{h_2^{j+1} - h_1^{j+1}}{\Delta x_i} + 1\right)$$

$$q_i^{j+1} = \frac{-K_{i+1/2}^{j+1}\left(\frac{h_{i+1}^{j+1} - h_i^{j+1}}{\Delta x_i} + 1\right)\Delta x_{i-1} - K_{i-1/2}^{j+1}\left(\frac{h_i^{j+1} - h_{i-1}^{j+1}}{\Delta x_{i-1}} + 1\right)\Delta x_i}{\Delta x_{i-1} + \Delta x_i} \tag{7.21}$$

$$q_N^{j+1} = -K_{N-1/2}^{j+1}\left(\frac{h_N^{j+1} - h_{N-1}^{j+1}}{\Delta x_{N-1}} + 1\right) - \frac{\Delta x_{N-1}}{2}\left(\frac{\theta_N^{j+1} - \theta_N^j}{\Delta t} + S_N^j\right)$$

7.4.6. *Water Uptake by Plant Roots*

HYDRUS considers the root zone to consist of all nodes, *n*, for which the potential root water uptake distribution, *b* (see Section 2.2), is greater than zero. The root water extraction rate is assumed to vary linearly over each element. The values of actual root extraction rate S_i in (7.1) are evaluated with (2.8). HYDRUS calculates the total rate of transpiration using the equation

$$T_a = \sum_e \Delta x_i \frac{S_i + S_{i+1}}{2} \tag{7.22}$$

in which the summation takes place over all elements within the root zone, and where S_i and S_{i+1} are the root water uptake rates evaluated at the corner nodes of element *e*.

7.4.7. *Evaluation of the Soil Hydraulic Properties*

At the beginning of a simulation, HYDRUS generates for each soil type in the flow domain a table of water contents, hydraulic conductivities, and specific water capacities from the specified set of hydraulic parameters [*Vogel*, 1987]. The values of θ_i, K_i and C_i in the table are evaluated at prescribed pressure heads h_i within a specified interval (h_a, h_b). The entries in the table are generated such that

$$\frac{h_{i+1}}{h_i} = \text{constant} \tag{7.23}$$

which means that the spacing between two consecutive pressure head values increases in a logarithmic fashion. Values for the hydraulic properties, $\theta(h)$, $K(h)$ and $C(h)$, are computed during the iterative solution process using linear interpolation between the entries in the table. If an argument h falls outside the prescribed interval (h_a, h_b), the hydraulic characteristics are evaluated directly from the hydraulic functions, i.e., without interpolation. The above interpolation technique was found to be much faster computationally than direct evaluation of the hydraulic functions over the entire range of pressure heads, except when very simple hydraulic models are used.

8. NUMERICAL SOLUTION OF THE SOLUTE TRANSPORT EQUATION

The Galerkin finite element method was used to solve the solute and heat transport equations subject to appropriate initial and boundary conditions. Since the heat transport equation (4.1) has the same mathematical form as the (linearized) solute transport equation (3.10), the numerical solution will be given here only for solute transport.

8.1. *Space Discretization*

The finite element method assumes that the dependent variable, the concentration function $c(x,t)$, can be approximated by a finite series $c'(x,t)$ of the form

$$c'(x,t) = \sum_{m=1}^{N} \phi_m(x) \, c_m(t) \tag{8.1}$$

where ϕ_m are the selected linear basis functions that fulfill the condition $\phi_m(x_n) = \delta_{nm}$, δ_{nm} is Kronecker delta ($\delta_{nm} = 1$ for $m = n$, and $\delta_{nm} = 0$ for $m \neq n$), c_m are the unknown time-dependent coefficients which represent solutions of (3.10) at the finite element nodal points, and N is the total number of nodal points. Linear basis functions have the following form:

$$\begin{aligned} \phi_1 &= 1 - \xi \\ \phi_2 &= \xi \end{aligned} \tag{8.2}$$

where ξ is the distance in the local coordinate system [-]. In the global coordinate system ξ is defined as

$$\xi = \frac{x - x_1}{\Delta x} \qquad x_1 \le x \le x_2 \tag{8.3}$$

where Δx ($= x_2 - x_1$) is the size of a finite element [L], i.e., the distance between two neighboring nodal points. The approximate solution $c'(x,t)$ converges to the correct solution $c(x,t)$ as the number of basis functions N increases.

Application of the Galerkin method which postulates that the differential operator associated with the transport equation is orthogonal to each of the N basis functions, we obtain the following system of N time-dependent differential equations with N unknown values $c_n(t)$.

$$\int_0^L \left[-\frac{\partial \theta R^1 c}{\partial t} - \theta R^2 \frac{\partial c}{\partial t} + \frac{\partial}{\partial x}\left(E\frac{\partial c}{\partial x} - Bc\right) + Fc + G \right] \phi_n \, dx = 0 \tag{8.4}$$

where, for notational convenience we have dropped the index k referring to the kth decay chain number. Integrating by parts the terms containing spatial derivatives leads to the following equation

$$\int_0^L \left[-\frac{\partial \theta R^1 c}{\partial t} - \theta R^2 \frac{\partial c}{\partial t} + Fc + G \right] \phi_n \, dx -$$
$$-\int_0^L \left(E\frac{\partial c}{\partial x} - Bc \right) \frac{\partial \phi_n}{\partial x} \, dx - q_{sL} \phi_n(L) + q_{s0} \phi_n(0) = 0 \tag{8.5}$$

where q_{s0} and q_{sL} are solute fluxes across the lower and upper boundaries, respectively. By substituting (8.1) for $c(x,t)$ we obtain

$$\sum_e \int_0^{L_e} \left[-\frac{\partial \theta R^1 c_m}{\partial t}\phi_m - \theta R^2 \frac{\partial c_m}{\partial t}\phi_m - Fc_m\phi_m + G \right] \phi_n \, dx -$$
$$-\sum_e \int_0^{L_e} \left(Ec_m \frac{\partial \phi_m}{\partial x} - Bc_m\phi_m \right) \frac{\partial \phi_n}{\partial x} \, dx - q_{sL}\phi_n(L) + q_{s0}\phi_n(0) = 0 \tag{8.6}$$

Equation (8.6) can be rewritten in matrix form as

$$\frac{d([Q^1]\{c\})}{dt} + [Q^2]\frac{d\{c\}}{dt} + [S]\{c\} = \{f\} \tag{8.7}$$

where the vector $\{c\}$ contains the unknown values of the nodal concentrations, and where

$$Q^1_{nm} = \int_0^{L_e} \theta R^1 \phi_m \phi_n dx \qquad (8.8)$$

$$Q^2_{nm} = \int_0^{L_e} \theta R^2 \phi_m \phi_n dx \qquad (8.9)$$

$$S_{nm} = \int_0^{L_e} [\, E \frac{d\phi_m}{dx} \frac{d\phi_n}{dx} - B \frac{d\phi_n}{dx} \phi_m - F \phi_m \phi_n \,] dx \qquad (8.10)$$

$$f_n = \int_0^{L_e} G\phi_n dx - q_{sL} \phi_n(L) + q_{s0} \phi_n(0) \qquad (8.11)$$

$$q_s = -\theta D \frac{\partial c'}{\partial x} + q c' \qquad (8.12)$$

In addition to the basic assumptions involving the Galerkin method, several additional assumptions are now made (*van Genuchten* [1978]). First, within each element and at a given time, the different coefficients or groups of coefficients in equations (8.8) through (8.11) (i.e., θR, θD, q, F, and G) are assumed to change linearly according to the expressions:

$$\theta R(t,x) = \sum_{m=1}^{2} \theta R(t, x_m) \phi_m(x)$$

$$E(t,x) = \sum_{m=1}^{2} E(t, x_m) \phi_m(x)$$

$$B(t,x) = \sum_{m=1}^{2} B(t, x_m) \phi_m(x) \qquad (8.13)$$

$$F(t,x) = \sum_{m=1}^{2} F(t, x_m) \phi_m(x)$$

$$G(t,x) = \sum_{m=1}^{2} G(t, x_m) \phi_m(x)$$

Because of (8.13) it is now not necessary to use numerical integration for evaluating the

coefficients from equation (8.7). Second, mass lumping will be invoked by redefining the nodal values of the time derivative in (8.4) as weighted averages over the entire flow region:

$$\frac{dc_n}{dt} = \frac{\int_0^L \theta R \frac{\partial c'}{\partial t} \phi_n dx}{\int_0^L \theta R \phi_n dx} \tag{8.14}$$

The above expansions lead to the following element matrices associated with global matrix equation (8.7). Note that $[S] = [S_1] + [S_2] + [S_3]$.

$$Q_{nm}{}^e = \int_1^2 \theta R \, \phi_m \phi_n \, dx = \frac{\Delta x}{12} \begin{vmatrix} 3\,\theta_1 R_1 + \theta_2 R_2 & \theta_1 R_1 + \theta_2 R_2 \\ \theta_1 R_1 + \theta_2 R_2 & \theta_2 R_2 + 3\,\theta_2 R_2 \end{vmatrix} \tag{8.15}$$

$$S_{nm}{}^e_1 = \int_1^2 E \frac{d\phi_m}{dx} \frac{d\phi_n}{dx} dx = \frac{1}{2\Delta x} \begin{vmatrix} E_1 + E_2 & -E_1 - E_2 \\ -E_1 - E_2 & E_2 + E_2 \end{vmatrix} \tag{8.16}$$

$$S_{nm}{}^e_2 = \int_1^2 B \frac{d\phi_n}{dx} \phi_m dx = \frac{1}{6} \begin{vmatrix} 2B_1 + B_2 & B_1 + 2B_2 \\ -2B_1 - B_2 & -B_1 - 2B_2 \end{vmatrix} \tag{8.17}$$

$$S_{nm}{}^e_3 = \int_1^2 F \phi_m \phi_n dx = \frac{\Delta x}{12} \begin{vmatrix} 3F_1 + F_2 & F_1 + F_2 \\ F_1 + F_2 & F_1 + 3F_2 \end{vmatrix} \tag{8.18}$$

$$f_n{}^e = \int_1^2 G \, \phi_n \, dx = \frac{\Delta x}{6} \begin{vmatrix} 2\,G_1 + G_2 \\ G_1 + 2\,G_2 \end{vmatrix} \tag{8.19}$$

8.2. *Time Discretization*

The Galerkin method is used only for approximating the spatial derivatives while the time derivatives are discretized by means of finite differences as follows

$$\frac{[Q^1]^{j+1}\{c\}^{j+1} - [Q^1]^j\{c\}^j}{\Delta t} + [Q^2]^{j+\varepsilon}\frac{\{c\}^{j+1} - \{c\}^j}{\Delta t} +$$

$$\varepsilon [S]^{j+1}\{c\}^{j+1} + (1-\varepsilon)[S]^j\{c\}^j = \varepsilon\{f\}^{j+1} + (1-\varepsilon)\{f\}^j \qquad (8.20)$$

where j and $j+1$ indicate previous and actual time level and Δt is time step, and where ε is a temporal weighting coefficient. Different finite difference schemes results depending upon the value of ε (=0: explicit scheme, =0.5: Crank-Nicholson scheme, =1.: fully implicit scheme). Equation (8.20) can be rewritten as:

$$[P_s]\{c\}^{j+1} = [T]\{c\}^j + \{R\} \qquad (8.21)$$

where

$$[P_s] = \frac{1}{\Delta t}\left([Q^1]^{j+1} + [Q^2]^{j+\varepsilon}\right) + \varepsilon[S]^{j+1}$$

$$[T] = \frac{1}{\Delta t}\left([Q^1]^j + [Q^2]^{j+\varepsilon}\right) - (1-\varepsilon)[S]^j \qquad (8.22)$$

$$\{R\} = \varepsilon\{f\}^{j+1} + (1-\varepsilon)\{f\}^j$$

Notice that we separated the retardation factor R into two parts, R^1 and R^2, leading to two matrices, $[Q^1]$ and $[Q^2]$, which are evaluated at different time levels. This approach was found to lead to much faster convergence when nonlinear adsorption isotherm is considered. Matrix $[Q^1]$ is evaluated at the previous and current time levels, while matrix $[Q^2]$ is evaluated using weighted averages of the current and previous nodal values of θ and R.

Higher-order approximations for the time derivative in the transport equation were derived by *van Genuchten* [1976, 1978]. The higher-order approximations may be incorporated into the transport equation by introducing time-dependent dispersion corrections as follows

$$D^- = D - \frac{q^2 \Delta t}{6\theta^2(R^1 + R^2)}$$

$$D^+ = D + \frac{q^2 \Delta t}{6\theta^2(R^1 + R^2)} \qquad (8.23)$$

where the superscripts + and - indicate evaluation at the old and the new time levels, respectively.

Evaluation of all integrals eventually leads to the following tridiagonal global matrices $[P_s]$ and $[T]$

$$[P_s] = \begin{vmatrix} d_1 & e_1 & 0 & & & & & 0 \\ b_2 & d_2 & e_2 & 0 & & & & 0 \\ 0 & b_3 & d_3 & e_3 & 0 & & & 0 \\ & & & . & & . & & \\ & & & . & & . & & \\ & & & . & & . & & \\ 0 & & 0 & b_{n-2} & d_{n-2} & e_{n-2} & 0 \\ 0 & & & 0 & b_{n-1} & d_{n-1} & e_{n-1} \\ 0 & & & & 0 & b_n & d_n \end{vmatrix} \tag{8.24}$$

with the individual entries of $[P_s]$ given in Table 8.1. In this table $\Delta x_{i-1} = x_i - x_{i-1}$, $\Delta x_i = x_{i+1} - x_i$, $\Delta x = (x_{i+1} - x_{i-1})/2$, $\Delta t = t_{j+1} - t_j$, i is the nodal index (increasing in the direction of the x-coordinate, $i=1,2,....,n$), and j is the time index. Individual entries of the vector $\{R\}$ have the following form

$$r_1 = \Delta x_{i-1}(2s_1 + s_2) + \varepsilon q_s(0,t^{j+1}) + (1-\varepsilon)q_s(0,t^j)$$
$$r_i = \Delta x_{i-1}(s_{i-1} + 2s_i) + \Delta x_i(2s_i + s_{i+1})$$
$$r_n = \Delta x_i(s_{n-1} + 2s_n) - \varepsilon q_s(L,t^{j+1}) - (1-\varepsilon)q_s(L,t^j) \tag{8.25}$$
$$s_i = \frac{1}{6}[\varepsilon G_i^{j+1} + (1-\varepsilon)G_i^j]$$

From equation (8.22) it follows that matrixes $[P_s]$ and $[T]$ are identical if the variables D^-, F, q and ε in $[P_s]$ are replaced by $-D^+$, $-F$, $-q$ and $(1-\varepsilon)$ to yield $[T]$.

Table 8.1. Values of the diagonal entries d_i, and off-diagonal entries b_i and e_i of matrix $[P_s]$ for linear finite elements.

$$d_1 = \frac{\Delta x_1}{12\Delta t}(3\theta_1 R_1 + \theta_2 R_2) + \frac{\varepsilon}{2\Delta x_1}(E_1 + E_2) + \frac{\varepsilon}{6}(2B_1 + B_2) + \frac{\varepsilon\Delta x_1}{12}(3F_1 + F_2)$$ (8.26)

$$b_i = \frac{\Delta x_{i-1}}{12\Delta t}(\theta_{i-1} R_{i-1} + \theta_i R_i) - \frac{\varepsilon}{2\Delta x_{i-1}}(E_{i-1} + E_i) - \frac{\varepsilon}{6}(2B_{i-1} + B_i) + \frac{\varepsilon\Delta x_{i-1}}{12}(F_{i-1} + F_i)$$ (8.27)

$$d_i = \frac{\Delta x_{i-1}}{12\Delta t}(\theta_{i-1} R_{i-1} + 3\theta_i R_i) + \frac{\Delta x_i}{12\Delta t}(3\theta_i R_i + \theta_{i+1} R_{i+1}) + \frac{\varepsilon}{2\Delta x_{i-1}}(E_{i-1} + E_i) + \frac{\varepsilon}{2\Delta x_i}(E_i + E_{i+1}) +$$

$$+ \frac{\varepsilon}{6}(B_{i+1} - B_{i-1}) + \frac{\varepsilon\Delta x_{i-1}}{12}(F_{i-1} + 3F_i) + \frac{\varepsilon\Delta x_i}{12}(3F_i + F_{i+1}) \qquad (i = 2,...,n-1)$$ (8.28)

$$e_i = \frac{\Delta x_i}{12\Delta t}(\theta_i R_i + \theta_{i+1} R_{i+1}) - \frac{\varepsilon}{2\Delta x_i}(E_i + E_{i+1}) + \frac{\varepsilon}{6}(2B_{i+1} + B_i) + \frac{\varepsilon\Delta x_i}{12}(F_i + F_{i+1})$$ (8.29)

$$d_N = \frac{\Delta x_{N-1}}{12\Delta t}(\theta_{N-1} R_{N-1} + 3\theta_N R_N) + \frac{\varepsilon}{2\Delta x_{N-1}}(E_{N-1} + E_N) - \frac{\varepsilon}{6}(B_{N-1} + 2B_N) + \frac{\varepsilon\Delta x_{N-1}}{12}(F_{N-1} + 3F_N)$$ (8.30)

Table 8.2. Values of the diagonal entries d_i, and off-diagonal entries b_i and e_i of matrix $[P_s]$ for linear finite elements with upstream weighting.

$$d_1 = \frac{\Delta x_1}{12\Delta t}(3\theta_1 R_1 + \theta_2 R_2) + \frac{\varepsilon}{2\Delta x_1}(E_1 + E_2) + \frac{\varepsilon}{6}[(2 + 3\alpha^+)B_1 + B_2] + \frac{\varepsilon \Delta x_1}{12}(3F_1 + F_2) \tag{8.31}$$

$$b_i = \frac{\Delta x_{i-1}}{12\Delta t}(\theta_{i-1}R_{i-1} + \theta_i R_i) - \frac{\varepsilon}{2\Delta x_{i-1}}(E_{i-1} + E_i) - \frac{\varepsilon}{6}[(2 + 3\alpha^-)B_{i-1} + B_i] + \frac{\varepsilon \Delta x_{i-1}}{12}(F_{i-1} + F_i) \tag{8.32}$$

$$d_i = \frac{\Delta x_{i-1}}{12\Delta t}(\theta_{i-1}R_{i-1} + 3\theta_i R_i) + \frac{\Delta x_i}{12\Delta t}(3\theta_i R_i + \theta_{i+1}R_{i+1}) + \frac{\varepsilon}{2\Delta x_{i-1}}(E_{i-1} + E_i) + \frac{\varepsilon}{2\Delta x_i}(E_i + E_{i+1}) +$$
$$+ \frac{\varepsilon}{6}[B_{i+1} + 3B_i(\alpha^+ + \alpha^-) - B_{i-1}] + \frac{\varepsilon \Delta x_{i-1}}{12}(F_{i-1} + 3F_i) + \frac{\varepsilon \Delta x_i}{12}(3F_i + F_{i+1}) \quad (i = 2,...,n-1) \tag{8.33}$$

$$e_i = \frac{\Delta x_i}{12\Delta t}(\theta_i R_i + \theta_{i+1}R_{i+1}) - \frac{\varepsilon}{2\Delta x_i}(E_i + E_{i+1}) + \frac{\varepsilon}{6}[(2 - 3\alpha^+)B_{i+1} + B_i] + \frac{\varepsilon \Delta x_i}{12}(F_i + F_{i+1}) \tag{8.34}$$

$$d_N = \frac{\Delta x_{N-1}}{12\Delta t}(\theta_{N-1}R_{N-1} + 3\theta_N R_N) + \frac{\varepsilon}{2\Delta x_{N-1}}(E_{N-1} + E_N) - \frac{\varepsilon}{6}[B_{N-1} + (2 - \alpha^-)B_N] + \frac{\varepsilon \Delta x_{N-1}}{12}(F_{N-1} + 3F_N) \tag{8.35}$$

8.3. Numerical Solution for Linear Nonequilibrium Solute Transport

The same solution procedure as described in Sections 8.1 and 8.2 is used here for either linear equilibrium or nonlinear (both equilibrium and nonequilibrium) solute transport. However, linear nonequilibrium transport is implemented somewhat differently. First, equation (3.9), simplified for linear adsorption, is discretized using finite differences as follows

$$
\frac{s^{t+\Delta t} - s^{t}}{\Delta t} = \varepsilon[\omega(1-f)k_s c - \omega s^k - \mu_s s^k + (1-f)\gamma]^{t+\Delta t} +
$$
$$
+ (1-\varepsilon)[\omega(1-f)k_s c - \omega s^k - \mu_s s^k + (1-f)\gamma]^t
$$

(8.36)

The new adsorbed concentration for type-2 sorption sites follows directly from (8.35):

$$
s^{t+\Delta t} = s^t \frac{2 - \Delta t(\omega + \mu_s)^t}{2 + \Delta t(\omega + \mu_s)^{t+\Delta t}} + \frac{\Delta t(1-f)[(\omega k_s c)^{t+\Delta t} + (\omega k_s c)^t + \gamma^{t+\Delta t} + \gamma^t]}{2 + \Delta t(\omega + \mu_s)^{t+\Delta t}}
$$

(8.37)

This term is incorporated directly into F and G so that they have the following values:

$$
F_*^{t+\Delta t} = F^{t+\Delta t} - \left\{ \frac{\rho\omega\Delta t(1-f)\omega k_s}{2 + \Delta t(\omega + \mu_s)} \right\}^{t+\Delta t}
$$

(8.38)

$$
G_*^{t+\Delta t} = G^{\{t+\Delta t\}} + \rho\omega^{t+\Delta t}\{s^t \frac{2 - \Delta t(\omega + \mu_s)^t}{2 + \Delta t(\omega + \mu_s)^{t+\Delta t}} + \frac{\Delta t(1-f)[(\omega k_s c)^t + \gamma^{t+\Delta t} + \gamma^t]}{2 + \Delta t(\omega + \mu_s)^{t+\Delta t}}\}
$$

(8.39)

where $F_*^{t+\Delta t}$ and $G_*^{t+\Delta t}$ are the values of parameters F and G for linear nonequilibrium solute transport, and $F^{t+\Delta t}$ and $G^{t+\Delta t}$ are the original values of F and G. The above procedure avoids having to solve two simultaneous equations for linear nonequilibrium transport. Once the transport equation with the modified F and G parameters is solved using the methods discussed earlier to yield the concentration $c^{t+\Delta t}$, equation (8.37) is used to update the adsorbed concentration $s^{t+\Delta t}$.

For physical nonequilibrium (dual-porosity) transport, equation (3.32), simplified for linear adsorption, is discretized using finite differences as follows

113

$$A \frac{c_{im}^{t+\Delta t} - c_{im}^{t}}{\Delta t} = \varepsilon [\omega(c - c_{im}) - Bc_{im} + E]^{t+\Delta t} + (1-\varepsilon)[\omega(c - c_{im}) - Bc_{im} + E]^{t}$$

where

$$A = \theta_{im} + (1-f)\rho k_s \tag{8.40}$$
$$B = \theta_{im}\mu_w + (1-f)\rho k_s \mu_s$$
$$E = \theta_{im}\gamma_w + (1-f)\rho \gamma_s$$

The new concentration in the immobile region follows directly from (8.39):

$$c_{im}^{t+\Delta t} = c_{im}^{t} \frac{2A - \Delta t(\omega + B)^{t}}{2A + \Delta t(\omega + B)^{t+\Delta t}} + \frac{\Delta t[(\omega\, c_{im})^{t+\Delta t} + (\omega c_{im})^{t} + E^{t+\Delta t} + E^{t}]}{2A + \Delta t(\omega + B)^{t+\Delta t}} \tag{8.41}$$

Similarly as for the chemical nonequilibrium case, equation (8.40) is incorporated directly into F and G to obtain following values:

$$F_*^{t+\Delta t} = F^{t+\Delta t} - \left\{ \frac{\omega\Delta t\omega}{2A + \Delta t(\omega + B)} \right\}^{t+\Delta t} \tag{8.42}$$

$$G_*^{t+\Delta t} = G^{\{t+\Delta t\}} + \omega^{t+\Delta t} \{c_{im}^{t} \frac{2A - \Delta t(\omega + B)^{t}}{2A + \Delta t(\omega + B)^{t+\Delta t}} + \frac{\Delta t[(\omega c)^{t} + E^{t+\Delta t} + E^{t}]}{2A + \Delta t(\omega + B)^{t+\Delta t}} \} \tag{8.43}$$

Numerical approaches very similar to those described above for the chemical nonequilibrium model were used also for the attachment/detachment model for colloid transport.

8.4. *Numerical Solution Strategy*

8.4.1. *Solution Process*

The solution process at each time step proceeds as follows. First, an iterative procedure is used to obtain the solution of the Richards' equation (2.1) (see Section 7.4.1). After achieving convergence, the solution of the transport equation (8.7) is implemented. This is done by first

114

determining the nodal values of the fluid flux from nodal values of the pressure head by applying Darcy's law. Nodal values of the water content and the fluid flux at the previous time level are already known from the solution at the previous time step. Values for the water content and the fluid flux are subsequently used as input to the transport equations (first for heat transport and then for solute transport), leading to a system of linear algebraic equations given by (8.7). The structure of the final set of equations depends upon the value of the temporal weighing factor, ε. The explicit ($\varepsilon = 0$) and fully implicit ($\varepsilon = 1$) schemes for the transport equation require that the global matrices $[P_s]$ and $[T]$ and the vector $\{R\}$ be evaluated at only one time level (the previous or current time level). All other schemes require evaluation at both time levels. Also, all schemes except for the explicit formulation ($\varepsilon = 0$) lead to an asymmetric banded matrix $[P_s]$.

Since the heat transport equation is linear, there is no need for an iterative solution process for heat flow. The same is true for the transport of solutes undergoing only linear sorption reactions. On the other hand, iteration is needed when a nonlinear reaction between the solid and liquid phase is considered. The iterative procedure for solute transport is very similar to that for water flow. The nonlinear coefficients in (8.7) are then re-evaluated at each iteration, and the new equations solved using results of the previous iteration. The iterative process continues until a satisfactory degree of convergence is obtained, i.e., until at all nodes the absolute change in concentration between two successive iterations becomes less than some small value determined by the imposed relative and absolute concentration tolerances.

The solution process for the carbon dioxide and major ion chemistry modules proceeds in a very similar manner. The nodal values of water content, velocity and temperature, obtained from solutions of the water flow and heat transport equations, are used to evaluate the coefficients of the discretized CO_2 transport equation (5.6). The CO_2 transport equation (5.6) is not linear because of the dependency of the production term P on the concentration of CO_2. To avoid the need to iterate, we evaluated this term using CO_2 concentrations from the previous time step. Finally, multicomponent solute transport was solved based on knowledge of the water contents, flow velocities, temperatures and CO_2 concentrations from the previous solution. The solution of the multicomponent chemical system and its coupling with solute transport is given in *Šimůnek et al.* [1996]. Water flow was considered to be invariant with respect to temperature, CO_2 and solute transport, while heat transport was similarly considered to be invariant with respect to both CO_2 and solute transport. Finally CO_2 transport was assumed to be independent of multicomponent solute transport. These assumptions make it possible to solve the various processes sequentially, rather than needing to solve all equations simultaneously.

8.4.2. *Upstream Weighted Formulation*

Upstream weighing is provided as an option in the HYDRUS to minimize some of the problems with numerical oscillations when relatively steep concentration fronts are being simulated. For this purpose the fourth (flux) term of equation (8.4) is not weighted using regular linear basis functions ϕ_n, but instead with the nonlinear functions ϕ_n^u

$$\phi_1^u = \phi_1 - 3\alpha^w \phi_1 \phi_2$$
$$\phi_2^u = \phi_2 + 3\alpha^w \phi_1 \phi_2 \tag{8.44}$$

where α_i^w is a weighing factor associated with the length of the element size. The weighing factors are evaluated using the equation of *Christie et al.* [1976]:

$$\alpha^w = \coth(\frac{uL}{2D}) - \frac{2D}{uL} \tag{8.45}$$

where *u, D* and *L* are the flow velocity, dispersion coefficient and length associated with side *i*. The weighing functions ϕ^u ensure that relatively more weight is placed on the flow velocities of nodes located at the upstream side of an element. Evaluating the integrals in (8.17) shows that the following terms must replace the entries of the global matrix S_{nm}:

$$S_{nm}{}^e{}_2 = \int_1^2 B \frac{d\varphi_n}{dx} \phi_m dx = \frac{1}{6} \begin{vmatrix} B_1(2+3\alpha^w) + B_2 & B_1 + B_2(2-3\alpha^w) \\ -B_1(2+3\alpha^w) - B_2 & -B_1 - B_2(2-3\alpha^w) \end{vmatrix} \tag{8.46}$$

The coefficients of matrix $[P_s]$ (8.24) for upstream weighting formulation are given in Table 8.2.

8.4.3. *Reverse Back-Step Particle Tracking*

The reverse back-step particle tracking method is another approach to stabilize numerical solutions of the convective-dispersive equation. A two-step procedure was followed for the mixed Lagrangian-Eulerian approach [*Molz*, 1981]. First, convective transport is considered using a Lagrangian approach in which the Lagrangian concentrations are estimated from particle

trajectories. Subsequently, all other processes including sinks and sources are modeled using the standard Eulerian approach involving the finite element method, thus leading to the final concentrations.

The single-step reverse particle tracking method [*Molz*, 1981] allows the initial position of particles arriving at the end of a time step at fixed nodal points to be calculated at each time step using

$$x_{n'} = x_n - \int_{t_k}^{t_{k+1}} v^* \, dt$$
(8.47)

where v^* represents the pore-water velocity (v/R) which accounts for all retardation processes. This equation states that a particle leaving location $x_{n'}$ at time t_k will reach the grid point location z_n exactly at time t_{k+1}. The concentration at location $x_{n'}$ at time t_k is then used in the discretized transport equation. The particle tracking method is used only for the transport of major ions.

8.4.4. *Mass Balance Calculations*

The total amount of mass in the entire flow domain, or in a preselected subregion, is given by

$$M = \sum_e \int_e (\theta c + a_v g + \rho s) dx = \sum_e \int_e [(\theta + a_v k_g + \rho f \frac{k_s c^{\beta-1}}{1 + \eta c^{\beta}}) c + \rho s^k] dx$$
(8.48)

where summation is taken over all elements within the specified region. The equations in this section pertain only to the equilibrium or chemical nonequilibrium models; the mass balance equations for physical nonequilibrium transport are very similar as those for chemical nonequilibrium. Similar calculations are carried out for the mobile and immobile regions of the dual-porosity model and for the matrix and fracture regions of the dual-permeability model.

The cumulative amounts M^0 and M^1 of solute removed from the flow region by zero- and first-order reactions, respectively, are calculated as follows

$$M^1 = \int_0^t \sum_e \int_e \left\{ \left[(\mu_w + \mu_w')\theta + (\mu_s + \mu_s')\rho f \frac{k_s c^{\beta-1}}{1+\eta c^\beta} + (\mu_g + \mu_g')a_v k_g \right]c + \right.$$
$$\left. + (\mu_s + \mu_s')\rho s^k \right\} dx\, dt \qquad (8.49)$$

$$M_1^0 = -\int_0^t \sum_e \int_e (\gamma_{w,1}\theta + \gamma_{s,1}\rho + \gamma_{g,1}\, a_v)\, dx\, dt$$

$$M_k^0 = -\int_0^t \sum_e \int_e \left[(\mu_{w,k-1}'\,\theta + \mu_{s,k-1}'\,\rho f \frac{k_{s,k-1}\, c_{k-1}^{\beta_{k-1}-1}}{1+\eta_{k-1}\, c_{k-1}^{\beta_{k-1}}} + \mu_{g,k-1}'\, a_v\, k_{g,k-1})c_{k-1} + \right. \qquad (8.50)$$
$$\left. + \mu_{s,k-1}'\, \rho\, s_{k-1}^k + \gamma_{w,k}\, \theta + \gamma_{s,k}\, \rho + \gamma_{g,k}\, a_v \right.$$

whereas the cumulative amount, M_r, of solute taken up by plant roots is given by

$$M_r = \int_0^t \sum_{e_R} \int_e S\, c_r\, dx\, dt \qquad (8.51)$$

where e_R represents the elements making up the root zone.

When the major ion chemistry module is considered, the total amount of mass in the entire flow domain, or in a preselected subregion, in solvent (M_l), mineral phase (M_p), and surface species (M_s), is given by

$$M_l = \sum_e \int_e \theta c\, dx = \sum_e \Delta x_i \frac{\theta_i c_i + \theta_{i+1} c_{i+1}}{2}$$

$$M_p = \sum_e \int_e \rho \bar{c}\, dx = \sum_e \Delta x_i \frac{\rho_i \bar{c}_i + \rho_{i+1} \bar{c}_{i+1}}{2} \qquad (8.52)$$

$$M_s = \sum_e \int_e \rho \hat{c}\, dx = \sum_e \Delta x_i \frac{\rho_i \hat{c}_i + \rho_{i+1} \hat{c}_{i+1}}{2}$$

where θ_i, θ_{i+1}, ρ_i, ρ_{i+1}, c_i, c_{i+1}, $\bar{c}_i$, $\bar{c}_{i+1}$, $\hat{c}_i$, and $\hat{c}_{i+1}$ represent, respectively, water contents, bulk densities and aqueous, mineral phase and surface concentrations evaluated at the corner nodes of element e. The summation is taken over all elements within the specified region. The total amount of solute in the entire flow domain, M_T [ML^{-1}], is then calculated as

$$M_T = M_l + M_p + M_s \tag{8.53}$$

Finally, when all boundary material fluxes, decay reactions, and root uptake mass fluxes have been computed, the following mass balance should hold for the flow domain as a whole:

$$M_t - M_0 = + \int_0^t q_{s0}\, dt - \int_0^t q_{sL}\, dt - M^0 - M^1 - M_r \tag{8.54}$$

where M_t and M_0 are the amounts of solute in the flow region at times t and zero, respectively, as calculated with (8.48). The difference between the left- and right-hand sides of (8.54) represents the absolute error, ε_a^c, in the solute mass balance. Similarly as for water flow, the accuracy of the numerical solution for solute transport is evaluated by using the relative error, ε_r^c [%], in the solute mass balance as follows

$$\varepsilon_r^c = \frac{100\,|\varepsilon_a^c|}{\max\left(\sum_e |M_t^e - M_0^e|,\ |M^0| + |M^1| + |M_r| + \int_0^t (|q_{s0}| + |q_{sL}|)\, dt\right)} \tag{8.55}$$

where M_0^e and M_t^e are the amounts of solute in element e at times 0 and t, respectively. Note again that HYDRUS does not relate the absolute error to the total amount of mass in the flow region. Instead, the program uses as a reference the maximum value of (1) the absolute change in element concentrations as summed over all elements, and (2) the sum of the absolute values of all cumulative solute fluxes across the flow boundaries including those resulting from sources and sinks in the flow domain.

The total amount of heat energy in the entire flow domain, or in a preselected subregion, is given by

$$W = \sum_e \int_e (C_n\theta_n + C_o\theta_o + C_w\theta + C_g a_v)T^A dx \tag{8.56}$$

where T^A is the absolute temperature [K]. The summation is again taken over all elements within

119

the specified region.

Total amount of carbon dioxide, M_{CO} [L], in the flow domain or in a preselected subregion, is given by

$$M_{CO} = \sum_e \int_e (\theta_w c_w + \theta_a c_a) dx = \sum_e \Delta x_i \frac{c_{a_i}(\theta_{a_i} + K_{CO2_i} R T_i \theta_{w_i}) + c_{a_{i+1}}(\theta_{a_{i+1}} + K_{CO2_{i+1}} R T_{i+1} \theta_{w_{i+1}})}{2} \quad (8.57)$$

The absolute error in the carbon dioxide mass balance ε_a^{CO} at time t is given by

$$\varepsilon_a^{CO} = M_{CO}^t - M_{CO}^0 - \int_0^t (q_0^{CO} - q_L^{CO} + P - S c_w)\, dt \quad (8.58)$$

where M_{CO}^0 and M_{CO}^t are the amounts of carbon dioxide in the flow region at times zero and t respectively, while the integral represents the amount of carbon dioxide added/removed from the flow region by boundary fluxes, CO_2 production and CO_2 root uptake.

8.4.5. *Oscillatory Behavior*

Numerical solutions of the transport equation often exhibit oscillatory behavior and/or excessive numerical dispersion near relatively sharp concentration fronts. These problems can be especially serious for convection-dominated transport characterized by small dispersivities. One way to partially circumvent numerical oscillations is to use upstream weighing as discussed in Section 8.4.2. Undesired oscillations can often be prevented also by selecting an appropriate combination of space and time discretizations. Two dimensionless numbers may be used to characterize the space and time discretizations. One of these is the grid Peclet number, Pe^e, which defines the predominant type of the solute transport (notably the ratio of the convective and dispersive transport terms) in relation to coarseness of the finite element grid:

$$Pe^e = \frac{q \Delta x}{\theta D} \quad (8.59)$$

where Δx is the characteristic length of a finite element. The Peclet number increases when the convective part of the transport equation dominates the dispersive part, i.e., when a relatively steep concentration front is present. To achieve acceptable numerical results, the spatial discretization must be kept relatively fine to maintain a low Peclet number. Numerical

oscillations can be virtually eliminated when the local Peclet numbers do not exceed about 5. However, acceptably small oscillations may be obtained with local Peclet numbers as high as 10 [*Huyakorn and Pinder*, 1983]. Undesired oscillations for higher Peclet numbers can be effectively eliminated by using upstream weighing (see Section 8.4.2).

A second dimensionless number which characterizes the relative extent of numerical oscillations is the Courant number, Cr^e. The Courant number is associated with the time discretization as follows

$$Cr^e = \frac{q\Delta t}{\theta R \Delta x} \tag{8.60}$$

Three stabilizing options are used in HYDRUS to avoid oscillations in the numerical solution of the solute transport equation [*Šimůnek and van Genuchten*, 1994]. One option is upstream weighing (see Section 8.4.2), which effectively eliminates undesired oscillations at relatively high Peclet numbers. A second option for minimizing or eliminating numerical oscillations uses the criterion developed by *Perrochet and Berod* [1993]

$$Pe \bullet Cr \leq \omega_s \quad (= 2) \tag{8.61}$$

where ω_s is the performance index [-]. This criterion indicates that convection-dominated transport problems having large *Pe* numbers can be safely simulated provided *Cr* is reduced according to (8. 60) [*Perrochet and Berod*, 1993]. When small oscillations in the solution can be tolerated, ω_s can be increased to about 5 or 10.

A third stabilization option implemented in HYDRUS also utilizes criterion (8.60). However, instead of decreasing *Cr* to satisfy equation (8.56), this option introduces artificial dispersion to decrease the Peclet number. The amount of additional longitudinal dispersion, D_L [L], is given by [*Perrochet and Berod*, 1993]

$$D_L{}^- = \frac{|q|\Delta t}{R\theta\omega_s} - D_L - \frac{\theta D_w \tau}{|q|} \tag{8.62}$$

The maximum permitted time step is calculated for all three options, as well as with the additional requirement that the Courant number must remain less than or equal to 1. The time

step calculated in this way is subsequently used as one of the time discretization rules (rule No. B) discussed in section 7.4.2.

9. PARAMETER OPTIMIZATION

Parameter optimization is an indirect approach for the estimation of soil hydraulic and/or solute transport parameters from transient flow and/or transport data. Inverse methods are typically based upon the minimization of a suitable objective function, which expresses the discrepancy between the observed values and the predicted system response. Soil hydraulic properties for this purpose are assumed to be described by an analytical model with unknown parameter values (see Section 2.3). The system response is represented by a numerical solution of the flow equation, augmented with the parameterized hydraulic functions, selected transport parameters, and suitable initial and boundary conditions. Initial estimates of the optimized system parameters are then iteratively improved during the minimization process until a desired degree of precision is obtained. This methodology was originally applied to one-step and multi-step column outflow data generated in the laboratory [see for example *Kool et al.*, 1985; *van Dam et al.*, 1994], and laboratory or field transport data during steady-state water flow [*van Genuchten*, 1981; *Toride et al.*, 1995]. HYDRUS now implements parameter optimization also for the estimation of the solute transport and reaction parameters from transient water flow and solute transport experiments.

9.1. *Definition of the Objective Function*

The objective function Φ to be minimized during the parameter estimation process may be defined as [*Šimůnek et al.*, 1998]:

$$
\begin{aligned}
\Phi(b,q,p) = &\sum_{j=1}^{m_q} v_j \sum_{i=1}^{n_{qj}} w_{i,j}[q_j^*(x,t_i) - q_j(x,t_i,b)]^2 + \\
&\sum_{j=1}^{m_p} \overline{v_j} \sum_{i=1}^{n_{pj}} \overline{w}_{i,j}[p_j^*(\theta_i) - p_j(\theta_i,b)]^2 + \\
&\sum_{j=1}^{n_b} \hat{v}_j[b_j^* - b_j]^2
\end{aligned}
\tag{9.1}
$$

where the first term on the right-hand side represents deviations between measured and calculated space-time variables, such as pressure heads, water contents, and/or concentrations at different locations and/or times in the flow domain, or actual or cumulative fluxes versus time across a certain boundary. Table 9.1 at the end of this chapter lists various options for defining

the first term of Eq. (9.1) for the different equilibrium and nonequilibrium water flow and solute transport models. In the first term, m_q is the number of different sets of measurements, n_{qj} is the number of measurements in a particular measurement set, $q_j^*(\boldsymbol{x}, t_i)$ represents specific measurements at time t_i for the jth measurement set at location $\boldsymbol{x}(r, z)$, $q_j(\boldsymbol{x}, t_i, \boldsymbol{b})$ are the corresponding model predictions for the vector of optimized parameters $\boldsymbol{b}$ (e.g., θ_r, θ_s, α, n, K_s, D_l, $k_{g,k}$, ...), and v_j and $w_{i,j}$ are weights associated with a particular measurement set or point, respectively. The second term of (9.1) represents differences between independently measured and predicted soil hydraulic properties (e.g., retention, $\theta(h)$ and/or hydraulic conductivity, $K(\theta)$ or $K(h)$ data), while the terms m_p, n_{pj}, $p_j^*(\theta_i)$, $p_j(\theta_i, \boldsymbol{b})$, $\overline{v}_j$ and $\overline{w}_{i,j}$ have similar meanings as for the first term but now for the soil hydraulic properties. The last term of (9.1) represents a penalty function for deviations between prior knowledge of the soil hydraulic parameters, b_j^*, and their final estimates, b_j, with n_b being the number of parameters with prior knowledge and $\hat{v}_j$ representing pre-assigned weights. Estimates, which make use of prior information (such as those used in the third term of (9.1)) are known as Bayesian estimates. We note that the covariance (weighting) matrices, which provide information about the measurement accuracy, as well as any possible correlation between measurement errors and/or parameters, are assumed to be diagonal in this study. The weighting coefficients v_j, which minimize differences in weighting between different data types because of different absolute values and numbers of data involved, are given by [*Clausnitzer and Hopmans*, 1995]:

$$v_j = \frac{1}{n_j \sigma_j^2} \tag{9.2}$$

which causes the objective function to become the average weighted squared deviation normalized by the measurement variances σ_j^2.

9.2. *Marquardt-Levenberg Optimization Algorithm*

Minimization of the objective function Φ is accomplished by using the Levenberg-Marquardt nonlinear minimization method (a weighted least-squares approach based on Marquardt's maximum neighborhood method) [*Marquardt*, 1963]. This method combines the Newton and steepest descend methods, and generates confidence intervals for the optimized parameters. The method was found to be very effective and has become a standard in nonlinear least-squares fitting among soil scientists and hydrologists [*van Genuchten*, 1981; *Kool et al.*,

1985, 1987].

9.3. *Statistics of the Inverse Solution*

As part of the inverse solution, HYDRUS produces a correlation matrix, which specifies degree of correlation between the fitted coefficients. The correlation matrix quantifies changes in model predictions caused by small changes in the final estimate of a particular parameter, relative to similar changes as a result of changes in the other parameters. The correlation matrix reflects the nonorthogonality between two parameter values. A value of ±1 suggests a perfect linear correlation whereas 0 indicates no correlation at all. The correlation matrix may be used to select which parameters, if any, are best kept constant in the parameter estimation process because of high correlation.

An important measure of the goodness of fit is the r^2 value for regression of the observed, $\hat{y}_i$, versus fitted, $y_i(\boldsymbol{b})$, values:

$$r^2 = \frac{\left[\sum w_i \ \hat{y}_i \ y_i - \dfrac{\sum \hat{y}_i \sum y_i}{\sum w_i} \right]^2}{\left[\sum w_i \hat{y}_i^2 - \dfrac{(\sum \hat{y}_i)^2}{\sum w_i} \right] \left[\sum y_i^2 - \dfrac{(\sum y_i)^2}{\sum w_i} \right]} \tag{9.3}$$

The r^2 value is a measure of the relative magnitude of the total sum of squares associated with the fitted equation; a value of 1 indicates a perfect correlation between the fitted and observed values.

HYDRUS provides additional statistical information about the fitted parameters such as the mean, standard error, T-value, and the lower and upper confidence limits (given in output file FIT.OUT). The standard error, s(b_j), is estimated from knowledge of the objective function, the number of observations, the number of unknown parameters to be fitted, and an inverse matrix [*Daniel and Wood*, 1971]. The T-value is obtained from the mean and standard error using the equation

$$T = \frac{b_j}{s(b_j)} \tag{9.4}$$

The values for T and s(b_j) provide absolute and relative measures of the deviations around the mean. HYDRUS also specifies the upper and lower bounds of the 95% confidence level around

each fitted parameter b_j. It is desirable that the real value of the target parameter always be located in a narrow interval around the estimated mean as obtained with the optimization program. Large confidence limits indicate that the results are not very sensitive to the value of a particular parameter.

Finally, because of possible problems related to convergence and parameter uniqueness, we recommend to routinely rerun the program with different initial parameter estimates to verify that the program indeed converges to the same global minimum in the objective function. This is especially important for field data sets, which often exhibit considerable scatter in the measurements, or may cover only a narrow range of soil water contents, pressure heads, and/or concentrations. Whereas HYDRUS will not accept initial estimates that are out of range, it is ultimately the user's responsibility to select meaningful initial estimates.

Comprehensive reviews of issues related to inverse parameter estimation were recently given by *Hopmans and Šimůnek* [1999], *Šimůnek and Hopmans* [2002], *Hopmans et al.* [2002], and *Šimůnek et al.* [2002].

Table 9.1. Definition of the objective function for different water flow and solute transport models.

Code (.iConcType)	Location	X	Y	Definition of Y
0	1	Time	Cumulative surface flux	W1-W2: cum(q_{top}) W3: cum(q_{top})=cum[$q_m(1-w)+q_f w$]
	2	Time	Cumulative bottom flux	W1-W2: cum(q_{bottom}) W3: cum(q_{bottom})=cum[$q_m(1-w)+q_f w$]
	3	Time	Cumulative surface matrix flux	W3: cum($q_{M,top}$)=cum[$q_m(1-w)$]
	4	Time	Cumulative surface fracture flux	W3: cum($q_{F,top}$)=cum[$q_f w$]
	5	Time	Cumulative bottom matrix flux	W3: cum($q_{M,bottom}$)=cum[$q_m(1-w)$]
	6	Time	Cumulative bottom fracture flux	W3: cum($q_{F,bottom}$)=cum[$q_f w$]
1	iObs	Time	Pressure head at observation node iObs (W2: mobile zone; W3: matrix)	W1: $h(iObs)$ W2: $h_{mo}(iObs)$ W3: $h_m(iObs)$
	-iObs	Time	Fracture pressure head at observation node iObs	W3: $h_f(iObs)$
2	iObs	Time	Water content at observation node iObs	W1: $\theta(iObs)$ W2: $\theta(iObs)=\theta_{mo}(iObs)+\theta_{im}(iObs)$ W3: $\theta(iObs)=w\theta_f(iObs)+(1-w)\theta_m(iObs)$
	-iObs	Time	Fracture water content at observation node iObs	W3: $\theta_F(iObs)=w\theta_f(iObs)$
	nObs+iObs	Time	Matrix water content at observation node iObs	W3: $\theta_M(iObs)=(1-w)\theta_m(iObs)$
	0	Time	Volume of water in the soil profile	W1: $W = \dfrac{1}{L}\displaystyle\int_{Bottom}^{Top}\theta dz$ W2: $W = \dfrac{1}{L}\displaystyle\int_{Bottom}^{Top}\left(\theta_m + \theta_{im}\right)dz$

				W3: $W = \dfrac{1}{L} \displaystyle\int_{Bottom}^{Top} \left[w\theta_f + (1-w)\theta_m \right] dz$
	-iLay	Time	Volume of water in the *iLay* subregion	W1: $W_i = \dfrac{1}{L_i} \displaystyle\int_{z_{i,Bottom}}^{z_{i,Top}} \theta\, dz$ W2: $W_i = \dfrac{1}{L_i} \displaystyle\int_{z_{i,Bottom}}^{z_{i,Top}} (\theta_m + \theta_{im})\, dz$
	-(nObs+iLay)	Time	Volume of water in the *iLay* subregion	W3: $W_i = \dfrac{1}{L_i} \displaystyle\int_{z_{i,Bottom}}^{z_{i,Top}} \left[w\theta_f + (1-w)\theta_m \right] dz$
3	1	Time	Surface Flux	W1-W2: q_{top} W3: $q_{top} = q_m(1-w) + q_f w$
	2	Time	Bottom Flux	W1-W2: q_{bottom} W3: $q_{bottom} = q_m(1-w) + q_f w$
	3	Time	Surface Matrix Flux	W3: $q_{M,top} = q_m(1-w)$
	4	Time	Surface Fracture Flux	W3: $q_{F,top} = q_f w$
	5	Time	Bottom Matrix Flux	W3: $q_{M,bottom} = q_m(1-w)$
	6	Time	Bottom Fracture Flux	W3: $q_{F,bottom} = q_f w$
4.0	0	Time	Solute mass in the transport domain	
4.0	*iObs*	Time	Liquid resident concentration at observation node *iObs* (W2: mobile zone; W3: matrix)	S1-S4: $c(iObs)$ S5-S6: $c_{mo}(iObs)$ S7-S9: $c_m(iObs)$
4.0	*-iObs*	Time	Liquid resident concentration of the second solute at observation node *iObs*	S1-S4: $c_2(iObs)$ S5-S6: $c_{2,mo}(iObs)$
4.1	0	Time	Logarithm of the solute mass in the transport domain	
4.1	*iObs*	Time	Logarithm of the liquid resident	S1-S4: $\log[c(iObs)]$

			concentration at observation node *iObs*	S5-S6: $\log[c_{mo}(iObs)]$
	iObs	Time	Liquid resident fracture concentration at observation node *iObs*	S7-S9: $c_f(iObs)$
4.1	*-iObs*	Time	Logarithm of the liquid resident concentration of the second solute at observation node *iObs*	S1-S4: $\log[c_2(iObs)]$ S5-S6: $\log[c_{2,mo}(iObs)]$
4.2	*iObs*	Time	S1-S6: Flux concentration at the observation node *iObs* S7-S9: Bottom flux concentration	S1-S4: $c_f(iObs)=c-\dfrac{D\theta}{q}\dfrac{\partial c}{\partial z}$ S5-S6: $c_{f,mo}(iObs)=c_{mo}-\dfrac{D_{mo}\theta_{mo}}{q_{mo}}\dfrac{\partial c_{mo}}{\partial z}$ S7-S9: $\dfrac{wc_f q_f+(1-w)c_m q_m}{wq_f+(1-w)q_m}$
4.3	*iObs*	Time	Total solute mass at observation node *iObs*	S1: $c(\theta+\rho K_d)$ S2: $c\theta+\rho s^k$ S3: $c(\theta+f_e\rho K_d)+\rho s^k$ S4: $c\theta+\rho s_1^k+\rho s_2^k$ S5: $c_{mo}(\theta_{mo}+f_{mo}\rho K_d)+c_{im}[\theta_{im}+(1-f_{mo})\rho K_d]$ S6: $c_{mo}(\theta_{mo}+f_{mo}f_{em}\rho K_d)+f_{mo}\rho s_{mo}^k+$ $\quad+c_{im}[\theta_{im}+(1-f_{mo})\rho K_d]$ S7: $w[c_f(\theta_f+\rho K_{df})]+(1-w)[c_m(\theta_m+\rho K_{dm})]$ S8: $w[c_f(\theta_f+f_f\rho K_{df})+\rho s_f^k]+$ $\quad(1-w)[c_m(\theta_m+f_m\rho K_{dm})+\rho s_m^k]$ S9:

				$w\left[c_f\left(\theta_f+\rho K_{df}\right)\right]+\left(1-w\right)$ $\left[c_{m,mo}\left(\theta_{m,mo}+f_{mo}\rho K_{dm}\right)+c_{m,im}\left(\theta_{m,im}+\left(1-f_{mo}\right)\rho K_{dm}\right)\right]$ Only for linear and isothermal transport
4.4	*iObs*	Time	Liquid resident concentration at observation node *iObs* for the dual-porosity model	S5-S6: $c(iObs)=\dfrac{c_{mo}\theta_{mo}+c_{im}\theta_{im}}{\theta_{mo}+\theta_{im}}$ S7-S9: $c(iObs)=\dfrac{wc_f\theta_f+(1-w)c_m\theta_m}{w\theta_f+(1-w)\theta_m}$
5	*iMat*	h	Water content, θ, at pressure head, *h*, for soil material *iMat*	$\theta(h)$
6	*iMat*	h	Hydraulic conductivity, *K*, at pressure head, *h*, for soil material *iMat*	$K(h)$
7	*iMat*		α	Retention curve parameter α for soil material *iMat*
8	*iMat*		*n*	Retention curve parameter *n* for soil material *iMat*
9	*iMat*		θ_r	Residual water content θ_r for soil material *iMat*
10	*iMat*		θ_s	W1: Saturated water content θ_s for soil material *iMat* W2: $\theta_s=\theta_{sm}+\theta_{sim}$ W3: $\theta_s=w\theta_{sf}+(1-w)\theta_{sm}$
11	*iMat*		K_s	W1-W2: Saturated hydraulic conductivity K_s for soil material *iMat* W3: $K_s=wK_{sf}+(1-w)K_{sm}$
12	*PLevel*	x	$h(x)$	W1-W2: Pressure head *h* (h_{mo}) at depth *x* at print time *PLevel* W3: Fracture pressure head h_f
13	*PLevel*	x	$\theta(x)$	W1: Water content θ at depth *x* at print time *PLevel* W2: $\theta=\theta_{mo}+\theta_{im}$ W3: $\theta=w\theta_f+(1-w)\theta_m$
14.0	*PLevel*	x	$c(x)$	S1-S6: Resident liquid concentration *c* at depth *x* at print time *PLevel*

				S7-S9: Resident liquid concentration c_f in the fracture domain at depth x at print time *PLevel*
14.1	*PLevel*	x	$\log[c(x)]$	S1-S6: Logarithm of the resident liquid concentration c at depth x at the print time *PLevel* S7-S9: Resident liquid concentration c in the matrix at depth x at print time *PLevel*
14.2	*PLevel*	x	$c(x)$	S1-S6: Flux concentration c at depth x at print time *PLevel* S7-S9: not implemented
14.3	*PLevel*	x	Total solute mass at depth x at print time *PLevel*	See 4.3 above for definitions
14.4	*PLevel*	x	Liquid resident concentration at depth x at print time *PLevel*	See 4.4 above for definitions
15	*PLevel*	x	Total sorbed concentration at depth x at print time *PLevel*	s_1+s_2 (usually used for attached and strained colloids)

S1: Uniform transport model
S2: One kinetic site model
S3: Two-site model
S4: Two kinetic sites model
S5: Dual-porosity model
S6: Dual-porosity model with one kinetic site
S7: Dual-permeability model
S8: Dual-permeability model with two-site model
S9: Dual-permeability model with immobile region in the matrix
W1: Uniform water flow model
W2: Dual-porosity model
W3: Dual-permeability model

10. PROBLEM DEFINITION

10.1. *Construction of Finite Element Mesh*

The finite element mesh is constructed by dividing the soil profile into linear elements whose sizes are defined by the *x*-coordinates of the nodes that form the element corners. Neighboring elements should have approximately the same size. The ratio of the sizes of two neighboring elements is not recommended to exceed about 1.5. The nodes are numbered sequentially from 1 to *NumNP* (total number of nodes) from the bottom of the soil profile to the soil surface.

The element dimensions must be adjusted to a particular problem. They should be made relatively small at locations where large hydraulic gradients are expected. Such a region is usually located close to the soil surface where highly variable meteorological factors can cause rapid changes in the soil water content and corresponding pressure heads. Therefore, it is usually recommended to use relatively small elements near the soil surface, and gradually larger sizes with depth. The element dimensions are also dependent on soil hydraulic properties. Coarse textured soils generally require a finer discretization than fine-textured soils (loams, clays). No special restrictions are necessary to facilitate the soil root zone.

10.2. *Coding of Soil Types and Subregions*

Soil Types - An integer code beginning with 1 and ending with *NMat* (the total number of soil materials) is assigned to each soil type in the flow region. The appropriate material code is subsequently assigned to each nodal point *n* of the finite element mesh.

Interior material interfaces do not coincide with element boundaries. When different material numbers are assigned to the nodes of a certain element, the finite element algorithm will assume that the material properties will change linearly over the element. This procedure will somewhat smooth soil interfaces. A set of soil hydraulic parameters, and solute and heat transport characteristics must be specified for each soil material.

Subregions - Water and solute mass balances are computed separately for each specified subregion. The subregions may or may not coincide with the material regions. Subregions are characterized by an integer code, which runs from 1 to *NLay* (the total number of subregions). A subregion code is assigned to each element in the flow domain.

10.3. *Coding of Boundary Conditions*

Boundary codes *KodTop* and *KodBot* must be assigned to surface and bottom boundary nodes, respectively. If a boundary node is to have a prescribed pressure head during a time step (a Dirichlet boundary condition), *KodTop* and *KodBot* must be set positive during that time step. If the volumetric flux of water entering or leaving the system is prescribed during a certain time step (a Neumann boundary condition), *KodTop* and *KodBot* must be negative or zero.

Constant Boundary Conditions - The value of a constant boundary condition for a particular boundary node, *n*, is given by the initial value of the pressure head, $h(n)$, in case of Dirichlet boundary conditions, or by the initial value of the recharge/discharge flux, *rTop* or *rBot*, in case of Neumann boundary conditions. Table 10.1 summarizes the use of the variables *KodTop* (*KodBot*), *rTop* (*rBot*), and $h(n)$ for various types of nodes.

Table 10.1. Initial settings of *KodTop* (*KodBot*), *rTop* (*rBot*), and $h(n)$ for constant boundary conditions.

Node Type	*KodTop* (*KodBot*)	*rTop* (*rBot*)	$h(n)$
Specified Head Boundary	1	0.0	Prescribed
Specified Flux Boundary	-1	Prescribed	Initial Value

Variable Boundary Conditions - Four types of variable boundary conditions can be imposed:
1. Atmospheric boundary conditions for which *TopInf=AtmInf=***.true.**,
2. Variable pressure head boundary conditions for which *TopInf=***.true.** and *KodTop*=+3, or *BotInf=***.true.** and *KodBot*=+3, or
3. Variable flux boundary conditions for which *TopInf=***.true.** and *KodTop*=-3, or *BotInf=***.true.** and *KodBot*=-3.
4. Variable pressure head/flux boundary conditions for which *TopInf=***.true.** and *KodTop*=-3 or +3.

Initial settings of the variables *KodTop* (*KodBot*), *rTop* (*rBot*), and $h(n)$ for the time-dependent boundary conditions are given in Table 10.2.

Table 10.2. Initial settings of *KodTop* (*KodBot*), *rTop* (*rBot*), and $h(n)$ for time-variable boundary conditions.

Node Type	*KodTop* (*KodBot*)	*rTop* (*rBot*)	$h(n)$
Atmospheric Boundary	-4	0.0	Initial Value
Variable Head Boundary	+3	0.0	Initial Value
Variable Flux Boundary	-3	0.0	Initial Value

Atmospheric boundary conditions are implemented when *TopInf=AtmInf=***.true.**, in which case time-dependent input data for the precipitation, *Prec*, and evaporation, *rSoil*, rates must be specified in the input file ATMOSPH.IN. The potential fluid flux across the soil surface is determined by *rAtm=rSoil-Prec*. The actual surface flux is calculated internally by the program. Two limiting values of surface pressure head must also be provided: *hCritS* which specifies the maximum allowed pressure head at the soil surface (usually 0.0), and *hCritA* which specifies the minimum allowed surface pressure head (defined from equilibrium conditions between soil water and atmospheric vapor). The program automatically switches the value of *KodTop* from -4 to +4 if one of these two limiting points is reached. Table 10.3 summarizes the use of the variables *rAtm*, *hCritS* and *hCritA* during program execution.

Variable head or flux boundary conditions on the soil surface (bottom of the soil profile) are implemented when *KodTop* (*KodBot*)=+3 or -3 and *TopInf* (*BotInf*)=**.true.**, respectively. In that case, the input file ATMOSPH.IN must contain the prescribed time-dependent values of the pressure head, *hT* (*hB*), or the flux, *rT* (*rB*), imposed on the boundary. The values of *hT* (*hB*) or *rT* (*rB*) are assigned to particular nodes at specified times according to rules given in Table 10.4.

Table 10.3. Definition of the variables *KodTop*, *rTop*, and *h*(*n*) when
an atmospheric boundary condition is applied.

KodTop	rTop	h(n)	Event
-4	rAtm	Unknown	rAtm=rSoil-Prec
+4	Unknown	hCritA	Evaporation capacity is exceeded
+4	Unknown	hCritS	Infiltration capacity is exceeded

Table 10.4. Definition of the variables *KodTop* (*KodBot*), *rTop* (*rBot*), and *h*(*n*)
when variable head or flux boundary conditions are applied.

Node Type	KodTop (KodBot)	rTop (rBot)	h(n)
Variable Head Boundary	+-3	Unknown	hT (hB)
Variable Flux Boundary	-3	rT (rB)	Unknown

Water Uptake by Plant Roots - The program calculates the rate at which plants extract water from the root zone by evaluating equation (2.8). Values of the potential transpiration rate, *rRoot*, must be specified at preselected times in the input file ATMOSPH.IN. These time-dependent values must be provided by the user and can be calculated in various ways, such as from the temperature and crop coefficients. Actual transpiration rates are calculated internally by the program as discussed in Section 2.2. The root water uptake parameters are taken from an input file, SELECTOR.IN. Values of the function *Beta*(*n*), which describes the potential water uptake distribution over the root zone, must be specified for each node in the flow domain. If the root growth model is considered, then the exponential function for the spatial distribution of the potential root water uptake is used (equation (2.16)). All parts of the flow region where *Beta*(*n*)>0 are treated as the soil root zone.

Root Growth Model - The program calculates the time variable rooting depth if the logical variable *lRoot* in input file SELECTOR.IN is equal to **.true.**. The classical Verhulst-Pearl logistic function (2.21) (see Section 2.2) is used to model the rooting depth. The exponential

(2.16) spatial distribution function for the root water uptake function is always used along with the time-variable rooting depth option. The root growth factor, *r*, can be calculated either from the known value of root depth (*xRMed*) at a specified time (*tRMed*), or from the assumption that 50% of the rooting depth is reached after 50% of the growing season.

Deep Drainage from the Soil Profile - Vertical drainage, *q*(*h*), across the lower boundary of the soil profile is sometimes approximated by a flux which depends on the position of the groundwater level [e.g., *Hopmans and Stricker*, 1989]. If available, such a relationship can be implemented in the form of a variable flux boundary condition; the code in that case internally sets the variable *KodBot* equal to -7. This boundary condition will be implemented in HYDRUS if the logical variable *qGWLF* in the input file SELECTOR.IN is set equal to **.true.**. The discharge rate *q*(*n*) assigned to bottom node *n* is determined by the program as *q*(*n*)=*q*(*h*), where *h* is the local value of the pressure head, and *q*(*h*) is given by

$$q(h) = -A_{qh} \exp(B_{qh} | h - GWL0L |) \qquad (10.1)$$

where A_{qh} and B_{qh} are empirical parameters which must be specified in input file SELECTOR.IN, together with *GWL0L* which represents the reference position of the groundwater level (sometimes set equal to the *x*-coordinate of the soil surface).

Free Drainage - Unit vertical hydraulic gradient boundary conditions can be implemented in the form of a variable flux boundary condition. The program in that case will internally set the variable *KodBot* equal to -5. This boundary condition is implemented in HYDRUS by setting the logical variable *FreeD* in the input file SELECTOR.IN equal to **.true.**. The discharge rate *q*(*n*) assigned to bottom node *n* is determined by the program as *q*(*n*)=-*K*(*h*), where *h* is the local value of the pressure head, and *K*(*h*) is the hydraulic conductivity corresponding to this pressure head.

Seepage Faces - The initial settings of the variables *KodBot*, *rBot* and *h*(*n*) for node on a seepage face are summarized in Table 10.5. This boundary condition is implemented in HYDRUS by setting the logical variable *SeepF* in the input file SELECTOR.IN equal to **.true.**

Table 10.5. Initial settings of *KodBot*, *rBot*, and *h*(*n*) for seepage faces.

Node Type	KodBot	rBot	h(n)
Seepage Face (initially saturated)	+2	0.0	0.0 (*hSeep*)
Seepage Face (initially unsaturated)	-2	0.0	Initial Value

Flow to Horizontal Drains - This boundary condition is implemented when the logical variable *lDrain* in the input file SELECTOR.IN is equal to .**true.**. Five conceptual models can be used to describe the tile-drained soil profile:

a) homogeneous soil profile; drain is located immediately above the impervious layer,

b) homogeneous soil profile; drain is located some distance above the impervious layer,

c) layered soil profile (two layers); drain is located at interface between soil layers,

d) layered soil profile (two layers); drain is located in the bottom layer,

e) layered soil profile (two layers); drain is located in the top layer.

The first three cases are solved with the Hooghoudt equation (2.51), and the last two cases with the Ernst equation (2.53).

Heat Transport Boundary Conditions - The type of applied boundary condition is specified by the input variables *kTopT* and *kBotT* for the upper and lower boundaries, respectively. Positive values for these variables means that a first-type boundary condition is used. When *kTopT* or *kBotT* is negative, then a third-type boundary condition is applied. On the other hand, when *kBotT* is equal to zero, a Neumann boundary condition with zero gradient is implemented. All initial and boundary conditions must be specified in ^{o}C.

Solute Transport Boundary Conditions - The type of applied boundary condition is specified by the input variables *kTopCh* and *kBotCh* for the upper and lower solute transport boundaries, respectively. Similarly as for heat transport, positive values for these variables means that a first-type boundary condition will be assumed. When *kTopCh* or *kBotCh* is negative, then a third-type boundary condition is applied. When *kBotCh* is equal to zero, a Neumann boundary condition with zero gradient is used.

10.4. *Program Memory Requirements*

One single parameter statement is used at the beginning of the code to define the problem dimensions. All major arrays in the program are adjusted automatically according to these dimensions. This feature makes it possible to change the dimensions of the problem to be simulated without having to recompile all program subroutines. Different problems can be investigated by changing the dimensions in the parameter statement at the beginning of the main program, and subsequently linking all previously compiled subroutines with the main program when creating an executable file. Table 10.6 lists the array dimensions, which must be defined in the parameter statement.

Table 10.6. List of the array dimensions.

Dimension	Current setting	Description
NumNPD	1001	Maximum number of nodes in finite element mesh
NMatD	20	Maximum number of materials
NTabD	100	Maximum number of items in the table of hydraulic properties generated by the program for each soil material
NObsD	10	Maximum number of observation nodes

11. EXAMPLE PROBLEMS

Eight example problems demonstrating direct problems and three examples for inverse problems are presented in this section. The first two examples are identical to those described in the SWMS_2D manual [*Šimůnek et al.*, 1992], while three other examples are the same as those discussed in the CHAIN_2D manual [*Šimůnek et al.*, 1994]. The three CHAIN_2D examples were included mainly for mathematical verification purposes, and for demonstrating new features of version 2.0 of HYDRUS, i.e., non-equilibrium and nonlinear adsorption, and sequential first-order decay reactions. Examples 9 through 11 demonstrate new features implemented into versions 3.0 and 4.0 of HYDRUS.

Examples 1 and 2 provide comparisons of the water flow part of the HYDRUS code with results from both the UNSAT2 code of *Neuman* [1972] and the SWATRE code of *Belmans et al.* [1983]. The results obtained with HYDRUS for these two examples were identical to those obtained with SWMS_2D. Example 3 serves to verify the accuracy of HYDRUS by comparing numerical results for a problem with three solutes involved in a sequential first-order decay reaction against results obtained with an analytical solution during one-dimensional steady-state water flow [*van Genuchten*, 1985]. Example 4 considers one-dimensional transport of a solute undergoing nonlinear cation adsorption. Numerical results are compared with experimental data and previous numerical solutions obtained with the MONOC code of *Selim et al.* [1987] and the previous version of HYDRUS (version 5.0) of *Vogel et al.* [1996]. Example 5 serves to test the performance of HYDRUS for nonequilibrium adsorption by comparing numerical results against experimental data and previous numerical predictions during one-dimensional steady-state water flow [*van Genuchten*, 1981]. Examples 6 through 8 demonstrate the inverse analyses of one- and multi-step outflow experiments, as well as of an evaporation experiment, for the purpose of estimating the unsaturated soil hydraulic parameters. Example 9 shows an application of the dual-porosity model, while example 10 demonstrates the new hysteresis model. Finally, example 11 demonstrates capabilities of HYDRUS-1D to simulate coupled water, vapor and heat transport.

Four additional examples are distributed with the HYDRUS-1D installation package demonstrating its use for simulating carbon dioxide transport and major ion chemistry. The first example simulates infiltration into a relatively dry soil column. This example shows predicted differences between the equilibrium and kinetic precipitation-dissolution model. The second example involving an irrigation problem with root water uptake demonstrates the importance of considering a proper model for calcite precipitation-dissolution. The third example simulating an irrigation problem with a periodic upper boundary condition demonstrates the important effects

of CO_2 concentration/transport on solution chemistry. The last example demonstrates the capabilities of HYDRUS for predicting carbon dioxide production and transport. The various major ion chemistry examples are not further described here since they are discussed in detail in the original UNSATCHEM manual [*Šimůnek et al.*, 1997].

A comprehensive list of publications showing a large number of HYDURS-1D applications can be found at www.pc-progress.cz/Pg_Hydrus1D_References.htm (for HYDRUS-1D and related software). Additional examples demonstrating HYDRUS capabilities to simulate nonequilibrium flow and transport can be downloaded from the HYDRUS web site (www.pc-progress.cz).

11.1. *Example 1 - Column Infiltration Test*

This example simulates a one-dimensional laboratory infiltration experiment initially discussed by *Skaggs et al.* [1970], and later used by *Davis and Neuman* [1983] as a test problem for the UNSAT2 code. Hence, the example provides a means of comparing results obtained with the HYDRUS and UNSAT2 codes.

The soil water retention and relative hydraulic conductivity functions of the sandy soil are presented in Figure 11.1. The sand was assumed to be at an initial pressure head of -150 cm. The soil was assumed to be homogenous and isotropic with a saturated hydraulic conductivity of 0.0433 cm/min. The column was subjected to ponded infiltration (a Dirichlet boundary condition) at the soil surface, resulting in one-dimensional vertical water flow. The open bottom boundary of the soil column was simulated by implementing a no-flow boundary condition during unsaturated flow ($h<0$), and a seepage face with $h=0$ when the bottom of the column becomes saturated (this last condition was not reached during the simulation).

The simulation was carried out for 90 min, which corresponds to the total time duration of the experiment. Figure 11.2 shows the calculated instantaneous (q_0) and cumulative (I_0) infiltration rates simulated with HYDRUS. The calculated results agree closely with those obtained by *Davis and Neuman* [1983] using their UNSAT2 code.
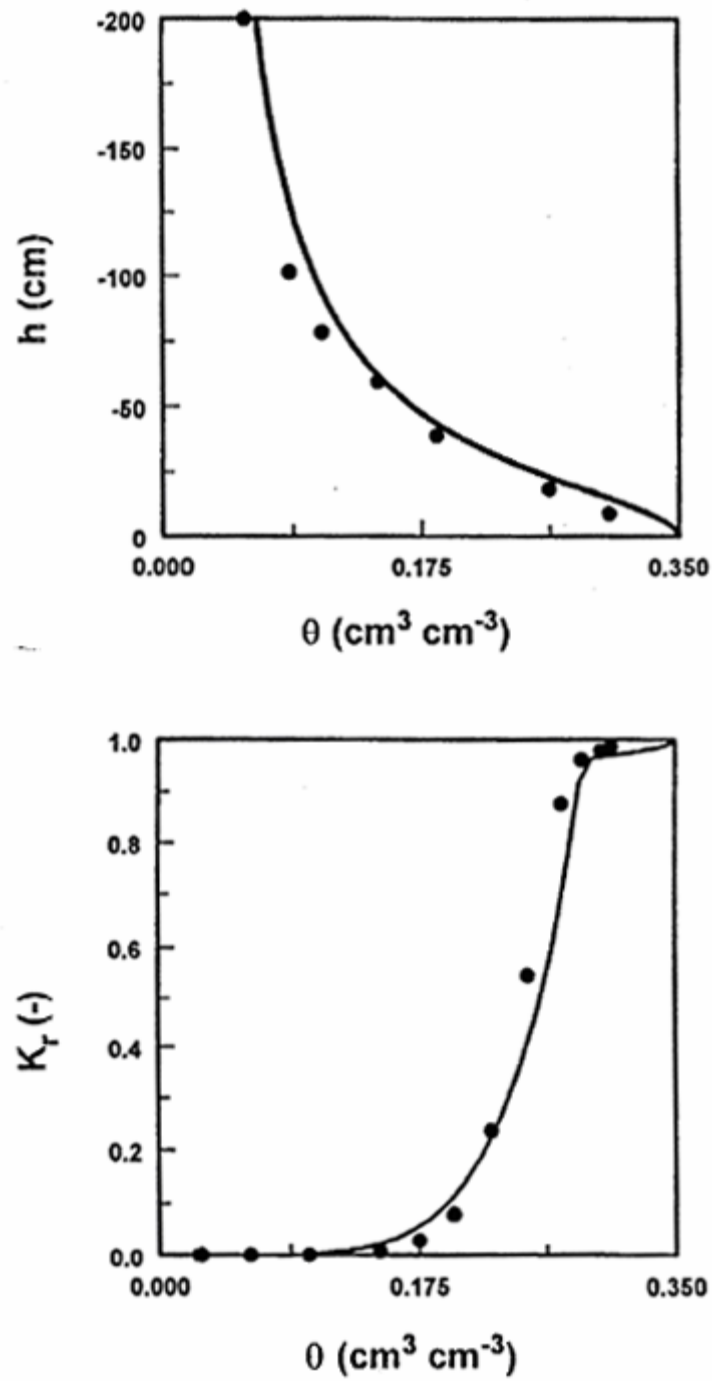
Fig. 11.1. Soil water retention and relative hydraulic conductivity functions for example 1. The solid circles are UNSAT2 input data [*Davis and Neuman*, 1983].
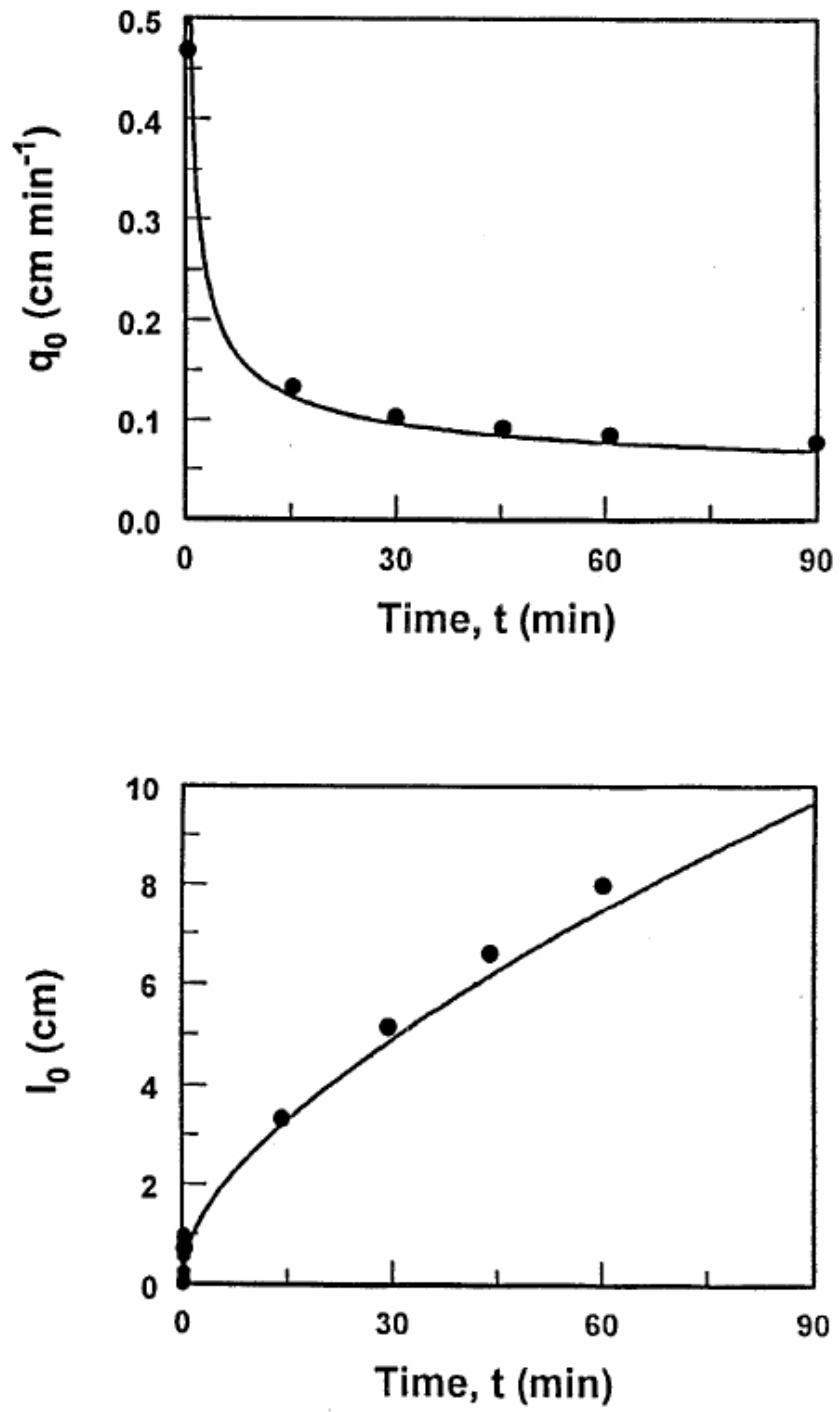
Fig. 11.2. Instantaneous, q_0, and cumulative, I_0, infiltration rates simulated with the HYDRUS (solid lines) and UNSAT2 (solid circles) computer codes (example 1).

144

11.2. *Example 2 - Water Flow in a Field Soil Profile Under Grass*

This example considers one-dimensional water flow in a field profile of the Hupselse Beek watershed in the Netherlands. Atmospheric data and observed ground water levels provided the required boundary conditions for the numerical model. Calculations were performed for the period of April 1 to September 30 of the relatively dry year 1982. Simulation results obtained with HYDRUS will be compared with those generated with the SWATRE computer program [*Feddes et al*., 1978, *Belmans et al*., 1983].

The soil profile consisted of two layers: a 40-cm thick A-horizon, and a B/C-horizon which extended to a depth of about 300 cm. The depth of the root zone was 30 cm. The mean scaled hydraulic functions of the two soil layers in the Hupselse Beek area [*Císlerová*, 1987; *Hopmans and Stricker*, 1989] are presented in Figure 11.3.

The soil surface boundary condition involved actual precipitation and potential transpiration rates for a grass cover. The surface fluxes were incorporated by using average daily rates distributed uniformly over each day. The bottom boundary condition consisted of a prescribed drainage flux - groundwater level relationship, $q(h)$, as given by equation (10.1). The groundwater level was initially set at 55 cm below the soil surface. The initial moisture profile was taken to be in equilibrium with the initial ground water level.

Figure 11.4 presents input values of the precipitation and potential transpiration rates. Calculated cumulative transpiration and cumulative drainage amounts as obtained with the HYDRUS and SWATRE codes are shown in Figure 11.5. The pressure head at the soil surface and the arithmetic mean pressure head of the root zone during the simulated season are presented in Figure 11.6. Finally, Figure 11.7 shows variations in the calculated groundwater level with time.
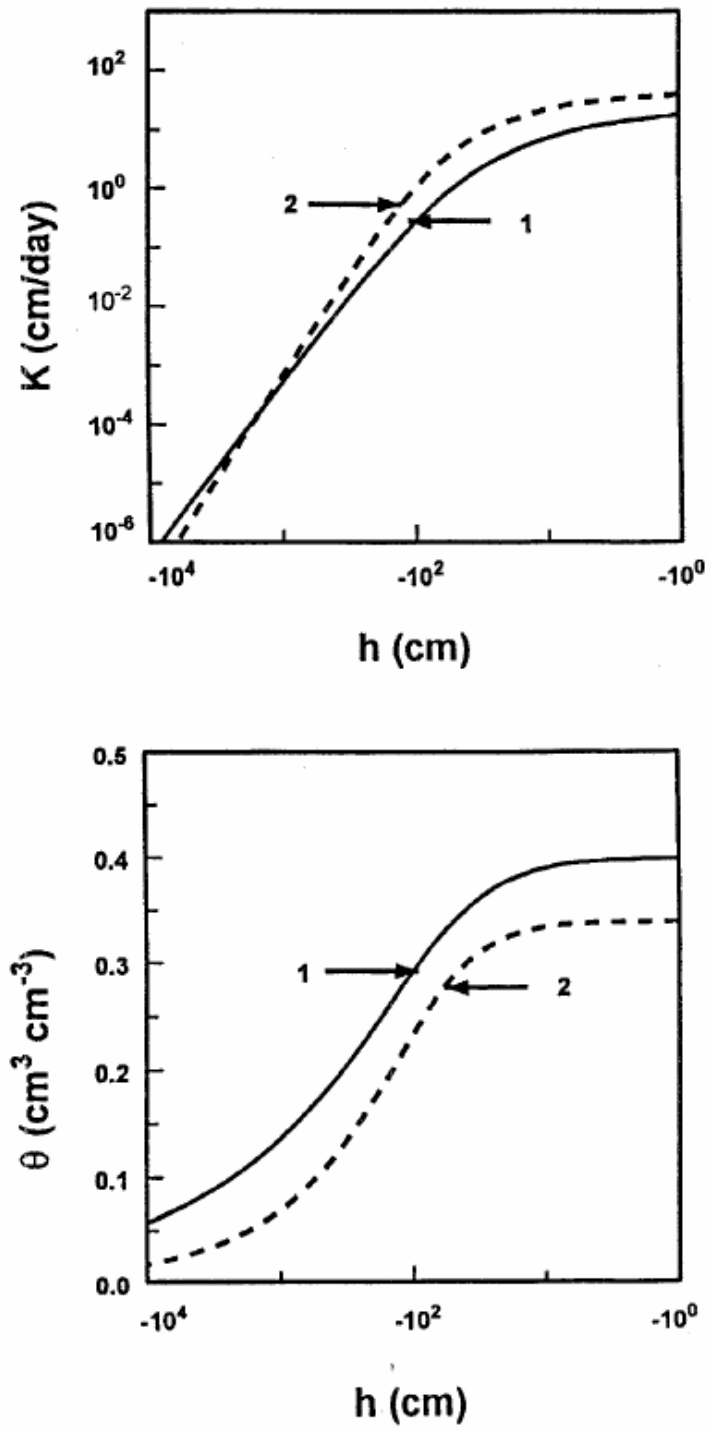
Fig. 11.3. Unsaturated hydraulic properties of the first and second soil layers (example 2).
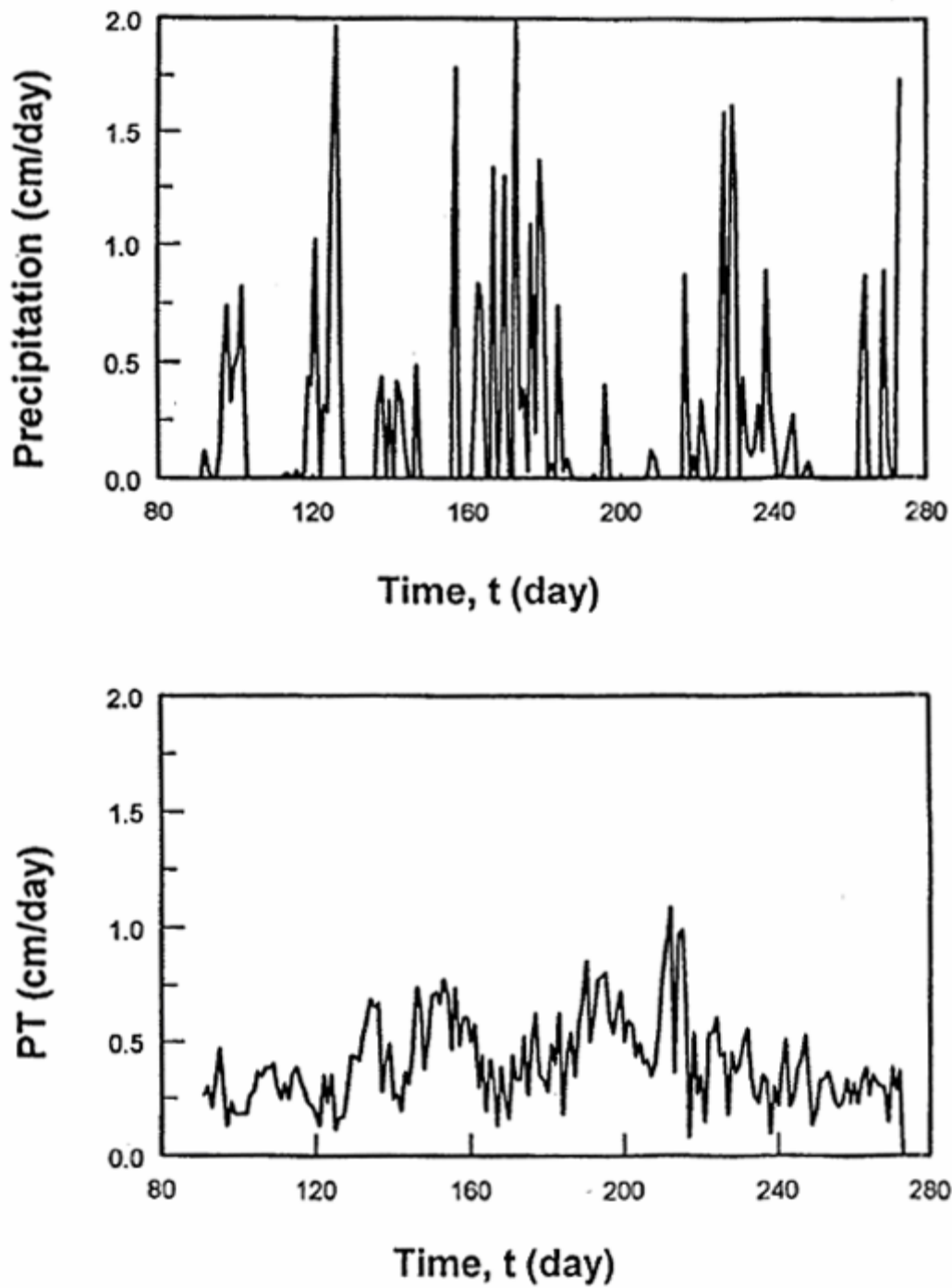
Fig. 11.4. Precipitation and potential transpiration rates (example 2).

147
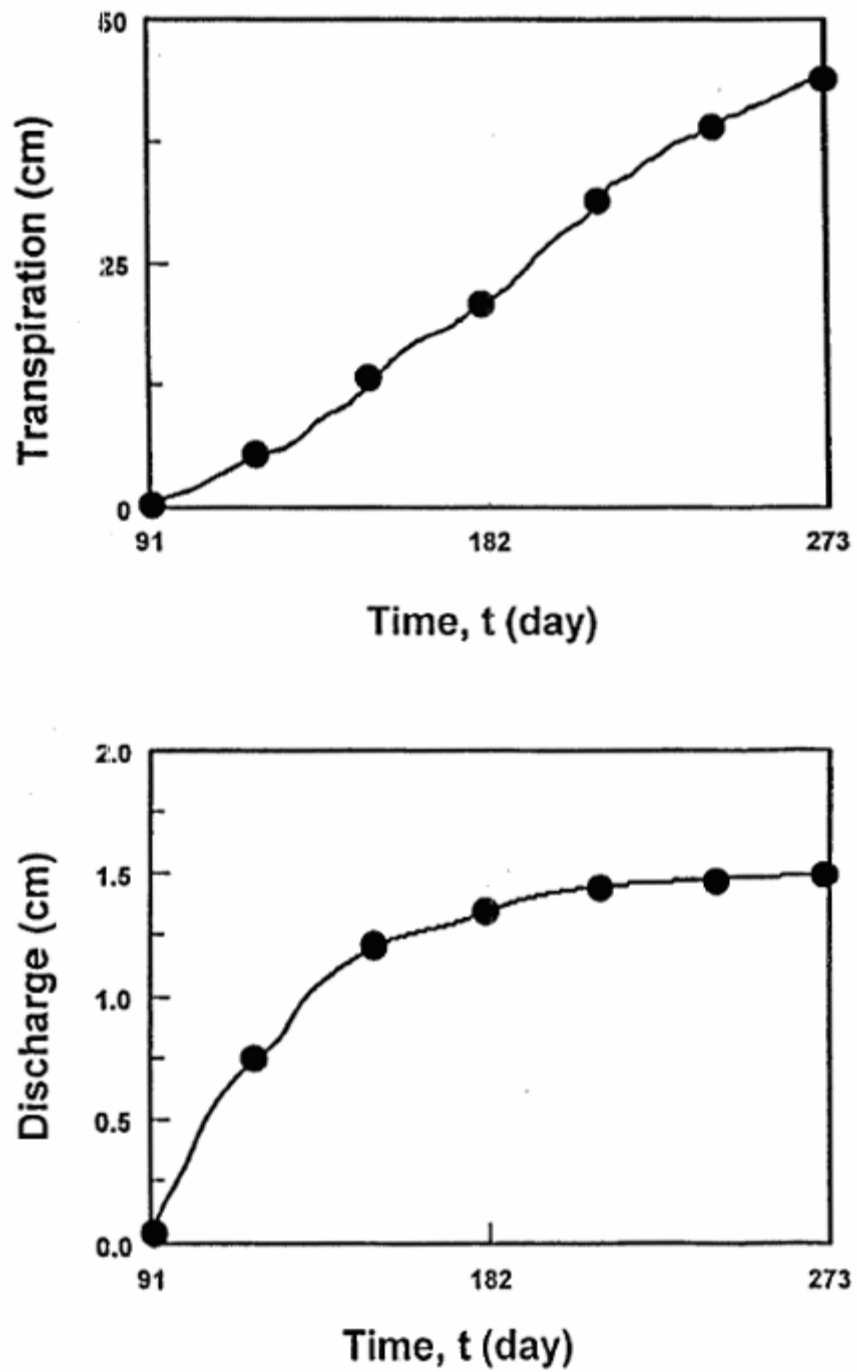
Fig. 11.5. Cumulative values for the actual transpiration and bottom leaching rates as simulated with the HYDRUS (solid line) and SWATRE (solid circles) computer codes (example 2).

148
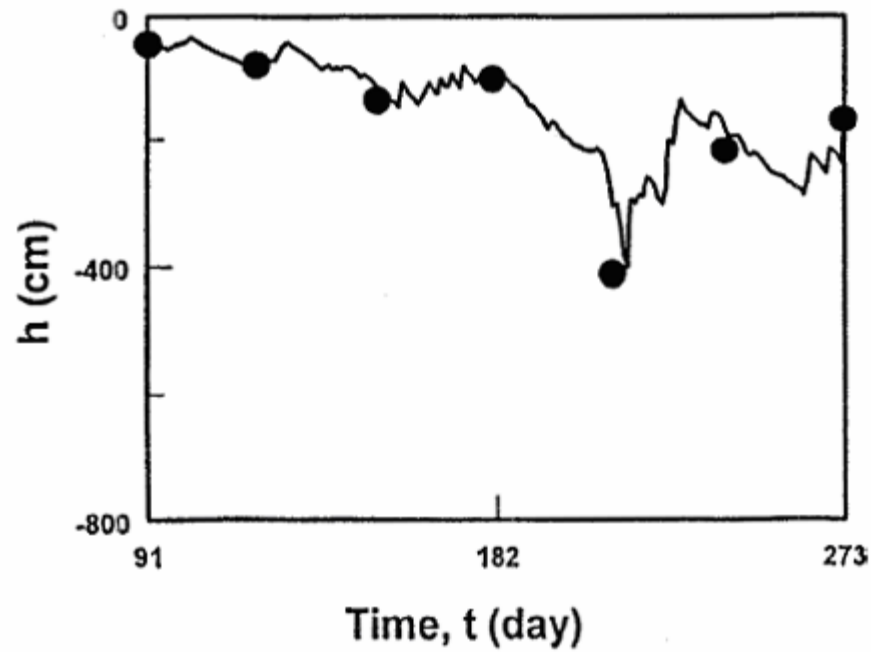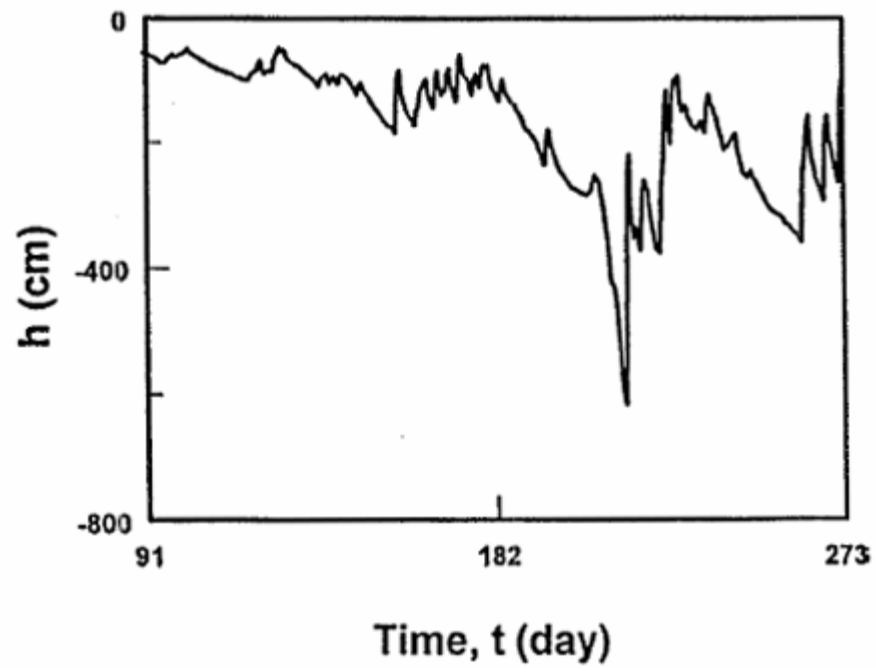
Fig. 11.6. Pressure head at the soil surface and mean pressure head of the root zone as simulated with the HYDRUS (solid lines) and SWATRE (solid circles) computer codes (example 2).

149
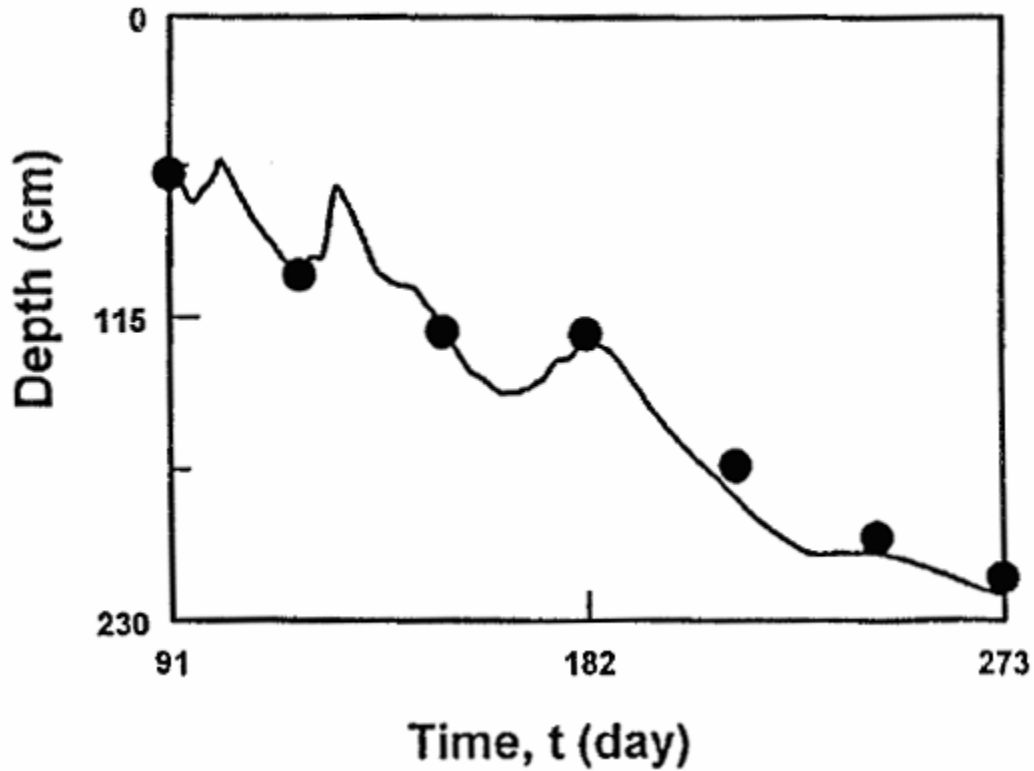
Fig. 11.7. Location of the groundwater table versus time as simulated with the HYDRUS (solid line) and SWATRE (solid circles) computer codes (example 2).

11.3. *Example 3 - Solute Transport with Nitrification Chain*

This example was used to verify in part the mathematical accuracy of the solute transport part of HYDRUS. Numerical results will be compared with results generated with an analytical solution published by *van Genuchten* [1985] for one-dimensional convective-dispersive transport of solutes involved in sequential first-order decay reactions. The analytical solution holds for solute transport in a homogeneous, isotropic porous medium during steady-state unidirectional groundwater flow. Solute transport equations (3.1) and (3.2) for this situation reduce to

$$R_1 \frac{\partial c_1}{\partial t} = D \frac{\partial^2 c_1}{\partial x^2} - v \frac{\partial c_1}{\partial x} - \mu_1 R_1 c_1 \qquad (11.1)$$

150

$$R_i \frac{\partial c_i}{\partial t} = D \frac{\partial^2 c_i}{\partial x^2} - v \frac{\partial c_i}{\partial x} + \mu_{i-1} R_{i-1} c_{i-1} - \mu_i R_i c_i \quad i = 2, 3 \qquad (11.2)$$

where μ is a first-order degradation constant, D is the dispersion coefficient, v is the average pore water velocity (q/θ) in the flow direction, x is the spatial coordinate in the direction of flow, and where it is assumed that 3 solutes participate in the decay chain. The specific example used here applies to the three-species nitrification chain

$$NH_4^+ \rightarrow NO_2^- \rightarrow NO_3^- \qquad (11.3)$$

and is the same as described by *van Genuchten* [1985], and earlier by *Cho* [1971]. The boundary conditions may be written as:

$$\left(-D \frac{\partial c_1}{\partial x} + v\, c_1 \right) = v\, c_{0,1}(0, t)$$

$$\left(-D \frac{\partial c_i}{\partial x} + v\, c_i \right) = 0 \qquad i = 2, 3 \qquad (11.4)$$

$$\lim_{x \to \infty} \frac{\partial c_i}{\partial x} = 0 \qquad i = 1, 2, 3$$

The experiment involves the application of a NH_4^+ solution to an initially solute-free medium ($c_i = 0$). The input transport parameters for the simulation are listed in Table 11.2.

Figure 11.8 shows concentration profiles for all three solutes at time 200 hours, calculated both numerically with HYDRUS and analytically with the CHAIN code of *van Genuchten* [1985]. Figure 11.9 shows the concentration profiles at three different times (50, 100, and 200 hours) for NH_4^+, NO_2^-, and NO_3^-, respectively. The numerical results in each case duplicated the analytical results.

Table 11.1. Input parameters for example 3.

Parameter	Value
v [cm/hour]	1.0
D [cm^2/hour]	0.18
μ_1 [hour^{-1}]	0.005
μ_2 [hour^{-1}]	0.1
μ_3 [hour^{-1}]	0.0
R_1 [-]	2.0
R_2 [-]	1.0
R_3 [-]	1.0
c_i [-]	0.0
$c_{0,1}$ [-]	1.0
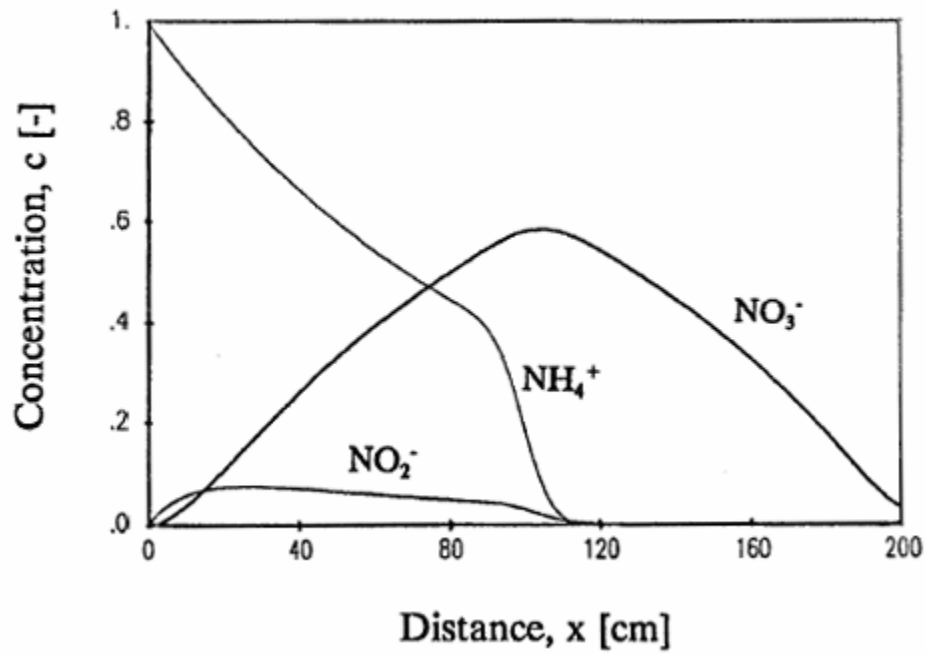
Fig. 11.8. Analytically and numerically calculated concentration profiles for NH_4^+, NO_2^-, and NO_3^- after 200 hours (example 3).
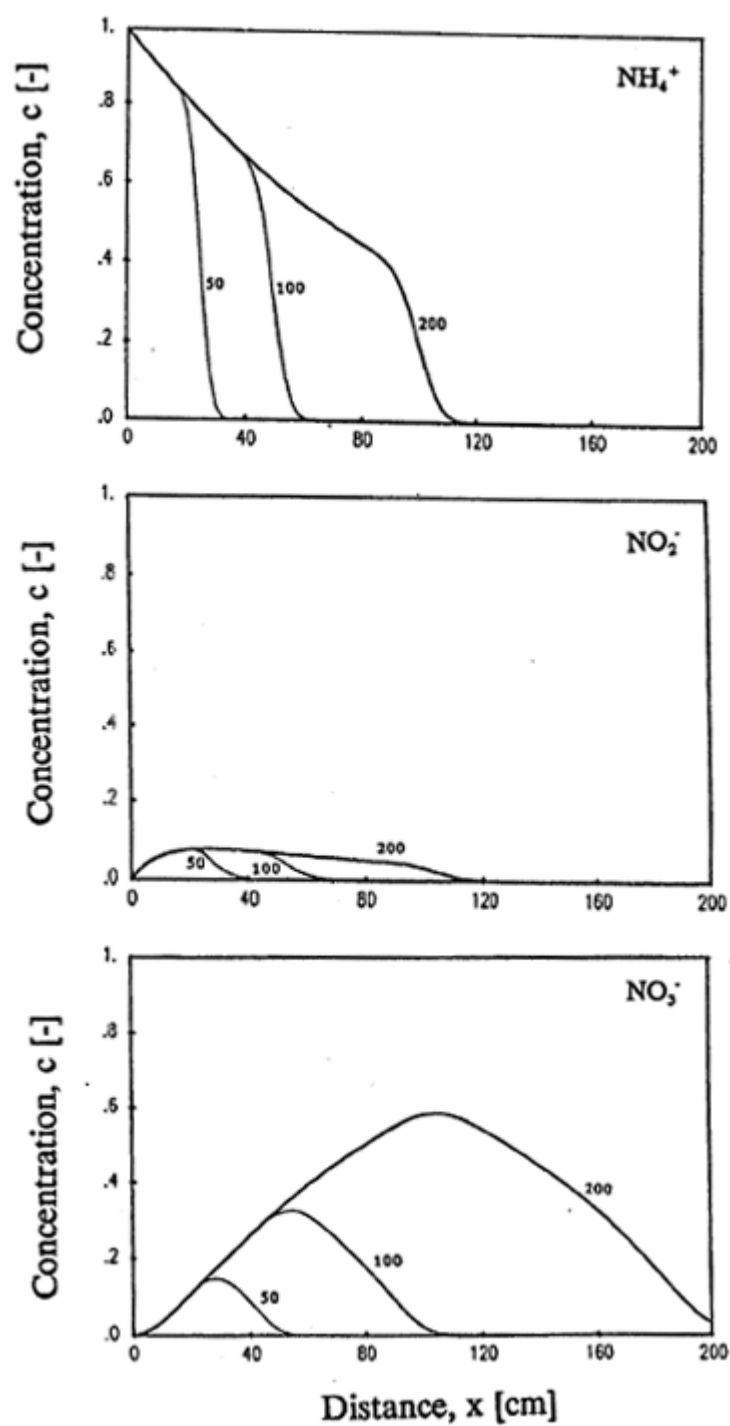
Fig. 11.9. Analytically and numerically calculated concentration profiles for NH_4^+ (top), NO_2^- (middle), NO_3^- (bottom) after 50, 100, and 200 hours (example 3).

153

11.4. *Example 4 - Solute Transport with Nonlinear Cation Adsorption*

The experiment discussed in this example was conducted by *Selim et al.* [1987], and used later for previous versions (version 3.1 and 5.0) of HYDRUS [*Kool and van Genuchten*, 1991; *Vogel et al.*, 1996]. The soil in this experiment was Abist loam. A 10.75-cm long soil column was first saturated with a 10 $mmol_cL^{-1}$ $CaCl_2$ solution. The experiment consisted of applying a 14.26 pore volume pulse (t = 358.05 hours) of a 10 $mmol_cL^{-1}$ $MgCl_2$ solution, followed by the original $CaCl_2$ solution. The adsorption isotherm was determined with the help of batch experiments [*Selim et al.*, 1987], and fitted with the Freundlich equation (3.3) [*Kool and van Genuchten*, 1991]. The Freundlich isotherm parameters, as well as other transport parameters for this problem, are listed in Table 11.2. First- and second-type boundary conditions were applied to the top and bottom of the soil column, respectively.

The observed Mg breakthrough curve is shown in Figure 11.10, together with simulated breakthrough curves obtained with HYDRUS, the MONOC code of *Selim et al.* [1987] and the previous versions of HYDRUS. The results indicate a reasonable prediction of the measured breakthrough curve using HYDRUS, and close correspondence between the simulated results obtained with the HYDRUS and MONOC models. The HYDRUS results became identical to those generated with previous versions of HYDRUS when a third-type boundary condition was invoked at the top of the soil column.

Table 11.2. Input parameters for example 4.

Parameter	Value
q [cm/hour]	0.271
D [cm^2/hour]	1.167
ρ [g/cm^3]	0.884
θ [-]	0.633
c_0 [mmol$_c$/L]	10.0
k_s [cm^3/g]	1.687
β [-]	1.615
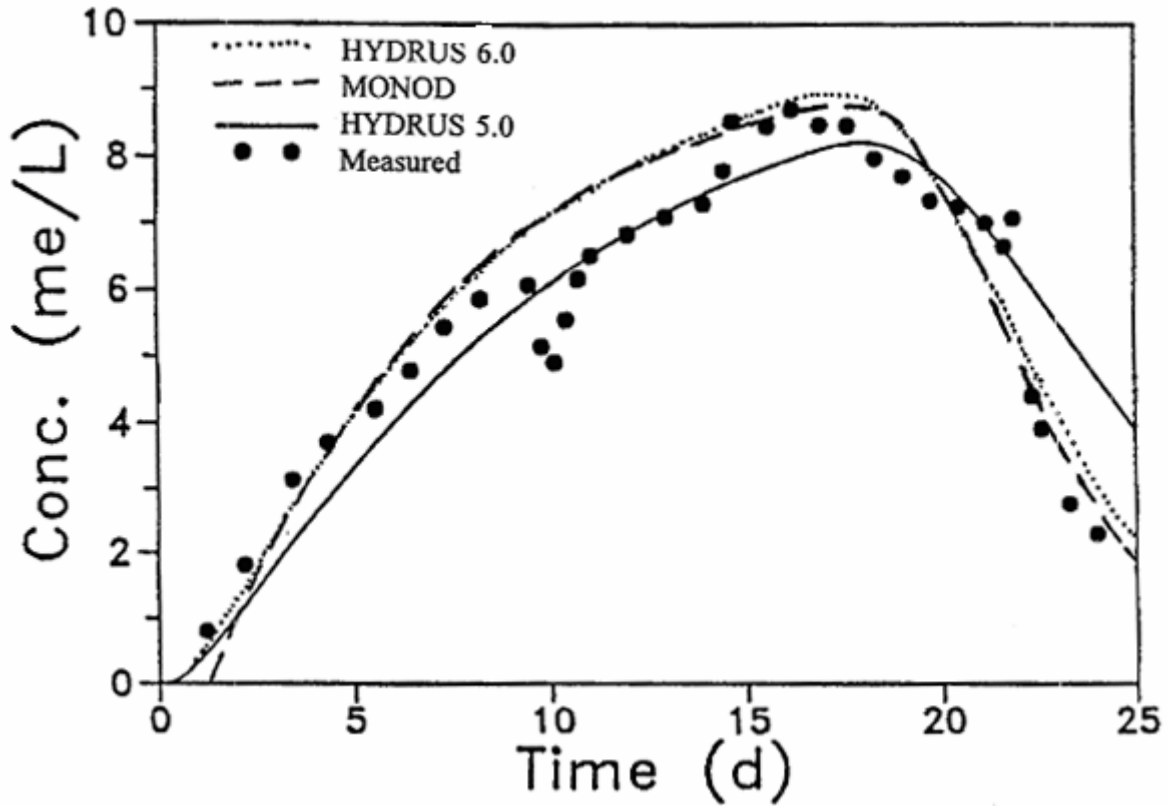
Fig. 11.10. Mg breakthrough curves for Abist loam calculated with the MONOD, HYDRUS, and new HYDRUS codes (data points from *Selim et al.*, 1978).

The Langmuir adsorption isotherm can also be used to model the exchange of homovalent ions. Parameters in the Langmuir adsorption isotherm for homovalent ion exchange may be derived as follows. Ion exchange for two ions with valences n and m can be expressed in a generalized form as [*Sposito*, 1981]

$$K_{ex} = \left(\frac{\overline{a_1}}{a_1}\right)^m \left(\frac{a_2}{\overline{a_2}}\right)^n \tag{11.5}$$

where K_{ex} is the dimensionless thermodynamic equilibrium constant, and a and $\overline{a}$ denote the ion activities in the soil solution and on the exchange surfaces [-], respectively:

$$a_i = \gamma_i c_i \qquad i = 1, 2$$

$$\overline{a}_i = \xi_i s_i \qquad i = 1, 2$$

(11.6)

where c_i [ML^{-3}] (mmol/l) and s_i [MM^{-1}] (mmol/kg) are solution and exchangeable concentrations, respectively, and γ_i and ξ_i are activity coefficients in the soil solution [L^{3}M^{-1}] (l/mmol) and on the exchange surfaces [MM^{-1}] (kg/mmol), respectively. Substituting (11.6) into (11.5) gives

$$K_{12} = K_v \frac{\gamma_1^m}{\gamma_2^n} = K_{ex} \frac{\xi_2^n \gamma_1^m}{\xi_1^m \gamma_2^n} = \frac{s_1^m c_2^n}{s_2^n c_1^m}$$

(11.7)

where K_v denotes the Vanselow selectivity coefficient [-], while K_{12} will be simply referred to as the selectivity coefficient [-]. Assuming that both the total solution concentration, C_T [ML^{-3}] (mmol$_c$/l), and the cation exchange capacity, S_T [MM^{-1}] (mmol$_c$/kg), are time invariant, i.e.,

$$n c_1 + m c_2 = C_T$$
$$n s_1 + m s_2 = S_T$$

(11.8)

the Langmuir parameters k_s and η in (3.3) for the incoming solute become

$$k_s = \frac{K_{12} S_T}{C_T}$$

$$\eta = \frac{\vartheta(K_{12} - 1)}{C_T}$$

(11.9)

whereas for the solute initially in the soil column:

$$k_s = \frac{S_T}{K_{12} C_T}$$

$$\eta = \frac{\vartheta(1 - K_{12})}{K_{12} C_T}$$

(11.10)

The parameter ϑ in (11.9) and (11.10) equals 1 for monovalent ions, and 2 for divalent ions.

The selectivity coefficient K_{12} for example 5 was measured by *Selim et al.* [1987] (K_{12}=0.51). From the total solution concentration (C_T=10 mmol$_c$/l) and the known cation exchange capacity (S_T=62 mmol$_c$/kg), it follows that the parameters in the Langmuir adsorption isotherm for the incoming solute (Mg) are k_s=3.126 and η=-0.098, while those for the solute initially in the soil profile (Ca) the parameters are k_s=12.157 and η=0.192. The observed Ca breakthrough curve is shown in Figure 11.11, together with the simulated breakthrough curves obtained with the HYDRUS2 and MONOC codes [*Selim et al.*, 1987]. Note the close agreement between the numerical results and the experimental data.
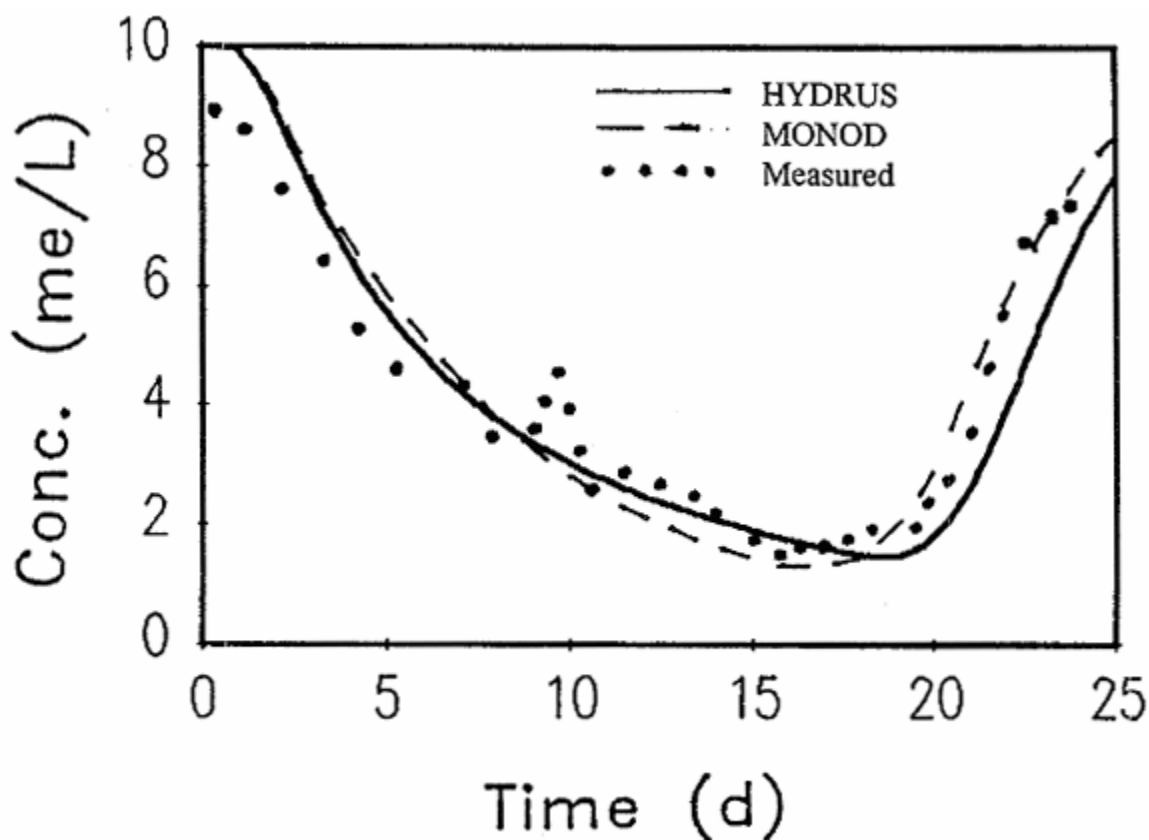
Fig. 11.11. Ca breakthrough curves for Abist loam calculated with the MONOD and HYDRUS codes (data points from *Selim et al.*, 1978) (example 4).

11.5. *Example 5 - Solute Transport with Nonequilibrium Adsorption*

     This example considers the movement of a boron (H_3BO_4) pulse through Glendale clay loam [*van Genuchten*, 1981]. The numerical simulation uses solute transport parameters that were fitted to the breakthrough curve with the CFITIM parameter estimation model [*van Genuchten*, 1981] assuming a two-site chemical nonequilibrium sorption model analogous to the formulation discussed in Section 3, but for steady-state water flow. Input parameters for example 5 are listed in Table 11.3. Figure 11.12 compares HYDRUS numerical results with the experimental data, and with a numerical simulation assuming physical nonequilibrium and nonlinear adsorption [*van Genuchten*, 1981].

Table 11.3. Input parameters for example 5.

Parameter	Value
q [cm/day]	17.12
D [cm^2/day]	49.0
θ [-]	0.445
ρ [g/cm$_3$]	1.222
c_0 [mmol$_c$/L]	20.0
k_s [cm^3/g]	1.14
β [-]	1.0
η [-]	0.0
f [-]	0.47
ω [1/day]	0.320
t_p [day]	6.494
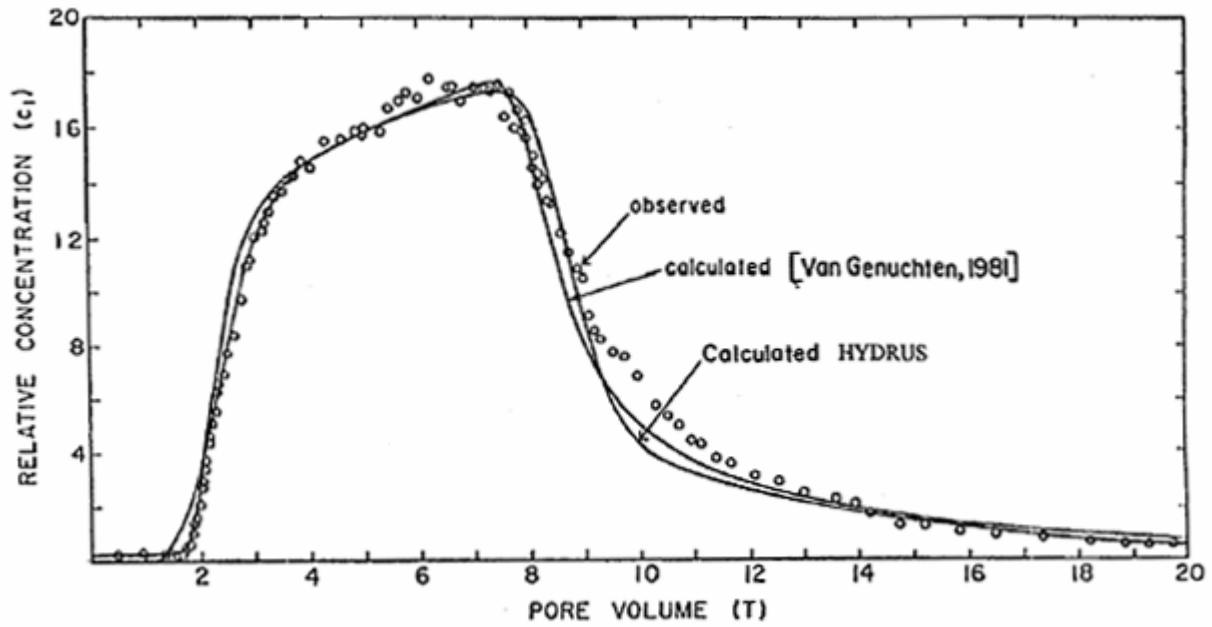
Fig. 11.12. Observed and calculated effluent curves for boron movement through Glendale clay (data points from *van Genuchten* [1981]) (example 5).

11.6. *Example 6 - Inverse Analysis of a One-Step Outflow Experiment*

The first example involving parameter estimation deals with a case first discussed by *Kool et al.* [1985]. An undisturbed core sample, having a length of 3.95 cm long and a diameter of 5.4 cm, was equilibrated at zero tension in a Tempe pressure cell. The retention curve was first measured for pressure heads up to -10 m. Water contents at pressure head of -30 and -150 m were measured on disturbed samples. After resaturating, the pneumatic pressure of 10 m was imposed at the top of the sample, and the cumulative outflow was recorded with time (Figure 11.13). The position of the measuring burette was adjusted manually every time a reading was made to maintain a constant head lower boundary condition. At the end of the experiment, the soil was resaturated and the saturated hydraulic conductivity of the soil and porous plate were measured with a falling head method.

Three hydraulic parameters (α, n, and θ_r) were estimated by numerical inversion of the observed cumulative outflow data and the measured water content at the pressure head of -150 m. Since water exits the soil column across a ceramic plate, the flow problem involves a two-layered system. To be able to simulate flow through the ceramic bottom plate without having to modify the code, the HYDRUS model must be able to simulate flow through materials with very high air entry values such that the ceramic plate remains saturated at all times during the outflow experiment. A relatively high air entry value of the plate was obtained by specifying parameter α to be 10^{-20} (1/cm). The soil profile was discretized into 50 nodes with five nodes representing the ceramic plate. Only a few nodes were used for the ceramic plate since the plate remains saturated during the entire experiment, thus causing the flow process in the plate to be linear.

Figure 11.13 shows the measured cumulative outflow curve versus time, as well as the best fit obtained with HYDRUS-1D. Initial and final parameter estimates are listed in Table 11.4. Notice the very good fit of the measured data in Fig. 11.13, with r^2 being 0.9987. Figure 11.14 shows a comparison of the predicted and measured retention curves, as well as a comparison of the diffusivity curve obtained by parameter estimation and $D(\theta)$ values calculated independently using the method of *Passioura* [1976]. Again, notice the very good agreement between predicted and measured values.

Table 11.4. Initial estimates of and optimized parameters for example 6.

Parameter	Initial Estimate	Final Value
θ_r [cm^3/cm^3]	0.15	0.166
θ_s [cm^3/cm^3]	0.388[+]	
α [1/cm]	0.025	0.0363
n [-]	1.5	1.42
K_s [cm/h]	5.4[+]	
$K_{s,cer}$ [cm/h]	0.003[+]	
l [-]	0.5[+]	

[+] Not optimized
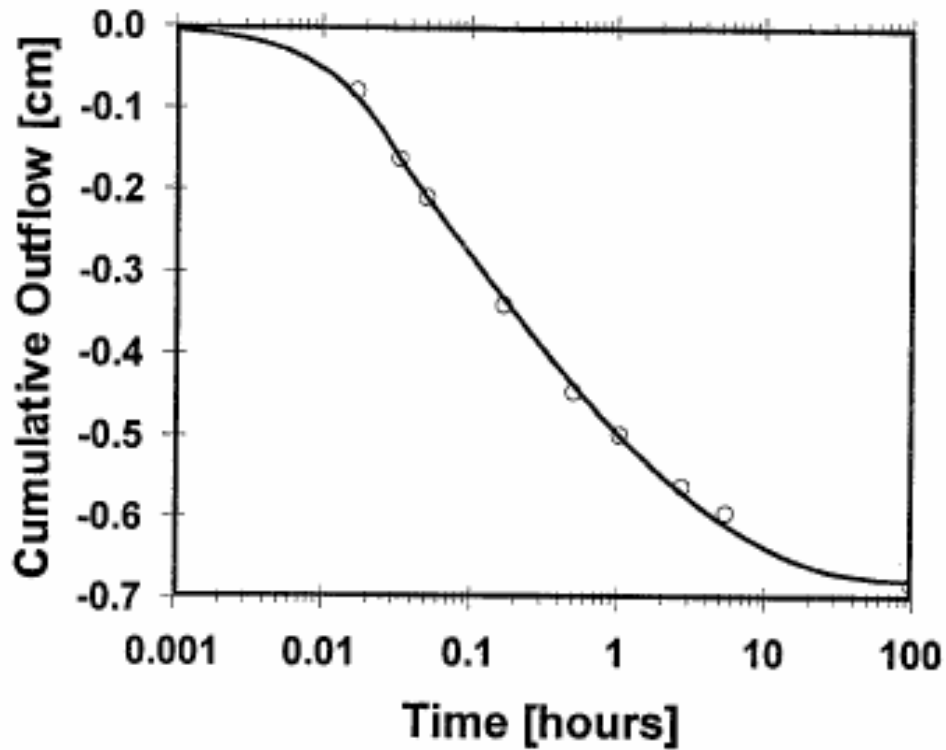
Fig. 11.13. Measured and optimized cumulative outflow versus time for a onestep outflow experiment (example 6).
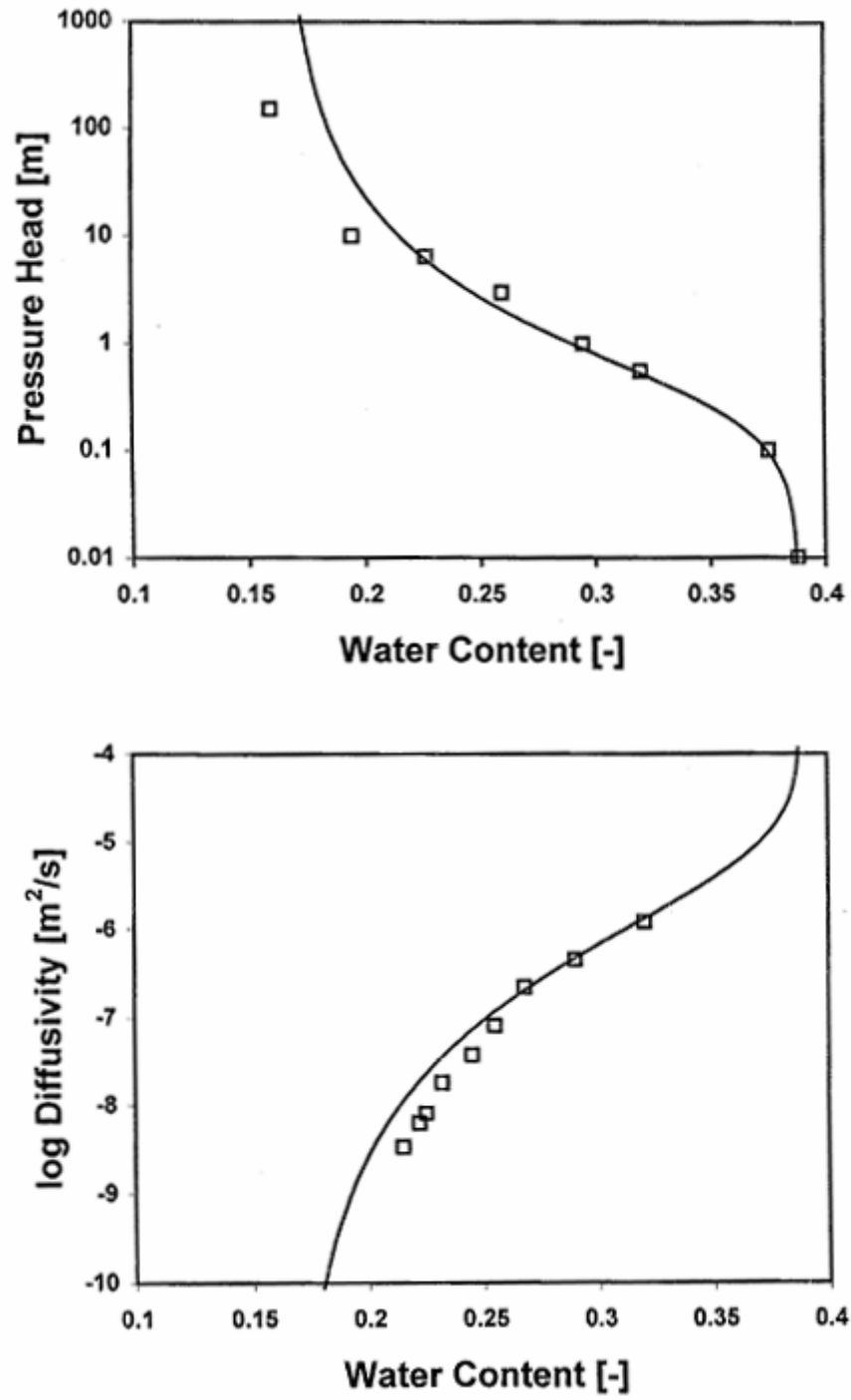
Fig. 11.14. Observed and predicted retention characteristics and calculated and predicted diffusivities (example 6).

11.7. *Example 7 - Inverse Analysis of a Multistep Outflow Experiment*

Although initial applications of the inverse approach to onestep outflow data appeared promising, later studies revealed possible problems in terms of non-uniqueness of the optimized parameters [e.g., *van Dam et al.,* 1992, 1994]. To circumvent uniqueness problems, *van Dam et al.* [1994] conducted and analyzed outflow experiments in which the pneumatic pressure was increased in several smaller steps. *Eching et al.* [1994] similarly estimated soil hydraulic parameters from simultaneous measurements of transient cumulative outflow and the soil water pressure head inside of the soil sample during a multistep outflow experiment.

In this test example we analyze a multistep outflow experiment with simultaneous measurement of the pressure head inside the soil sample [*Hopmans*, personal communication]. The experimental setup consisted of a 6-cm long soil column in a Tempe pressure cell modified to accommodate a microtensiometer-transducer system. A tensiometer was installed, with the cup centered 3 cm below the soil surface. The soil sample was saturated from the bottom and subsequently equilibrated to an initial soil water pressure head of -25 cm at the soil surface. Pressures of 100, 200, 400, and 700 cm were applied subsequently in consecutive steps at 0, 12.41, 48.12, and 105.92 hours, respectively.

Figure 11.15 compares the measured and optimized cumulative outflow curves for the soil sample, while Fig. 11.16 compares measured and optimized pressure heads. Excellent agreement was obtained for both variables. The final fit had an r^2 of 0.9995. Table 11.5. lists initial estimates and final values of the six optimized parameters.

Table 11.5. Initial estimates and optimized parameters for example 7.

Parameter	Initial Estimate	Final Value
θ_r [cm^3/cm^3]	0.078	0.197
θ_s [cm^3/cm^3]	0.43	0.438
α [1/cm]	0.036	0.0101
n [-]	1.56	1.434
K_s [cm/h]	1.04	0.521
l [-]	0.5	3.80
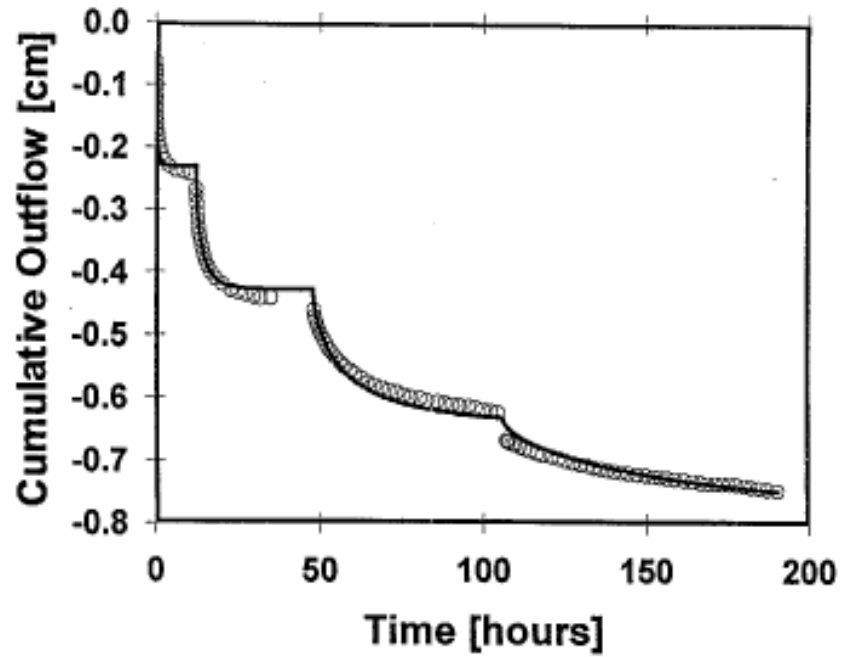
Fig. 11.15. Measured and optimized cumulative bottom flux for a multistep outflow experiment (example 7).
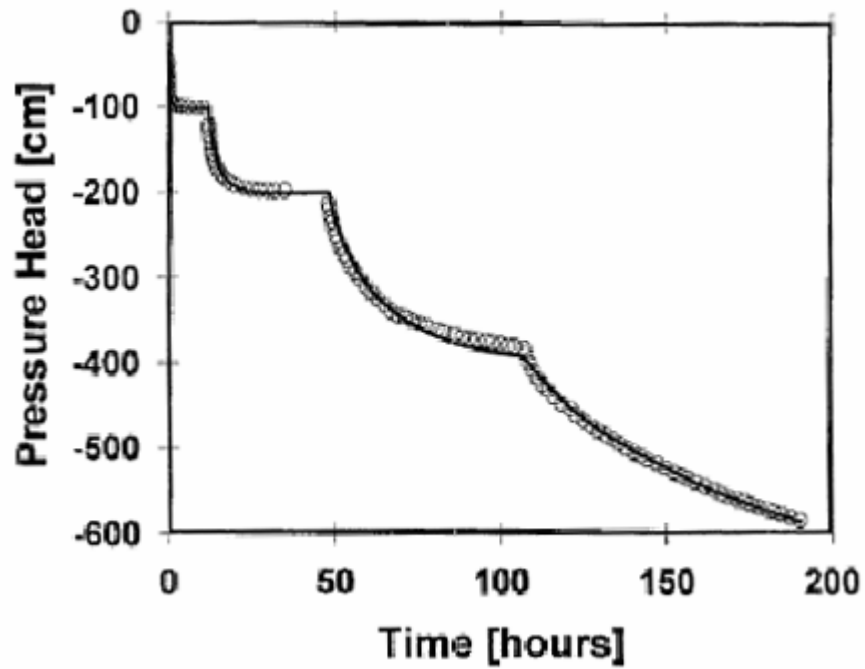
Fig. 11.16. Measured and optimized pressure heads inside the soil sample for a multistep outflow experiment (example 7).

11.8. *Example 8 - Inverse Analysis of an Evaporation Experiment*

This example demonstrated application of the parameter estimation method to an evaporation experiment. Details about the experiment are given in *Šimůnek et al.* [1998]. An undisturbed soil core sample with a height of 10 cm and inside diameter of 10 cm was placed on a ceramic plate and saturated with deionized water. The soil had a bulk density of 1.59 g cm^{-3}, and sand, silt and clay fractions of 7.4, 79.3 and 13.3%, respectively. Five tensiometers with cups having a length of 6 cm and outside diameter of 0.6 cm were inserted horizontally through drill holes into the soil cores at locations 1, 3, 5, 7, and 9 cm below the sample surface. Following previous disc infiltrometer experiments on the same soil column, the sample was moved onto impermeable plates for the evaporation experiment. An initial pressure head of -15.4 cm was measured in the middle of the soil sample.

Evaporation was subsequently allowed to start. After each pressure reading the soil samples with the tensiometers were weighted to determine the evaporative water loss as a function of time. The evaporation rate at the beginning of the experiments was artificially increased to approximately 1.2 cm d^{-1} by using of a fan to blow air away from the soil surface at room temperature [*Wendroth et al.*, 1993]. Once the gradient between the tensiometers reached a value between 1.5 and 2.5 m/m, the top of the soil sample was covered to prevent further evaporation. After re-establishing hydraulic equilibrium in the samples, evaporation was allowed to continue, without the fan, at a rate of approximately 0.2 cmd^{-1}. Measurements were taken every 30 min during the initial high-evaporation rate period, and every 4 hours during the second stage when the rate was relatively low. The evaporation experiment was terminated when the upper tensiometer recorded a pressure head value of -650 cm. Water losses between consecutive measurements were used to calculate the average evaporation rate for a given time interval; this information was subsequently used as the upper boundary condition in the numerical simulations.

The laboratory experiment was first analyzed using the modified Wind method as described by *Wendroth et al.* [1993]. The soil hydraulic parameters were obtained by simultaneous fitting of the resulting $\theta(h)$ and $K(h)$ data using the RETC code [*van Genuchten et al.*, 1991]. The final parameters are given in Table 11.6. Data obtained with Wind's method and the subsequently fitted hydraulic functions are shown in Fig. 11.17.
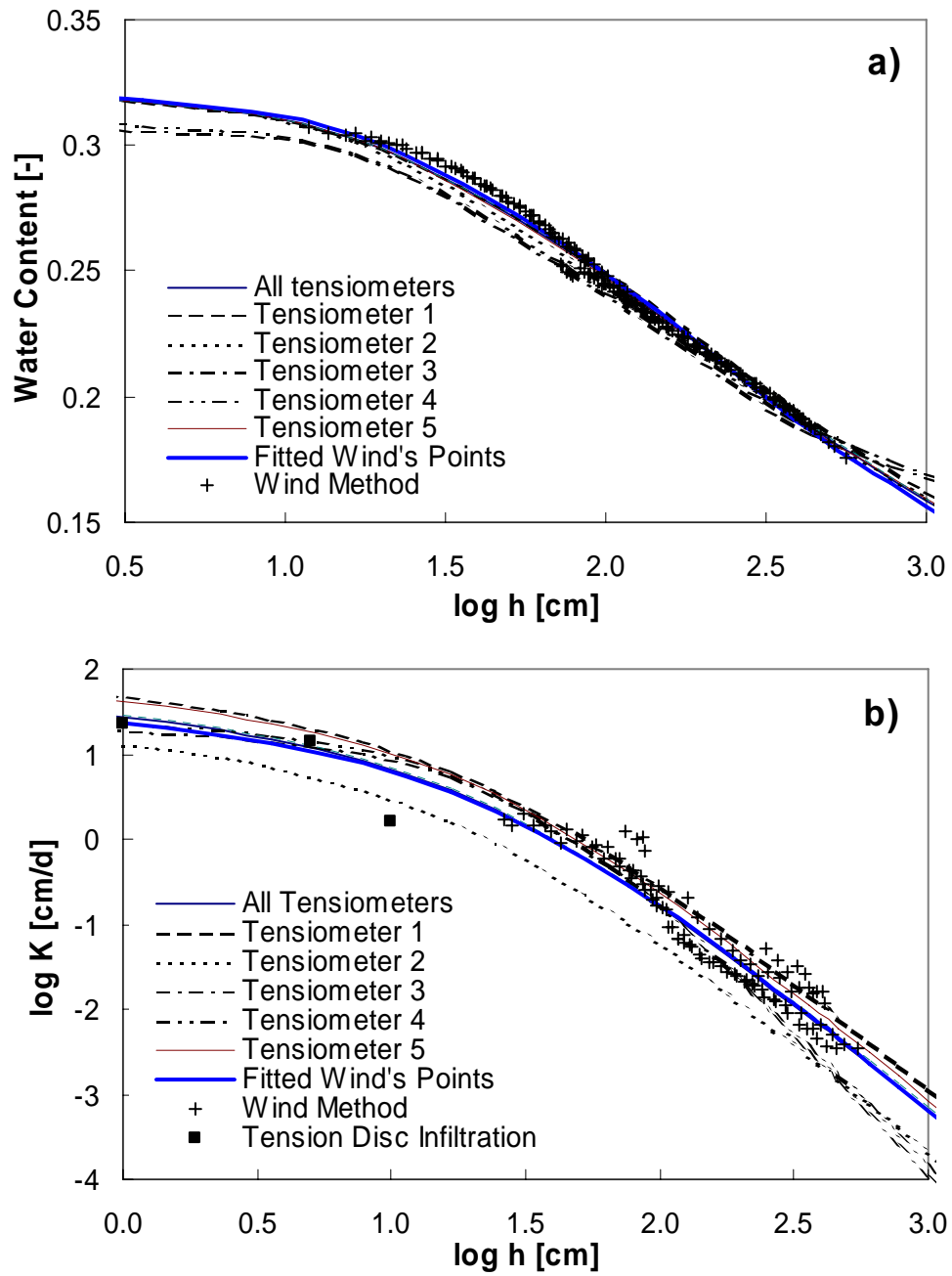
Fig. 11.17. Water retention (a) and hydraulic conductivity (b) functions determined with inverse parameter estimation and Wind's method (example 8).

The soil hydraulic parameters were also estimated from the evaporation experiment using parameter inversion. We used for this purpose the tensiometer readings as a function of time and the total water volume at the end of the experiment. The resulting optimized soil hydraulic parameters are listed in Table 11.6, together with the r^2 of the regression between predicted and measured values. Soil hydraulic characteristics obtained by numerical inversion and using Wind's method are compared in Figure 11.17.

Notice a very good correspondence between retention curves obtained by parameter optimization and the $\theta(h)$ data points determined with Wind's method or their analytical fit (Fig. 11.17a). The soil-water retention parameters obtained with Wind's method and by parameter optimization are almost identical and undistinguishable from each other (Fig. 11.17a). The estimated unsaturated hydraulic conductivity functions obtained with the two methods (Fig. 11.17b) are also almost identical. Figure 11.17 also shows results of inversions when the objective function was alternatively defined in terms of readings obtained with only one tensiometer. Results apparently remain relatively close to those obtained when readings from all tensiometers were used simultaneously.

Measured and fitted tensiometer readings are shown in Figure 11.18. The largest deviations were about 5 and 20 cm for the first and second evaporation rates, respectively, with most deviations being much lower.

Table 11.6. Hydraulic parameters obtained from an evaporation experiment using parameter estimation and Wind's method (example 8).

Method of Analysis	θ_r	θ_s	α	n	K_s	R^2
	(-)	(-)	(cm^{-1})	(-)	(cm d^{-1})	
Parameter Estimation	0.0055	0.321	0.0274	1.22	93.1	0.9987
Wind's Method	0.0045	0.321	0.0249	1.23	73.3	0.992
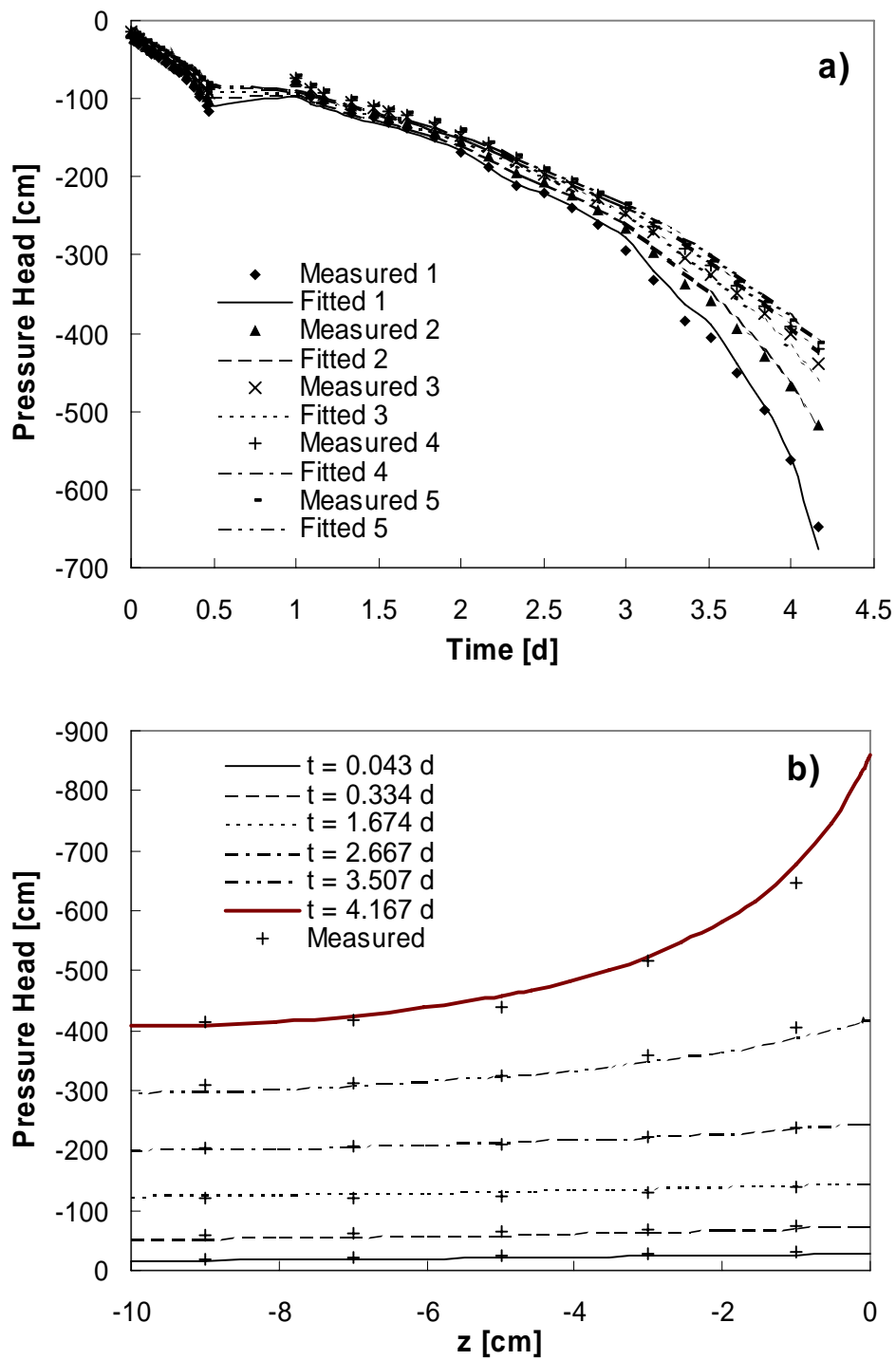
Fig. 11.18. Measured and fitted tensiometer readings as a function of time (a) and depth (b) (example 8).

11.9. *Example 9 – Infiltration into Structured Soil*

This example shows an application of the dual-porosity model described in Section 2.1.2. Figure 11.19 shows computed water and solute distributions during infiltration obtained with the model [*Šimůnek et al.,* 2003]. The soil hydraulic parameters of the macropore (mobile) domain were taken as follows: θ_r=0.0, θ_s=0.200, α_1=0.041 cm^{-1}, n=1.964, l=0.5, K_s=0.000722 cm s^{-1}, while the (immobile) matrix domain was assumed to have a saturated water content, θ_{sm}, of 0.15. Initial conditions were set equal to a pressure head of −150 cm. We assumed that water mass transfer was described with Eq. (2.92), in which the mass transfer constant ω was set at 0.00001 s^{-1}. For simplicity we considered only convective solute mass transfer between the two pore regions (i.e. no diffusive transfer), with the dispersivity again fixed at 2 cm. While for ponded surface conditions water in the fracture domain quickly reached full saturation (Fig. 11.19a), the water content of the matrix increased only gradually with time. Consequently, the total water content, defined as the sum of the water contents of both the fracture and matrix domains, also increased only gradually. The total water content would be the quantity measured with most field water content measurement devices, such as a TDR or neutron probe. Pressure head measurements using tensiometers are, on the other hand, often dominated by the wetter fracture domain that reaches equilibrium relatively quickly. The dual-porosity model can therefore explain often observed nonequilibrium between pressure heads and water contents (e.g. *Šimůnek et al.* [1999, 2001], among others). Similar nonequilibrium profiles as for the water content were also obtained for the solute concentration (Fig. 11.19b).
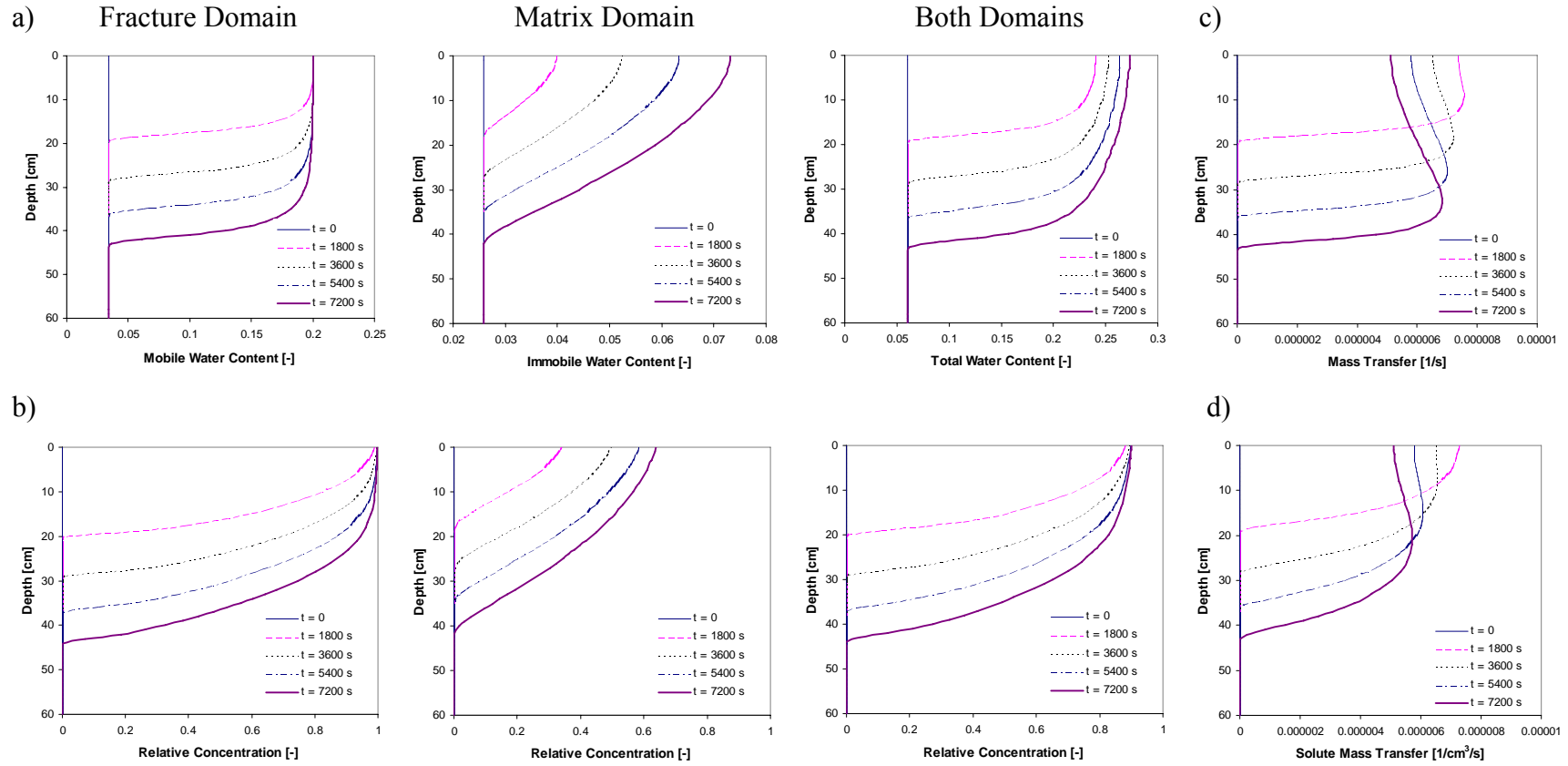
Fig. 11.19. Water content (a) and concentration (b) profiles in the fracture (mobile) domain, the matrix (immobile) domain, and both domains combined, as well as the water (c) and solute (d) mass transfer terms as calculated with the dual-porosity model [*Šimůnek et al.,* 2003].

11.10. *Example 10 – Evaluation of Hysteretic Models*

The new hysteresis model is demonstrated on a data set reported by *Lenhard et al.* [1991]. In this experiment, the sand (97.5% sand, 0.8% silt, and 1.7% clay) was packed in a column with a cross-sectional area of approximately 39 cm² and 72 cm height. Porous ceramic tensiometers connected to pressure transducers were installed 70, 60, 50, 40, 30, and 20 cm above the soil bottom. Water contents were measured using a gamma radiation attenuation system at the same locations. The water table was raised initially to the soil surface by wetting the dry soil column. The water table at the beginning of the experiment (i.e., at $t = 0$ hours) was lowered 5 cm. Every 10 min thereafter the water table was lowered an additional 5 cm until reaching an elevation of 7 cm at $t = 2$ hours, where it remained stationary for an hour. At $t = 3$ hours the water table was raised 5 cm every 10 min to a final elevation of 42 cm where it remained for an hour until $t = 5$ hours. The first lowering and raising of the water table produced main drainage and imbibition scanning paths, respectively. A drying scanning path was subsequently generated by lowering the water table at the prescribed rate from 42 cm at $t = 5$ hours to 17 cm where again the water table remained stationary for an hour until $t = 6.67$ hours. The final saturation path, an imbibition scanning path, was produced by raising the water table elevation from 17 cm back to the soil surface at 72 cm, which was reached at $t = 8.33$ hours. In the last path, as the water table was raised past 42 cm, all internal scanning loops should have been closed. The soil hydraulic parameters were also reported by *Lenhard et al.* [1991] (θ_r=0.0612, θ_s^d=0.36, α_d=0.042 cm⁻¹, n=5.25, K_s=119 cm h⁻¹, l=0.5, θ_s=0.36, θ_s^w=0.27, α_w=0.084 cm⁻¹). Since the collected data are described in detail by *Lenhard et al.* [1991], we show here only the simulation results.

Figure 11.20 compares the original and newly-implemented hysteresis models by showing the main drainage curve, and the imbibition (wetting) and drainage (drying) scanning curves measured at elevations of 30, 40, 50, and 60 cm. The original model clearly shows the pumping effect after the process reversal. Figure 11.21 shows pressure heads and water contents at elevations of 20, 30, 40, 50, 60, and 70 cm as calculated with the new model. Calculated results are essentially identical to those presented by *Lenhard et al.* [1991].
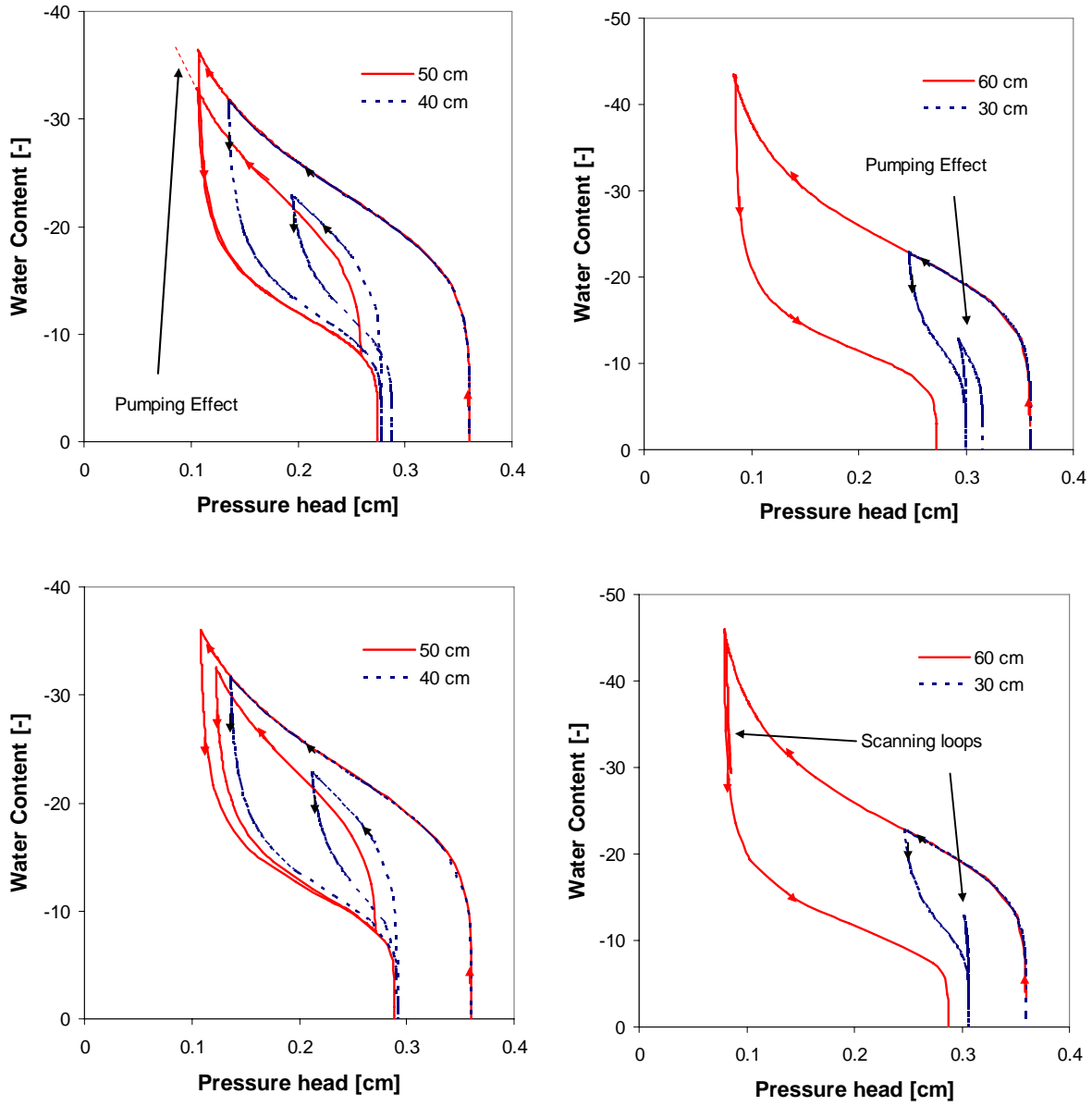
Fig. 11.20. Main drainage curves, and imbibition and drainage scanning curves, as calculated at elevations of 40 and 50 (left figure) and 30 and 60 cm (right figure) using the original (top) and new (bottom) hysteresis models.
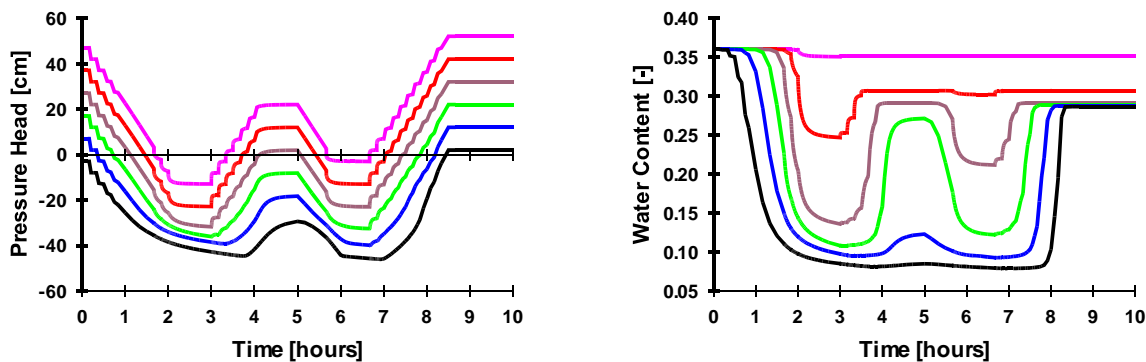
Fig. 11.21. Calculated pressure heads (left) and water contents (right) at elevations of 20 (N6), 30 (N5), 40 (N4), 50 (N3), 60 (N2), and 70 (N1) cm.

11.11. *Example 11 – Coupled Water, Vapor, and Heat Transport*

Example 11 demonstrates capabilities of HYDRUS-1D to simulate coupled water, vapor and heat transport [*Šimůnek et al.*, 2007]. Figure 11.21 shows calculated water content, total flux, temperature and concentration profiles for a 10-cm long soil sample with zero water fluxes at both the top and bottom boundaries, and with a specified temperature gradient along the sample. Increasing temperatures (Fig. 11.21c) from the top to the bottom of the sample cause vapor flow (Fig. 11.21b) from the warmer bottom end of the sample toward the colder end. Water evaporates at the warmer end, flows upward as vapor and condensates at the colder end. Water contents correspondingly decrease at the warmer end, and increase at the colder bottom (Fig. 11.21a). As a consequence of changing water contents, a pressure head gradient develops in the sample, leading to water flow in a direction opposite to vapor flow. A steady-state is eventually reached when upward vapor flow fully balances downward liquid flow (Fig. 11.21b). Since water evaporates at the bottom of the sample and condensates at the top, solute becomes more concentrated near the bottom and more diluted near the top (Fig. 11.21d). Also, the concentration profile should eventually reach steady-state, although at a much later time, when the downward advective solute flux balances the upward diffusive flux.

173
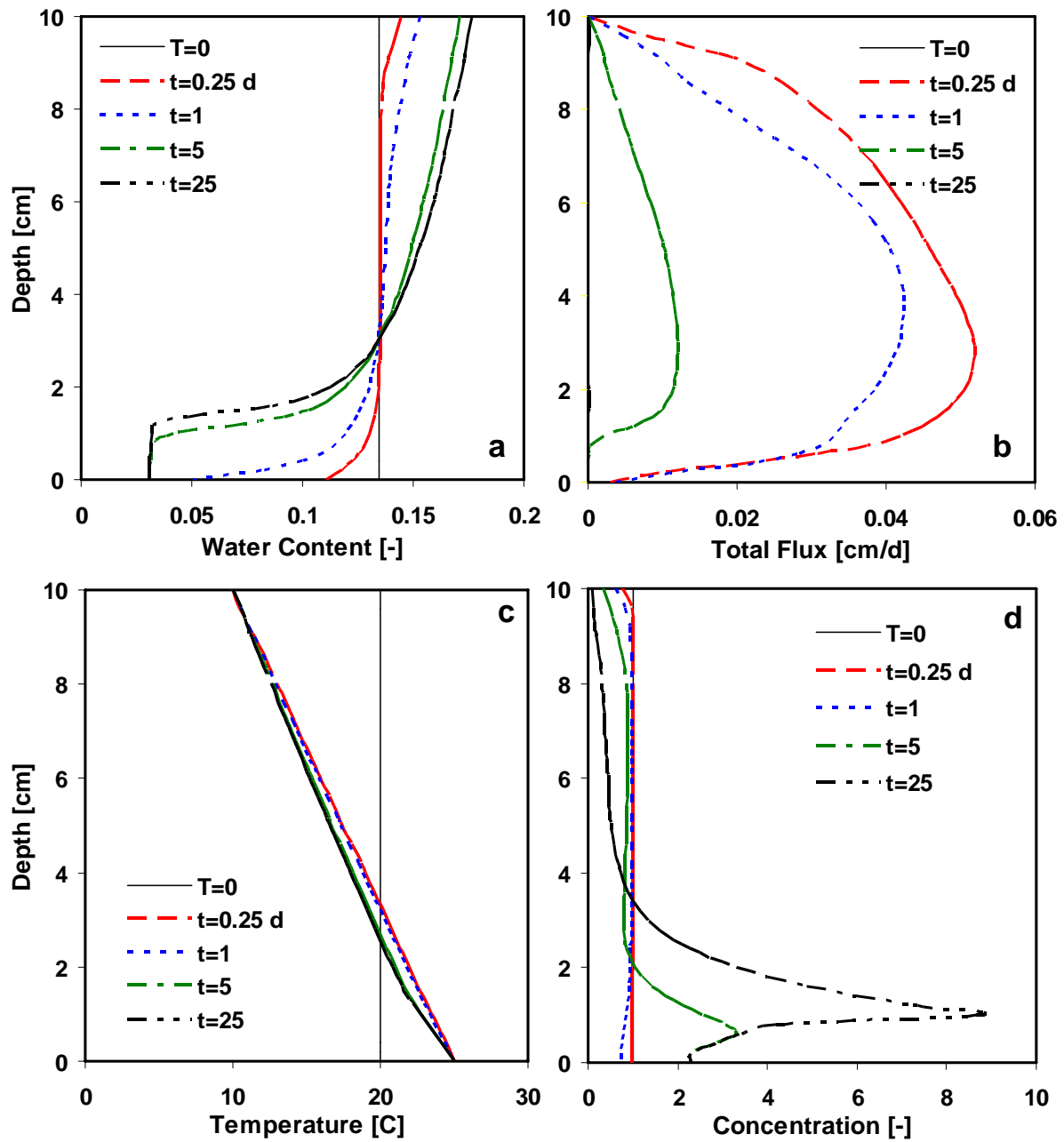
Fig. 11.22. Water content (a), total flux (b), temperature (c), and solute concentration (d) distributions in a 10-cm long vertical soil sample with zero water fluxes across the top and bottom boundaries, and with temperature increasing from top to bottom.

12. INPUT DATA

The input data for HYDRUS are given in five separate input files. These input files consist of one or more input blocks identified by the letters from A through M. The input files and blocks must be arranged as follows:

SELECTOR.IN
    A. Basic Information
    B. Water Flow Information
    C. Time Information
    D. Root Growth Information
    E. Heat Transport Information
    K. Carbon Dioxide Transport Information
    F. Solute Transport Information
    L. Major Ion Chemistry Information
    G. Root Water Uptake Information

PROFILE.DAT
    H. Nodal Information

ATMOSPH.IN
    I. Atmospheric Information

FIT.IN
    J. Inverse Solution Information

METEO.IN
    M. Meteorological Information

All input files must be placed into one subdirectory. Output files are printed into the same subdirectory. Another file, **HYDRUS1D.DAT**, which is not read by the executable code, enables communication between particular modules of the user-interface and will be described in part B of this manual. The input files can be created manually or with the graphics-based user-friendly interface **HYDRUS1D** also described in part B.

Tables 12.1 through 12.13 describe the data required for each input block. All data are read in using list-directed formatting (free format). Comment lines are provided at the beginning of, and within, each input block to facilitate, among other things, proper identification of the function of the block and the input variables. The comment lines are ignored during program execution; hence, they may be left blank but should not be omitted. The program assumes that all input data are specified in a consistent set of units for mass M, length L, and time T. The values

of temperature should be specified in degrees Celsius. Several variables in the METEO.IN file must be specified in the requested units.

Most of the information in Tables 12.1 through 12.13 should be self-explanatory. Table 12.8 (Block H) is used to define, among other things, the nodal coordinates and initial conditions for the pressure head, temperature and solute concentrations. One short-cut may be used when generating the nodal coordinates. The short-cut is possible when two nodes (e.g., N_1 and N_2), not adjacent to each other, are located such that N_2 is greater than N_1+1. The program will automatically generate nodes between N_1 and N_2, provided all of the following conditions are met simultaneously: (1) all nodes between nodes N_1 and N_2 are spaced at equal intervals, (2) values of the input variables $hNew(n)$, $Beta(n)$, $Axz(n)$, $Bxz(n)$, $Dxz(n)$, $Temp(n)$, $Conc(1,n)$ through $Conc(NS,n)$, and $Sorb(1,n)$ through $Sorb(NS,n)$ vary linearly between nodes N_1 and N_2, and (3) values of $LayNum(n)$ and $MatNum(n)$ are the same for all $n = N_1, N_1+1,..., N_2-1$ (see Table 12.8).

The major ion chemistry module requires four additional input files containing input data for the Pitzer equations. These four input files are provided together with the program and should not be changed by the user. The four input files, which were adopted from *Felmy* [1990], must be placed in the same directory as the executable program.

COMP.DAT   contains the species ID numbers, species names, and species charge.

BINARYP.DAT   contains the ID number of each species in each binary interaction considered (e.g., $CaHCO_3^+$) and the Pitzer ion interaction parameters $\beta^{(0)}$, $\beta^{(1)}$, $\beta^{(2)}$, and C^{φ} for binary systems.

TERNARYP.DAT   contains the Pitzer ion-interaction parameters for the common ion ternary systems, θ, and ψ. The first two columns include the cation-cation or anion-anion ID numbers associated with the ion-interaction parameter, θ, in column three. Subsequent columns include the anion or cation ID number and the triple ion-interaction parameter, ψ, associated with that triple ion interaction.

LAMBDA.DAT   contains the Pitzer ion-interaction parameters for the neutral species, λ and δ. The first column of this file contains the ID number for the neutral species, and the second column the ID number for the cation or anion involved in the neutral-cation or neutral-anion interaction parameterized by the Pitzer λ parameter included in the third column. Subsequent columns are for higher-order neutral interactions.

176

Table 12.1. Block A - Basic Information.

Record	Type	Variable	Description
0	Char	*iVer*	HYDRUS-1D version
1,2	-	-	Comment lines.
3	Char	*Hed*	Heading.
4	-	-	Comment line.
5	Char	*LUnit*	Length unit (e.g., 'cm').
6	Char	*TUnit*	Time unit (e.g., 'min').
7	Char	*MUnit*	Mass unit for concentration (e.g., 'g', 'mol', '-').
8	-	-	Comment line.
9	Logical	*lWat*	Set this logical variable equal to **.true.** when transient water flow is considered. Set this logical variable equal to **.false.** when initial condition is to be kept constant during the simulation.
9	Logical	*lChem*	Set this logical variable equal to **.true.** if solute transport is to be considered.
9	Logical	*lTemp*	Set this logical variable equal to **.true.** if heat transport is to be considered.
9	Logical	*lSink*	Set this logical variable equal to **.true.** if water extraction from the root zone occurs.
9	Logical	*lRoot*	Set this logical variable equal to **.true.** if root growth is to be considered.
9	Logical	*lShort*	**.true.** if information is to be printed only at preselected times, but not at each time step (T-level information, see Section 10), **.false.** if information is to be printed at each time step.
9	Logical	*lWDep*	**.true.** if hydraulic properties are to be considered as temperature dependent. **.false.** otherwise (see Section 2.5).
9	Logical	*lScreen*	**.true.** if information is to be printed on the screen during code execution.
9	Logical	*AtmInf*	**.true.** if variable boundary conditions are supplied via the input file ATMOSPH.IN, **.false.** if the file ATMOSPH.IN is not provided (i.e., in case of time independent boundary conditions).
9	Logical	*lEquil*[*]	**.true.** if equilibrium or no adsorption is considered in the solute transport equation. **.false.** if nonequilibrium adsorption is considered for at least one solute species.
9	Logical	*lInverse*[+]	**.true.** if inverse problem is to be solved. **.false.** if direct problem is to be solved.
10	-	-	Comment line.
11	Logical	*lSnow*	Set this logical variable equal to **.true.** if snow accumulation of the soil surface is to be considered (heat transport needs to be considered as well).

Table 12.1. (continued)

Record	Type	Variable	Description
11	Logical	*lHP1*	Set this logical variable equal to **.true.** when the HP1 module (obtained by coupling HYDRUS-1D and PHREEQC models) is to be run.
11	Logical	*lMeteo*	**.true.** if meteorological information is supplied via the input file METEO.IN. **.false.** if the file METEO.IN is not provided.
11	Logical	*lVapor*	**.true.** if vapor transport is to be considered (see section 2.1.1), **.false.** if vapor transport is not to be considered.
11	Logical	*lDummy*	Dummy variable (six times) (prepared for further expansions of the HYDRUS program). Set equal to .false..
12	-	-	Comment line.
13	Integer	*NMat*	Number of soil materials. Materials are identified by the material number, *MatNum*, specified in Block H.
13	Integer	*NLay*	Number of subregions for which separate water balances are being computed. Subregions are identified by the subregion number, *LayNum*, specified in Block H.
13	Real	*CosAlfa*	Cosine of the angle between the flow direction and the vertical axis (i.e., cos α = 1 for vertical flow, cos α = 0 for horizontal flow, and 0 < cos α < 1 for inclined flow.

[*]Parameter *lEquil* is replaced with parameter *lCO2* when the major ion chemistry module is used, indicating whether or not the carbon dioxide transport is to be considered.

[+]Parameter *lInverse* is replaced with parameter *lKRed* when the major ion chemistry module is used, indicating that a reduction in the hydraulic conductivity due to solution composition is to be considered.

Table 12.2. Block B - Water Flow Information.

Record	Type	Variable	Description
1,2	-	-	Comment lines.
3	Integer	*MaxIt*	Maximum number of iterations allowed during any time step (usually 20).
3	Real	*TolTh*	Absolute water content tolerance for nodes in the unsaturated part of the flow region [-] (its recommended value is 0.0001). *TolTh* represents the maximum desired absolute change in the value of the water content, θ, between two successive iterations during a particular time step.
3	Real	*TolH*	Absolute pressure head tolerance for nodes in the saturated part of the flow region [L] (its recommended value is 0.1 cm). *TolH* represents the maximum desired absolute change in the value of the pressure head, *h*, between two successive iterations during a particular time step.
4	-	-	Comment line.
5	Logical	*TopInf*	**.true.** if time dependent boundary condition is to be imposed at the top of the profile; data are supplied via input file ATMOSPH.IN. **.false.** in the case of time independent surface boundary conditions.
5	Logical	*WLayer*	Set this variable equal to **.true.** if water can accumulate at the surface with zero surface runoff.
5	Integer	*KodTop*	Code specifying type of boundary condition (BC) for water flow at the surface. Code number is positive for Dirichlet BC and negative for Neumann BC. In the case of 'Atmospheric BC' set *KodTop*=-1. Set *KodTop*=0 when a prescribed BC can change from Dirichlet BC to Neumann BC and vice versa.
5	Logical	*lInitW*	Set this variable equal to **.true.** if the initial condition is given in terms of the water content. Set this variable equal to **.false.** if the initial condition is given in terms of the pressure head
6	-	-	Comment line.
7	Logical	*BotInf*	**.true.** if time dependent boundary condition is to be imposed at the bottom of the profile; control data are supplied via input file ATMOSPH.IN. **.false.** in the case of time independent bottom boundary conditions.
7	Logical	*qGWLF*	Set this variable equal to **.true.** if the discharge-groundwater level relationship *q*(*GWL*) is applied as bottom boundary condition.
7	Logical	*FreeD*	**.true.** if free drainage is to be considered as bottom boundary condition.
7	Logical	*SeepF*	**.true.** if seepage face is to be considered as the bottom boundary condition.
7	Integer	*KodBot*	Code specifying type of boundary condition for water flow at the bottom of the profile. Code number is positive for a Dirichlet BC and negative for a Neumann BC. In case of a seepage face or free drainage BC set *KodBot*=-1.
7	Logical	*qDrain*	**.true.** if flow to horizontal drains is considered as bottom boundary condition.
7	Real	*hSeep*	Pressure head (i.e., 0) that initiates flow over the seepage face bottom boundary.

Table 12.2. (continued)

Record	Type	Variable	Description
8a	-	-	Comment line.
9a	Real	*rTop*	Prescribed top flux [LT^{-1}] (in case of a Dirichlet BC set this variable equal to zero).
9a	Real	*rBot*	Prescribed bottom flux [LT^{-1}] (in case of a Dirichlet BC set this variable equal to zero).
9a	Real	*rRoot*	Prescribed potential transpiration rate [LT^{-1}] (if no transpiration occurs or if transpiration is variable in time set this variable equal to zero).
			Records 8a and 9a are provided only when lower or upper boundary conditions are independent of time and at least one of them is a Neumann BC.
8b	-	-	Comment line.
9b	Real	*GWL0L*	Reference position of the groundwater table (e.g., the *x*-coordinate of the soil surface).
9b	Real	*Aqh*	Value of the parameter A_{qh} [LT^{-1}] in the *q*(*GWL*)-relationship, equation (10.1); set to zero if *qGWLF*=**.false.**
9b	Real	*Bqh*	Value of the parameter B_{qh} [L^{-1}] in the *q*(*GWL*)-relationship, equation (10.1); set to zero if *qGWLF* =**.false.**
			Records 8b and 9b are provided only when the logical variable *qGWLF*=**.true.**.
8c	-	-	Comment line.
9c	Integer	*iPosDr*	Code for position of the drain. = 1: Homogeneous profile; drain on top of impervious layer. = 2: Homogeneous profile; drain above impervious layer. = 3: Layered profile; drain at interface between both soil layers. = 4: Layered profile; drain in bottom layer. = 5: Layered profile; drain in top layer.
10c	-	-	Comment line.
11c	Real	*zBotDr*	Coordinate of the bottom of the drain system [L].
11c	Real	*rSpacing*	Drain spacing, L_{dr} [L].
11c	Real	*Entres*	Entrance resistance, γ_{entr} [T].
12c	-	-	Comment line.
			The following value is specified when *iPosDr* = 1.
13c	Real	*KhTop*	Horizontal saturated hydraulic conductivity above the drain, K_{hTop} [LT^{-1}].
			The following three values are specified when *iPosDr* = 2.
13c	Real	*BaseGW*	Coordinate of the impervious layer [L].
13c	Real	*KhTop*	Horizontal saturated hydraulic conductivity above the drain, K_{hTop} [LT^{-1}].

Table 12.2. (continued)

Record	Type	Variable	Description
13c	Real	*WetPer*	Wet perimeter of the drain, u [L].
			The following four values are specified when *iPosDr* = 3.
13c	Real	*BaseGW*	Coordinate of the impervious layer [L].
13c	Real	*KhTop*	Horizontal saturated hydraulic conductivity above the drain, K_{hTop} [LT^{-1}].
13c	Real	*KhBot*	Horizontal saturated hydraulic conductivity below the drain, K_{hBot} [LT^{-1}].
13c	Real	*WetPer*	The wet perimeter, u, of the drain [L].
			The following six values are specified when *iPosDr* = 4.
13c	Real	*BaseGW*	Coordinate of the impervious layer [L].
13c	Real	*KvTop*	Vertical saturated hydraulic conductivity above the drain, K_{vTop} [LT^{-1}].
13c	Real	*KvBot*	Vertical saturated hydraulic conductivity below the drain, K_{vBot} [LT^{-1}].
13c	Real	*KhBot*	Horizontal saturated hydraulic conductivity below the drain, K_{hBot} [LT^{-1}].
13c	Real	*WetPer*	The wet perimeter, u, of the drain [L].
13c	Real	*zInTF*	Coordinate of the transition between the upper and lower soil layer [L].
			The following seven values are specified when *iPosDr* = 5.
13c	Real	*BaseGW*	Coordinate of the impervious layer [L].
13c	Real	*KhTop*	Horizontal saturated hydraulic conductivity above the drain, K_{hTop} [LT^{-1}].
13c	Real	*KvTop*	Vertical saturated hydraulic conductivity above the drain, K_{vTop} [LT^{-1}].
13c	Real	*KhBot*	Horizontal saturated hydraulic conductivity below the drain, K_{hBot} [LT^{-1}].
13c	Real	*WetPer*	The wet perimeter, u, of the drain [L].
13c	Real	*zInTF*	Coordinate of the transition between the upper and lower soil layers [L].
13c	Real	*GeoFac*	Geometry factor, a_{dr} [-], as obtained by the relaxation method [*Ernst*, 1962] (see Table below).

K_{hbot}/K_{htop}	D_{bot}/D_{top}					
	1 2	4	8	16	32	
1	2.0	3.0	5.0	9.0	15.0	30.0
2	2.4	3.2	4.6	6.2	8.0	10.0
3	2.6	3.3	4.5	5.5	6.8	8.0
5	2.8	3.5	4.4	4.8	5.6	6.2
10	3.2	3.6	4.2	4.5	4.8	5.0
20	3.6	3.7	4.0	4.2	4.4	4.6
50	3.8	4.0	4.0	4.0	4.2	4.6

Record	Type	Variable	Description
10	-	-	Comment line.
11	Real	*ha*	Absolute value of the upper limit [L] of the pressure head interval below which a table of hydraulic properties will be generated internally for each material (h_a must be greater than 0.0; e.g. 0.001 cm) (see Section 5.4.7).

Table 12.2. (continued)

Record	Type	Variable	Description
11	Real	*hb*	Absolute value of the lower limit [L] of the pressure head interval for which a table of hydraulic properties will be generated internally for each material (e.g. 1000 m). One may assign to h_b the highest (absolute) expected pressure head to be expected during a simulation. If the absolute value of the pressure head during program execution lies outside of the interval $[h_a, h_b]$, then appropriate values for the hydraulic properties are computed directly from the hydraulic functions (i.e., without interpolation in the table).
12	-	-	Comment line.
13	Integer	*iModel*	Soil hydraulic properties model: = 0; *van Genuchten*'s [1980] model with six parameters. = 1; modified van Genuchten's model with ten parameters [*Vogel and Císlerová, 1988*]. = 2; *Brooks and Corey*'s [1964] model with six parameters. = 3; *van Genuchten*'s [1980] model with air-entry value of -2 cm and with six parameters. = 4; *Kosugi*'s [1996] model with six parameters. = 5; dual porosity model of *Durner* [1994] with nine parameters. = 6; dual-porosity system with transfer proportional to the effective saturation (9 parameters) (see Sections 2.1.3. and 2.8.). = 7; dual-porosity system with transfer proportional to the pressure head (11 parameters) (see Sections 2.1.3. and 2.8.). = 9; dual-permeability system with transfer proportional to the pressure head (17 parameters) (see Sections 2.1.4. and 2.8.). iModel>3 options are not available with the major ion chemistry module.
13	Integer	*iHyst*	Hysteresis in the soil hydraulic properties: = 0; No hysteresis = 1; Hysteresis in the retention curve only = 2; Hysteresis in both the retention and hydraulic conductivity functions = 3; Hysteresis using Robert Lenhard's model [*Lenhard et al.*, 1991; *Lenhard and Parker*, 1992]. (Not available with major ion chemistry module.)
14	-	-	Comment line.
15	Integer	*iKappa*	= -1 if the initial condition is to be calculated from the main drying branch. = 1 if the initial condition is to be calculated from the main wetting branch. Records 14 and 15 are provided only when *iHyst* > 0.
16	-	-	Comment line.
17	Real	*Par*(1,M)	Parameter θ_r for material *M* [-].
17	Real	*Par*(2,M)	Parameter θ_s for material *M* [-].
17	Real	*Par*(3,M)	Parameter α for material *M* [L^{-1}].

Table 12.2. (continued)

Record	Type	Variable	Description
17	Real	*Par*(4,*M*)	Parameter n for material M [-].
17	Real	*Par*(5,*M*)	Parameter K_s for material M [LT^{-1}].
17	Real	*Par*(6,*M*)	Parameter l for material M [-].
			The previous six parameters are specified for the matrix region when *iModel*=9.
			The following four parameters are specified only when *iModel*=1.
17	Real	*Par*(7,*M*)	Parameter θ_m for material M [-].
17	Real	*Par*(8,*M*)	Parameter θ_a for material M [-].
17	Real	*Par*(9,*M*)	Parameter θ_k for material M [-].
17	Real	*Par*(10,*M*)	Parameter K_k for material M [LT^{-1}].
			The following four parameters are specified only when *iModel*=0 and *iHyst*>1.
17	Real	*Par*(7,*M*)	Parameter θ_m for material M [-].
17	Real	*Par*(8,*M*)	Parameter θ_s^w for material M [-].
17	Real	*Par*(9,*M*)	Parameter α^w for material M [L^{-1}].
17	Real	*Par*(10,*M*)	Parameter K_s^w for material M [LT^{-1}].
			The following three parameters are specified only when *iModel*=5 [*Durner*, 1994].
17	Real	*Par*(7,*M*)	Parameter w for material M [-]. The weighting factor for the sub-curve for the second overlapping subregion.
17	Real	*Par*(8,*M*)	Parameter α for material M [L^{-1}] for the second overlapping subregion.
17	Real	*Par*(9,*M*)	Parameter n for material M [-] for the second overlapping subregion.
			The following four parameters are specified only when *iModel*=6 (dual-porosity system with transfer proportional to the water content gradient).
17	Real	*Par*(7,*M*)	Parameter θ_r^{im} for the immobile region of material M [-].
17	Real	*Par*(8,*M*)	Parameter θ_s^{im} for the immobile region of material M [-].
17	Real	*Par*(9,*M*)	Parameter ω (mass transfer coefficient in (2.92)) for material M [-].
			The following four parameters are specified only when *iModel*=7 (dual-porosity system with transfer proportional to the pressure head gradient).
17	Real	*Par*(7,*M*)	Parameter θ_r^{im} for the immobile region of material M [-].
17	Real	*Par*(8,*M*)	Parameter θ_s^{im} for the immobile region of material M [-].
17	Real	*Par*(9,*M*)	Parameter α^{im} for the immobile region of material M [-].
17	Real	*Par*(10,*M*)	Parameter n^{im} for the immobile region of material M [-].
17	Real	*Par*(11,*M*)	Parameter K_a (mass transfer coefficient in (2.96)) for material M [-].
			Record 17 information is provided for each material M (from 1 to *NMat*).
			If *lWDep*=**.true.** (Block A) then the soil hydraulic parameters *Par*(i,*M*) must be specified at reference temperature T_{ref}=20°C.
18	-	-	Comment line.
19	Real	*ParF*(1,*M*)	Parameter θ_r for material M [-].
19	Real	*ParF*(2,*M*)	Parameter θ_s for material M [-].
19	Real	*ParF*(3,*M*)	Parameter α for material M [L^{-1}].

Table 12.2. (continued)

Record	Type	Variable	Description
19	Real	*ParF*(4,*M*)	Parameter *n* for material *M* [-].
19	Real	*ParF*(5,*M*)	Parameter K_s for material *M* [LT^{-1}].
19	Real	*ParF*(6,*M*)	Parameter *l* for material *M* [-]. The previous six parameters are specified for the fracture region when *iModel*=9 (dual-permeability model).
19	Real	*ParAF*(1,*M*)	Parameter *w* for material *M* [-]. *w* is the ratio of the volumes of the macropore or fracture domain and the total soil system (for *iModel*=9, i.e., the dual-permeability model).
19	Real	*ParAF*(2,*M*)	Parameter β (a shape factor that depends on the geometry) for material *M* [-]. See eq. (2.94).
19	Real	*ParAF*(3,*M*)	Parameter γ (a scaling factor) for material *M* [-]. See eq. (2.94).
19	Real	*ParAF*(4,*M*)	Parameter *d* (an effective 'diffusion' pathlength) for material *M* [L]. See eq. (2.94).
19	Real	*ParAF*(5,*M*)	Parameter K_a (the effective hydraulic conductivity K_a [LT^{-1}] of the fracture-matrix interface) for material *M* [LT^{-1}]. See eq. (2.94).
			Record 19 information is provided for each material *M* (from 1 to *NMat*).
			Records 18 and 19 are provided only when *iModel* = 9, i.e., for the dual-permeability model.

Table 12.3. Block C - Time information.

Record	Type	Variable	Description
1,2	-	-	Comment lines.
3	Real	*dt*	Initial time increment, Δt [T]. Initial time step should be estimated in dependence on the problem being solved. For problems with high-pressure gradients (e.g. infiltration into an initially dry soil), Δt should be relatively small.
3	Real	*dtMin*	Minimum permitted time increment, Δt_{min} [T].
3	Real	*dtMax*	Maximum permitted time increment, Δt_{max} [T].
3	Real	*dMul*	If the number of required iterations at a particular time step is less than or equal to *ItMin*, then Δt for the next time step is multiplied by a dimensionless number $dMul \geq 1.0$ (its value is recommended not to exceed 1.3).
3	Real	*dMul2*	If the number of required iterations at a particular time step is greater than or equal to *ItMax*, then Δt for the next time step is multiplied by $dMul2 \leq 1.0$ (e.g. 0.33).
3	Integer	*ItMin*	If the number of required iterations at a particular time step is less than or equal to *ItMin*, then Δt for the next time step is multiplied by a dimensionless number $dMul \geq 1.0$ (its value is recommended not to exceed 1.3).
3	Integer	*ItMax*	If the number of required iterations at a particular time step is greater than or equal to *ItMax*, then Δt for the next time step is multiplied by $dMul2 \leq 1.0$ (e.g. 0.33).
3	Integer	*MPL*	Number of specified print-times at which detailed information about the pressure head, water content, flux, temperature, concentrations, and the water and solute balances will be printed.
4	-	-	Comment line.
5	Real	*tInit*	Initial time of the simulation [T].
5	Real	*tMax*	Final time of the simulation [T].
6	-	-	Comment line.
7	Logical	*lPrint*	Set this logical variable equal to **.true.** if information about the pressure heads, water contents, temperatures, and concentrations in observation nodes, and the water and solute fluxes is to be printed at a constant time interval *tPrintInterval*.
7	Integer	*nPrintSteps*	Information to the screen and output files is not printed at each time step, but after each *nPrintSteps*.
7	Real	*tPrintInterval*	A constant time interval after which information about the pressure heads, water contents, temperatures, and concentrations in observation nodes, and the water and solute fluxes is to be printed.

Table 12.3. (continued)

Record	Type	Variable	Description
7	Logical	*lEnter*	Set this logical variable equal to **.true.** if the Enter key is to be pressed at the end of simulation.
8	-	-	Comment line.
9	Real	*TPrint*(1)	First specified print-time [T].
9	Real	*TPrint*(2)	Second specified print-time [T].
.	.	.	.
.	.	.	.
9	Real	*TPrint*(*MPL*)	Last specified print-time [T]. (Maximum six values on one line.)

Table 12.4. Block D - Root Growth Information.[+]

Record	Type	Symbol	Description
1,2	-	-	Comment lines.
3	Integer	*iRootIn*	= 0; the root depth is specified together with other time-variable boundary condition, such as atmospheric fluxes. = 1; the root depth is given in a table = 2; the root depth is calculated using the growth function.
			The following lines 4-7 are given only when *iRootIn* =1, i.e., using a table of *RootDepth* values.
4	-	-	Comment line
5	Integer	*nGrowth*	Number of data points in the root depth table.
6	-	-	Comment line
7 7	Real Real	*tGrowth* *RootDepth*	Day Rooting depth [L] Line 7 is given *nGrowth* times.
			The following lines 8 and 9 are given only when *iRootIn* =2.
8	-	-	Comment lines.
	Integer	*iRFak*	Method to calculate the root growth factor, *r*.
9			= 0; the root growth factor is calculated from given data [*xRMed*, *tRMed*].
			= 1; the root growth factor is calculated based on the assumption that 50% of the rooting depth, (*xRMax*+*xRMin*)/2., is reached at the midpoint of the growing season, (*tRMin*+*tRHarv*)/2.
9	Real	*tRMin*	Initial time of the root growth period [T].
9	Real	*tRMed*	Time of known rooting depth (set equal to zero if *iRFak*=1) [T].
9	Real	*tRHarv*	Time at the end of the root water uptake period [T].
9	Real	*xRMin*	Initial value of the rooting depth at the beginning of the growth period (recommended value = 1 cm) [L].
9	Real	*xRMed*	Value of known rooting depth (set equal to zero if *iRFak*=1) [L].
9	Real	*xRMax*	Maximum rooting depth, which may be reached at infinite time [L].
9	Real	*tRPeriod*	Time period at which the growth function repeat itself.

[+] Block D is not needed if the logical variable *lRoot* (Block A) is set equal to **.false.**

Table 12.5. Block E - Heat transport information.[+]

Record	Type	Symbol	Description
1,2	-	-	Comment lines.
3	Real	TPar(1,M)	Volumetric solid phase fraction of material M, θ_n [-].
3	Real	TPar(2,M)	Volumetric organic matter fraction of material M, θ_o [-].
3	Real	TPar(3,M)	Longitudinal thermal dispersivity of material M, λ_L [L].
3	Real	TPar(4,M)	Coefficient b_1 in the thermal conductivity function [$MLT^{-3}K^{-1}$] (e.g. $Wm^{-1}K^{-1}$) (see equation (4.8)).
3	Real	TPar(5,M)	Coefficient b_2 in the thermal conductivity function [$MLT^{-3}K^{-1}$] (e.g. $Wm^{-1}K^{-1}$) (see equation (4.8)).
3	Real	TPar(6,M)	Coefficient b_3 in the thermal conductivity function [$MLT^{-3}K^{-1}$] (e.g. $Wm^{-1}K^{-1}$) (see equation (4.8)).
3	Real	TPar(7,M)	Volumetric heat capacity of solid phase of material M, C_n [$ML^{-1}T^{-2}K^{-1}$] (e.g. $Jm^{-3}K^{-1}$).
3	Real	TPar(8,M)	Volumetric heat capacity of organic matter of material M, C_o [$ML^{-1}T^{-2}K^{-1}$] (e.g. $Jm^{-3}K^{-1}$).
3	Real	TPar(9,M)	Volumetric heat capacity of liquid phase of material M, C_w [$ML^{-1}T^{-2}K^{-1}$] (e.g. $Jm^{-3}K^{-1}$).
			Record 3 is required for each soil material M (from 1 to NMat).
4	-	-	Comment line.
5	Real	Ampl	Temperature amplitude at the soil surface [K].
5	Real	tPeriod	Time interval for completion of one temperature cycle (usually 1 day) [T].
5	Integer	iCampbell	Set equal to 1 if Campbell [1985] formula is to be used to calculate the thermal conductivity. Set equal to 0, when Chung and Horton [1987] formula is to be used.
5	Real	SnowMF	Amount of snow that will melt during one day for each ^{o}C (e.g., 0.43 cm).
5	Logical	lDummy	Dummy variable (five times) (reserved for further expansions of HYDRUS). Set equal to .false..
6	-	-	Comment line.
7	Integer	kTopT	Code which specifies the type of upper boundary condition =1: Dirichlet boundary condition, =-1: Cauchy boundary condition.
7	Real	tTop	Temperature of the upper boundary, or temperature of the incoming fluid [^{o}C].
7	Integer	kBotT	Code which specifies the type of lower boundary condition =1: Dirichlet boundary condition, =0: continuous temperature profile, zero gradient, =-1: Cauchy boundary condition.
7	Real	tBot	Temperature of lower boundary, or temperature of the incoming fluid [^{o}C].

[+] Block E is not needed if logical variable lTemp (Block A) is set equal to **.false.**

Table 12.6. Block F - Solute transport information.[+]

Record	Type	Variable	Description
1,2	-	-	Comment lines.
3	Real	*Epsi*	Temporal weighing coefficient. =0.0 for an explicit scheme. =0.5 for a Crank-Nicholson implicit scheme. =1.0 for a fully implicit scheme.
3	Logical	*lUpW*	**.true.** if upstream weighing formulation is to be used. **.false.** if the original Galerkin formulation is to be used.
3	Logical	*lArtD*	**.true.** if artificial dispersion is to be added in order to fulfill the stability criterion *PeCr* (see Section 8.4.4). **.false.** otherwise.
3	Logical	*lTDep*	**.true.** if at least one transport or reaction coefficient (*ChPar*) is temperature dependent. **.false.** otherwise. If *lTDep*=**.true.**, then all values of *ChPar*(i,M) should be specified at a reference temperature T_r=20°C.
3	Real	*cTolA*	Absolute concentration tolerance [ML^{-3}], the value is dependent on the units used (set equal to zero if nonlinear adsorption is not considered).
3	Real	*cTolR*	Relative concentration tolerance [-] (set equal to zero if nonlinear adsorption is not considered).
3	Integer	*MaxItC*	Maximum number of iterations allowed during any time step for solute transport - usually 20 (set equal to zero if nonlinear adsorption is not considered).
3	Real	*PeCr*	Stability criteria (see Section 8.4.4). Set equal to zero when *lUpW* is equal to **.true.**.
3	Integer	*NS*	Number of solutes.
3	Logical	*lTort*	**.true.** if the tortuosity factor [*Millington and Quirk,* 1961] is to be used. **.false.** if the tortuosity factor is assumed to be equal to one.
3	Integer	*iBacter*	Set equal to 1 if attachment/detachment approach is to be used to calculate nonequilibrium transport of viruses, colloids, or bacteria. Set equal to 0 if original formulations, i.e., physical nonequilibrium or two-site sorption is to be used to describe nonequilibrium solute transport.
3	Logical	*lFiltr*	Set this logical variable equal to **.true.** if the attachment coefficient is to be evaluated using the filtration theory (eq. (3.24)).
3	Integer	*nChPar*	Number of solute transport parameters specific for each solute.
4	-	-	Comment line.

Table 12.6. (continued)

Record	Type	Variable	Description
5	Integer	*iNonEqual*	Code describing type of nonequilibrium considered for solute transport: = 0: equilibrium solute transport = 1: one-site sorption model (chemical nonequilibrium) = 2: two-site sorption model (chemical nonequilibrium) = 3: two kinetic sorption sites model (attachment/detachment; chemical nonequilibrium). This model is often used for particle (viruses, colloids, bacteria) transport. = 4: two kinetic sorption sites model (attachment/detachment) (chemical nonequilibrium). Attachment coefficients are calculated using filtration theory. = 5: dual-porosity model (mobile-immobile regions; physical nonequilibrium). = 6: dual-porosity model (mobile-immobile regions) with two-site sorption in the mobile zone (physical and chemical nonequilibrium). = 7: dual-permeability model (physical nonequilibrium). = 8: dual-permeability model with either an immobile region in the matrix domain (physical nonequilibrium) or with two-site sorption in both domains (physical and chemical nonequilibrium).
5	Logical	*lWatDep*	**.true.** if at least one degradation coefficient (*ChPar*) is water content dependent. **.false.** otherwise. If *lWatDep*=**.true.**, then values of all degradation coefficients should be specified at a reference water content.
5	Logical	*lDualNEq*	**.true.** if the dual-porosity model (mobile-immobile regions) with two-site sorption in the mobile zone (physical and chemical nonequilibrium) is to be considered (*iNonEqual* =6).
5	Logical	*lDummy*	Dummy variable (eight times) (reserved for further expansions of HYDRUS). Set equal to .false..
6	-	-	Comment line.
7	Real	*ChPar*(1,*M*)	Bulk density of material *M*, ρ [ML^{-3}].
7	Real	*ChPar*(2,*M*)	Longitudinal dispersivity for material type *M*, D_L [L].
7	Real	*ChPar*(3,*M*)	Dimensionless fraction of the adsorption sites classified as type-1, i.e., sites with instantaneous sorption, when the **chemical nonequilibrium** option is considered. Set equal to 1 if equilibrium transport is to be considered. Dimensionless fraction of the adsorption sites in contact with mobile water when the **physical nonequilibrium** option is considered. Set equal to 1 if all sorption sites are in contact with the mobile water.
7	Real	*ChPar*(4,*M*)	Immobile water content. Set equal to 0 when the **physical nonequilibrium** option is not considered.

Table 12.6. (continued)

Record	Type	Variable	Description
			The parameters $ChPar(i,M)$ below are to be reinterpreted when the variable $iNonEqual$ =7 or 8 (for the dual-permeability model).
7	Real	$ChPar(2,M)$	Longitudinal dispersivity in the matrix domain for material type M, D_L [L].
7	Real	$ChPar(3,M)$	Dimensionless fraction of adsorption sites classified as type-1 (i.e., sites with instantaneous sorption) in the matrix domain when the **chemical nonequilibrium** option is considered ($iNonEqual$=2). Set equal to 1 if equilibrium transport is to be considered ($iNonEqual$=0). Set equal to 0 when one-site kinetic sorption is to be considered ($iNonEqual$=1). Dimensionless fraction of adsorption sites in contact with mobile water in the matrix domain when the **physical nonequilibrium** option is considered ($iNonEqual$=5 or 6). Set equal to 1 if all sorption sites are in contact with the mobile water.
7	Real	$ChPar(4,M)$	Immobile water content of the matrix domain. Set equal to 0 when the **physical nonequilibrium** option is not considered or if $iModel$=6 or 7.
			Record 7 information is provided for each material M (from 1 to $NMat$).
8	-	-	Comment line.
9	Real	$ChPar(5,M)$	Ionic or molecular diffusion coefficient in free water, D_w [L^{2}T^{-1}].
9	Real	$ChPar(6,M)$	Ionic or molecular diffusion coefficient in gas phase, D_g [L^{2}T^{-1}].
			The parameter $ChPar(6,M)$ is to be reinterpreted when the variable $iNonEqual$ =7 or 8:
9	Real	$ChPar(6,M)$	Mass transfer coefficient, ω_{dp} [T^{-1}], for solute mass transfer between the fracture and matrix domains. See eq. (3.38).
10	-	-	Comment line.
11	Real	$ChPar(7,M)$	Adsorption isotherm coefficient, k_s, for material type M [L^{3}M^{-1}]. Set equal to zero if no adsorption is to be considered.
11	Real	$ChPar(8,M)$	Adsorption isotherm coefficient, η, for material type M [L^{3}M^{-1}]. Set equal to zero if Langmuir adsorption isotherm is not to be considered.
11	Real	$ChPar(9,M)$	Adsorption isotherm coefficient, β, for material type M [-]. Set equal to one if Freundlich adsorption isotherm is not to be considered.
11	Real	$ChPar(10,M)$	Equilibrium distribution constant between liquid and gas phases, k_g, material type M [-].
11	Real	$ChPar(11,M)$	First-order rate constant for the dissolved phase, μ_w, material type M [T^{-1}].
11	Real	$ChPar(12,M)$	First-order rate constant for the solid phase, μ_s, material type M [T^{-1}].
11	Real	$ChPar(13,M)$	First-order rate constant for the gas phase, μ_g, material type M [T^{-1}].
11	Real	$ChPar(14,M)$	Rate constant, $\mu_w{'}$, representing a first-order decay for the first solute and zero-order production for the second solute in the dissolved phase, material type M [T^{-1}].
11	Real	$ChPar(15,M)$	Same as above for the solid phase, $\mu_s{'}$, material type M [T^{-1}].
11	Real	$ChPar(16,M)$	Same as above for the gas phase, $\mu_g{'}$, material type M [T^{-1}].
11	Real	$ChPar(17,M)$	Zero-order rate constant for the dissolved phase, γ_w, material type M [ML^{-3}T^{-1}].

Table 12.6. (continued)

Record	Type	Variable	Description
11	Real	$ChPar(18,M)$	Zero-order rate constant for the solid phase, γ_s, of material type M [T^{-1}].
11	Real	$ChPar(19,M)$	Zero-order rate constant for the gas phase, γ_g, of material type M [ML^{-3}T^{-1}].
11	Real	$ChPar(20,M)$	First-order rate transfer coefficient for nonequilibrium adsorption, or the mass transfer coefficient for solute exchange between mobile and immobile liquid regions, ω, material type M [T^{-1}].
			The parameters $ChPar(6,M)$ and $ChPar(13,M)$ through $ChPar(20,M)$ are to be reinterpreted when the variable $iBacter$=1 ($iNonEqual$ =3):
11	Real	$ChPar(6,M)$	Diameter of the sand grains, d_c [L].
11	Integer	$ChPar(13,M)$	Type of blocking, $iPsi$, used in (3.19) for the second sorption sites. $= 0$: No blocking. $= 1$: Langmuirian dynamics, (3.20). $= 2$: ripening, (3.21). $= 3$: random sequential adsorption, (3.22). $= 4$: depth dependent blocking coefficient, (3.23).
11	Integer	$ChPar(14,M)$	Same for the first sorption sites.
11	Real	$ChPar(15,M)$	Parameter in the blocking function for the second sorption sites (s_{max} for (3.20), (3.21) and (3.22), β in (3.23)).
11	Real	$ChPar(16,M)$	The first-order deposition (attachment) coefficient, k_a [T^{-1}], for the second sorption sites.
11	Real	$ChPar(17,M)$	The first-order entrainment (detachment) coefficient, k_d [T^{-1}], for the second sorption sites.
11	Real	$ChPar(18,M)$	Parameter in the blocking function for the first sorption sites.
11	Real	$ChPar(19,M)$	The first-order deposition (attachment) coefficient, k_a [T^{-1}], for the first sorption sites.
11	Real	$ChPar(20,M)$	The first-order entrainment (detachment) coefficient, k_d [T^{-1}], for the first sorption sites.
			The parameters $ChPar(13,M)$ through $ChPar(20,M)$ are to be reinterpreted when the variable $iBacter$=1 and $lFilter$=.true. ($iNonEqual$ =4):
11	Integer	$ChPar(13,M)$	Diameter of the sand grains, d_c [L].
11	Integer	$ChPar(14,M)$	Diameter of the particle, d_p (e.g., virus, bacteria) (= 0.95 μm or 0.95e-6 m) [L].
11	Real	$ChPar(15,M)$	Parameter s_{max} in the blocking function for the second sorption sites (3.20).
11	Real	$ChPar(16,M)$	Sticking efficiency, α [-], for the second sorption sites.
11	Real	$ChPar(17,M)$	The first-order entrainment (detachment) coefficient, k_d [T^{-1}], for the second sorption sites.
11	Real	$ChPar(18,M)$	Parameter s_{max} in the blocking function for the first sorption sites (3.20).
11	Real	$ChPar(19,M)$	Sticking efficiency, α [-], for the first sorption sites.
11	Real	$ChPar(20,M)$	The first-order entrainment (detachment) coefficient, k_d [T^{-1}], for the first sorption sites.
			The parameters $ChPar(i,M)$ must be reinterpreted when the variable $iNonEqual$ =6:
11	Real	$ChPar(10,M)$	Must be set equal to zero.

Table 12.6. (continued)

Record	Type	Variable	Description
11	Real	$ChPar(13,M)$	Dimensionless fraction of adsorption sites classified as type-1 (i.e., sites with instantaneous sorption in contact with the mobile domain). Remaining sites are classified as type-2 sites (i.e., with kinetic sorption). See eq. (3.37).
11	Real	$ChPar(16,M)$	First-order rate transfer coefficient for nonequilibrium adsorption to type-2 sorption sites in the mobile region, α_{ch}, material type M [T^{-1}]. See eq. (3.37).
11	Real	$ChPar(20,M)$	Mass transfer coefficient for solute exchange between mobile and immobile liquid regions, ω_{ph}, for material type M [T^{-1}]. See eq. (3.37).
			The parameters $ChPar(i,M)$ must be reinterpreted when the variable $iNonEqual$ =7 or 8 (for the dual-permeability model):
11	Real	$ChPar(7,M)$	Adsorption isotherm coefficient, K_{dm}, for the matrix domain, for material type M [L^{3}M^{-1}]. Set equal to zero if no adsorption is to be considered.
11	Real	$ChPar(10,M)$	First-order rate transfer coefficient for nonequilibrium adsorption in the matrix domain, $\alpha_{ch,m}$, material type M [T^{-1}]. See eq. (3.41).
11	Real	$ChPar(13,M)$	Longitudinal dispersivity in the fracture domain for material type M, D_L [L].
11	Real	$ChPar(16,M)$	Dimensionless fraction of adsorption sites classified as type-1 (i.e., sites with instantaneous sorption) in the fracture domain when the **chemical nonequilibrium** option is considered.
11	Real	$ChPar(19,M)$	Adsorption isotherm coefficient, K_{df}, for the fracture domain, for material type M [L^{3}M^{-1}]. Set equal to zero if no adsorption is to be considered.
11	Real	$ChPar(20,M)$	First-order rate transfer coefficient for nonequilibrium adsorption in the fracture domain, $\alpha_{ch,f}$, for material type M [T^{-1}]. See eq. (3.41).
			Record 11 information is provided for each material M (from 1 to $NMat$).
			Record 7 through 11 information is provided for each solute (from 1 to NS).
12,13	-	-	Comment lines.
14	Real	$TDep(5)$	Activation energy for parameter $ChPar(5,M)$ [ML^{2}T^{-2}M^{-1}] (see Section 3.4). This parameter should be specified in J mol^{-1}. Set equal to 0 if $ChPar(5,M)$ is temperature independent.
14	Real	$TDep(6)$	Same for parameter $ChPar(6,M)$ [ML^{2}T^{-2}M^{-1}].
15	-	-	Comment line.
16	Real	$TDep(7)$	Same for parameter $ChPar(7,M)$ [ML^{2}T^{-2}M^{-1}].
.	.	.	.
.	.	.	.
16	Real	$TDep(20)$	Same for parameter $ChPar(20,M)$ [ML^{2}T^{-2}M^{-1}].
			Record 12 through 16 information is provided only when the logical variable $lTDep$ of record 3 is set equal to **.true.**.
17,18	-	-	Comment lines.
19	Integer	$nParWD$	Number of parameters whose values are water content dependent.

Table 12.6. (continued)

Record	Type	Variable	Description
20	-	-	Comment line.
21	Real	$WDep(1)$	First parameter for the water content dependence of degradation coefficients (see Section 3.4). Set equal to 0 if $ChPar(11,M)$ is water content independent.
.	.	.	.
.	.	.	.
21	Real	$WDep(nParWD)$	Same for parameter $ChPar(19,M)$.
22	Real	$WDep(1)$	Second parameter for the water content dependence of degradatioin coefficients (see Section 3.4). Set equal to 0 if $ChPar(11,M)$ is water content independent.
.	.	.	.
.	.	.	.
22	Real	$WDep(nParWD)$	Same for parameter $ChPar(19,M)$.
			Record 17 through 22 information is provided only when the logical variable $lWatDep$ of record 5 is set equal to **.true.**.
23	-	-	Comment line.
24	Integer	$kTopCh$	Code which specifies the type of upper boundary condition =1: Dirichlet boundary condition, =-1: Cauchy boundary condition. =-2: a special type of boundary condition for volatile solutes as described by equation (3.46).
24	Real	$cTop(1)$	Concentration of the upper boundary, or concentration of the incoming fluid, for the first solute $[ML^{-3}]$.
24	Real	$cTop(2)$	Concentration of the upper boundary, or concentration of the incoming fluid, for the second solute $[ML^{-3}]$ (not specified if $NS < 2$).
.	.	.	.
24	Real	$cTop(NS)$	Concentration of the upper boundary, or concentration of the incoming fluid, for the NSth solute $[ML^{-3}]$.
24	Integer	$kBotCh$	Code which specifies the type of lower boundary condition =1: Dirichlet boundary condition, =0: continuous concentration profile, =-1: Cauchy boundary condition.
24	Real	$cBot(1)$	Concentration of lower boundary, or concentration of the incoming fluid, for the first solute $[ML^{-3}]$.
24	Real	$cBot(2)$	Concentration of lower boundary, or concentration of the incoming fluid, for the second solute $[ML^{-3}]$ (not specified if $NS < 2$).
.	.	.	.
24	Real	$cBot(NS)$	Concentration of lower boundary, or concentration of the incoming fluid, for the NSth solute $[ML^{-3}]$.

Table 12.6. (continued)

Record	Type	Variable	Description
25	-	-	Comment line.
26	Real	*dSurf*	Thickness of the stagnant boundary layer, d [L] (see equation (3.46)).
26	Real	*cAtm*	Concentration above the stagnant boundary layer, g_{atm} [ML^{-3}] (see equation (3.46)).
			Records 17 and 18 information is provided only when *kTopCh*=-2.
27	-	-	Comment line.
28	Real	*tPulse*	Time duration of the concentration pulse [T].

[+] Block F is not needed when the logical variable *lChem* in Block A is set equal to **.false.** .

Table 12.7. Block G - Root water uptake information. [+]

Record	Type	Variable	Description
1,2	-	-	Comment lines.
3	Integer	*iMoSink*	Type of root water uptake stress response function. = 0; *Feddes et al.* [1978] = 1; S-shaped, *van Genuchten* [1987]
3	Real	*cRootMax*(1)	Maximum allowed concentration in the root solute uptake term for the first solute [ML^{-3}]. When the nodal concentration is lower than *cRootMax*, all solute is taken up. When the nodal concentration is higher than *cRootMax*, additional solute stays behind.
.	.	.	.
.	.	.	.
3	Real	*cRootMax*(*NS*)	Maximum allowed concentration in the root solute uptake term for the last solute [ML^{-3}].
3	Real	*OmegaC*	Critical root water uptake index. Set equal to zero for a noncompensated root water uptake and smaller than zero for compensated root water uptake [-].
4	-	-	Comment line.
			The following records (records 5a, 6a, 7a) are given only if *iMoSink*=0.
5a	Real	*P0*	Value of the pressure head, h_1 (Fig. 2.1), below which roots start to extract water from the soil.
5a	Real	*P2H*	Value of the limiting pressure head, h_3, below which the roots cannot extract water at the maximum rate (assuming a potential transpiration rate of *r2H*).
5a	Real	*P2L*	As above, but for a potential transpiration rate of *r2L*.
5a	Real	*P3*	Value of the pressure head, h_4, below which root water uptake ceases (usually equal to the wilting point).
5a	Real	*r2H*	Potential transpiration rate [LT^{-1}] (currently set at 0.5 cm/day).
5a	Real	*r2L*	Potential transpiration rate [LT^{-1}] (currently set at 0.1 cm/day).
			The above input parameters permit one to make the variable h_3 a function of the potential transpiration rate, T_p (h_3 presumably decreases at higher transpiration rates). HYDRUS currently implements the same linear interpolation scheme as used in several versions of the SWATRE code (e.g., *Wesseling and Brandyk* [1985]) and in the SWMS_2D [*Šimůnek et al.*, 1992] and HYDRUS 5.0 [*Vogel et al.*, 1996] codes. The scheme is based on the following interpolation:

$$h_3 = P2H + \frac{P2L - P2H}{r2H - r2L} (r2H - T_p) \quad \text{for} \quad r2L < T_p < r2H$$

$$h_3 = P2L \quad \text{for } T_a \leq r2L$$

$$h_3 = P2H \quad \text{for } T_a \geq r2H$$

Table 12.7. (continued)

Record	Type	Variable	Description
6a	-	-	Comment line.
7a	Real	*POptm*(1)	Value of the pressure head, h_2, below which roots start to extract water at the maximum possible rate (material number 1).
7a	Real	*POptm*(2)	As above (material number 2).
.	.	.	.
.	.	.	.
7a	Real	*POptm*(*NMat*)	As above (for material number *NMat*).
			The following record (record 5b) is given only if *iMoSink*=1.
5b	Real	*P50*	Value of the pressure head, h_{50} (Fig. 2.1), at which the root water uptake is reduced by 50%.
5b	Real	*P3*	Exponent, *p*, in the S-shaped root water uptake stress response function. Recommended value is 3.
			The following records are given only if *lChem*=**.true.** .
8	-	-	Comment line.
9	Logical	*lSolRed*	=**.true.** : root water uptake is reduced due to salinity. =**.false.**: otherwise.
			The following records are given only if *lSolRed*=**.true.** .
10	-	-	Comment line.
11	Logical	*lSolAdd*	=**.true.** if the effect of salinity stress is additive to the pressure head stress. =**.false.** if the effect of salinity stress is multiplicative to the pressure head stress.
12	-	-	Comment line.
			The following two values are specified when the root water uptake salinity stress response function is described with the S-shaped function (2.10) or (2.11), i.e., *lMsSink*=**.true.**.
13a	Real	*c50*	Value of the osmotic head $h_{\varphi 50}$, at which the root water uptake is reduced by 50%. This value is specified only when *lSolAdd*=**.false.**.
13a	Real	*P3c*	Exponent, *p*, in the S-shaped root water uptake salinity stress response function. Recommended value is 3. This value is specified only when *lSolAdd*=**.false.**.
			The following two values are specified when the root water uptake salinity stress response function is described with the threshold-slope function of *Maas* [1990], i.e., *lMsSink*=**.false.**.

Table 12.7. (continued)

Record	Type	Variable	Description

$$\alpha(h_\phi) = 1 \qquad\qquad h_\phi{}^M \leq h_\phi < 0$$

$$\alpha(h_\phi) = \max[0\,,1. - 0.01(h_\phi - h_\phi{}^M)s_\phi] \quad h_\phi < h_\phi{}^M$$

Record	Type	Variable	Description
13a	Real	*c50*	Value of the minimum osmotic head (the salinity threshold) $h_\phi{}^M$, above which root water uptake is not reduced. This value is specified only when *lSolAdd*=**.false.**.
13a	Real	*P3c*	Slope, s_ϕ, of the curve determining fractional root water uptake decline per unit increase in salinity below the threshold. This value is specified only when *lSolAdd*=**.false.**.
13	Real	*aOsm*(1)	Osmotic coefficient, a_1, for the first solute [L^4M^{-1}].
13	Real	*aOsm*(2)	Osmotic coefficient, a_2, for the second solute [L^4M^{-1}].
.	.	.	.
.	.	.	.
.	.	.	.
13	Real	*aOsm*(NSD)	Osmotic coefficient, a_n, for the last solute [L^4M^{-1}].
13	Logical	*lMsSink*	=**.true.** : S-shaped root water uptake salinity stress response function. =**.false.**: threshold function according *Maas* [1990].

[+] Block G is not needed when the logical variable *SinkF* (Block A) is set equal to **.false.** .

Table 12.8. Block H - Nodal information.

Record	Type	Variable	Description
0	Char	*iVer*	HYDRUS-1D version
1	Integer	*NFix*	Number of fixed nodes.
2	Integer	*i*	Fixed node.
2	Real	*xFix*(*i*)	*x*-coordinate of the fixed node *i*.
2	Real	*wTop*(*i*)	Nodal density above fixed node *i*.
2	Real	*wBot*(*i*)	Nodal density below fixed node *i*.
			Record 2 must be specified for each fixed node.
			Records 1 and 2 have relevant information only for the module PROFILE of the user interface. When the code is used without the user interface, then only two fixed points (top and bottom of the soil profile) with unit nodal density have to be specified.
3	Integer	*NumNP*	Number of nodal points.
3	Integer	*NS*	Number of solutes (set equal to zero if *lChem* is equal to **.false.**).
3	Integer	*iTemp*	This variable is read only if the user interface is used. = 1; initial condition for the temperature is specified (must be equal to 1 when *lTemp* or *lChem* is equal to **.true.**). = 0; initial condition for the temperature is not specified.
3	Integer	*iEquil*	This variable is read only if the user interface is used. = 1; Equilibrium solute transport is considered. = 0; Nonequilibrium solute transport is considered.
			Set equal to 1 if *lChem* is equal to **.false.**.
4	Integer	*n*	Nodal number.
4	Real	*x*(*n*)	*x*-coordinate of node *n* [L].
4	Real	*hNew*(*n*)	Initial value of the pressure head at node *n* [L]. If *lWat*=**.false.** in Block A, then *hNew*(*n*) represents the pressure head which will be kept constant during simulation.
4	Integer	*MatNum*(*n*)	Index for material whose hydraulic and transport properties are assigned to node *n*.
4	Integer	*LayNum*(*n*)	Subregion number assigned to node *n*.
4	Real	*Beta*(*n*)	Value of the water uptake distribution, $b(x)$ [L^{-1}], in the soil root zone at node *n*. Set *Beta*(*n*) equal to zero if node *n* lies outside the root zone.
			Following three numbers, i.e., *Ah*(*n*), *Ak*(*n*), and *Ath*(*n*), are given only when neither carbon dioxide transport nor major ion chemistry is considered.

Table 12.8. (continued)

Record	Type	Variable	Description
4	Real	*Ah*(*n*)	Nodal value of the dimensionless scaling factor α_h [-] associated with the pressure head.
4	Real	*Ak*(*n*)	Nodal value of the dimensionless scaling factor α_K [-] associated with the saturated hydraulic conductivity.
4	Real	*Ath*(*n*)	Nodal value of the dimensionless scaling factor α_θ [-] associated with the water content.
			The following number, i.e., CO2(*n*), is given only when either carbon dioxide transport or major ion chemistry is considered.
4	Real	*CO2*(*n*)	Initial value of the carbon dioxide concentration at node *n* [L^3L^{-3}].
4	Real	*Temp*(*n*)	Initial value of the temperature at node *n* [^oC] (do not specify if both *lTemp* or *lChem* are equal to **.false.**; if *lTemp*=**.false.** and *lChem*=**.true.** then set equal to 0 or any other initial value to be used later for temperature dependent water flow and solute transport).
			Following dissolved and sorbed concentrations, i.e., *Conc*(*i,n*) and *Sorb*(*i,n*), are given only when neither carbon dioxide transport nor major ion chemistry is considered.
4	Real	*Conc*(1,*n*)	Initial value of the concentration of the first solute at node *n* [ML^{-3}] (omit if *lChem*=**.false.**).
4	Real	*Conc*(2,*n*)	Initial value of the concentration of the second solute at node *n* [ML^{-3}] (omit if *lChem*=**.true.** and *NS* < 2).
.	.	.	.
.	.	.	.
4	Real	*Conc*(*i,n*)	Initial value of the concentration of the last solute at node *n* [ML^{-3}] (omit if *lChem*=**.true.** and *NS* < *i*).
4	Real	*Sorb*(1,*n*)	Initial value of the adsorbed concentration on type-2 sites of the first solute at node *n* [ML^{-3}]. Omit this variable if *lChem*=**.false.** or *lEquil*=**.true.** .
4	Real	*Sorb*(2,*n*)	Initial value of the adsorbed concentration on type-2 sites of the second solute at node *n* [ML^{-3}]. Omit this variable if *lChem*=**.false.** or *lEquil*=**.true.** or *NS* < 2.
.	.	.	.
4	Real	*Sorb*(*i,n*)	Initial value of the adsorbed concentration on type-2 sites of the *NS*th solute at node *n* [ML^{-3}]. This variable does not have to be specified if *lChem*=**.false.** or *lEquil*=**.true.** and *NS* < *i*).
			Following three numbers, i.e., *nC*(*n*), *nX*(*n*), and *nS*(*n*), are given only when major ion chemistry is considered.
4	Integer	*nC*(*n*)	Code which specifies which solution concentration combination (see Block H) is to be used as an initial condition at node *n* [-] (omit if *lChem*=**.false.**).
4	Integer	*nX*(*n*)	Code which specifies which surface species combination (see Block H) is to be used as an initial condition at node *n* [-] (omit if *lChem*=**.false.**).

Table 12.8. (continued)

Record	Type	Variable	Description
4	Integer	$nS(n)$	Code which specifies which mineral phase combination (see Block H) is to be used as an initial condition at node n [-] (omit if $lChem$=**.false.**).
			In general, record 4 information is required for each node n, starting with n=1 and continuing sequentially until n=$NumNP$. Record 4 information for certain nodes may be skipped if several conditions are satisfied (see beginning of this section).
5	Integer	$NObs$	Number of observation nodes for which values of the pressure head, the water content, temperature (for $lTemp$=**.true.**), and the solution and sorbed concentrations (for $lChem$=**.true.**) are printed at each time level.
6	Integer	$iObs(1)$	Nodal number of the first observation node.
6	Integer	$iObs(2)$	Nodal number of the second observation node.
.	.	.	.
.	.	.	.
6	Integer	$iObs(NObs)$	Nodal number of the last observation node.

Table 12.9. Block I - Atmospheric information.[+]

Record	Type	Variable	Description
0	Char	*iVer*	HYDRUS-1D version
1,2	-	-	Comment lines.
3	Integer	*MaxAl*	Number of atmospheric data records.
4	-	-	Comment line.
5	Logical	*lDailyVar*	**.true.** if HYDRUS-1D is to generate daily variations in evaporation and transpiration (see section 2.7.2.). **.false.** otherwise.
5	Logical	*lSinusVar*	**.true.** if HYDRUS-1D is to generate sinusoidal variations in precipitation (see section 2.7.2.). **.false.** otherwise.
5	Logical	*lDummy*	Dummy variable (eight times) (reserved for further expansions of HYDRUS). Set equal to .false..
6	-	-	Comment line.
7	Real	*hCritS*	Maximum allowed pressure head at the soil surface [L].
8	-	-	Comment line.
9	Real	*tAtm*(i)	Time for which the i-th data record is provided [T].
9	Real	*Prec*(i)	Precipitation rate [LT^{-1}] (in absolute value).
9	Real	*rSoil*(i)	Potential evaporation rate [LT^{-1}] (in absolute value). *rSoil*(i) is interpreted as *KodTop* when a time variable Dirichlet or Neumann boundary condition is specified.
9	Real	*rRoot*(i)	Potential transpiration rate [LT^{-1}] (in absolute value).
9	Real	*hCritA*(i)	Absolute value of the minimum allowed pressure head at the soil surface [L].
9	Real	*rB*(i)	Bottom flux [LT^{-1}] (set equal to 0 if *KodBot* is positive, or if one of the logical variables *qGWLF*, *FreeD* or *SeepF* is **.true.**).
9	Real	*hB*(i)	Groundwater level [L], or any other prescribed pressure head boundary condition as indicated by a positive value of *KodBot* (set equal to 0 if *KodBot* is negative, or if one of the logical variables *qGWLF*, *FreeD* or *SeepF* is **.true.**).
9	Real	*hT*(i)	Prescribed pressure head [L] at the surface (set equal to 0 if *KodBot* is negative).
9	Real	*tTop*(i)	Soil surface temperature [^{o}C] (omit if both *lTemp* and *lChem* are equal to **.false.**).
9	Real	*tBot*(i)	Soil temperature at the bottom of the soil profile [^{o}C] (omit if both *lTemp* and *lChem* are equal to **.false.**, set equal to zero if *kBotT*=0).
9	Real	*Ampl*(i)	Temperature amplitude at the soil surface [K] (omit if both *lTemp* and *lChem* are equal to **.false.**).

Table 12.9. (continued)

Record	Type	Variable	Description
			The following parameters (i.e., *cTop*(*i,j*) and *cBot*(*i,j*)) are to be specified only when neither carbon dioxide transport nor major ion chemistry is considered.
9	Real	*cTop*(*i*,1)	Soil surface concentration [ML^{-3}] for the first solute (not needed if *lChem* is equal to **.false.**).
9	Real	*cTop*(*i*,2)	Soil surface concentration [ML^{-3}] for the second solute (not needed if *lChem* is equal to **.false.** or *NS* < 2).
.	.	.	.
.	.	.	.
9	Real	*cTop*(*i,NS*)	Soil surface concentration [ML^{-3}] for the *NS*th solute (not needed if *lChem* is equal to **.false.**).
9	Real	*cBot*(*i*,1)	Concentration at the bottom of the soil profile [ML^{-3}] for the first solute (not needed if *lChem* is equal to **.false.**, set equal to zero if *cBotSolute*=0).
9	Real	*cBot*(*i*,2)	Concentration at the bottom of the soil profile [ML^{-3}] for the second solute (not needed if *lChem* is equal to **.false.**, set equal to zero if *cBotSolute*=0 or *NS* < 2).
9	Real	*cBot*(*i,NS*)	Concentration at the bottom of the soil profile [ML^{-3}] for the *NS*th solute (not needed if *lChem* is equal to **.false.**, set equal to zero if *cBotSolute*=0).
			Following two number, i.e., *kTopCh*(*i*) and *kBotCh*(*i*), are given only when major ion chemistry is considered.
9	Real	*kTopCh*(*i*)	Code which refers to the field *ConcTab* for the value of the solute transport upper boundary condition. Sign of *kTopCh*(*i*) indicates whether a Dirichlet (positive) or Neumann (negative) boundary condition is to be applied at the soil surface. *ConcTab*(abs(*kTopCh*(*i*)),*j*) is the boundary condition for the soil surface for species *j*. Permissible values are ±1,±2,±3,...,±*nSolConc*.
9	Real	*kBotCh*(*i*)	Code which refers to the field *ConcTab* for the value of the solute transport lower boundary condition. Sign of *kBotCh*(*i*) indicates whether a Dirichlet (positive) or Neumann (negative) boundary condition is to be applied at the bottom of the soil profile. *ConcTab*(abs(*kBotCh*(*i*)),*j*) is the boundary condition for the bottom of the soil profile for species *j*. Permissible values are ±1,±2,±3,...,±*nSolConc*.
9	Real	*RootDepth*	Rooting depth [L] (given only when *iRootIn* =0).
			The total number of atmospheric data records is *MaxAl* (i=1,2, ..,*MaxAl*).

[+] Block I is not needed if the logical variable *AtmInf* (Block A) is set equal to **.false.** .

Table. 12.10. Block J - Inverse solution information.[+]

Record	Type	Variable	Description
0	Char	*iVer*	HYDRUS-1D version
1	Integer	*NCase*	Number of cases being considered (only for the first data set).
2	Char	*Title1*	Descriptive title for simulation.
3	Char	*Title2*	Descriptive title for simulation.
4	-	-	Comment line.
5	Integer	*NOBB*	Number of observed data.
5	Integer	*MIT*	Maximum number of iterations for the inverse problem.
5	Integer	*iWeight*	Type of weighting used for the data set. = 0; no internal weighting. = 1; weighting by mean ratio. = 2; weighting by standard deviation.
6	-	-	Comment line.
7	Logical	*lWatF*	Set this logical variable equal to **.true.** when the soil hydraulic parameters are to be optimized.
7	Logical	*lChemF*	Set this logical variable equal to **.true.** when the solute transport parameters are to be optimized.
7	Integer	*NMat*	Number of soil materials. Materials are identified by the material number, *MatNum*, specified in Block H.
7	Logical	*lTempF*	Set this logical variable equal to **.true.** when the heat transport parameters are to be optimized.
8	-	-	Comment line.
9	Integer	*iModel*	Soil hydraulic properties model: = 0; *van Genuchten*'s [1980] model containing six parameters. = 1; modified van Genuchten's model containing ten parameters, *Vogel and Císlerová* [1988]. = 2; *Brooks and Corey*'s [1964] model containing six parameters.
9	Integer	*iHyst*	Hysteresis in the soil hydraulic properties: = 0; no hysteresis = 1; hysteresis in the retention curve only = 2; hysteresis in both the retention and hydraulic conductivity functions
10	-	-	Comment line.
11	Integer	*iQSame*	Parameter constraints = 0: $\theta_s^d > \theta_s^w$ = 1: $\theta_s^d = \theta_m^d$, $\theta_s^w = \theta_m^w$ = 2: $\theta_s^d = \theta_s^w = \theta_m$
11	Logical	*lAw2Ad*	**.true.** if parameter constraint $\alpha^w = 2\,\alpha^d$ is to be considered. **.false.** if no constraint on α^w and α^d is imposed.

Record	Type	Variable	Description
11	Logical	*lKSame*	**.true.** if parameter constraint $K_s^w = K_s^d$ is to be considered. **.false.** if no constraint on K_s^w and K_s^d is imposed.
11	Integer	*iKappa*	= -1 if the initial condition is to be calculated from the main drying branch. = 1 if the initial condition is to be calculated from the main wetting branch.
			Records 10 and 11 are provided only when *iHyst* > 0.
			Records 8 through 11 are specified only when the logical variable *lWatF* is equal to .true.
12	-	-	Comment line.
13	Integer	*NS*	Number of solutes (must be equal to 1).
13	Real	*iConcType*	Type of concentration that is used in the objective function [-]. = 0: resident concentration (concentration in the mobile region) = 1: log resident concentration = 2: flux concentration = 3: total resident concentration (includes sorbed phase) = 4: resident concentration (includes mobile and immobile regions)
			Records 12 and 13 are specified only when the logical variable *lChemF* is equal to .true.
14	-	-	Comment line.
15	Real	*Par*(1,*M*)	Initial estimate of parameter θ_r for material *M* [-].
15	Real	*Par*(2,*M*)	Initial estimate of parameter θ_s for material *M* [-].
15	Real	*Par*(3,*M*)	Initial estimate of parameter α for material *M* [L^{-1}].
15	Real	*Par*(4,*M*)	Initial estimate of parameter n for material *M* [-].
15	Real	*Par*(5,*M*)	Initial estimate of parameter K_s for material *M* [LT^{-1}].
15	Real	*Par*(6,*M*)	Initial estimate of parameter l for material *M* [-].
			The following four parameters are specified only when *iModel*=1.
15	Real	*Par*(7,*M*)	Initial estimate of parameter θ_m for material *M* [-].
15	Real	*Par*(8,*M*)	Initial estimate of parameter θ_a for material *M* [-].
15	Real	*Par*(9,*M*)	Initial estimate of parameter θ_k for material *M* [-].
15	Real	*Par*(10,*M*)	Initial estimate of parameter K_k for material *M* [LT^{-1}].
			The following four parameters are specified only when *iModel*=0 and *iHyst*>1.
15	Real	*Par*(7,*M*)	Initial estimate of parameter θ_m for material *M* [-].
15	Real	*Par*(8,*M*)	Initial estimate of parameter θ_s^w for material *M* [-].
15	Real	*Par*(9,*M*)	Initial estimate of parameter α^w for material *M* [L^{-1}].
15	Real	*Par*(10,*M*)	Initial estimate of parameter K_s^w for material *M* [LT^{-1}].
16	Integer	*Index*(1,*M*)	Parameter estimation index for parameter θ_r for material *M* [-]. = 0; Coefficient is known and kept constant during optimization. = 1; Coefficient is unknown and estimated by curve fitting the data.
16	Integer	*Index*(2,*M*)	Parameter estimation index for parameter θ_s for material *M* [-].

Record	Type	Variable	Description
16	Integer	$Index(3,M)$	Parameter estimation index for parameter α for material M [-].
16	Integer	$Index(4,M)$	Parameter estimation index for parameter n for material M [-].
16	Integer	$Index(5,M)$	Parameter estimation index for parameter K_s for material M [-].
16	Integer	$Index(6,M)$	Parameter estimation index for parameter l for material M [-].
			The following four parameter estimation indices are specified only when $iModel=1$.
16	Integer	$Index(7,M)$	Parameter estimation index for parameter θ_m for material M [-].
16	Integer	$Index(8,M)$	Parameter estimation index for parameter θ_a for material M [-].
16	Integer	$Index(9,M)$	Parameter estimation index for parameter θ_k for material M [-].
16	Integer	$Index(10,M)$	Parameter estimation index for parameter K_k for material M [-].
			The following four parameter estimation indices are specified only when $iModel=0$ and $iHyst>1$.
16	Integer	$Index(7,M)$	Parameter estimation index for parameter θ_m for material M [-].
16	Integer	$Index(8,M)$	Parameter estimation index for parameter θ_s^w for material M [-].
16	Integer	$Index(9,M)$	Parameter estimation index for parameter αw^w for material M [-].
16	Integer	$Index(10,M)$	Parameter estimation index for parameter K_s^w for material M [-].
17	Real	$BMn(1,M)$	Minimum constraint for parameter θ_r for material M [-] (dummy value if $Index(1,M)=0$).
17	Real	$BMn(2,M)$	Minimum constraint for parameter θ_s for material M [-].
17	Real	$BMn(3,M)$	Minimum constraint for parameter α for material M [L^{-1}].
17	Real	$BMn(4,M)$	Minimum constraint for parameter n for material M [-].
17	Real	$BMn(5,M)$	Minimum constraint for parameter K_s for material M [LT^{-1}].
17	Real	$BMn(6,M)$	Minimum constraint for parameter l for material M [-].
			The following four minimum parameter constraints are specified only when $iModel=1$.
17	Real	$BMn(7,M)$	Minimum constraint for parameter θ_m for material M [-].
17	Real	$BMn(8,M)$	Minimum constraint for parameter θ_a for material M [-].
17	Real	$BMn(9,M)$	Minimum constraint for parameter θ_k for material M [-].
17	Real	$BMn(10,M)$	Minimum constraint for parameter K_k for material M [LT^{-1}].
			The following four minimum parameter constraints are specified only when $iModel=0$ and $iHyst>1$.
17	Real	$BMn(7,M)$	Minimum constraint for parameter θ_m for material M [-].
17	Real	$BMn(8,M)$	Minimum constraint for parameter θ_s^w for material M [-].
17	Real	$BMn(9,M)$	Minimum constraint for parameter α^w for material M [L^{-1}].
17	Real	$BMn(10,M)$	Minimum constraint for parameter K_s^w for material M [LT^{-1}].
18	Real	$BMx(1,M)$	Maximum constraint for parameter θ_r for material M [-] (dummy value if $Index(1,M)=0$).
18	Real	$BMx(2,M)$	Maximum constraint for parameter θ_s for material M [-].
18	Real	$BMx(3,M)$	Maximum constraint for parameter α for material M [L^{-1}].
18	Real	$BMx(4,M)$	Maximum constraint for parameter n for material M [-].
18	Real	$BMx(5,M)$	Maximum constraint for parameter K_s for material M [LT^{-1}].

Record	Type	Variable	Description
18	Real	$BMx(6,M)$	Maximum constraint for parameter l for material M [-].
			The following four maximum parameter constraints are specified only when $iModel$=1.
18	Real	$BMx(7,M)$	Maximum constraint for parameter θ_m for material M [-].
18	Real	$BMx(8,M)$	Maximum constraint for parameter θ_a for material M [-].
18	Real	$BMx(9,M)$	Maximum constraint for parameter θ_k for material M [-].
18	Real	$BMx(10,M)$	Maximum constraint for parameter K_k for material M [LT^{-1}].
			The following four maximum parameter constraints are specified only when $iModel$=0 and $iHyst$>1.
18	Real	$BMx(7,M)$	Maximum constraint for parameter θ_m for material M [-].
18	Real	$BMx(8,M)$	Maximum constraint for parameter θ_s^w for material M [-].
18	Real	$BMx(9,M)$	Maximum constraint for parameter α^w for material M [L^{-1}].
18	Real	$BMx(10,M)$	Maximum constraint for parameter K_s^w for material M [LT^{-1}].
			Records 14 through 18 provide information for each material M (from 1 to $NMat$).
			If $lWDep$=**.true.** (Block A) then the soil hydraulic parameters $Par(i,M)$ must be specified at reference temperature T_{ref}=20°C.
19	-	-	Comment line.
20	Real	$ChPar(1,M)$	Initial estimate of bulk density of material M, ρ [ML^{-3}].
20	Real	$ChPar(2,M)$	Initial estimate of longitudinal dispersivity for material type M, D_L [L].
20	Real	$ChPar(3,M)$	Initial estimate of dimensionless fraction of the adsorption sites classified as type-1, i.e., sites with instantaneous sorption when the **chemical nonequilibrium** option is considered. Set equal to 1 if equilibrium transport is to be considered.
			Dimensionless fraction of the adsorption sites in contact with mobile water when the **physical nonequilibrium** option is considered. Set equal to 1 if all sorption sites are in contact with mobile water.
20	Real	$ChPar(4,M)$	Initial estimate of the immobile water content. Set equal to 0 when the **physical nonequilibrium** option is not considered.
20	Real	$ChPar(5,M)$	Initial estimate of the ionic or molecular diffusion coefficient in free water, D_w [$L^2 T^{-1}$].
20	Real	$ChPar(6,M)$	Initial estimate of the ionic or molecular diffusion coefficient in the gas phase, D_g [$L^2 T^{-1}$].
20	Real	$ChPar(7,M)$	Initial estimate of the adsorption isotherm coefficient, k_s, for material type M [$L^3 M^{-1}$]. Set equal to zero if no adsorption is to be considered.
20	Real	$ChPar(8,M)$	Initial estimate of the adsorption isotherm coefficient, η, for material type M [$L^3 M^{-1}$]. Set equal to zero if a Langmuir adsorption isotherm is not to be considered.
20	Real	$ChPar(9,M)$	Initial estimate of the adsorption isotherm coefficient, β, for material type M [-]. Set equal to one if a Freundlich adsorption isotherm is not to be considered.

Record	Type	Variable	Description
20	Real	$ChPar$(10,M)	Initial estimate of the equilibrium distribution constant between the liquid and gas phases, k_g, material type M [-].
20	Real	$ChPar$(11,M)	Initial estimate of the first-order rate constant for the dissolved phase, μ_w, material type M [T^{-1}].
20	Real	$ChPar$(12,M)	Initial estimate of the first-order rate constant for the solid phase, μ_s, material type M [T^{-1}].
20	Real	$ChPar$(13,M)	Initial estimate of the first-order rate constant for the gas phase, μ_g, material type M [T^{-1}].
20	Real	$ChPar$(14,M)	Initial estimate of the rate constant, μ_w', representing first-order decay for the first solute and zero-order production for the second solute in the dissolved phase, material type M [T^{-1}].
20	Real	$ChPar$(15,M)	Initial estimate of the rate constant for the solid phase, μ_s', material type M [T^{-1}].
20	Real	$ChPar$(16,M)	Initial estimate of the rate constant for the gas phase, μ_g', material type M [T^{-1}].
20	Real	$ChPar$(17,M)	Initial estimate of the zero-order rate constant for the dissolved phase, γ_w, material type M [ML^{-3}T^{-1}].
20	Real	$ChPar$(18,M)	Initial estimate of the zero-order rate constant for the solid phase, γ_s, material type M [T^{-1}].
20	Real	$ChPar$(19,M)	Initial estimate of the zero-order rate constant for the gas phase, γ_g, material type M [ML^{-3}T^{-1}].
20	Real	$ChPar$(20,M)	Initial estimate of the first-order mass transfer coefficient for nonequilibrium adsorption, ω, material type M [T^{-1}].
21	Integer	$Index$(1,M)	Parameter estimation index for parameter $ChPar$(1,M). = 0; Coefficient is known and kept constant during optimization. = 1; Coefficient is unknown and estimated by curve fitting the data.
.	.	.	.
21	Integer	$Index$(20,M)	Parameter estimation index for parameter $ChPar$(20,M).
22	Real	BMn(1,M)	Minimum constraint for parameter $ChPar$(1,M) (dummy value if $Index$(1,M)=0).
.	.	.	.
.	.	.	.
22	Real	BMn(20,M)	Minimum constraint for parameter $ChPar$(20,M).
23	Real	BMx(1,M)	Maximum constraint for parameter $ChPar$(1,M) (dummy value if $Index$(1,M)=0).
.	.	.	.
.	.	.	.
23	Real	BMx(20,M)	Maximum constraint for parameter $ChPar$(20,M).
			Records 19 through 23 provide information for each material M (from 1 to $NMat$).
24	-	-	Comment line.
25	Real	HO(i)	Observation data. Time t for $iType$(i)=0,1,2,3,4; Pressure head h for $iType$(i)=5,6; Dummy for $iType$(i)=7,8,9,10,11;

Record	Type	Variable	Description
25	Real	*FO*(*i*)	Observation data. When *iType*(*i*)=2 and *iPos*(*i*)=0, then *FO*(*i*) represents the average water content in the entire flow domain. When *iType*(*i*)=4 and *iPos*(*i*)=0, then *FO*(*i*) represents the total solute amount in the entire flow domain.
25	Integer	*iType*(*i*)	Type of observed data: = 0: cumulative boundary water flux = 1: $h(x,t)$ measurement = 2: $\theta(x,t)$ measurement = 3: boundary flux = 4: $Conc(x,t)$ measurement = 5: $h(\theta)$ measurement = 6: $K(h)$ measurement = 7: prior knowledge of parameter α = 8: prior knowledge of parameter n = 9: prior knowledge of parameter θ_r = 10: prior knowledge of parameter θ_s = 11: prior knowledge of parameter K_s =12: Pressure head at location *HO*(*i*) at print time *iPos*(*i*). =13: Water content at location *HO*(*i*) at print time *iPos*(*i*). =14: Concentration at location *HO*(*i*) at print time *iPos*(*i*). =15: Kinetically sorbed concentration at location *HO*(*i*) at print time *iPos*(*i*).
25	Integer	*iPos*(*i*)	Position of the observation node for *iType*(*i*)=1,2,4; allowed values are 1, 2,...*NObs*. When *iType*(*i*)=0 or 3, then *iPos*(*i*) is equal to 1 for the upper boundary and 2 for the lower boundary. When *iType*(*i*)=5,6,7,8,9,10, or 11, then *iPos*(*i*) represents the material number *M*; allowed values are 1, 2,...*NMat*. When *iType*(*i*)=2 then *iPos*(*i*)=0 represents the average water content in the entire transport domain. When *iType*(*i*)=2 then *iPos*(*i*)=-*iLay* represents the average water content in the subregion *iLay*.
25	Real	*Weight*(*i*)	Weight associated with a particular data point.

[+] Block J is not needed if only the direct solution is calculated.

Record	Type	Variable	Description
1..2	-	-	Comment lines.
3	Logical	*lStagn*	Set this variable equal to **.true.** if the gas phase is to be considered stagnant, i.e., there is no gas convection. Otherwise the simplified gas convection expression is considered (see Section 5.1).
4	-	-	Comment line.
5	Integer	*kTopCO*	Code specifying type of boundary condition (BC) for the CO_2 transport at the soil surface. Code number is positive for Dirichlet BC and negative for stagnant boundary layer at the soil surface.
5	Real	*CO2Top*	Value of the time independent BC at the surface [L^3L^{-3}]. For *kTopCO*<0 *CO2Top* represents the thickness of the stagnant boundary layer [L].
5	Integer	*kBotCO*	Code specifying type of boundary condition at the bottom of the profile. Code number is positive for Dirichlet and negative for Cauchy BC. In the case of 'Free drainage' set *kBotCO*=0.
5	Real	*CO2Bot*	Value of the time independent BC at the bottom of the soil profile [L^3L^{-3}]. In case of 'Free drainage' set *CO2Bot*=0.
6	-	-	Comment line.
7	Real	*Par*(11,*M*)	Molecular diffusion coefficient of CO_2 in air at 20^oC, D_a [L^2T^{-1}].
7	Real	*Par*(12,*M*)	Molecular diffusion coefficient of CO_2 in water at 20^oC, D_w [L^2T^{-1}].
7	Real	*Par*(13,*M*)	Longitudinal dispersivity of CO_2 of material *M*, D_L [L].
			The same record as above must be provided for each material *M* (from 1 to *NMat*).
8	-	-	Comment line.
9	Real	*GamR*0	Optimal CO_2 production by plant roots for the entire soil profile at 20^oC under optimal water, solute, and CO_2 concentration conditions, γ_{r0} [$L^3L^{-2}T^{-1}$].
9	Real	*GamS*0	Optimal CO_2 production by soil microorganisms for the whole soil profile at 20^oC under optimal water, solute, and CO_2 concentration conditions, γ_{s0} [$L^3 L^{-2} T^{-1}$].
9	Real	*PDDMax*	Cumulative value of temperature when CO_2 production reaches its maximum value. Set equal to zero if the degree day concept is not used to calculate the time reduction coefficient for plant CO_2 production. In that case the time reduction coefficient is equal to one during the whole season.
9	Integer	*kProd*	Code specifying the type of spatial distribution function for CO_2 production by soil microorganisms. =0: Exponential function. =1: van Genuchten's distribution function.
10	-	-	Comment line.

Table 12.11. (continued)

Record	Type	Symbol	Description
11	Real	*rAlfa*	Coefficient in the exponential function (only if *kProd*=0) [L^{-1}].
11	Real	*xR*	Maximum depth of CO_2 production in the soil profile (only if *kProd*=1) [L].
12	-	-	Comment line.
13	Real	*B*2	Activation energy for CO_2 production by plant roots, E_2 [$ML^2T^{-2}M^{-1}$], divided by universal gas constant, R [$ML^2T^{-2}K^{-1}M^{-1}$]; $B_2=E_2/R$ [K].
13	Real	*B*1	Activation energy for CO_2 production by soil microorganisms, E_1 [$ML^2T^{-2}M^{-1}$], divided by universal gas constant, R [$ML^2T^{-2}K^{-1}M^{-1}$]; $B_1=E_1/R$ [K].
13	Real	*cM*2	Michaelis' constant for CO_2 production by plant roots [L^3L^{-3}]. Equal to the CO_2 concentration at which CO_2 production is reduced by half from the optimal value γ_{r0}.
13	Real	*cM*1	Michaelis' constant for CO_2 production by soil microorganisms [L^3L^{-3}]. Equal to the CO_2 concentration at which CO_2 production is reduced by half from the optimal value γ_{s0}.
13	Real	*hB*1	Value of the pressure head at which CO_2 production by soil microorganisms is at the optimal level [L].
13	Real	*hB*2	Value of the pressure head below which CO_2 production by soil microorganisms ceases [L].
13	Real	*P*0*c*	The coefficient b in the CO_2 soil production reduction function due to salinity stress [-]. The recommended value is 3.
13	Real	*P*50*c*	The value $h_{\varphi50}$ in the CO_2 soil production reduction function due to salinity stress [L]. There is a 50% reduction in the CO_2 production by soil microorganisms at this osmotic head.

[†] Block K is not needed if the logical variable *lCO*2 (Block A) is set equal to **.false.**.

Table. 12.12. Block L – Major ion chemistry information.[+]

Record	Type	Variable	Description
1,2	-	-	Comment lines.
3	Real	*Epsi*	Temporal weighing coefficient. =0.0 for an explicit scheme, =0.5 for a Crank-Nicholson implicit scheme. =1.0 for a fully implicit scheme.
3	Logical	*lUpW*	**.true.** if upstream weighing formulation is to be used (see Section 8.3.2). **.false.** if the original Galerkin formulation is to be used.
3	Logical	*lArtD*	**.true.** if artificial dispersion is to be added in order to fulfill the *PeCr* stability criterion (see Section 8.4.5). **.false.** otherwise.
3	Logical	*lLagr*	**.true.** if the Eulerian-Lagrangian single-step reverse particle tracking technique is to be used to solve the solute transport equation. This method is useful for convection dominated problems (see Section 8.4.3). **.false.** if the Eulerian finite differences approach is to be used to solve the solute transport equation.
3	Real	*PeCr*	Stability criteria (see Section 8.4.5). Set equal to zero when *lUpW* is equal to **.true.**.
3	Logical	*lTort*	**.true.** if tortuosity factor [*Millington and Quirk*, 1961] is to be used. **.false.** if tortuosity factor is assumed to be equal to one.
4	-	-	Comment line.
5	Logical	*lRate*	Set this logical variable equal to **.true.** if kinetic precipitation-dissolution of calcite and kinetic dissolution of dolomite is to be considered. Set this logical variable equal to **.false.** if only equilibrium reactions are to be considered.
5	Logical	*lSilic*	Set this logical variable equal to **.true.** if the silica content of the soil solution is to be calculated based on the solution pH. Set this logical variable equal to **.false.** if the silica content of the soil solution is not considered.
5	Real	*UCrit*	Value of ionic strength below which the extended Debye-Hückel equation is used to calculate ion activity coefficients. Pitzer's virial-type equations are used above this value. It is suggested that either one or the other be used.
5	Integer	*MaxCh*	Maximum number of iterations allowed during any time step between the solute transport and chemical modules. When the maximum number of iterations is reached for *MaxCh*>5 then the time step is divided by three and the particular time level is restarted again. When the maximum number of iterations is reached for *MaxCh*≤5 then the code proceeds to the new time level. Recommended value (from experience) is 5. Set equal to one if no iteration is required.
5	Real	*xConv*	Length conversion factor. Multiplication factor to convert the length unit *LUnit* into meters.

Table 12.12. (continued)

Record	Type	Variable	Description
5	Real	*tConv*	Time conversion factor. Multiplication factor to convert the time unit *TUnit* into seconds.
6	-	-	Comment line.
7	Real	*ChPar*(1,*M*)	Bulk density of material *M* [ML^{-3}].
7	Real	*ChPar*(2,*M*)	Molecular diffusion coefficient in free water, D_w [L^2T^{-1}].
7	Real	*ChPar*(3,*M*)	Longitudinal dispersivity for material type *M*, D_L [L].
7	Real	*ChPar*(4,*M*)	Cation exchange capacity for material type *M*, c_T ($mmol_c$ kg^{-1} of soil).
7	Real	*ChPar*(5,*M*)	Calcite surface area A^C (m^2l^{-1} of soil matrix). Set this variable equal to zero when *lRate*=**.false.**.
7	Real	*ChPar*(6,*M*)	Dolomite surface area A^D (m^2l^{-1} of soil matrix). Set this variable equal to zero when *lRate*=**.false.** or dolomite is not present in the soil profile.
7	Real	*ChPar*(7,*M*)	Dissolved organic carbon (μmol l^{-1}). This variable is used to calculate the reduction in the precipitation-dissolution rates of calcite.
7	Real	*ChPar*(8,*M*)	Gapon' selectivity constant between calcium and magnesium, K_{13} [-].
7	Real	*ChPar*(9,*M*)	Gapon' selectivity constant between calcium and sodium, K_{14} [-].
7	Real	*ChPar*(10,*M*)	Gapon' selectivity constant between calcium and potassium, K_{15} [-].
			Record 7 information is provided for each material *M* (from 1 to *NMat*).
8	-	-	Comment line.
9	Integer	*kTopCh*	Code which specifies the type of upper boundary condition =+1: Dirichlet boundary condition, =-1: Cauchy boundary condition.
9	Integer	*nTop*	Code which in case of a time-independent upper boundary condition (*TopInf*=**.false.** - see Block A), refers to the field *ConcTab* for the value of the solute transport boundary condition. *ConcTab*(*nTop*,*i*) is the boundary condition for the soil surface for species *i*. Permissible values are 1,2,3,...,*nSolConc*.
9	Integer	*kBotCh*	Code which specifies the type of lower boundary condition = 1: Dirichlet boundary condition, = 0: Continuous boundary condition, free drainage, =-1: Cauchy boundary condition.
9	Integer	*nBot*	Code which in case of a time-independent upper boundary condition (*BotInf*=**.false.** - see Block A), refers to the field *ConcTab* for the value of the solute transport boundary condition. *ConcTab*(*nBot*,*i*) is the boundary condition at the soil surface for species *i*. Permissible values are 1,2,3,...,*nSolConc*.
10	-	-	Comment line.
11	Integer	*nSolConc*	Number of different solutions used in a particular application.

Table 12.12. (continued)

Record	Type	Variable	Description
11	Integer	*nAdsConc*	Number of surface species combinations used in a particular application.
11	Integer	*nPrecConc*	Number of mineral phase combinations used in a particular application.
12	-	-	Comment line.
13	Real	*ConcTab*(1,1)	Analytical concentration of calcium for the first solution concentration combination, Ca_T ($mmol_c l^{-1}$ of solution).
13	Real	*ConcTab*(1,2)	Analytical concentration of magnesium for the first solution concentration combination, Mg_T ($mmol_c l^{-1}$ of solution).
13	Real	*ConcTab*(1,3)	Analytical concentration of sodium for the first solution concentration combination, Na_T ($mmol_c l^{-1}$ of solution).
13	Real	*ConcTab*(1,4)	Analytical concentration of potassium for the first solution concentration combination, K_T ($mmol_c l^{-1}$ of solution).
13	Real	*ConcTab*(1,5)	Analytical concentration of alkalinity for the first solution concentration combination, Alk ($mmol_c l^{-1}$ of solution).
13	Real	*ConcTab*(1,6)	Analytical concentration of sulfate for the first solution concentration combination, SO_{4T} ($mmol_c l^{-1}$ of solution).
13	Real	*ConcTab*(1,7)	Analytical concentration of chloride for the first solution concentration combination, Cl_T ($mmol_c l^{-1}$ of solution).
13	Real	*ConcTab*(1,8)	Analytical concentration of hypothetical tracer for the first solution concentration combination [-].
			In general, one record as described above is required for each solution concentration combination, starting with the first solution concentration combination and continuing in sequence up to the *nSolConc*th combination.
14	-	-	Comment line.
15	Real	*XConcTab*(1,1)	Adsorbed (surface species) calcium concentration for the first surface species combination, a ($mmol_c kg^{-1}$ of soil matrix).
15	Real	*XConcTab*(1,2)	Adsorbed magnesium concentration for the first surface species combination, g ($mmol_c kg^{-1}$ of soil matrix).
15	Real	*XConcTab*(1,3)	Adsorbed sodium concentration for the first surface species combination, a ($mmol_c kg^{-1}$ of soil matrix).
15	Real	*XConcTab*(1,4)	Adsorbed potassium concentration for the surface species combination, ($mmol_c kg^{-1}$ of soil matrix).
			In general, one record as described above is required for each surface species combination, starting with the first surface species combination and continuing in sequence up to the *nAdsConc*th combination.
16	-	-	Comment line.
17	Real	*SConcTab*(1,1)	Solid phase calcite concentration for the first mineral phase combination expressed in $mmol_c$ of Ca per kg of soil matrix, $CaCO_3$ (divide by $2*10^{-3}$ to obtain moles of calcite per kg of soil matrix).

Table 12.12. (continued)

Record	Type	Variable	Description
17	Real	*SConcTab*(1,2)	Solid phase gypsum concentration for the first mineral phase combination expressed in $mmol_c$ of Ca per kg of soil matrix, $CaSO_4$ (divide by $2*10^{-3}$ to obtain moles of gypsum per kg of soil matrix).
17	Real	*SConcTab*(1,3)	Solid phase dolomite concentration for the first mineral phase combination expressed in $mmol_c$ of Ca per kg of soil matrix, $CaMg(CO_3)_2$ (divide by $2*10^{-3}$ to obtain moles of dolomite per kg of soil matrix).
17	Real	*SConcTab*(1,4)	Solid phase hydromagnesite concentration for the first mineral phase combination expressed in $mmol_c$ of Mg per kg of soil matrix, $Mg_5(CO_3)_4(OH)_2 \cdot 4H_2O$ (divide by 10^{-4} to obtain moles of hydromagnesite per kg of soil matrix).
17	Real	*SConcTab*(1,5)	Solid phase nesquehonite concentration for the first mineral phase combination expressed in $mmol_c$ of Mg per kg of soil matrix, $MgCO_3 \cdot 3H_2O$ (divide by $2*10^{-3}$ to obtain moles of nesquehonite per kg of soil matrix).
17	Real	*SConcTab*(1,6)	Solid phase sepiolite concentration for the first mineral phase combination expressed in $mmol_c$ of Mg per kg of soil matrix, $Mg_2Si_3O_{7.5}(OH) \cdot 3H_2O$ (divide by $4*10^{-3}$ to obtain moles of nesquehonite per kg of soil matrix).
			In general, one record as described above is required for each mineral phase combination, starting with the first mineral phase combination and continuing in sequence up to the *nPrecConc*th combination.

[†]Block L is not needed when the logical variable *lChem* in Block A is set equal to **.false.** .

215

Table 12.13. Block M – Meteorological information. [†]

Record	Type	Variable	Description
1	char	*cVersion*	Set text equal to "Pcp_File_Version="
1		*iVer*	HYDRUS-1D version
2,3	-	-	Comment line
4	Integer	*MaxAlMeteo*	Number of meteorological records
4	Integer	*iRadiation*	Index specifying how the radiation term is entered or calculated: =0: potential value calculated based on latitude, altitude and time of year =1: solar radiation is specified =2: net radiation is specified
4	Logical	*lHargr*	**.false.** if potential evapotranspiration is to be calculated using the Penman-Monteith combination equation (2.81). **.true.** if potential evapotranspiration is to be calculated using the Hargreaves equation (2.87).
5	-	-	Comment line
6	Logical	*lDummy*	Dummy variable (ten times) (reserved for further expansions of HYDRUS). Set equal to .false.. The following records 7 through 14 are specified only when *iRadiation* <2.
7	-	-	Comment line
8	Real	*Latitude*	Latitude (deg)
8	Real	*Altitude*	Altitude (m)
9	-	-	Comment line
10	Real	*ShortWaveRadA*	Angstrom value a_s in (2.84), recommended value is 0.25
10	Real	*ShortWaveRadB*	Angstrom value b_s in (2.84), recommended value is 0.5
11	-	-	Comment line
12	Real	*LongWaveRadA*	Value of a_1 in (A16) for calculating the effect of the cloudiness factor on long wave radiation, recommended value is 0.9
12	Real	*LongWaveRadB*	Value of b_1 in (A16) for calculating the effect of the cloudiness factor on long wave radiation, recommended value is 0.1
13	-	-	Comment line
14	Real	*LongWaveRadA1*	Value of a_l in (A.14) for calculating the effect of emissivity on long wave radiation, recommended value is 0.34
14	Real	*LongWaveRadB1*	Value of b_l in (A.14) for calculating the effect of emissivity on long wave radiation, recommended value is –0.139
15	-	-	Comment line
16	Real	*WindHeight*	Height of wind speed measurements (usually 200 cm)
16	Real	*TempHeight*	Height of temperature and humidity measurements (usually 200 cm)

Table 12.13. (continued)

Record	Type	Variable	Description
17	-	-	Comment line
18	Integer	*iCrop*	=0: No crop (no values for *Crop height*, *LAI*, and *RootDepth* are specified) =1: *Crop height*, *Albedo*, *LAI*, and *RootDepth* are constant with time =2: A table of *Crop height*, *Albedo*, *LAI*, and *RootDepth* versus time is provided. Values are interpolated linearly with time between entered values. =3: *Crop height*, *Albedo*, *LAI*, and *RootDepth* are given daily
18	Integer	*iSunSh*	=0: Sunshine hours are specified =1: Cloudiness is specified =2: The transmission coefficient is specified
18	Integer	*iRelHum*	=0: Relative humidity is specified =1: Vapor pressure is specified
			The following two lines (19 and 20) are specified only when *iCrop* = 0:
19	-	-	Comment line
20	Real	*Albedo*	Albedo
			The following four lines (21 through 24) are specified only when *iCrop* > 0:
21	-	-	Comment line
22	Integer	*iLai*	Defines how the leaf area index is calculated or specified: =1: calculated from crop height using equation for grass (i.e., *LAI*=0.24*CropHeight), =2: calculated from crop height using equation for alfalfa (*LAI*=1.5*log(*CropHeight*)+5.5), =3: calculated from surface fraction, SCF, using

$$SCF = 1 - \exp\left(-a_i \cdot LAI\right) \quad \text{or} \quad LAI = -\frac{1}{a_i} \ln\left(1 - SCF\right), \text{ where } a_i = rExtinct = 0.463$$

Record	Type	Variable	Description
22	Real	*rExtinct*	constant for the radiation extinction by the canopy [-]
23	-	-	Comment line
24	Integer	*iIntercept*	=0: no interception =1: interception according to

$$I = a \cdot LAI \left(1 - \frac{1}{1 + \dfrac{bP}{a \cdot LAI}} \right)$$

Table 12.13. (continued)

Record	Type	Variable	Description
			where *P* is precipitation, *I* is interception, and *a* and *b*(*SCF*) are empirical constants.
			Lines 25 and 26 below are needed only when *iCrop*=1, i.e., when *CropHeight*, *Albedo*, *LAI*, and *RootDepth* are constant with time.
25	-	-	Comment line
26	Real	*CropHeight*	Crop height [L]
26	Real	*Albedo*	Albedo [-]
26	Real	*LAI*	Leaf area index for *iLai*=1 or 2; soil cover fraction for *iLai*=3.
26	Real	*RootDepth*	Rooting depth [L]
			Lines 25-28 below are needed only when *iCrop*=2, i.e., when using a table of *CropHeight*, *Albedo*, *LAI*, and *RootDepth* values.
25	-	-	Comment line
26	Integer	*nGrowth*	Number of data points in the crop growth table.
27	-	-	Comment line
28	Real	*tGrowth*	Day
28	Real	*CropHeight*	Crop height [L]
28	Real	*Albedo*	Albedo [-]
28	Real	*LAI*	Leaf area index for *iLai*=1 or 2; soil cover fraction for *iLai*=3.
28	Real	*RootDepth*	Rooting depth [L] Line 28 is given *nGrowth* times.
			Lines 29 and 30 below are needed only when *iIntercept*=1 and *iCrop*>0.
29	-	-	Comment line
30	Real	*aInterc*	Constant *a* in the interception model (=0.25).
			The previous lines 21-30 are not needed if *iCrop*=0.
31-33	-	-	Comment lines
34	Real	*tMeteo*	Day
34	Real	*Rad*	Net radiation flux at the surface [MJ/m^2]
34	Real	*TMax*	Maximum temperature [$^{\circ}$C]
34	Real	*TMin*	Minimum temperature [$^{\circ}$C]
34	Real	*RHMean*	Relative humidity [%]
34	Real	*Wind*	Average daily wind speed at height *WindHeight* [km/d]
34	Real	*SunHours*	Bright sunshine hours per day [hr], or cloudiness, or the transmission coefficient (based on *iSunSh*)
			The next four entries are needed only when *iCrop*=3.
34	Real	*CropHeight*	Crop height [L]
34	Real	*Albedo*	Albedo [-]

Table 12.13. (continued)

Record	Type	Variable	Description
34	Real	*LAI*	Leaf area index for *iLai*=1 or 2; soil cover fraction for *iLai*=3.
34	Real	*RootDepth*	Rooting depth [L]

[†]Block M is not needed when the logical variable *lMeteo* in Block A is set equal to **.false.** .

13. OUTPUT DATA

The program output consists of 9+(n_s-1) output files (when major ion chemistry or dua-permeability are not considered), where n_s is the number of solutes considered in the first-order decay chain. When major ion chemistry is considered the program output consists of 13 output files. The output is organized into 3 groups:

> T-level information
> > T_LEVEL.OUT
> > RUN_INF.OUT
> > SOLUTE.OUT
> > OBS_NODE.OUT
> > CO2_INF.OUT[*]
> > SOLUTEF.OUT[+]
> > SOLUTEM.OUT[+]
> > OBS_NODF.OUT[+]
>
> P-level information
> > NOD_INF.OUT
> > BALANCE.OUT
> > CONC.OUT[*]
> > SOLID.OUT[*]
> > EQUIL.OUT[*]
> > CHEMBAL.OUT[*]
>
> A-level information
> > A_LEVEL.OUT
> > METEO.OUT

[*]Major ion chemistry module output files

[+]Dual-permeability module output files

In addition, some of the input data are printed to files I_CHECK.OUT and PROFILE.OUT. A separate output file SOLUTE.OUT is created for each solute. Results of the inverse solution are directed into an output file FIT.OUT. All output files are directed to the same directory as the input files, which must be created by the user prior to program execution (the directory is created automatically if the user interface is used). The various output files are described in detail in this section.

File I_CHECK.OUT contains a complete description of the space discretization, the hydraulic characteristic, and the transport properties of each soil material.

T-level information - This group of output files contains information, which is printed at the end of each time step. Printing can be suppressed by setting the logical variable *ShortF* in input Block A equal to .true.; the information is then printed only at selected print times. Output files printed at the T-level are described in Tables 13.1 through 13.3. Output file OBS_NODE. OUT gives transient values of the pressure head, water content, temperature, and solution and sorbed concentrations, as obtained during the simulation at specified observation nodes.

P-level information - P-level information is printed only at prescribed print times. The following output files are printed at the P-level:

NOD_INF.OUT	Nodal values of the pressure head, the water content, the solution and sorbed concentrations, and temperature, etc. (Table 13.4).
BALANCE.OUT	This file gives the total amount of water, heat and solute inside each specified subregion, the inflow/outflow rates to/from each subregion, together with the mean pressure head (*hMean*), mean temperature (*TMean*) and the mean concentration (*cMean*) of each subregion (see Table 13.5). Absolute and relative errors in the water and solute mass balances are also printed to this file.
CONC.OUT	Nodal values of the aqueous concentrations for calcium, magnesium, sodium, potassium, alkalinity, sulfate, chloride, and hypothetical tracer (see Table 13.9).
SOLID.OUT	Nodal values of the mineral phase concentrations for calcite, gypsum, dolomite, hydromagnesite, nesquehonite, and sepiolite and nodal values of the adsorbed concentrations for calcium, magnesium, sodium, and potassium (see Table 13.10).
EQUIL.OUT	This file contains the chemical information such as activities of calcium, bicarbonate and water, alkalinity, *p*H, *SAR*, electric conductivity of the solution, ionic strength, osmotic coefficient, osmotic pressure head, and ion activity products for calcite, gypsum and dolomite (see Table 13.11).
CHEMBAL.OUT	This file contains the information about the total amount of particular species (e.g. Ca, Mg, SO_4,..) in solution, mineral phase and surface species form in the entire flow region, as well as the cumulative boundary fluxes and absolute mass error in particular species.

A-level information - A-level information is printed each time a time-dependent boundary condition is specified. The information is directed to output file A_LEVEL.OUT (Table 13.6). Meteorological information is directed into the METEO.OUT output file (Table 13.14).

Table 13.1. T_LEVEL.OUT - pressure heads and fluxes on the boundaries and in the root zone.

Time	Time, *t*, at current time-level [T].
rTop	Potential surface flux [LT^{-1}] (infiltration/evaporation: -/+).
rRoot	Potential transpiration rate [LT^{-1}].
vTop	Actual surface flux [LT^{-1}] (infiltration/evaporation: -/+).
vRoot	Actual transpiration rate [LT^{-1}].
vBot	Actual flux across the bottom of the soil profile [LT^{-1}] (inflow/outflow: +/-).
sum(*rTop*)	Cumulative value of the potential surface flux [L] (infiltration/evaporation: -/+).
sum(*rRoot*)	Cumulative value of the potential transpiration rate [L].
sum(*vTop*)	Cumulative value of the actual surface flux [L] (infiltration/evaporation: -/+).
sum(*vRoot*)	Cumulative value of the actual transpiration rate [L].
sum(*vBot*)	Cumulative value of the actual flux across the bottom of the soil profile [L] (inflow/outflow: +/-).
hTop	Pressure head at the soil surface [L].
hRoot	Mean value of the pressure head over the region for which *Beta(n)*>0 (i.e., within the root zone) [L].
hBot	Pressure head at the bottom of the soil profile [L].
RunOff	Surface runoff [LT^{-1}].
sum(*RunOff*)	Cumulative surface runoff [L]
Volume	Volume of water in the entire flow domain [L].
sum(*Infil*)	Cumulative infiltration [L]
sum(*Evap*)	Cumulative evaporation [L]
TLevel	Time-level (current time-step number) [-].
sum(*WTrans*)	Cumulative mass transfer of water between mobile and immobile regions for dual porosity model [L]
SnowLayer	Thickness of the snow layer [L]

Table 13.2. RUN_INF.OUT - time and iteration information.

TLevel	Time-level (current time-step number) [-].
Time	Time, t, at current time-level [T].
dt	Time step, Δt [T].
IterW	Number of iterations necessary for solution of the water flow equation [-].
IterC	Number of iterations necessary for solution of the solute transport equation [-].
ItCum	Cumulative number of iterations [-].
KodT	Code for the boundary condition at the soil surface.
KodB	Code for the boundary condition at the bottom of the soil profile.
Converg	Information whether or not the numerical convergence was achieved at the current time-level.
Peclet	Maximum local Peclet number [-].
Courant	Maximum local Courant number [-].

Table 13.3. SOLUTE.OUT - actual and cumulative concentration fluxes.[+][◆]

Time	Time, t, at current time-level [T].
cvTop	Actual solute flux across the soil surface [$ML^{-2}T^{-1}$] (inflow/outflow: +/-).
cvBot	Actual solute flux across the bottom of the soil profile [$ML^{-2}T^{-1}$] (inflow/outflow: +/-).
sum(*cvTop*)	Cumulative solute flux across the soil surface [ML^{-2}] (inflow/outflow: +/-).
sum(*cvBot*)	Cumulative solute flux across the bottom of the soil profile [ML^{-2}] (inflow/outflow: +/-).
sum(*cvCh*0)	Cumulative amount of solute removed from the flow region by zero-order reactions (positive when removed from the system) [ML^{-2}].
sum(*cvCh*1)	Cumulative amount of solute removed from the flow region by first-order reactions [ML^{-2}].
cTop	Solute concentration at the soil surface [ML^{-3}].
cRoot	Mean solute concentration of the root zone [ML^{-3}].
cBot	Solute concentration at the bottom of the soil profile [ML^{-3}].
cvRoot	Actual root solute uptake in the root zone [$ML^{-2}T^{-1}$].
sum(*cvRoot*)	Cumulative amount of solute removed from the flow region by root water uptake S [ML^{-2}].
sum(*cvNEql*)	Cumulative mass transfer to either kinetic adsorption sites (type-2 adsorption sites), or to the immobile liquid region [ML^{-2}] (inflow/outflow: +/-).
TLevel	Time-level (current time-step number) [-].
vFracS[*]	Mass transfer between the matrix and fracture domains of the dual-permeability model [$ML^{-2}T^{-1}$].
vFracS[*]	Cumulative mass transfer between the matrix and fracture domains of the dual-permeability model [ML^{-2}].

[+] Similar output files are created for each solute from 1 to *NS*.

[◆] Similar output files are created separately for the matrix (SoluteM) and fracture (SoluteF) domains of the dual-permeability model.

[*] Provided only for the dual-permeability model.

Table 13.4. NOD_INF.OUT - profile information.

Node	Number of nodal point n.
Depth	x-coordinate of node n.
Head	Nodal value of the pressure head [L].
Moisture	Nodal value of the water content [-].
K	Nodal value of the hydraulic conductivity [LT^{-1}].
C	Nodal value of the hydraulic capacity [L^{-1}].
Flux	Nodal value of the Darcian velocity [LT^{-1}].
Sink	Nodal value of the root water uptake [T^{-1}].
Ks/KsTop	Ratio between the local hydraulic conductivity and the saturated hydraulic conductivity at the soil surface [-].
v/KsTop	Ratio between the local velocity and the saturated hydraulic conductivity at the soil surface [-].
Temp	Nodal value of the temperature [K].
Conc(1,..,*NS*)	Nodal value of the concentration [ML^{-3}]. Only given when *lChem*=.true. .
Sorb(1,..,*NS*)	Nodal value of the sorbed concentration [MM^{3}] or concentration in the immobile regions [ML^{-3}]. Only given when *lChem*=.true. and *lEquil*=.false. .

The following information is printed when dual-porosity models are used:

WTrans	Water mass transfer between mobile and immobile regions [T^{-1}].
Im.Moist.	Water content in the immobile region [-].
STrans	Solute mass transfer between mobile and immobile regions [T^{-1}]. Only given when *lChem*=.true.

The following information is printed when dual-permeability models are used:

HeadF	Nodal value of the pressure head of the fracture region [L].
MoistureF	Nodal value of the water content of the fracture region [-].
FluxF	Nodal value of the Darcian velocity of the fracture region [LT^{-1}].
Transf	Water mass transfer between the matrix and fracture regions [T^{-1}].
TranS	Solute mass transfer between the matrix and fracture regions [T^{-1}]. Only given when *lChem*=.true.
ConcF	Nodal value of the concentration of the fracture region [ML^{-3}]. Only given when *lChem*=.true. .

Table 13.5. BALANCE.OUT - mass balance variables.

Area	Length of the entire flow domain or a specified subregion [L].
W-Volume	Volume of water in the entire flow domain or in a specified subregion [L].
InFlow	Inflow/outflow to/from the entire flow domain or a specified subregion [LT^{-1}].
hMean	Mean pressure head in the entire flow domain or a specified subregion [L].
TVol	Amount of heat in the entire flow domain or a specified subregion [MT^{-2}].
TMean	Mean temperature in the entire flow domain or a specified subregion [K].
COVol	Volume of CO_2 in the entire flow domain or in a specified subregion [L^3L^{-2}].
COMean	Mean CO_2 concentration in the entire flow domain or in a specified subregion [L^3L^{-3}].
ConcVol	Amount of solute in the entire flow domain or a specified subregion [ML^{-2}] excluding *ConcVolIm*. This variable is given for all solutes from 1 to *NS*.
ConcVolIm	Amount of solute in the entire flow domain, or in a specified subregion, either adsorbed at type-2 (kinetic) adsorption sites or in the immobile liquid region [ML^{-2}]. This information is given for all solutes from 1 to *NS*.
cMean	Mean concentration in the entire flow domain or a specified subregion [ML^{-3}]. This information is given for all solutes from 1 to *NS*.
Top Flux	Actual surface flux [LT^{-1}] (infiltration/evaporation: -/+).
Bot Flux	Actual flux across the bottom of the soil profile [LT^{-1}] (inflow/outflow: +/-).
WatBalT	Absolute error in the water mass balance of the entire flow domain [L].
WatBalR	Relative error in the water mass balance of the entire flow domain [%].
CncBalT	Absolute error in the solute mass balance of the entire flow domain [%]. This information is given for all solutes from 1 to *NS*.
CncBalR	Relative error in the solute mass balance of the entire flow domain [%]. This information is given for all solutes from 1 to *NS*.

The following information is printed when carbon dioxide transport is considered:

CO2BalT	Absolute error in the CO_2 mass balance for the entire flow domain [L].
CncBalT	Absolute error in the solute mass balance of the entire flow domain [ML^{-2}]. This information is given for all solutes from 1 to *NS*.

The following information is printed when dual-porosity models are used.

W-VolumeI	Volume of water in the immobile domain of the entire flow domain or a specified subregion [L].
cMeanIm	Mean concentration in the immobile domain of the entire flow domain or a specified subregion [ML^{-3}]. This variable is given for all solutes from 1 to *NS*.

Table 13.5. (continued)

The following information for the fracture domain is printed when dual-permeability models are used:

W-VolumeF Volume of water in the entire flow domain or in a specified subregion [L].

InFlowF Inflow/outflow to/from the entire flow domain or a specified subregion [LT^{-1}].

ConcVolF Amount of solute in the entire flow domain or a specified subregion [ML^{-2}] excluding *ConcVolIm*. This variable is given for all solutes from 1 to *NS*.

ConcVolIF Amount of solute in the entire flow domain, or in a specified subregion, either adsorbed at type-2 (kinetic) adsorption sites or in the immobile liquid region [ML^{-2}]. This information is given for all solutes from 1 to *NS*.

cMeanF Mean concentration in the entire flow domain or a specified subregion [ML^{-3}]. This information is given for all solutes from 1 to *NS*.

WatBalTF Absolute error in the water mass balance of the entire flow domain [L].

WatBalRF Relative error in the water mass balance of the entire flow domain [%].

CncBalTF Absolute error in the solute mass balance of the entire flow domain [%]. This information is given for all solutes from 1 to *NS*.

CncBalRF Relative error in the solute mass balance of the entire flow domain [%]. This information is given for all solutes from 1 to *NS*.

Table 13.6. A_LEVEL.OUT - pressure heads and cumulative fluxes on the boundary and in the root zone.

Time	Time, *t*, at current time-level [T].
sum(rTop)	Cumulative potential surface flux [L] (infiltration/evaporation: -/+).
sum(rRoot)	Cumulative potential transpiration [L].
sum(vTop)	Cumulative value of the actual surface flux [L] (infiltration/evaporation: -/+).
sum(vRoot)	Cumulative value of the actual transpiration [L].
sum(vBot)	Cumulative value of the bottom boundary flux [L] (inflow/outflow: +/-).
hTop	Pressure head at the soil surface [L].
hRoot	Mean value of the pressure head in the soil root zone for which *Beta(n)*>0 [L].
hBot	Pressure head at the bottom of the soil profile [L].
ALevel	A-level number (current variable boundary condition number) [-].

Table 13.7. FIT.OUT - parameter estimation related information.

SSQ	Value of the objective function Φ being minimized during the parameter optimization process.
S.E.Coeff	Standard error.
RSQUARE	r^2 value for regression of observed versus fitted values.
Quantity	Measured data, e.g., the pressure head, water content, cumulative flux.
Type	Type of measured data (see Table 12.10).
Position	Position of the measurement (see Table 12.10).
Weight	Weight associated with a particular data point.
Residual	Residual between measured and fitted quantity.

Table 13.8. CO2_INF.OUT - CO_2 concentrations and CO_2 fluxes on the boundaries and in the root zone. [+]

CvTop	Actual CO_2 flux at the soil surface $[L^3L^{-2}T^{-1}]$ (inflow/outflow: -/+).
CvBot	Actual CO_2 flux at the bottom of the soil profile $[L^3L^{-2}T^{-1}]$ (inflow/outflow: +/-).
sum(*CvTop*)	Cumulative CO_2 flux at the soil surface $[L^3L^{-2}]$.
sum(*CvBot*)	Cumulative CO_2 flux at the bottom of the soil profile $[L^3L^{-2}]$.
cTop	CO_2 concentration at the soil surface $[L^3L^{-3}]$.
cRoot	Mean CO_2 concentration in the root zone $[L^3L^{-3}]$.
cBot	CO_2 concentration at the bottom of the soil profile $[L^3L^{-3}]$.
vProd	CO_2 production by soil microorganisms and plant roots in the soil profile $[L^3L^{-2}T^{-1}]$.
sum(*vProd*)	Cumulative CO_2 production by soil microorganisms and plant roots in the soil profile $[L^3L^{-2}]$.
sum(*Sink*)	Cumulative CO_2 root uptake in the soil profile $[L^3L^{-2}]$.

[+] This output file is created only when carbon dioxide transport is calculated.

Table 13.9. CONC.OUT - solute concentration information.[+]

Node	Number of nodal point n.
Depth	x-coordinate of node n.
Ca	Analytical concentration of calcium ($mmol_c l^{-1}$) at node n.
Mg	Analytical concentration of magnesium ($mmol_c l^{-1}$) at node n.
Na	Analytical concentration of sodium ($mmol_c l^{-1}$) at node n.
K	Analytical concentration of potassium ($mmol_c l^{-1}$) at node n.
HCO3	Analytical concentration of alkalinity ($mmol_c l^{-1}$) at node n.
SO4	Analytical concentration of sulfate ($mmol_c l^{-1}$) at node n.
Cl	Analytical concentration of chloride ($mmol_c l^{-1}$) at node n.
Tracer	Analytical concentration of hypothetical tracer [-] at node n.

[+] This output file is created only when carbonate chemistry is considered.

Table 13.10. SOLID.OUT - precipitated and adsorbed concentrations.[+]

Node	Number of nodal point n.
Depth	x-coordinate of node n.
Calcite	Mineral phase Ca concentration present as calcite at node n (mmol$_c$kg^{-1}).
Gypsum	Mineral phase Ca concentration present as gypsum at node n (mmol$_c$kg^{-1}).
Dolomite	Mineral phase Ca concentration present as dolomite at node n (mmol$_c$kg^{-1}).
Nesqeh.	Mineral phase Mg concentration present as nesquehonite at node n (mmol$_c$kg^{-1}).
HydroMg.	Mineral phase Mg concentration present as hydromagnesite at node n (mmol$_c$kg^{-1}).
Sepiol.	Mineral phase Mg concentration present as sepiolite at node n (mmol$_c$kg^{-1}).
XCa	Surface species concentration of calcium at node n (mmol$_c$kg^{-1}).
XMg	Surface species concentration of magnesium at node n (mmol$_c$kg^{-1}).
XNa	Surface species concentration of sodium at node n (mmol$_c$kg^{-1}).
XK	Surface species concentration of potassium at node n (mmol$_c$kg^{-1}).

[+] This output file is created only when carbonate chemistry is considered.

Table 13.11. EQUIL.OUT - chemical information.[+]

Node	Number of nodal point n.
Depth	x-coordinate of node n.
aCa	Activity of Ca^{2+} [-].
aHCO$_3$	Activity of HCO_3^- [-].
aH$_2$O	Activity of water [-].
Alk	Alkalinity ($mmol_c kg^{-1}$).
pH	Negative logarithm of hydrogen activity, -log(H), [-].
SAR	Sodium adsorption ratio, defined as $[Na/(Ca+Mg)^{0.5}]$ $(mmol^{0.5}l^{-0.5})$.
EC	Electric conductivity of the soil solution (dSm^{-1}).
U	Ionic strength ($mol\ kg^{-1}$).
pIAP(c)	Negative logarithm of the ion activity product for calcite, $-log[(Ca^{2+})(CO_3^{2-})]$, [-].
pIAP(g)	Negative logarithm of the ion activity product for gypsum, $-log[(Ca^{2+})(SO_4^{2-})(H_2O)^2]$, [-].
pIAP(d)	Negative logarithm of the ion activity product for dolomite, $-log[(Ca^{2+})(Mg^{2+})(CO_3^{2-})^2]$, [-].
phi	Osmotic coefficient [-].
hphi	Osmotic pressure head [L].

[+] This output file is created only when carbonate chemistry is considered.

Table 13.12. METEO.OUT - meteorological information.[+]

Time	Time, t, at current time-level [T].
ET	Potential evapotranspiration (calculated using either the Penman-Monteith combination equation or the Hargreaves equation) [mm/d].
Evap	Potential evaporation (evaluated from ET using LAI or SCF) [mm/d].
Transp	Potential transpiration (evaluated from ET using LAI or SCF) [mm/d].
Rns	Shortwave net radiation (calculated using the Penman-Monteith combination equation) [MJ/m^2/d].
Rnl	Longwave net radiation (calculated using the Penman-Monteith combination equation) [MJ/m^2/d].
RadTerm	Radiation term in the Penman-Monteith combination equation [mm/d].
AeroTerm	Aerodynamic term in the Penman-Monteith combination equation [mm/d].
Prec	Precipitation [mm/d].
Interc	Interception [mm/d].
ExInterc	Excess interception, i.e., potential transpiration minus interception [mm/d].

[+] This output file is created only when meteorological information is considered.

15. REFERENCES

Adamczyk, Z., B. Siwek, M Zembala, and P. Belouschek, Kinetics of localized adsorption of colloid particles , *Adv. Colloid Interface Sci.*, *48*, 151-280, 1994.

Alexander, M., and K. M. Scow, Kinetics of biodegradation in soil, In *Reactions and Movement of Organic Chemicals in Soils*, edited by B. L. Sawhney and K. Brown, Spec. Publ. No. 22, 243-270, Soil Science Society of America, Madison, WI, 1989.

Aziz, K., and A. Settari, *Petroleum Reservoir Simulation*, pp. 395-401, Applied Science, Barking, United Kingdom, 1979.

Bear, J., *Dynamics of Fluid in Porous Media*, Elsevier, New York, NY, 1972.

Belmans, C., J. G. Wesseling and R. A. Feddes, Simulation model of the water balance of a cropped soil: SWATRE, *J. Hydrol., 63*, 271- 286, 1983.

Bell, R. P., and J. H. B. George, Dissociation of thallus and Ca sulfate salts at different temperatures, *Trans. Faraday Soc., 49*, 619-627, 1953.

Bradford, S. A., S. R. Yates, M. Bettahar, and J. Šimůnek, Physical factors affecting the transport and fate of colloids in saturated porous media, *Water Resour. Res.* 38(12), 1327, doi:10.1029/2002WR001340, 2002.

Bradford, S. A., J. Šimůnek, M. Bettahar, M. Th. van Genuchten, and S. R. Yates, Modeling colloid attachment, straining, and exclusion in saturated porous media, *Environ. Sci. Technol.*, *37*, 2242-2250, 2003.

Bradford, S. A., M. Bettahar, J. Šimůnek, and M. Th. Van Genuchten, Straining and attachment of colloids in physically heterogeneous porous media, *Vadose Zone J.*, *3*, 384-394, 2004.

Bromilow, R. H., and M. Leistra, Measured and simulated behavior of aldicarb and its oxidation products in fallow soils, *Pestic. Sci., 11*(4), 389-395, 1980.

Brooks, R. H., and A. T. Corey, Properties of porous media affecting fluid flow, *J. Irrig. Drainage Div.*, ASCE Proc. 72(IR2), 61-88, 1966.

Brunt D., *Physical and Dynamical Meteorology*, 2nd ed. University Press, Cambridge, 428 pp., 1952.

Busenberg, E., and L. N. Plummer, The kinetics of dissolution of dolomite in CO_2-H_2O systems at 1.5 to 65 C and 0 to 1 ATM P_{CO2}, *Am. J. Sci., 282*, 45-78, 1982.

Campbell, G. S., *Soil Physics with Basic; Transport Models for Soil-Plant Systems*, Elsevier, New York, 1985.

Casey, F. X. M., and J. Šimůnek, Inverse analyses of the transport of chlorinated hydrocarbons subject to sequential transformation reactions, *J. Environ. Quality*, *30*(4), 1354-1360, 2001.

Casey, F. X. M., G. L. Larsen, H. Hakk, and J. Šimůnek, Fate and transport of 17β-Estradiol in soil-water systems, *Environ.l Sci. Technol.*, *37*(11), 2400-2409, 2003.

Casey, F.X.M., G. L. Larsen, H. Hakk, and J. Šimůnek, Fate and transport of testosterone in agriculturally significant soils. *Environ. Sci. Technol.*, *38*(3), 790-798, 2004.

Cass, A., G. S. Campbell, and T. L. Jones, Enhancement of thermal water vapor diffusion in soil, *Soil Sci. Soc. Am. J.*, *48*, 25-32, 1984.

Castro, C. L., and D. E. Rolston, Organic phosphate transport and hydrolysis in soil: theoretical and experimental evaluation, *Soil Sci. Soc. Am. J., 41*(6), 1085-1092, 1977.

Celia, M. A., and E. T. Bououtas, R. L. Zarba, A general mass-conservative numerical solution for the unsaturated flow equation, *Water Resour. Res., 26*, 1483-1496, 1990.

Chiou, C. T., Theoretical consideration of the partition uptake of nonionic organic compounds by soil organic matter, In *Reactions and Movement of Organic Chemicals in Soils*, edited by B. L. Sawhney and K. Brown, Spec. Publ. Number 22, 1-30, Soil Science Society of America, Madison, WI, 1989.

Chung S.-O., and R. Horton, Soil heat and water flow with a partial surface mulch, *Water Resour. Res., 23*(12), 2175-2186, 1987.

Cho, C. M., Convective transport of ammonium with nitrification in soil, *Can. Jour. Soil Sci., 51*(3), 339-350, 1971.

Christie, L. D., D. F. Griffiths, A. R. Mitchell, and O. C. Zienkiewicz, Finite element methods for second order differential equations with significant first derivatives, *Int. J. Num. Methods in Engineering, 10*, 1389-1396, 1976.

Císlerová, M., Comparison of simulated water balance for ordinary and scaled soil hydraulic characteristics, *Publ. No. 82*, Dept. of Hydraulics and Catchment Hydrology, Agricultural Univ., Wageningen, The Netherlands, 1987.

Clausnitzer, V., and J. W. Hopmans, Non-linear parameter estimation: LM_OPT. General-purpose optimization code based on the Levenberg-Marquardt algorithm, *Land, Air and Water Resources Paper No. 100032*, University of California, Davis, CA, 1995.

Cleary, R. W., and M. J. Ungs, Groundwater pollution and hydrology, Mathematical models and computer programs, *Research Rep. No. 78-WR-15*, Water Resour. Program, Princeton Univ. Princeton, NJ, 1978.

Constantz, J., Temperature dependence of unsaturated hydraulic conductivity of two soils. *Soil Sci. Soc. Am. J., 46*(3), 466-470, 1982.

Daniel, C., and F. S. Wood, *Fitting Equations to Data*. Wiley-Interscience, New York, 1971.

Davis, L. A., and S. P. Neuman, Documentation and user's guide: UNSAT2 - Variably saturated flow model, *Final Rep., WWL/TM-1791-1,* Water, Waste & Land, Inc., Ft. Collins, CO, 1983.

de Marsily, G., *Quantitative Hydrogeology*, Academic Press, London, 1986.

de Vries, D. A., Simultaneous transfer of heat and moisture in porous media, Transactions, *American Geophysical Union*, *39*(5), 909-916, 1958.

de Vries, D. A., The thermal properties of soils, In *Physics of Plant Environment*, edited by R. W. van Wijk, pp. 210-235, North Holland, Amsterdam, 1963.

Dontsova, K. M., S. L. Yost, J. Šimůnek, J. C. Pennington, C. Williford, Dissolution and transport of TNT, RDX, and Composition B in saturated soil columns, *J. Environ. Quality*, *35*, 2043-2054, 2006.

Durner, W., Hydraulic conductivity estimation for soils with heterogeneous pore structure, *Water Resour. Res.*, *32*(9), 211-223, 1994.

Durner, W., E. Priesack, H.-J. Vogel, and T. Zurmühl, Determination of parameters for flexible hydraulic functions by inverse modeling. In: M. Th. van Genuchten, F. J. Leij, L. Wu (Editors), *Characterization and Measurement of the Hydraulic Properties of Unsaturated Porous Media*. University of California, Riverside, CA, pp. 817-829, 1999.

Eching, S. O., and J. W. Hopmans, Optimization of hydraulic functions from transient outflow and soil water pressure data, *Soil Sci. Soc. Am. J. 57*, 1167-1175, 1993.

Ekpete, D. M., and A. H. Cornfield, Effect of varying static and changing moisture levels during incubation on the mineralization of carbon in soil, *J. Agric. Sci., 64*, 205-209, 1965.

Ernst, L. F., Groundwaterstromingen in de verzadigde zone en hun berekening bij aanwezigheid van horizontale evenwijdige open leidengen (Groundwater flow in the saturated zone and its calculation when horizontal parallel open conduits are present), Versl. Landbouwk. Onderz. 67.1, Pudoc, Wageningen, 189 pp., the Netherlands (in Dutch), 1962.

Fayer, M. J. UNSAT-H version 3.0: Unsaturated soil water and heat flow model, theory, user manual, and examples, *Rep. 13249*, Pacific Northwest National Laboratory, Richland, Washington, 2000.

Feddes, R. A., E. Bresler, and S. P. Neuman, Field test of a modified numerical model for water uptake by root systems, *Water Resour. Res., 10*(6), 1199-1206, 1974.

Felmy, A. R., and J. H. Weare, The prediction of borate mineral equilibria in natural waters: Application to Searles Lake, California, *Geochim. Cosmochim. Acta, 50*, 2771-2783, 1986.

Felmy, A. R., *GMIN: A computerized chemical equilibrium model using a constrained minimization of the Gibbs free energy*, Pacific Northwest Lab., Richland, Washington, 1990.

Feddes, R. A., P. J. Kowalik, and H. Zaradny, *Simulation of Field Water Use and Crop Yield*, John Wiley & Sons, New York, NY, 1978.

Flint, A. L., L. E. Flint, G. S. Bodvarsson, E. M. Kwicklis, and J. Fabryka-Martin, Development of the conceptual model of unsaturated zone hydrology at Yucca Mountain, Nevada, In: *Conceptual Models of Flow and Transport in the Fractured Vadose zone*, National Research Council, National Academy Press, Washington, D.C., pp. 47-85, 2001.

Food and Agriculture Organization of the United Nations, Expert consultation on revision of FAO methodologies for crop water requirements, *ANNEX V*, FAO Penman-Monteith Formula, Rome Italy, 1990.

Gerke, H. H., and M. Th. van Genuchten, A dual-porosity model for simulating the preferential movement of water and solutes in structured porous media, *Water Resour. Res., 29*, 305-319, 1993a.

Gerke, H. H., and M. Th. van Genuchten, Evaluation of a first-order water transfer term for variably saturated dual-porosity flow models, *Water Resour. Res., 29*, 1225-1238, 1993b.

Gerke, H. H., and M. Th. van Genuchten, Macroscopic representation of structural geometry for simulating water and solute movement in dual-porosity media, *Adv. Water Resour., 19*, 343-357, 1996.

Germann, P. F., Kinematic wave approach to infiltration and drainage into and from soil macropores, *Trans. ASAE, 28*, 745-749, 1985.

Germann, P. F., and G. Beven, Kinematic wave approximation to infiltration into soils with sorbing macropores, *Water Resour. Res.*, *21*(7), 990-996, 1985.

Glinski, J., and W. Stepniewski, *Soil aeration and its role for plants*, CRC Press, Boca Raton, Florida, 1985.

Glotfelty, D. E., and C. J. Schomburg, Volatilization of pesticides from soil, In *Reactions and Movement of Organic Chemicals in Soils*, edited by B. L. Sawhney and K. Brown, Spec. Publ. Number 22, 181-208, Soil Science Society of America, Madison, WI, 1989.

Gureghian, A. B., A two-dimensional finite-element solution for the simultaneous transport of water and multi-solutes through a nonhomogeneous aquifer under transient saturated-unsaturated flow conditions, *Sci. Total Environ., 21*, 329-337, 1981.

Gureghian, A. B., and G. Jansen, LAYFLO: A one-dimensional semianalytical model for the migration of a three-member decay chain in a multilayered geologic medium, *Tech. Rep. ONWI-466*, Office of Nuclear Waste Isolation, Battelle Memorial Institute, Columbus, OH, 1983.

Harada, M., P. L. Chambre, M. Foglia, K. Higashi, F. Iwamoto, D. Leung, T. H. Pigford, and D. Ting, Migration of radionuclides through sorbing media, analytical solutions - I, *Rep. no. LBL-10500 (UC-11)*, Lawrence Berkeley Laboratory, Univ. of California, Berkeley, CA, 1980.

Harned, H. S., and R. Davis, Jr., The ionization constant of carbonic acid and the solubility of carbon dioxide in water and aqueous salt solutions from 0 to 50 C, *J. Am. Chem. Soc., 653*, 2030-2037, 1943.

Higashi, K., and T. H. Pigford, Analytical models for migration of radionuclides in geologic sorbing media, *J. Nucl. Sci. and Techn., 7*(9), 700-709, 1980.

Hoffman, G. J., and M. Th. van Genuchten, Soil properties and efficient water use: Water namagement for salinity control. In: H. M. Taylor, W. R. Jordan, and T. R. Sinclair (eds.), Limitations and Efficient Water Use in Crop Production, Am. Soc. Of Agron., Madison, WI, pp. 73-85, 1983.

Hooghoudt, S. B., Bijdrage tot de kennis van enige natuutkundige grootheden van de grond (Contribution to the knowledge of several physical soil parameters), Versl. Landbouwk. Onderz. 46 (14) B, 515-707, Wageningen, the Netherlands (in Dutch), 1940.

Hopmans, J. W., and J. N. M. Stricker, Stochastic analysis of soil water regime in a watershed, *J. Hydrol., 105*, 57-84, 1989.

Hopmans, J. W., and J. Šimůnek, Review of inverse estimation of soil hydraulic properties, In: van Genuchten, M. Th., F. J. Leij, and L. Wu (eds.), *Characterization and Measurement of the Hydraulic Properties of Unsaturated Porous Media*, University of California, Riverside, CA, pp. 643-659, 1999.

Hopmans, J. W., J. Šimůnek, N. Romano, and W. Durner, Inverse Modeling of Transient Water Flow, In: *Methods of Soil Analysis, Part 1, Physical Methods,* Chapter 3.6.2, Eds. J. H. Dane and G. C. Topp, Third edition, SSSA, Madison, WI, 963-1008, 2002.

Huyakorn, P. S., and G. F. Pinder, *Computational Methods in Subsurface Flow*, Academic Press, London, United Kingdom, 1983.

Inskeep, W. P., and P. R. Bloom, An evaluation of rate equations for calcite precipitation kinetics at pCO$_2$ less than 0.01 atm and pH greater than 8, *Geochim. Cosmochim. Acta, 49*, 2165-2180, 1985.

Inskeep, W. P., and P. R. Bloom, Kinetics of calcite precipitation in the presence of water-soluble organic ligands, *Soil Sci. Soc. Am. J., 50*, 1167-1172, 1986.

Jacobson, R., *Controls on the quality of some carbonate ground waters: dissociation constant of calcite and CaHCO$_3^+$ from 0 to 50 ^{o}C*, Ph. D. Thesis, Pennsylvania State Univ, 131p., 1973.

Jacques, D., and J. Šimůnek, User Manual of the Multicomponent Variably-Saturated Flow and Transport Model HP1, Description, Verification and Examples, Version 1.0, *SCK•CEN-BLG-998,* Waste and Disposal, SCK•CEN, Mol, Belgium, 79 pp., 2005.

Jacques, D., J. Šimůnek, D. Mallants, and M. Th. van Genuchten, Operator-splitting errors in coupled reactive transport codes for transient variably saturated flow and contaminant transport in layered soil profiles, *J. Contam. Hydrol.*, *88*, 197-218, 2006.

Jensen, D. T., G. H. Hargreaves, B. Temesgen, and R. G. Allen, Computation of Eto under nonideal conditions, *J. Irrig. Drainage*, 123(5), 394-400, 1997.

Javandel, I., Ch. Doughty, Chin-Fu Tsang, *Groundwater Transport: Handbook of Mathematical Models*, Water Resour. Monograph No. 10, Am. Geophys. Union, Washington, D.C., 1984.

Johnson, P. R., and M. Elimelech, Dynamics of colloid deposition in porous media: Blocking based on random sequential adsorption, *Langmuir*, *11*, 801-812, 1995.

Jury, W. A., W. F. Spencer, and W. J. Farmer, Behavior assessment model for trace organics in soil, I. Model description, *J. Environ. Qual., 12*, 558-564, 1983.

Kirkham, D., and W. L. Powers, *Advanced Soil Physics*, John Wiley & Sons, New York, NY, 1972.

Köhne, J. M., S. Köhne, B. P. Mohanty, and J. Šimůnek, Inverse mobile-immobile modeling of transport during transient flow: Effect of between-domain transfer and initial water content, *Vadose Zone Journal*, *3*(4), 1309-1321, 2004.

Köhne, S., B. Lennartz, J. M. Köhne, and J. Šimůnek, Bromide transport at a tile-drained field site: experiment, one- and two-dimensional equilibrium and non-equilibrium numerical modeling, *J. Hydrology*, (submitted September, 2004).

Kool, J. B., J. C. Parker, and M. Th. van Genuchten, ONESTEP: A nonlinear parameter estimation program for evaluating soil hydraulic properties from one-step outflow experiments, *Bulletin 58-3*, Virginia Agr. Exp. Station, Virginia, 1985.

Kool, J. B., J. C. Parker, and M. Th. van Genuchten, Determining soil hydraulic properties from one-step outflow experiments by parameter estimation: I. Theory and numerical studies, *Soil Sci. Soc. Am. J., 49*, 1348-1354, 1985.

Kool, J. B., J. C. Parker, and M. Th. van Genuchten, Parameter estimation for unsaturated flow and transport models - A review, *J. Hydrol., 91*, 255-293, 1987.

Kool, J. B., and J. C. Parker, Development and evaluation of closed-form expressions for hysteretic soil hydraulic properties, *Water Resour. Res., 23*(1), 105-114, 1987.

Kool, J. B., and M. Th. van Genuchten, HYDRUS - One-dimensional variably saturated flow and transport model, including hysteresis and root water uptake, Version 3.3, *Research Report No. 124*, U. S. Salinity Laboratory, USDA, ARS, Riverside, CA, 1991.

Kosugi K., Lognormal distribution model for unsaturated soil hydraulic properties, *Water Resour. Res.*, *32*(9), 2697-2703, 1996.

Leij, F. J., T. H. Skaggs, and M. Th. van Genuchten, Analytical solutions for solute transport in three-dimensional semi-infinite porous media, *Water Resour. Res., 27*(10), 2719-2733, 1991.

Leij, F. J., and S. A. Bradford, 3DADE: A computer program for evaluating three-dimensional equilibrium solute transport in porous media, *Research Report No. 134*, U. S. Salinity Laboratory, USDA, ARS, Riverside, CA, 1994.

Lenhard, R. J., J. C. Parker, and J. J. Kaluarachchi, Comparing simulated and experimental hysteretic two-phase transient fluid flow phenomena, *Water Resour. Res., 27*(8), 2113-2124, 1991.

Lenhard, R. J., and J. C. Parker, Modeling multiphase fluid hysteresis and comparing results to laboratory investigations, In, Proc. Intl. Workshop on *Indirect Methods for Estimating the Hydraulic Properties of Unsaturated Soils,* edited by M. Th van Genuchten, F. J. Leij, and L. J. Lund, University of California, Riverside, pp. 233-248, 1992.

Lester, D. H., G. Jansen, and H. C. Burkholder, Migration of radionuclide chains through an adsorbing medium, In: *Adsorption and Ion Exchange,* Am. Inst. Chem. Eng., Symp. Series no. 152, 71, 202-213, 1975.

Liu, Chen Wuing, and T. N. Narasimhan, Redox-controlled multiple-species reactive chemical transport. 2. Verification and application, *Water Resour. Res., 25*(5), 883-910, 1989.

Logan, B. E., D. G. Jewett, R. G. Arnold, E. J. Bouwer, and C. R. O'Melia, Clarification of clean-bed filtration models, *J. Environ. Eng.*, *121*, 869-873, 1995.

Luckner, L., M. Th. van Genuchten, and D. R. Nielsen, A consistent set of parametric models for the two-phase flow of immiscible fluids in the subsurface, *Water Resour. Res., 25*(10), 2187-2193, 1989.

Lynch, D., Mass conservation in finite element groundwater models, *Adv. Water Resour., 7*, 67-75, 1984.

Marquardt, D. W., An algorithm for least-squares estimation of nonlinear parameters, *SIAM J. Appl. Math., 11*, 431-441, 1963.

Maas, E. V., Crop salt tolerance. In "Agricultural salinity assessment and management", K. K. Tanji (ed.), ASCE Manuals and Reports on Engineering practice, No 71, New York, 1990.

McNeal, B. L, Prediction of the effect of mixed-salt solutions on soil hydraulic conductivity, *Soil Sci. Soc. Amer. Proc., 32*, 190-193, 1968.

McNeal, B. L., J. D. Oster, and J. T. Hatcher, Calculation of electrical conductivity from solution composition data as an aid to in-situ estimation of soil salinity, *Soil Sci., 110*, 405-414, 1970.

McNeal, B. L, Soil salts and their effects on water movement, In: *Drainage for Agriculture*, Edited by J. van Schilfgaarde, Agronomy No 17, Am. Soc. Agr., Madison, Wi. 1974.

Miller, E. E., and R. D. Miller, Physical theory for capillary flow phenomena, *J. Appl. Phys., 27*, 324-332, 1956.

Millington, R. J., and J. M. Quirk, Permeability of porous solids, *Trans. Faraday Soc., 57*, 1200-

1207, 1961.

Misra, C., D. R. Nielsen, and J. W. Biggar, Nitrogen transformations in soil during leaching: I. Theoretical considerations, *Soil Sci. Soc. Am. Proc., 38*(2), 289-293, 1974.

Mls, J., Formulation and solution of fundamental problems of vertical infiltration, *Vodohosp. Čas., 30*, 304-313 (in Czech), 1982.

Mohammad, F. S., and R. W. Skaggs, Drain tube opening effects on drain inflow, *J. Irrig. Drain. Div., Am. Soc. Civ. Eng., 109*(4), 393-404, 1983.

Monteith, J. L., Evaporation and surface temperature, *Quarterly J. Royal Meteo. Soc.*, 107, 1-27, 1981.

Monteith, J. L. and M. H. Unsworth, *Principles of Environmental Physics*, Edward Arnold, London, 1990.

Mualem, Y., A new model for predicting the hydraulic conductivity of unsaturated porous media, *Water Resour. Res., 12*(3), 513-522, 1976.

Murray F. W., On the computation of saturation vapor pressure, *J. Appl. Meteor.*, 6, 203-204, 1967.

Nassar, I. N., and R. Horton, Water transport in unsaturated nonisothermal salty soil: II. Theoretical development, *Soil Sci. Soc. Am. J.*, 53, 1330-1337, 1989.

Nassar, I. N., and R. Horton, Simultaneous transfer of heat, water, and solute in porous media: I. Theoretical development, *Soil Sci. Soc. Am. J.*, 56, 1350-1356, 1992.

Neuman, S. P., Finite element computer programs for flow in saturated-unsaturated porous media, *Second Annual Report, Project No. A10-SWC-77*, Hydraulic Engineering Lab., Technion, Haifa, Israel, 1972.

Neuman, S. P., Saturated-unsaturated seepage by finite elements, *J. Hydraul. Div.*, ASCE, 99 (HY12), 2233-2250, 1973.

Neuman, S. P., R. A. Feddes, and E. Bresler, Finite element simulation of flow in saturated-unsaturated soils considering water uptake by plants, *Third Annual Report*, *Project No. A10-SWC-77*, Hydraulic Engineering Lab., Technion, Haifa, Israel, 1974.

Neuman, S. P., Galerkin approach to saturated-unsaturated flow in porous media, Chapter 10 in *Finite Elements in Fluids, Vol. I, Viscous Flow and Hydrodynamics*, edited by R. H. Gallagher, J. T. Oden, C. Taylor, and O.C. Zienkiewicz, John Wiley & Sons, London, pp. 201-217, 1975.

Nielsen, D. R., and L. M. Luckner, Theoretical aspects to estimate reasonable initial parameters and range limits in indentification procedures for soil hydraulic properties. In, Proc. Intl. Workshop on *Indirect Methods for Estimating the Hydraulic Properties of Unsaturated Soils,* edited by M. Th van Genuchten, F. J. Leij, and L. J. Lund, University of California, Riverside, pp. 147-160, 1992.

Nimmo, J. R., and E. E. Miller, The temperature dependence of isothermal moisture vs. potential characteristics of soils, *Soil Sci. Soc. Am. J.*, *50*, 1105-1113, 1986.

Noborio, K., K. J. McInnes, and J. L. Heilman, Two-dimensional model for water, heat, and solute transport in furrow-irrigated soil: I. Theory, *Soil Sci. Soc. Am. J.*, *60*, 1001-1009, 1996a.

Noborio, K., K. J. McInnes, and J. L. Heilman, Two-dimensional model for water, heat, and solute transport in furrow-irrigated soil: II. Field evaluation, *Soil Sci. Soc. Am. J.*, *60*, 1010-1021, 1996b.

Ou, L. T., P. S. C. Rao, K. S. V. Edvardson, R. E. Jessup, A. G. Hornsby, and R. L. Jones, Aldicarb degradation in sandy soils from different depths, *Pesticide Sci., 23*, 1-12, 1988.

Parkhurst, D. L. and C. A. J. Appelo, User's guide to PHREEQC (Version 2) – A computer program for speciation, batch-reaction, one-dimensional transport and inverse geochemical calculations. Water-Resources Investigations, *Report 99-4259*, Denver, Co, USA, 312 pp, 1999.

Passioura, J. B., Determining soil water diffusivities from one-step outflow experiments, *Aust. J. Soil Res., 15*, 1-8, 1976.

Patwardhan, A. S., J. L. Nieber, and I. D. Moore, Oxygen, carbon dioxide, and water transfer in soils: mechanism and crop response, *Transaction of ASEA, 31*(5), 1383-1395, 1988.

Perrochet, P., and D. Berod, Stability of the standard Crank-Nicolson-Galerkin scheme applied to the diffusion-convection equation: some new insights, *Water Resour. Res., 29*(9), 3291-3297, 1993.

Peters, R. R., and E. A. Klavetter, A continuum model for water movement in an unsaturated fractured rock mass, *Water Resour. Res., 24*(3), 416-430, 1988.

Philip, J. R., and D. A. de Vries, Moisture movement in porous media under temperature gradients, *Eos Trans. AGU, 38*(2), 222-232, 1957.

Phillip, J. R., The theory of absorption in aggregated media, *Aust. J. Soil Res., 6*, 1-19, 1968.

Pignatello, J. J., Sorption dynamics of organic compounds in soils and sediments, In *Reactions and Movement of Organic Chemicals in Soils*, edited by B. L. Sawhney and K. Brown, Spec. Publ. Number 22, 45-80, Soil Science Society of America, Madison, WI, 1989.

Pinder, G. F., and W. G. Gray, *Finite Element Simulation in Surface and Subsurface Hydrology*, Academic Press, New York, N.Y., 1977.

Pitzer, K. S., Thermodynamics of electrolytes I: Theoretical basis and general equations, *J. Phys. Chem., 77*, 268-277, 1973.

Pitzer, K. S., *Activity Coefficients in Electrolyte Solutions*, Chap. 7, CRC Press, Boca Raton, Fl., 1979.

Plummer, L. N., T. M. Wigley, and D. L. Parkhurst, The kinetics of calcite dissolution in CO_2 systems at 5° to 60^oC and 0.0 to 1.0 atm CO_2, *Am. J. Sci., 278*, 179-216, 1978.

Plummer, L. N., and E. Busenberg, The solubilities of calcite, aragonite and vaterite in CO_2-H_2O solutions between 0 and 90^oC, and an evaluation of the aqueous model for the system $CaCO_3$-CO_2-H_2O, *Geochim. Cosmochim. Acta, 46*, 1011-1040, 1982.

Pot, V., J. Šimůnek, P. Benoit, Y. Coquet, A. Yra and M.-J. Martínez-Cordón, Impact of rainfall intensity on the transport of two herbicides in undisturbed grassed filter strip soil cores, *J. Contam. Hydrol.*, *81*, 63-88, 2005.

Pruess, K., and J. S. Y. Wang, Numerical modeling of isothermal and non-isothermal flow in unsaturated fractured rock - a review, In: D. D. Evans, and T. J. Nicholson (Editors), Flow and Transport Through Unsaturated Fractured Rock, *Geophysics Monograph 42*, American Geophysical Union, Washington, D.C., pp. 11-22, 1987.

Raats, P. A. C., Steady flows of water and salt in uniform soil profiles with plant roots, *Soil Sci. Soc. Am. Proc., 38*, 717-722, 1974.

Rajagopalan, R., and Tien, C., 1976. Trajectory analysis of deep-bed filtration with the sphere-in-cell porous media model, *AIChE. J.*, 22, 523-533.

Reardon, E. J., *Thermodynamic Properties of Some Sulfate, Carbonate and Bicarbonate Ion Pairs*, Ph.D. Thesis, Pennsylvania State Univ, 85p., 1974.

Reardon, E. J., and D. Langmuir, Thermodynamic properties of the ion pairs $MgCO_3^o$ and $CaCO_3^o$ from 10 to 50^oC, *Am. J. Sci., 274*, 599-612, 1974.

Reardon, E. J., and D. Langmuir, Activity coefficients of $MgCO_3^o$ and $CaSO_4^o$ ion pairs as a

function of ionic strength, *Geochim. Cosmochim. Acta, 40*, 549-554, 1976.

Ritchie, J. T., Model for predicting evaporation from a row crop with incomplete cover, *Water Resour. Res., 8*(5), 1204-1213, 1972.

Rixon, A. J., Oxygen uptake and nitrification at various moisture levels by soils and mats from irrigated pastures, *J. Soil. Sci., 19*, 56-66, 1968.

Robinson, R. A., and R. H. Stokes, *Electrolyte Solutions*, Butterworths, London, 571p., 1965.

Rogers, V. C., Migration of radionuclide chains in groundwater, *Nucl. Techn., 40*(3), 315-320, 1978.

Rogers, J. S., and J. L. Fouss, Hydraulic conductivity determination from vertical and horizontal drains in layered soil profiles, *Transaction of the ASAE, 32*(2), 589-595, 1989.

Saito, H., J., Šimůnek, and B. Mohanty, Numerical analyses of coupled water, vapor and heat transport in the vadose zone, *Vadose Zone J.*, *5*, 784–800, 2006.

Scanlon, B., K. Keese, R. C. Reedy, J. Šimůnek, and B. Andraski, Variations in flow and transport in thick desert vadose zones in response to paleoclimatic forcing (0 − 90 kyr): Monitoring, modeling, and uncertainties, *Water Resour. Res.*, *39*(7), 1179, doi:10.1029/2002WR001604, 13.1-13.7, 2003.

Schaerlaekens, J., D. Mallants, J. Šimůnek, M. Th. van Genuchten, and J. Feyen, Numerical simulation of transport and sequential biodegradation of chlorinated aliphatic hydrocarbons using CHAIN_2D, *J. of Hydrological Processes*, *13*(17), 2847-2859, 1999.

Schijven, J., and J. Šimůnek, Kinetic modeling of virus transport at field scale, *J. of Contam. Hydrology*, *55*(1-2), 113-135, 2002.

Scott, P. S., G. J. Farquhar, and N. Kouwen, Hysteresis effects on net infiltration, Advances in Infiltration, *Publ. 11-83*, pp.163-170, Am. Soc. Agri. Eng., St. Joseph, Mich., 1983.

Selim, H. M., R. Schulin, and H. Flühler, Transport and ion exchange of calcium and magnesium in an aggregated soil, *Soil Sci. Soc. Am. J., 51*(4), 876-884, 1987.

Shainberg, I., and G. J. Levy, Physico-chemical effects of salts upon infiltration and water movement in soils, In: *Interacting Processes in Soil Science*, edited by R. J. Wagenet, P. Baveye, B. A. Stewart, Lewis Publishers, CRC Press, Boca Raton, Florida, 1992.

Simmons, C. S., D. R. Nielsen, and J. W. Biggar, Scaling of field-measured soil water properties, *Hilgardia, 47*, 101-122, 1980.

Šimůnek, J., T. Vogel and M. Th. van Genuchten, The SWMS_2D code for simulating water flow and solute transport in two-dimensional variably saturated media, Version 1.1, *Research Report No. 126*, U. S. Salinity Laboratory, USDA, ARS, Riverside, CA, 1992.

Šimůnek, J., *Numerical modeling of transport processes in unsaturated porous media,* Dissertation, Czech Academy of Sciences, Prague (in Czech), 1993.

Šimůnek, J., and D. L. Suarez, Modeling of carbon dioxide transport and production in soil: 1. Model development, *Water Resour. Res.*, *29*(2), 487-497, 1993a.

Šimůnek, J., and D. L. Suarez, UNSATCHEM-2D code for simulating two-dimensional variably saturated water flow, heat transport, carbon dioxide production and transport, and multicomponent solute transport with major ion equilibrium and kinetic chemistry, Version 1.1, *Research Report No. 128*, U. S. Salinity Laboratory, USDA, ARS, Riverside, CA, 1993b.

Šimůnek, J., and D. L. Suarez, The SOILCO2 code for simulating one-dimensional carbon dioxide production and transport in variably saturated porous media, Version 1.1, *Research Report No. 127*, U.S. Salinity Laboratory, USDA, ARS, Riverside, California, 1993c.

Šimůnek, J., and D. L. Suarez, Major ion chemistry model for variably saturated porous media, *Water Resour. Res.*, *30*(4), 1115-1133, 1994.

Šimůnek, J., and M. Th. van Genuchten, The CHAIN_2D code for simulating two-dimensional movement of water flow, heat, and multiple solutes in variably-saturated porous media, Version 1.1, *Research Report No 136*, U.S. Salinity laboratory, USDA, ARS, Riverside, California, 1994.

Šimůnek, J., and M. Th. van Genuchten, Numerical model for simulating multiple solute transport in variably-saturated soils, *Proc. "Water Pollution III: Modelling, Measurement, and Prediction*, Ed. L. C. Wrobel and P. Latinopoulos, Computation Mechanics Publication, Ashurst Lodge, Ashurst, Southampton, UK, pp. 21-30, 1995.

Šimůnek, J., D. L. Suarez, and M. Šejna, The UNSATCHEM software package for simulating one-dimensional variably saturated water flow, heat transport, carbon dioxide production and transport, and multicomponent solute transport with major ion equilibrium and kinetic chemistry, Version 2.0, *Research Report No. 141*, U.S. Salinity Laboratory, USDA, ARS, Riverside, California, 186pp., 1996.

Šimůnek, J., M. Šejna, and M. Th. van Genuchten, The HYDRUS-1D software package for simulating the one-dimensional movement of water, heat, and multiple solutes in variably-saturated media, Version 2.0. *IGWMC - TPS - 70,* International Ground Water Modeling Center, Colorado School of Mines, Golden, Colorado, 162pp., 1998.

Šimůnek, J., O. Wendroth, and M. Th. van Genuchten, A parameter estimation analysis of the evaporation method for determining soil hydraulic properties, *Soil Sci. Soc. Am. J.*, *62*(4), 894-905, 1998.

Šimůnek, J., M. Th. van Genuchten, M. M. Gribb, and J. W. Hopmans, Parameter estimation of unsaturated soil hydraulic properties from transient flow processes, *Soil & Tillage Research*, *47*/1-2, Special issue "State of the art in soil physics and in soil technology of antrophic soils", 27-36, 1998.

Šimůnek, J., and J. W. Hopmans, Parameter Optimization and Nonlinear Fitting, In: *Methods of Soil Analysis, Part 1, Physical Methods,* Chapter 1.7, Eds. J. H. Dane and G. C. Topp, Third edition, SSSA, Madison, WI, 139-157, 2002.

Šimůnek, J., D. Jacques, J. W. Hopmans, M. Inoue, M. Flury, and M. Th. van Genuchten, Solute Transport During Variably-Saturated Flow - Inverse Methods, In: *Methods of Soil Analysis, Part 1, Physical Methods,* Chapter 6.6, Eds. J. H. Dane and G. C. Topp, Third edition, SSSA, Madison, WI, 1435-1449, 2002.

Šimůnek, J. and A. J. Valocchi, Geochemical Transport, In: *Methods of Soil Analysis, Part 1, Physical Methods,* Chapter 6.9, Eds. J. H. Dane and G. C. Topp, Third edition, SSSA, Madison, WI, 1511-1536, 2002.

Šimůnek, J., N. J. Jarvis, M. Th. van Genuchten, and A. Gärdenäs, Review and comparison of models for describing non-equilibrium and preferential flow and transport in the vadose zone, *Journal of Hydrology*, 272, 14-35, 2003.

Šimůnek, J., M. Th. van Genuchten, and M. Šejna, The HYDRUS-1D software package for simulating the one-dimensional movement of water, heat, and multiple solutes in variably-saturated media. Version 3.0, *HYDRUS Software Series 1*, Department of Environmental Sciences, University of California Riverside, Riverside, CA, 270 pp., 2005.

Šimůnek, J., M. Th. van Genuchten, and M. Šejna, The HYDRUS Software Package for Simulating Two- and Three-Dimensional Movement of Water, Heat, and Multiple Solutes in Variably-Saturated Media, Technical Manual, Version 1.0, PC Progress, Prague, Czech Republic, pp. 241, 2006a.

Šimůnek, J., M. Šejna, and M. Th. van Genuchten, The HYDRUS Software Package for Simulating Two- and Three-Dimensional Movement of Water, Heat, and Multiple Solutes in Variably-Saturated Media, User Manual, Version 1.0, PC Progress, Prague, Czech Republic, pp. 161, 2006b.

Šimůnek, J., D. Jacques, M. Th. van Genuchten, and D. Mallants, Multicomponent geochemical transport modeling using the HYDRUS computer software packages, *J. Am. Water Resour. Assoc.*, *42*(6), 1537-1547, 2006c.

Šimůnek, J., M. Th. van Genuchten, and M. Šejna, Modeling Subsurface Water Flow and Solute Transport with HYDRUS and Related Numerical Software Packages, In: Garcia-Navarro & Playán (eds.), Numerical Modelling of Hydrodynamics for Water Resources, An International Workshop, Centro Politecnico Superior, University of Zaragoza Spain, June 18-21 2007. Taylor & Francis Group, London, ISBN 978-0-415-44056-1, 95-114, 2007.

Šimůnek, J., M. Th. van Genuchten, and M. Šejna, Development and applications of the HYDRUS and STANMOD software packages, and related codes, *Vadose Zone J.*, Special Issue "Vadose Zone Modeling", (in press). 2008.

Šimůnek, J. and M. Th. van Genuchten, Modeling nonequilibrium flow and transport with HYDRUS, *Vadose Zone J.*, Special Issue "Vadose Zone Modeling", (in press), 2008.

Šír, M., T. Vogel, and M. Císlerová, Analytical expression of the retention curve and hydraulic conductivity for porous material, *Vodohosp. Čas., 33*(1), 74-85 (in Czech), 1985.

Sisson, J. B., Drainage from layered field soils: Fixed gradient models, *Water Resour. Res., 23*(11), 2071-2075, 1987.

Skaggs, R. W., E. J. Monke, and L. F. Huggins, An approximate method for determining the hydraulic conductivity function of an unsaturated soil, *Techn. Rep. No. 11*, Water Resour. Res. Center, Purdue University, Lafayette, IN, 1970.

Sleep, B. E. and J. F. Sykes, Modeling the transport of volatile organics in variably saturated media, *Water Resour. Res., 22*(1), 81-92, 1989.

Sophocleous, M., Analysis of water and heat flow in unsaturated-saturated porous media, *Water Resour. Res., 15*(5), 1195-1206, 1979.

Spencer, W. F., Volatilization of pesticides from soil: processes and measurement, *Pesticide Res. J., 3*(1), 1-14, 1991.

Sposito, G., *The Thermodynamics of Soil Solutions*. Oxford University Press, New York, NY, 1981.

Stumm, W., and J. J. Morgan, *Aquatic Chemistry: An Introduction Emphasizing Chemical Equilibria in Natural Waters*, John Wiley & Sons, New York, NY, 1981.

Suarez, D. L., Magnesium, carbonate, and silica interactions in soils, *U.S. Salinity Laboratory Annual Report*, USDA, 120 pp., 1977.

Suarez, D. L., J. D. Rhoades, R. Lavado, and C. M. Grieve, Effect of pH on saturated hydraulic conductivity and soil dispersion, *Soil Sci. Soc. Am. J., 48*, 50-55, 1984.

Suarez, L. D., and J. Šimůnek, Modeling of carbon dioxide transport and production in soil: 2. Parameter selection, sensitivity analysis and comparison of model predictions to field data, *Water Resour. Res., 29*(2), 499-513, 1993.

Suarez, D. L., and J. Šimůnek, UNSATCHEM: Unsaturated water and solute transport model with equilibrium and kinetic chemistry, *Soil Sci. Soc. Am. J., 61*, 1633-1646, 1997.

Stokes, R. H., Thermodynamics of solutions, In: R. M. Pitkowicz, *Activity Coefficients in Electrolyte Solutions*, CRC Press, Inc., Boca Raton, Florida, 1979.

Stumm, W., and J. J. Morgan, *Aquatic Chemistry: An Introduction Emphasizing Chemical Equilibria in Natural Waters*, John Wiley & Sons, New York, 1981.

Sudicky, E. A., and P. S. Huyakorn, Contaminant migration in imperfectly known heterogeneous groundwater systems, *Review of Geophysics*, Supplement, U. S. National Rep. to Inter. Union of Geodesy and Geophysics 1987-1990, 240-253, 1991.

Tetens O., Uber einige meteorologische Begriffe, *Z. Geophys*., *6*, 297-309, 1930.

Tillotson, W. R., C. W. Robbins, R. J. Wagenet, and R. J. Hanks, Soil water, solute and plant growth simulation, *Bulletin 502,* Utah Agricultural Experiment Station, 53 p., 1980.

Toride, N., F. J. Leij, and M. Th. van Genuchten, A comprehensive set of analytical solutions for nonequilibrium solute transport with first-order decay and zero-order production, *Water Resour. Res., 29*(7), 2167-2182, 1993.

Toride, N., F. J. Leij, and M. Th. van Genuchten, The CXTFIT code for estimating transport parameters from laboratory or field tracer experiments, Version 2.0, *Research Report No 137*, U.S. Salinity laboratory, USDA, ARS, Riverside, California, 1995.

Truesdell, A. H., and B. F. Jones, WATEQ, a computer program for calculating chemical equilibria of natural waters, *J. Res. U. S. Geol. Surv., 2*(2), 233-248, 1974.

van Dam, J. C., J. N. M. Stricker, and P. Droogers, Inverse method for determining soil hydraulic functions from one-step outflow experiment, *Soil Sci. Soc. Am. J., 56*, 1042-1050, 1992.

van Dam, J. C., J. N. M. Stricker, and P. Droogers, Inverse method to determine soil hydraulic functions from multistep outflow experiment, *Soil Sci. Soc. Am. J., 58*, 647-652, 1994.

van Dam, J. C., J. Huygen, J. G. Wesseling, R. A. Feddes, P. Kabat, P. E. V. van Walsum, P. Groenendijk, and C. A. van Diepen, Theory of SWAP version 2.0, *Report 71*, Dept. of Water Resour., Wageningen Agricultural University, Wageningen, the Netherlands, 1997.

van Genuchten, M. Th., On the accuracy and efficiency of several numerical schemes for solving the convective-dispersive equation, in *Finite Elements in Water Resources*, edited by W. G. Gray et al., Pentech Press, London, pp. 1.71-1.90, 1976.

van Genuchten, M. Th., and P. J. Wierenga, Mass transfer studies in sorbing porous media, I. Analytical solutions, *Soil Sci. Soc. Am. J.*, *40*, 473-481, 1976.

van Genuchten, M. Th., Mass transport in saturated-unsaturated media: one-dimensional solutions, *Research Rep. No. 78-WR-11*, Water Resources Program, Princeton Univ., Princeton, NJ, 1978.

van Genuchten, M. Th., A closed-form equation for predicting the hydraulic conductivity of unsaturated soils, *Soil Sci. Soc. Am. J., 44*, 892-898, 1980.

van Genuchten, M. Th., Non-equilibrium transport parameters from miscible displacement experiments. *Research Report No. 119*, U.S. Salinity Laboratory, Riverside, CA, 1981.

van Genuchten, M. Th., Convective-dispersive transport of solutes involved in sequential first-order decay reactions, *Computers & Geosciences, 11*(2), 129-147, 1985.

van Genuchten, M. Th., and J. Parker, Boundary conditions for displacement experiment through short laboratory soil columns, *Soil Sci. Soc. Am. J., 48*, 703-708, 1984.

van Genuchten, M. Th., and F. N. Dalton, Models for simulating salt movement in aggregated field soils, *Geoderma*, *38*, 165-183, 1986.

van Genuchten, M. Th., A numerical model for water and solute movement in and below the root zone. *Research Report No 121*, U.S. Salinity laboratory, USDA, ARS, Riverside, California, 1987.

van Genuchten, M. Th., and R. J. Wagenet, Two-site/two-region models for pesticide transport and degradation: Theoretical development and analytical solutions, *Soil Sci. Soc. Am. J., 53*,

1303-1310, 1989.

van Genuchten, M. Th., and P. J. Wierenga, Mass transfer studies in sorbing porous media, I. Analytical solutions, *Soil Sci. Soc. Am. J., 40*, 473-481, 1976.

van Horn, J. W., Drainage for salinity control, Dept. of Water Resour., Wageningen Agricultural University, Wageningen, the Netherlands, 1997.

Vogel, T., SWMII - Numerical model of two-dimensional flow in a variably saturated porous medium, *Research Rep. No. 87*, Dept. of Hydraulics and Catchment Hydrology, Agricultural Univ., Wageningen, The Netherlands, 1987.

Vogel, T., and M. Císlerová, On the reliability of unsaturated hydraulic conductivity calculated from the moisture retention curve, *Transport in Porous Media, 3*, 1-15, 1988.

Vogel, T., *Numerical modeling of water flow in non-homogeneous soil profile*, Dissertation, Czech Technical Univ., Prague (in Czech), 1990.

Vogel, T., M. Císlerová, and J. W. Hopmans, Porous media with linearly variable hydraulic properties, *Water Resour. Res., 27*(10), 2735-2741, 1991.

Vogel, T., K. Huang, R. Zhang, and M. Th. van Genuchten, The HYDRUS code for simulating one-dimensional water flow, solute transport, and heat movement in variably-saturated media, Version 5.0, *Research Report No 140*, U.S. Salinity Laboratory, USDA, ARS, Riverside, CA, 1996.

Wagenet, R. J., J. W. Biggar, and D. R. Nielsen, Analytical solutions of miscible displacement equations describing the sequential microbiological transformations of urea, ammonium and nitrate, *Research Rep. no 6001,* Dept. of Water Science and Engineering, Univ. California, Davis, CA, 1976.

Wagenet R. J., and J. L. Hutson, LEACHM: Leaching Estimation And CHemistry Model, A process-based model of water and solute movement, transformations, plant uptake and chemical reactions in the unsaturated zone, *Continuum 2*, Dept. of Agronomy, Cornell University, Ithaca, New York, NY, 1987.

Walker, A., A simulation model for prediction of herbicide persistence, *J. Environ. Quality, 3*(4), 396-401, 1974.

Wendroth, O., W. Ehlers, J. W. Hopmans, H. Kage, J. Halbertsma, and J. H. M. Wösten, Reevaluation of the evaporation method for determining hydraulic functions in unsaturated soils, *Soil Sci. Soc. Am. J., 57*, 1436-1443, 1993.

Wesseling, J. G., and T. Brandyk, Introduction of the occurrence of high groundwater levels and surface water storage in computer program SWATRE, *Nota 1636*, Institute for Land and Water Management Research (ICW), Wageningen, The Netherlands, 1985.

Westall, J. C., J. L. Zachary, and F. M. M. Morel, MINEQL: A computer program for the calculation of chemical equilibrium composition of aqueous systems, *Tech. Note 18,* 91pp., Dep. of Civ. Eng., Mass. Inst. of Technol., Cambridge, 1976.

White, N., and L. W. Zelazny, Charge properties in soil colloids, In: *Soil Physical Chemistry*, edited by D. L. Sparks, CRC Press, BOCA Raten, Florida, 1986.

Williams, S. T., M. Shameemullah, E. T. Watson, and C. I. Mayfield, Studies on the ecology of actinomycetes in soil. IV. The influence of moisture tension on growth and survival, *Soil Biol. Biochem., 4*, 215-225, 1972.

Wilson, J. M., and D. M. Griffin, Water potential and the respiration of microorganisms in the soils, *Soil Biol. Biochem., 7*, 199-204, 1975.

Yeh, G. T., and V. S. Tripathi, HYDROGEOCHEM: A coupled model of HYDROlogic transport and GEOCHEMical equilibria in reactive multicomponent systems, *Environs Sci. Div., Publ. No. 3170.*, Oak Ridge National Lab., Oak Ridge, TN, 1990.

Yeh, G. T., and V. S. Tripathi, A model for simulating transport of reactive multispecies components: Model development and demonstration, *Water Resour. Res., 27*(12), 3075-3094, 1991.

Zienkiewicz, O. C., *The Finite Element Method*, 3rd ed., McGraw-Hill, London, United Kingdom, 1977.

Appendix A

Variables in the Penman-Monteith combination equation can be calculated using the following equations [*FAO*, 1990].

1. *Latent Heat of Vaporization*

$$\lambda = 2.501 - (2.361 \times 10^{-3})T \qquad\qquad (A.1)$$

where λ is the latent heat of vaporization [MJ kg^{-1}], and T is air temperature [$^{\circ}$C] [*Harrison*, 1963].

2. *Atmospheric Pressure*

$$P = P_0\left(\frac{T_{k0} - \alpha(z - x_o)}{T_{k0}}\right)^{\frac{g}{\alpha R}} = 101.3\left(\frac{293 - 0.0065z}{293}\right)^{5.26} \qquad\qquad (A.2)$$

where P is atmospheric pressure at elevation z [kPa], P_0 is atmospheric pressure at sea level (=101.3 kPa), z is the elevation [m], z_0 is elevation at the reference level (= 0 m), g is the gravitational acceleration (= 9.81 m s^{-2}), R is the specific gas constant (= 287 J kg^{-1}K^{-1}), T_{k0} is the reference temperature at z_0 (= 20 $^{\circ}$C), and α is the constant lapse rate saturated air (= 0.0065 K m^{-1}) [*Burman et al.*, 1987].

3. *Atmospheric Density*

$$\rho = \frac{1000P}{T_{kv}R} = 3.486\frac{P}{T_{kv}} \qquad\qquad (A.3)$$

where ρ is the atmospheric density [kg m^{-3}], and T_{kv} is the virtual temperature [K].

$$T_{kv} = T_k \left(1 - 0.378 \frac{e_d}{P} \right)^{-1} \approx 1.01 (T + 273) \qquad (A.4)$$

where T_k is the absolute temperature [K], and e_d is the vapor pressure at dew point [kPa].

4. *Saturation Vapor Pressure*

$$e_a = 0.611 \exp \left(\frac{17.27 \, T}{T + 237.3} \right) \qquad (A.5)$$

where e_a is the saturation vapor pressure [kPa] [*Tetens*, 1930].

5. *Crop Canopy Resistance*

$$r_c = \frac{R_l}{0.5 \, LAI} = \frac{200}{LAI} \qquad (A.6)$$

where r_c is the crop canopy resistance [s m^{-1}], R_l is the average daily (24 hours) stomata resistance of a single leaf ($\cong 100$ s m^{-1}), and *LAI* is the leaf area index [-] [*Allen et al.*, 1989]. *LAI* can be calculated using the following approaches:

(a)   For clipped grass (crop height $h_c = 0.05$ - 0.15 m):

$$LAI = 24 \, h_c \qquad (A.7)$$

(b)   For alfalfa and other field crops ($h_c = 0.10$ - 0.50 m):

$$LAI = 5.5 + 1.5 \ln (h_c) \qquad (A.8)$$

(c)   From the surface cover fraction (*SCF*):

$$LAI = -\frac{1}{a_i} \ln\left(1 - SCF\right) \tag{A.9}$$

where a_i is a constant for the radiation extinction by the canopy (i.e., 0.463) [-].

6. *Aerodynamic Resistance*

$$r_a = \frac{\ln\left(\dfrac{z_m - d}{z_{om}}\right) \cdot \ln\left(\dfrac{z_h - d}{z_{oh}}\right)}{k^2\, U_z} \tag{A.10}$$

where r_a is the aerodynamic resistance [s m^{-1}], z_m is the height of windspeed measurements [m], z_h is the height of the temperature and humidity measurements [m], k is the von Karman constant (= 0.41), U_z is the measured windspeed [m s^{-1}] [*Allen et al.*, 1989], and d is the zero plane displacement of the wind profile [m] [*Monteith*, 1981]:

$$d = \frac{2}{3} h_c \tag{A.11}$$

where z_{om} is the roughness parameter for momentum [m] [*Brutsaert*, 1975],

$$z_{om} = 0.123\, h_c \tag{A.12}$$

and z_{oh} is the roughness parameter for heat and water vapor [m].

$$z_{oh} = 0.1 z_{om} = 0.0123 h_c \tag{A.13}$$

7. Net Emissivity

$$\varepsilon' = (\varepsilon_a - \varepsilon_{vs}) \approx \left(a_l + b_l \sqrt{e_d}\right) \tag{A.14}$$

where ε' is the net emissivity [-], ε_a is the effective emissivity of the atmosphere [-], ε_{vs} is the emissivity by vegetation and soil [-], e_d is the actual vapor pressure [kPa], and a_l and b_l are correlation coefficients (i.e., $a_l = 0.34$, $b_l = -0.14$) [*Brunt*, 1932; *Jensen et al.*, 1990].

8. Cloudiness Factor

The cloudiness factor f [-] can be calculated in three different ways:
  (a) From measured solar radiation data:

$$f = \frac{R_{nl}}{R_{nl0}} = \left(a_c \frac{R_s}{R_{s0}} + b_c \right) \tag{A.15}$$

where R_{nl} is the net longwave radiation [MJ m^{-2}d^{-1}], R_{nl0} is the net longwave radiation for clear skies [MJ m^{-2}d^{-1}], R_s is the measured shortwave solar radiation [MJ m^{-2}d^{-1}], R_{s0} is the shortwave solar radiation for clear skies (extraterrestrial radiation) [MJ m^{-2}d^{-1}], and a_c and b_c are calibration values (i.e., $a_c = 1.35$, $b_c = -0.35$) [*Wright and Jensen*, 1972; *Jensen et al.*, 1990].

  (b) From measured sunshine hour data:

$$f = \frac{R_{nl}}{R_{nl0}} = a_1 \frac{n}{N} + b_1 \tag{A.16}$$

where n is the measured sunshine hours per day [hr], N is the total day length (= 24 hr), and a_1 and b_1 are parameters for cloudiness effect (i.e., $a_1 = 0.9$, $b_1 = 0.1$).

  (c) From the atmospheric transmission coefficient :

$$f = 1 - c = 1 - \left(0\,; 2.33 - 3.33T_t\,; 1\right) \tag{A.17}$$

where c is the fractional cloud cover [-], and T_t is the atmospheric transmission coefficient for solar radiation [-] [*Campbell*, 1985].

Appendix References

Allen, R. G., M. E. Jensen, J. L. Wright and R. D. Burman, Operational estimates of evapotranspiration, *Agron. J.*, *81*, 650-662, 1989.

Harrison, L. P., Fundamental concepts and definitions relating to humidity, In: *Humidity and Moisture*, Vol. 3, Wexler A. (ed.), Reinhold Publishing Company, New York, 1963.

Brunt, D., Notes on radiation in the atmosphere, *Quart. J. Roy. Meteorol. Soc*, *58*, 389-418, 1932.

Brutsaert, W., The roughness length for water vapor, sensible heat and other scalars, *J. Atm. Sci.*, *32*, 2028-2031, 1975.

Burman R. D., M. E. Jensen, and R. G. Allen, Thermodynamic factors in evapotranspiration, In: *Proc. Irrig. and Drain. Spec. Conf.*, James L.G. and M. J. English (eds). ASCE, Portland, Ore., July. pp. 28-30, 1987.

Campbell, G. S., *Soil Physics with Basic, Transport Models for Soil-Plant Systems*, Elsevier, New York, 1985.

Harrison, L. P., Fundamental concepts and definitions relating to humidity, In: *Humidity and Moisture*, Vol. 3, Wexler A. (ed), Reinhold Publishing Company, New York, 1963.

Jensen, M. E., R. D. Burman, and R. G. Allen, Evapotranspiration and irrigation water requirements. *ASCE Manual No. 70*, 1990.

Monteith, J. L., Evaporation and surface temperature, *Quarterly J. Royal Meteo. Soc.*, *107*, 1-27, 1981.

Tetens, O., Uber einige meteorologische Begriffe, *Z. Geophys.*, *6*, 297-309, 1930.

Wright, J. L., and M. J. Jensen, Peak water requirements of crops in Southern Idaho, *J. Irrig. Drain. Div.*, *ASCE*, *96*(IR1), 193-201, 1972.

PART B

Interactive Graphics-Based User Interface

HYDRUS1D

Version 4.0

by

J. Šimůnek, M. Šejna, and M. Th. van Genuchten

Even with well-documented numerical computer models available, one major problem often preventing the use of such codes is the extensive work required for data preparation, finite element grid design, and graphical presentation of the output results. Hence, a more widespread use of numerical models requires techniques which make it easier to create, manipulate and display large data files, and which facilitate interactive data management. Introducing such techniques will free users from cumbersome manual data processing, and should enhance the efficiency in which programs are being implemented for a particular example. To avoid or simplify the preparation and management of relatively complex input data files and to graphically display final simulation results, we developed an interactive graphics-based user-friendly interface HYDRUS1D for the MS Windows environment. The graphics interface is connected directly to the HYDRUS FORTRAN code.

In addition to information given in this chapter, extensive context-sensitive on-line help is made part of every module of the interface. By pushing the F1 button, or clicking on the Help button while working in any window, the user obtains information about the window content. In addition, context-sensitive help is available in every module using the "SHIFT+F1" help button. In this mode, the mouse cursor changes to a help cursor (a combination arrow + question mark), and the user proceeds to click on the object for which he needs help (i.e, a menu item, toolbar button, or other features). At that point, a help file will be displayed giving information about the item on which the user clicked. Except for the HYDRUS FORTRAN application itself, all modules are written in C++.

Table B.1. Main modules of the HYDRUS-1D software package.

HYDRUS1D	main program unit, input parameters, output graphics
POSITION	project manager (PCP_BASE.DLL)
PROFILE	transport domain geometry, finite element mesh generator, boundary and initial conditions, material distribution
H1D_calc	FORTRAN application for the direct solution
H1D_clci	FORTRAN application for the inverse solution
H1D_dual	FORTRAN application for the direct solution (dual-permeability model)
H1D_dlin	FORTRAN application for the inverse solution (dual-permeability model)
H1D_unsc	FORTRAN application for the major ion chemistry model
HP1	C application for running the coupled HP1 biogeochemical model
Hydrus.dll	HYDRUS part of the HP1 model
Phreeqc.dll	PHREEQC part of the HP1 model

B. *Brief Description of Selected Modules*

B.1. *Module **HYDRUS1D***

HYDRUS1D (Fig. B.1) is the main program unit defining the overall computational environment of the system. This module controls execution of the program and determines which other optional modules are necessary for a particular application. The module contains a project manager and both the pre-processing and post-processing units. The pre-processing unit includes specification of all necessary parameters to successfully run the **HYDRUS** FORTRAN codes, a small catalog of soil hydraulic properties, and a plant salt tolerance database. Table B.2 lists all commands accessible through the menu, whereas Table B.3 gives a brief discussion of the action taken with the particular commands. More detailed descriptions are available through

the on-line help. The post-processing unit consists of simple x-y graphics for graphical presentation of soil hydraulic properties, as well as such output as transient values of a particular variable at selected observation points in the domain, and actual or cumulative water and solute fluxes across boundaries. Table B.4 gives an overview of the different graph options made available through the interface. The **HYDRUS1D** and **PROFILE** modules mutually communicate through the file **HYDRUS1D.DAT**, a description of which is given in Table B.5.

The work for a new project should begin by opening the Project Manager (see Section B.2), and giving a name and brief description to this new project. Then select the <u>Main Processes</u> command from the Main Information Menu. From this point on, the program will navigate the user through the entire process of entering input files. The user may either select particular commands from a menu, or allow the interface to lead him through the process of entering input data by selecting the <u>Next</u> buttons. Alternatively, clicking the <u>Previous</u> button will return the user to the previous window.
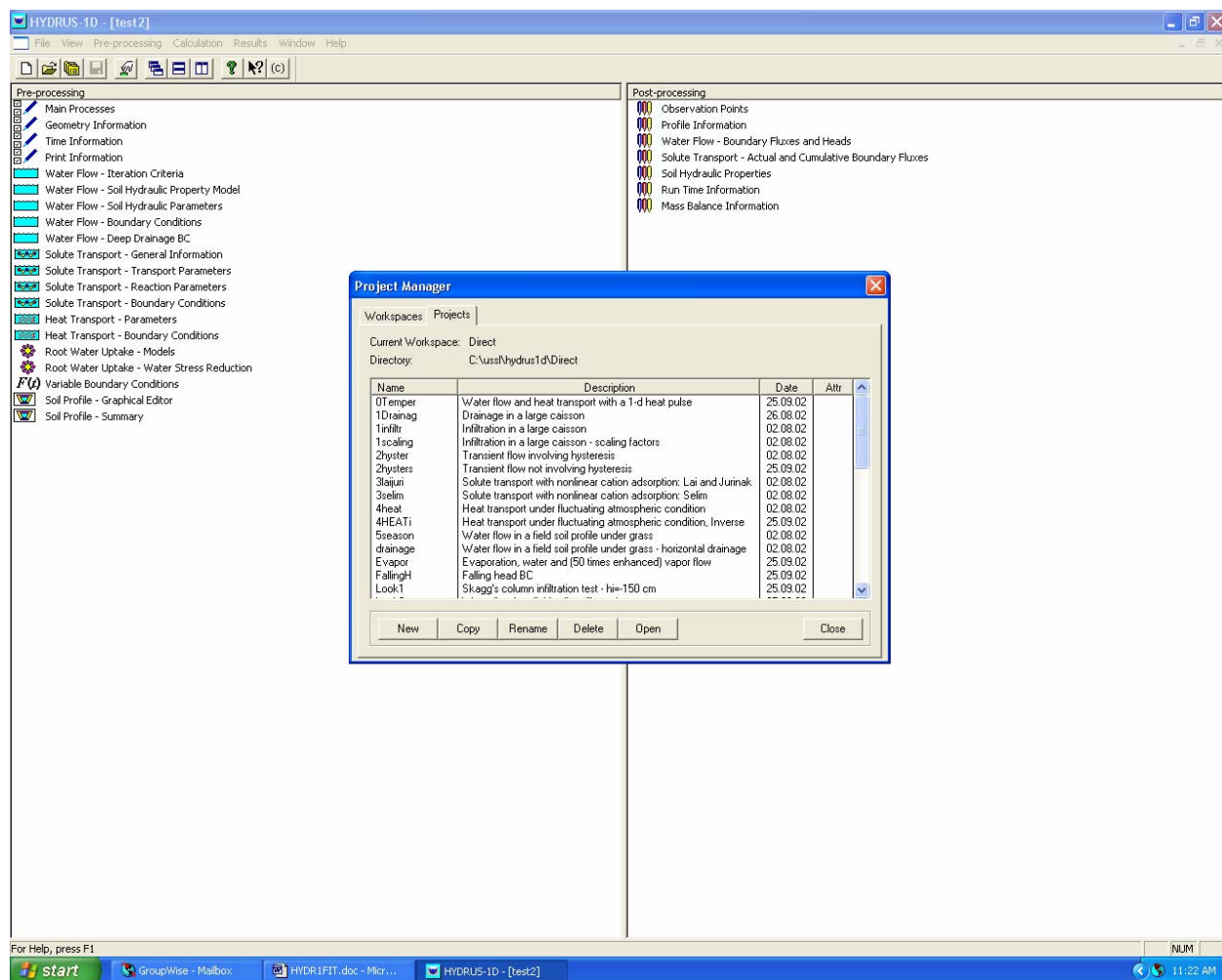
Fig. B.1. The main window of the HYDRUS1D module, including the project manager.

Table B.2. Menu commands in the main module HYDRUS1D.

Group	Menu	Submenu	Sub-Submenu
A	Project	New	
		Open	
		Project Manager	
		Save	
		Save As	
		Exit	
B	View	Toolbar	
		Status Bar	
		List Boxes for Inverse Data	
C	Pre-processing	Main Processes	
		Inverse Solution	
		Geometry Information	
		Time Information	
		Print Information	
		Water Flow	Iteration Criteria
			Hydraulic Properties Model
			Soil Hydraulic Properties
			Boundary Conditions
			Constant Boundary Fluxes
			Deep Drainage BC
		Solute Transport	General Solute Transport Information
			HP1 Components
			Solute Transport Parameters
			Solute Reaction Parameters
			Temperature Dependence
			Water Content Dependence
			Boundary Conditions
		Heat Transport	Heat Transport Parameters
			Boundary Conditions
		Carbon Dioxide Transport	CO2 Transport Parameters
			Soil CO2 Production Parameters
			Root CO2 Production Parameters
		Root Water Uptake	Root Water Uptake Models
			Pressure Head Reduction
			Osmotic Head Reduction
		Root Growth Parameters	
		Meteorological Parameters	
		Variable Boundary Conditions	
		Meteorological Boundary Conditions	
		Data for Inverse Solution	
		Profile Information	
		Profile Summary	
D	Calculation	Execute HYDRUS	

Group	Menu	Submenu	Sub-Submenu
E	Results	Observation Points	

Group	Menu	Submenu	Sub-Submenu
		Profile Informations	Basic Information
			Solution Concentrations
			Solid Concentrations
			Chemical Information
		Boundary Informations	Water Flow
			Solute Transport
			CO2 Transport
		Soil Hydraulic Properties	
		Run Time Information	
		Mass Balance Information	
		Inverse Solution	
		Meteorological Information	
		Solute Mass Balance Information	
F	Options	Program Options	
G	Window	Cascade	
		Tile Horizontally	
		Tile Vertically	
		Arrange Icons	
H	Help	Index	
		Help On	
		About HYDRUS-1D	

Table B.3. Description of all menu commands in the main module HYDRUS1D.

Group	Command	Brief description of the command
A	New	Creates a new project.
	Open	Open an existing project (represented by *project_name*.h1d file)
	Project Manager	Calls the project manager to manage data of existing projects; helps to locate, open, copy, delete or rename the desired projects and their data.
	Save	Saves the input data of an actual project specified in the main program module if the data were either newly created or changed during an application run. This command deletes at the same time all existing output files of a selected project since the output data are no longer consistent with the changed input data. A warning is issued to the user before doing so.
	Save as	Saves data of a particular project under a new project name.

Group	Command	Brief description of the command
	Exit	Closes a project and leaves the program. This command informs the user before exiting the application whether or not the input data of an actual project were changed during the application run. If changes did occur, the user is given a possibility to save data before exiting the application.
B	Toolbar	Shows or hides the toolbar.
	Status Bar	Shows or hides the status bar.
	List Boxes for Inverse Data	Shows a text information in the inverse data list.
C	Main Processes	Selects the title which is printed into output files, and specifies the processes to be simulated, i.e., water flow, multiple solute transport, heat transport, root growth, and/or root water uptake.
	Inverse Solution	Selects type of weighting of measured data, whether soil hydraulic parameters, solute transport parameters, or both are to be fitted.
	Main Geometry Information	Selects the length unit, specifies the depth and inclination of the soil profile to be analyzed, and determines the number of materials to be used.
	Main Time Information	Selects time units, and gives the time discretization information.
	Print Information	Specifies print options.
	Iteration Criteria	Specifies iteration criteria for the solution precision, and parameters for the time step control.
	Hydraulic Properties Model	Selects the type of model used for the soil hydraulic properties, and decides whether the hysteresis is to be considered.
	Soil Hydraulic Properties	Specifies parameters in the soil hydraulic model.
	Boundary Conditions	Specifies the types of upper and lower boundary conditions.
	Constant Boundary Fluxes	Specifies constant boundary fluxes and constant root water uptake when no time-variable boundary conditions are given.
	Deep Drainage BC	Specifies parameters for the deep drainage function.
	General Solute Transport Information	Selects the time and spatial weighting schemes for numerical solution of the solute transport equation; specifies the number of solutes to be considered.
	HP1 Components	Selects the main components of the biogeochemical system and pathways to the geochemical database.
	Solute Transport Parameters	Specifies solute transport parameters.
	Solute Reaction Parameters	Specifies solute reaction parameters.
	Temperature Dependence	Specifies parameters, which define the temperature dependence of reaction and transport parameters.
	Water Content Dependence	Specifies parameters, which define the water content dependence of reaction and transport parameters.
	ST Boundary Conditions	Specifies the upper and lower boundary conditions for solute transport.

Group	Command	Brief description of the command
	Chemical Parameters	Selects kinetic or equilibrium model for calcite precipitation/dissolution, specifies critical ionic strength and maximum number of iterations.
	Solution Compositions	Specifies different solution, adsorbed and mineral phase compositions.
	CO_2 Transport Parameters	Specifies carbon dioxide transport parameters including boundary conditions.
	Soil CO_2 Production Parameters	Specifies soil (microbial) CO_2 production parameters.
	Root CO_2 Production Parameters	Specifies root CO_2 production parameters.
	Heat Transport Parameters	Specifies heat transport parameters.
	Heat Transport Boundary Conditions	Specifies the upper and lower boundary conditions for heat flow.
	Root Water Uptake Models	Selects the root water uptake stress response models for both salinity and water stress.
	Pressure Head Reduction	Specifies parameters in the root water uptake water stress response model.
	Osmotic Head Reduction	Specifies parameters in the root water uptake salinity stress response model.
	Root Growth	Specifies parameters in the Verhulst-Pearl logistic growth function used to describe root growth during the growing season.
	Meteorological Parameters	Specifies meteorological parameters required by the Penman-Monteit combination or Hargreaves equations.
	Variable Boundary Condition	Specifies time-dependent boundary conditions for all transport processes.
	Meteorological Boundary Conditions	Specifies meteorological variables (radiation, temperatures, wind speed, relative humidity) required by the Penman-Monteit combination or Hargreaves equations.
	Data for Inverse Solution	Specifies data for the inverse solution, their type, location and associated weight.
	Profile Information	Calls external module PROFILE, for users to discretize the soil profile and to specify the vertical distribution of relevant parameters.
	Profile Summary	Summarizes in tabular form the spatial discretization and spatial distribution of soil properties, initial conditions, and other variable. This command allows the user to summarize and modify the parameters setup in the external module PROFILE.
D	Execute HYDRUS	Executes a HYDRUS FORTRAN application.
E	Observation Points	Graphical presentation of changes in water content, pressure head, temperature, and/or solute and sorbed concentration at specified observation nodes.

273

Table B.3. (continued).

Group	Command	Brief description of the command
	Basic Informations	Graphical presentation of pressure head, water content, flow velocity, root water uptake, temperature, and concentration profiles at different times.
	Solution Concentrations	Graphical presentation of major ion concentrations: Ca, Mg, Na, K, alkalinity, SO_4, Cl, and tracer.
	Solid Concentrations	Graphical presentation of surface species and mineral phase concentrations:Ca, Mg, Na, K, calcite, gypsum, dolomite, nesquehonite, hydromagnesite, sepiolite.
	Chemical Information	Graphical presentation of major chemical information (pH, SAR, (H_2O^0), (Ca^{2+}), (HCO_3^-), $p\mathrm{IAP}^C$, $p\mathrm{IAP}^D$, $p\mathrm{IAP}^G$, EC, ..
	Boundary Informations	Graphical presentation of actual and cumulative boundary water and solute fluxes, and surface, root zone, and bottom pressure heads and concentrations.
	Carbon Dioxide Transport	Graphical presentation of actual and cumulative boundary CO_2 fluxes, and surface, root zone, and bottom boundary CO_2 concentrations.
	Soil Hydraulic Properties	Graphical presentation of the soil hydraulic properties.
	Run Time Information	Graphical presentation of information about the number of iterations, time step, and Peclet and Courant numbers.
	Mass Balance Information	Displays mass balance information and mean profile properties
	Inverse Solution	Displays information about the inverse solution.
	Meteorological Information	Displays components of the surface energy balance (ET, E, T, aerodynamic and radiation terms of the Penman-Monteith combination equation).
	Solute Mass Balance Information	Displays mass balance information for particular major ions.
F	Program Options	Displays pathways for HYDRUS settings and configuration files, as well as for HYDRUS projects.
H	Index	Offers an index of topics for which help is available.
	Using Help	Provides general instructions on using help.
	About HYDRUS-1D	Displays the version and authors of the HYDRUS-1D application.

Table B.4. Graph options in the HYDRUS-1D interface.

Command	Horizontal Axis	Vertical Axis
Observation Points	Time	Pressure Head Water Content Temperature Concentration – x^+ Sorbed Concentration - x^+
Profile Information - Basic Information	Pressure Head$^\blacklozenge$ Water Content$^\blacklozenge$ Hydraulic Conductivity Soil Water Capacity Water Flux$^\blacklozenge$ Root Water Uptake Temperature Immobile Water Content[*] Water Mass Transfer[*] Solute Mass Transfer[*] Concentration - $x^{+\blacklozenge}$ Sorbed Concentration - x^+	Depth
- Solution Concentrations	Calcium Magnesium Sodium Potassium Alkalinity Sulfate Chloride Tracer	Depth
Solid Concentrations	Calcite Gypsum Dolomite Nesquehonite Hydromagnesite Sepiolite Adsorbed Calcium Adsorbed Magnesium Adsorbed Sodium Adsorbed Potassium	Depth
Chemical Information	Calcium Activity Bicarbonate Activity Water Activity Alkalinity pH SAR Electric Conductivity	Depth

Command	Horizontal Axis	Vertical Axis
	Ionic Strength	
	pIAP Calcite	
	pIAP Gypsum	
	pIAP Dolomite	
	Osmotic Coefficient	
	Osmotic Pressure Head	
T_Level Information		
- Water Flow	Time	Potential Surface Flux
		Potential Root Water Uptake Rate
		Actual Surface Flux
		Actual Root Water Uptake Rate
		Bottom Flux
		Cumulative Potential Surface Flux
		Cumulative Potential Root Water Uptake Rate
		Cumulative Actual Surface Flux
		Cumulative Actual Root Water Uptake Rate
		Cumulative Bottom Flux
		Surface Pressure Head
		Average Root Zone Pressure Head
		Bottom Pressure Head
- Solute Transport[+]	Time	Surface Solute Flux
		Bottom Solute Flux
		Cumulative Surface Solute Flux
		Cumulative Bottom Solute Flux
		Cumulative Zero-Order Reactions
		Cumulative First-Order Reactions
		Surface Concentration
		Average Root Zone Concentration
		Bottom Concentration
		Root Solute Uptake
		Cumulative Root Solute Uptake
		Cumulative Mass Transfer Flux
- CO_2 Transport	Time	Surface CO_2 Flux
		Bottom CO_2 Flux
		Cumulative Surface CO_2 Flux
		Cumulative Bottom CO_2 Flux
		Surface CO_2 Concentration
		Average Root Zone CO_2 Concentration
		Bottom CO_2 Concentration
		CO_2 Production
		Cumulative CO_2 Production
		Cumulative CO_2 Root Uptake

Command	Horizontal Axis	Vertical Axis
Soil Hydraulic Properties	Pressure Head Log Pressure Head Water Content	Water Content Soil Water Capacity Hydraulic Conductivity Log Hydraulic Conductivity Effective Water Content
Run-Time Information	Time Level Time	Time Step Number of Iterations Cumulative Number of Iterations Peclet Number Courant Number Number of Solute Iterations

[+] This value is given for each solute
[*] This value is given when dual porosity model is used
◆ These variables are displayed for both matrix and fracture regions when the dual-permeability model is used

B.2. *Module **POSITION***

A project manager, **POSITION** (PCP_BASE.DLL) (Fig. B.1), is used to manage data of existing projects, and to help locating, opening, copying, deleting and/or renaming desired projects or their input or output data. A "project" represents any particular problem to be solved by HYDRUS-1D. The project name (8 letters), as well as a brief description of the project helps to locate a particular problem. Input and output data for selected projects are grouped into **Workspaces** (represented by subdirectories) which can be located anywhere on accessible hard discs of a particular PC or network.

Table B.5. Information in the HYDRUS1D.DAT file.

Group	Variable	Type	Description
Main	WaterFlow	Int	Variable, which specifies whether or not transient water flow is to be calculated.
	SoluteTransport	Int	Variable, which specifies whether or not solute transport is to be calculated.
	HeatTransport	Int	Variable, which specifies whether or not heat transport is to be calculated.
	EquilibriumAdsorption	Int	Variable, which specifies whether or not adsorption is considered as equilibrium process.
	RootWaterUptake	Int	Variable, which specifies whether or not root water uptake is to be calculated.
	RootGrowth	Int	Variable, which specifies whether or not root water growth is to be calculated.
	MaterialNumbers	Int	Number of materials considered.
	SubregionNumbers	Int	Number of subregions considered for mass balance calculation.
	SpaceUnit	String	Space units.
	TimeUnit	String	Time units.
	PrintTimes	Int	Number of print-times.
	NumberOfSolutes	Int	Number of solutes considered in the application.
	CO2Transport	Int	Variable which specifies whether or not carbon dioxide transport is to be calculated.
	SolutionConc	Int	Number of solution combinations considered in the application.
	AdsorbedConc	Int	Number of surface species combinations considered in the application.
	PrecipConc	Int	Number of mineral phase combinations considered in the application.
	Unsatchem	Int	Variable, which specifies whether or not major ion solute transport is to be calculated.
Profile	NumberOfNodes	Int	Number of nodes used to discretize the soil profile.
	ProfileDepth	Float	Depth of the soil profile.
	ObservationNodes	Int	Number of observation nodes.
	GridVisible	Int	Variable, which specifies whether or not the grid is to be visible.
	SnapToGrid	Int	Variable, which specifies whether or not the mouse should move in steps defined by the grid.
	ProfileWidth	Int	Number of pixels for graphical display of the soil profile.
	LeftMargin	Int	Number of pixels for graphical display of the nodal discretization.
	GridOrgX	Real	X-coordinate of the grid origin.
	GridOrgY	Real	Y-coordinate of the grid origin.
	GridDX	Real	Step in the x direction between grid nodes.
	GridDY	Real	Step in the y direction between grid nodes.

B.3. *Module* **PROFILE**

B.3.1. *Soil Profile Discretization*

The module **PROFILE** (Fig. B.2) is used, among other things, to discretize a one-dimensional soil profile into discrete nodes. Nodes are generated by dividing the soil profile into small elements. If no previous nodes exist, the program automatically generates a default equidistant point distribution. The location of nodes can be edited by the user to optimize the thickness of the different elements. There are two ways of specifying appropriate distributions of the nodes, i.e., by (1) editing the number of points, and (2) specifying fixed points and nodal densities. The nodal density determines the relative length of the elements, and can be specified only at fixed points. Fixed points can be inserted or deleted anywhere in the soil profile. The user can edit the nodal density at a fixed point in order to locally refine the nodal distribution around this point. Careful placement of the nodes is important since the nodal distribution determines in a very substantial manner the ultimate quality and speed of the calculations.
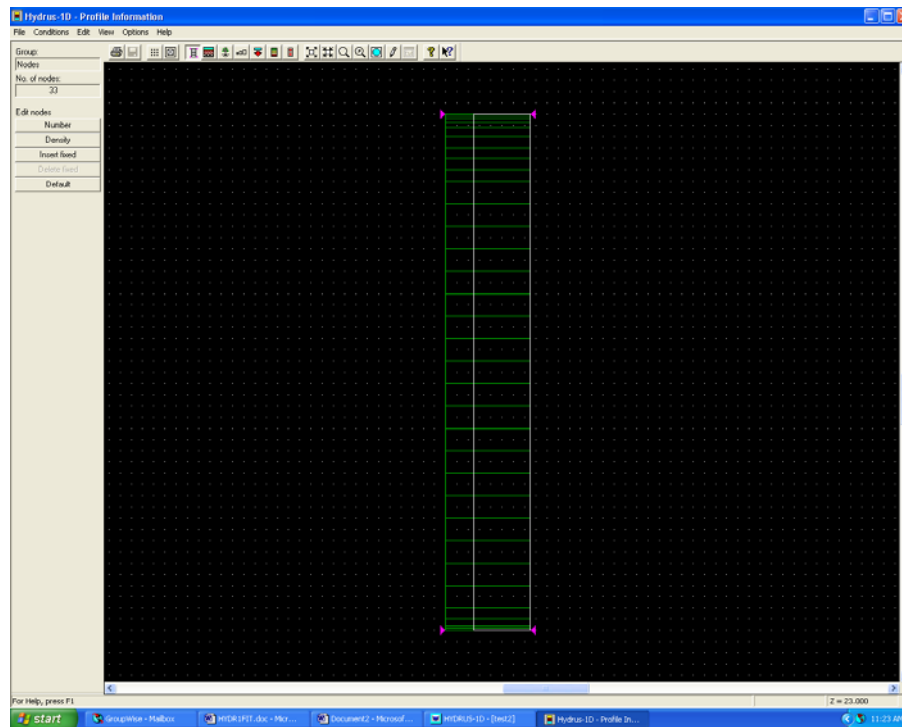

Fig. B.2. The main window of the PROFILE module; when used for soil profile discretization.

Table B.6. Definition of terms used in module PROFILE.

Nodal Point	Nodal points are nodes which discretize the soil profile and which are marked by green crosses. These nodes are ordered from the top (node number 1) to the bottom (node *NumNP*).
Elements	Elements are layers discretizing the soil profile. They connect the generated nodal points.
Fixed Points	Fixed points are points in the soil profile marked by purple stars. These points may be used to adjust the local discretization density of nodal points. By default, fixed points are placed at the top and bottom of the soil profile, but they can be inserted or deleted also at any other point in the soil profile.
Nodal Density	The nodal density is a real number in the range <0.01, 100.> specifying the local density of nodal points. The density can be specified only at fixed points. The program distinguishes between top and bottom density. The top (bottom) density at a fixed point specifies the relative thickness of the elements above (or below) this point. If the top and bottom densities are equal then the nodal density is continuous throughout the profile, i.e., both elements have the same thickness. If the top and bottom density values are different then the element thicknesses will be different as well. For example: if $DT = 3.$, $DB = 2.$ then $LT/LB = 1.5$, where DT and DB are the top and bottom densities at a fixed point, respectively, and LT and LB are the thicknesses of elements above and below that fixed point, respectively.

B.3.2. *Specification of Soil Properties within the Soil Profile*

The **PROFILE** module (Fig. B.3.) helps a user to define also the spatial distribution of parameters characterizing the flow domain (e.g., spatial distribution of soil materials, hydraulic scaling factors, root-water uptake parameters) and/or observation nodes. All parameters in this module are specified in a graphical environment with the help of a mouse.

Specification of parameters characterizing the flow domain (initial conditions, material distribution) is relatively straightforward. The user must first select that part of the transport domain to which he/she wants to assign a particular value of the selected variable. It is possible

to select the entire transport domain, part of it, or only individual nodes. A particular part of the transport domain can be selected as follows: the user must first click the Edit Condition button, and then move the mouse to a selected position. The beginning and end of the selection operation is framed by clicking the left button. The selected area is the vertical defined by the two mouse positions when the left button was clicked. When the selection is completed, the window Condition Specification pops up and the user must specify the value of a particular variable. That value will then be assigned to the selected area. When specifying the initial condition, the user has the possibility of assigning either a constant value to a selected domain, or specifying different values to the top and bottom of the selected region, in which case the program will linearly interpolate the variable within the selected region. Variables are always assigned to nodal points, not to elements.
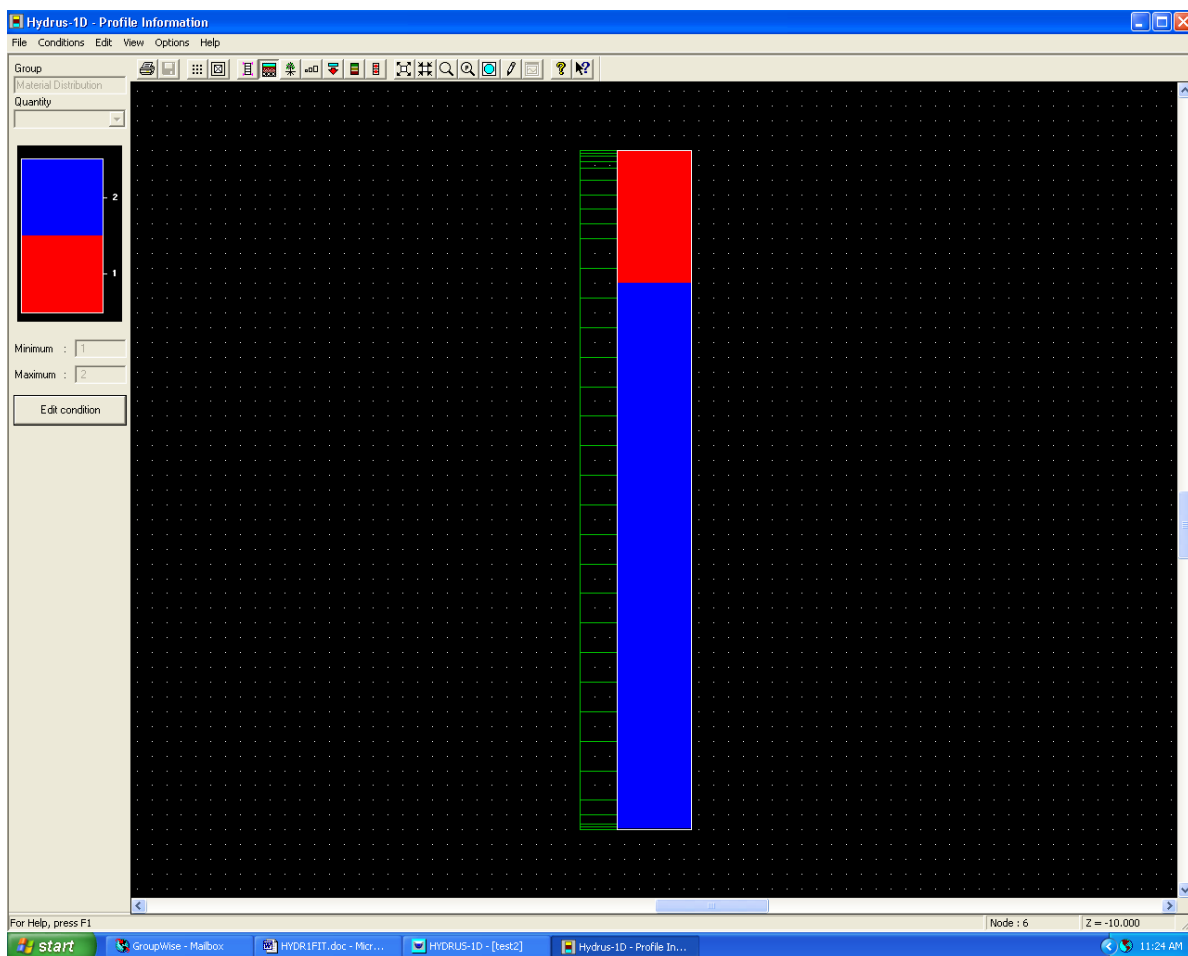

Fig. B.3. The main window of the PROFILE module; when used for specification of soil properties.